

EEG Analysis: Theory and Practice

FERNANDO H. LOPES DA SILVA

54

Analysis of electroencephalography (EEG) signals always involves questions of quantification; such questions may concern the precise value of the dominant frequency and the similarity between two signals recorded from symmetric derivations at the same time or different times. In these examples, there is a question that can be solved only by taking measures with regard to the EEG signal. Without such measures, EEG appraisal remains subjective and can hardly lead to logical systematization. Classic EEG evaluation has always involved measuring frequency and/or amplitude with the help of simple rulers. The limitations of such simple methods are severe, particularly when large amounts of EEG data must be evaluated and the need for data reduction is felt strongly, as well as when rather sophisticated questions are being asked, such as whether EEG signal changes occur in relation to internal or external factors, and how synchronous are EEG phenomena occurring in different derivations.

Clear replies to these questions require some form of EEG analysis. However, such analysis not only is a problem of quantification, but also involves elements of pattern recognition. Every electroencephalographer knows that it is sometimes extremely difficult to cite exact measures for such EEG phenomena as spikes, sharp waves, or other abnormal patterns; the experienced specialist is able to detect them only by “eyeballing.” These types of problems may be solved using pattern recognition analysis techniques, based on the principle that features characteristic of the EEG phenomena have to be measured. This phase of *feature extraction* is followed by *classification* of the phenomena into different groups. EEG analysis thus implies not only simple quantification, but also feature extraction and classification.

The primary aim of EEG analysis is to support electroencephalographers' evaluations with objective data in numerical or graphic form. EEG analysis, however, can go further, actually extending electroencephalographers' capabilities by giving them new tools with which they can perform such difficult tasks as quantitative analysis of long-duration EEG in epileptic patients and sleep and psychopharmacologic studies.

The choice of analytic method should be determined mainly by the goal of the application, although budget limitations must also be taken into consideration. The development of an appropriate strategy rests on such practical facts as whether analysis results must be available in real time and online or may be presented offline. In the past, the former requirement would pose considerable problems, solvable only by adopting a rather simple form of analysis; the development of new computer technology has provided more acceptable solutions. Another

practical consideration is the number of derivations to be analyzed and whether the corresponding topographic relations have to be determined or the analysis of one or two derivations is enough; the latter may suffice during anesthesia monitoring or in sleep research. Whether the analysis of a relatively short EEG epoch is sufficient or must involve very long records, for instance, up to 24 hours is another important factor.

In short, the *method* of analysis must be suited to the *purpose* of the analysis. Among the different purposes are the following: (i) determining whether a relatively short EEG record taken in a routine laboratory is normal or abnormal; (ii) classifying an EEG as abnormal, for example, as epileptiform or hypofunctional; (iii) evaluating changes occurring in serial EEG; and (iv) evaluating trends during many hours of EEG monitoring, such as under intensive care conditions for heart surgery or in long-term recordings in epileptic patients.

GENERAL CHARACTERISTICS

The EEG is a complex signal, the statistical properties of which depend on both time and space. Regarding the temporal characteristics, it is essential to note that EEG signals are ever-changing. However, they can be analytically subdivided into representative epochs (i.e., with more or less constant statistical properties).

Estimates of the length of such epochs vary considerably because of dependence on the subject's behavioral state. When the latter is kept almost constant, Isaksson and Wennberg (1) found that, over relatively short-time intervals, epochs can be defined that can be considered representative of the subject's state; in this study, some 90% of the EEG signals investigated had time-invariant properties after 20 seconds, whereas less than 75% remained time invariable after 60 seconds. Empirical observations indicate that EEG records obtained under equivalent behavioral conditions show highly stable characteristics; for example, Dumermuth et al. (2) showed that variations in mean peak (beta activity) of only 0.8 Hz were obtained in a series of 11 EEGs over 29 weeks. In this respect it is interesting to consider the studies of Jansen (3) and Grosveld et al. (4); these authors investigated the possibility of correctly assigning EEG epochs (duration 10.24 seconds) to the corresponding subject by means of multivariate analysis, using half of the EEG epochs recorded from 16 subjects as a training set for the classification algorithm. Using 4 to 10 EEG features, it was found that in 80% to 90% of the cases of EEG epochs were assigned correctly to the corresponding subject. McEwen and Anderson (5) introduced the concept of wide-sense stationarity in EEG analysis; they

proposed a procedure for determining whether a set of signal samples (e.g., an EEG signal) can be considered to belong to a wide-sense stationarity process. Their procedure consisted of calculating the amplitude distributions and power spectra of sample subsets and showing that they do not differ significantly using the Kolmogorov–Smirnov statistic. From this study it was concluded that, for EEG epochs (awake condition or during anesthesia) of less than 32 seconds, the assumption of wide-sense stationarity was valid more than 50% of the time.

On the basis of this type of empirical observation, it can be assumed that relatively short EEG epochs (~10 seconds) recorded under constant behavioral conditions are quasi-stationary. Elul (6) remarked that the EEG is related to intermittent changes in the synchrony of cortical neurons; thus, he characterized the EEG as a series of short epochs rather than a continuous process.

The fact that EEG signals have different characteristics depending on the place over the head where they are recorded is essential to all EEG recordings. Therefore, in any method of EEG analysis, topographic characteristics have to be taken into account. This means that one should choose EEG montages carefully, in view of the objectives of the analysis. The topographic aspects appear most clearly in the simple case of comparing EEG records from symmetric derivations; indeed, the use of the subject as his or her own control through right–left comparisons is a cornerstone of the neurologic examination. Therefore, right–left comparisons are also paramount in any practical clinical system of EEG analysis.

BASIC STATISTICAL PROPERTIES

Some of the underlying assumptions of the most common methods of EEG analysis will be discussed briefly. Gasser (7) has provided a more fundamental discussion of this topic; here, general concepts will suffice.

The exact characteristics of EEG signals are, in general terms, unpredictable. This means that one cannot foresee precisely the amplitude of an EEG graphoelement or the duration of an EEG wave. Therefore, it is said that an EEG signal is a realization of a *random* or *stochastic* process. Indeed, it is possible to determine some statistical measures of EEG signals that show considerable regularity, such as an average amplitude or an average frequency. This is a general characteristic of random processes, which are characterized by probability distributions and their moments (e.g., mean, variance, skewness, and kurtosis) or by frequency spectra or correlation functions. Such a description of an EEG signal as a realization of a random process implies a mathematical, but not a biophysical, model.

It should be stressed (8) that the biophysical process underlying EEG generation is not necessarily random in nature, but it may have such a high degree of complexity that only a description in statistical terms is justified. Gasser (7) has also emphasized this point; even in the case of signals that are deterministic (e.g., sinusoids) but very complex (e.g., made of many components), a stochastic approach may be the most adequate.

EEG signals are, of course, time series; they are characterized by a set of values as a function of time. An important problem, however, is whether the general methods for analyzing time series can be applied without restrictions to EEG signals.

In Chapter 4, which discusses EEG dynamics, it was mentioned that modern mathematical tools are being used to analyze EEG signals, assuming that signal generation can be described using sets of nonlinear differential equations. These techniques have been developed within the active field of mathematical research called “deterministic chaos.” In essence, nonlinear dynamical systems such as the neuronal networks generating EEG signals can display chaotic behavior; that is, their behavior can become unpredictable for relatively long periods, and EEG signals may be an expression of chaotic behavior. Since new mathematical tools, based on the analysis of complex nonlinear systems such as the correlation dimension, were introduced in EEG, it became clear that EEG signals may be high-dimensional so that in many cases it is difficult, or even impossible, to distinguish whether these signals are generated by random or by high-dimensional nonlinear deterministic processes (9).

SAMPLING, PROBABILITY DISTRIBUTIONS, CORRELATION FUNCTIONS, AND SPECTRA

EEG signals are continuous variations of potential as a function of time. However, in most practical cases where quantitative analysis is applied, signals must be digitized so that they can be processed by digital computer. This means that the EEG signal must be processed in such a way that the random variable, potential as a function of time, will have only one set of discrete values at a set of discrete time instances. In technical terms, the process of analog-to-digital (AD) conversion involves *sampling* combined with the operation of *quantizing*. According to definitions commonly used (10), sampling is the “process of obtaining a sequence of instantaneous values of a wave at regular or intermittent intervals” and quantization is the “process in which the continuous range of values of an input signal is divided into nonoverlapping subranges and to each subrange a discrete value of the output is uniquely assigned.”

EEG signal sampling must be performed without changing the statistical properties of the continuous signal. Generally, one samples an EEG signal at equidistant time intervals (Δt), thus transforming the continuous signal into a set of impulses with different heights separated by intervals Δt (Fig. 54.1). An important question is the choice of the sampling frequency. This choice is based on the *sampling theorem*: assuming that a signal $x(t)$ has a frequency spectrum $X(f)$ such that $X(f) = 0$ for f_N , no information is lost by sampling $x(t)$ at equidistant intervals Δt with $f_N = 1/(2 \Delta t)$; f_N is called the folding or Nyquist frequency. The sampling frequency, therefore, must be at least equal to $2f_N$. A consequence of this theorem is that care has to be taken to ensure that the signal to be sampled has no frequency components above f_N . Therefore, before sampling, all frequency components greater than f_N should be eliminated by low-pass filtering. One should keep in mind that sampling at a frequency below $2f_N$ is not equivalent to filtering; it would produce aliasing

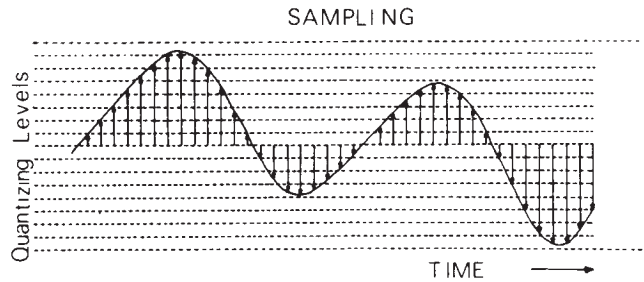


Figure 54.1 Analog-to-digital (AD) conversion of the continuous signal is performed at equidistant time intervals, digitizing its amplitude according to the corresponding quantizing levels. (Adapted from Lopes da Silva FH, Cooper R, Dumermuth G, et al. Sampling, conversion, and measurement of bioelectrical phenomena. In: Remond A, ed-in-chief; Brazier MA, ed. *Handbook of Electroencephalography and Clinical Neurophysiology*. Vol 4. Part A. Amsterdam: Elsevier; 1976.)

or signal distortion due to folding of frequency components larger than f_N onto lower frequencies (11). The analog voltages of the signal at the sampling moments are converted to a number corresponding to the amplitude subrange or level. Most EEG analysis can be performed using 512 to 2048 amplitude levels (i.e., 9 to 11 bits). Technical details of AD conversion may be found in Susskind (12) and, for the special case of EEG signals, in Lopes da Silva et al. (11) and Steineberg and Paine (13).

The continuous EEG signal is thus replaced by a string of numbers $x(t_i)$ representing the signal amplitude at sequential sample moments; the latter are indicated by the index i along the time axis. The signal is assumed to be a realization of a stationary random process $\underline{x}(t_i)$, which is indicated by underlining the letter (\underline{x}). In general, a collection of EEG signals of a certain length recorded under equivalent conditions is available for analysis. The entire collection of EEG signals is called an *ensemble*; each member of the ensemble is called a *sample function* or a *realization*.

PROBABILITY DISTRIBUTIONS

The digitized EEG signal values $x(t_i)$ can be considered realizations of one stochastic variable $\underline{x}(t_i)$ and may be characterized when stationarity is assumed by a histogram; when in an interval $0 > t > T$ there are n_a sample points in the interval $\pm 1/2\Delta$, n_a/N is called the relative frequency of occurrence of the value a , where N is the total number of samples available. One can define the relative frequencies of all other values similarly. When N becomes infinitely large and Δ infinitely small, n_a/N will tend to a limit value $p(x(t_i) = a)$, called the probability of occurrence of $x(t_i) = a$. The set of values of $p(x(t_i))$ is called the signal *probability distribution*, characterized by a mean and a number of moments. Considering that the discrete random variable x can take any of a set of values from 1 to M , the mean or *average* of the sample functions is given as follows (E is the symbol for expectation):

$$E[\underline{x}(t_i)] = \left[\sum_{a=1}^M a \cdot p(\underline{x}(t_i) = a) \right] = m_1 \quad (54.1)$$

Also definable is a class of statistical functions characteristic of the random process: $m_n = E[\underline{x}^n(t_i)]$ with $n = 1, 2, 3, \dots$; these functions are called the *n*th moments of the discrete random variable $\underline{x}(t_i)$. The implicit assumption here and in the following discussion is that the statistical properties of the signal do not change in the interval T . Therefore, the moments are independent of time t_i .

The first moment $E[\underline{x}(t_i)]$ is called the *mean* of $\underline{x}(t_i)$. It is often preferable to consider the *central moments* (i.e., the moments around the mean); the second central moment is then:

$$E[(\underline{x}(t_i) - E(\underline{x}(t_i)))^2] = m_2 \quad (54.2)$$

or σ^2 or *variance* of $\underline{x}(t_i)$.

Similarly, the third central moment $E[(\underline{x}(t_i) - E(\underline{x}(t_i)))^3] = m_3$ can be defined; from this can be derived the *skewness* factor $\beta_1 = m_3/(m_2)^{3/2}$. The fourth central moment is $E[(\underline{x}(t_i) - E(\underline{x}(t_i)))^4] = m_4$, from which can be derived the *kurtosis excess*: $\beta_2 = m_4/(m_2)^2$. In case of a symmetric amplitude distribution is $\beta_1 = 0$; all odd moments are equal to zero. For a gaussian distribution the even moments have specific values, for example, $\beta_2 = 3$; derivatives from this value indicate the peakedness ($\beta_2 > 3$) or flatness ($\beta_2 < 3$) of the distribution (Fig. 54.2).

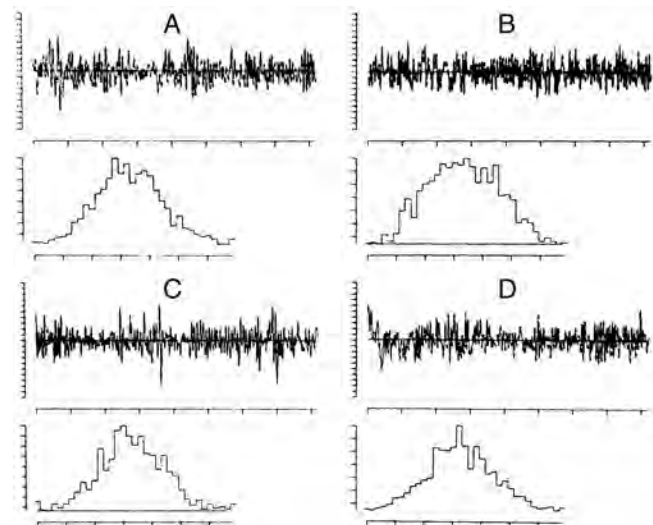


Figure 54.2 Examples of EEG signals with corresponding amplitude distributions. For the EEG signals, the time marks along the horizontal axis give the intervals in seconds; the vertical axis is in microvolts; for the amplitude distributions, the horizontal axis is in microvolts, and the vertical axis gives the number (N) of times a certain amplitude class has been measured in the corresponding EEG epoch. The signals were sampled at 20 Hz. The amplitude distribution of the four EEG signals has the following values of skewness (S) and kurtosis (K): (A) $S = 0.17$, $K = 3.09$; (B) $S = 0.09$, $K = 2.41$; (C) $S = 0.10$, $K = 3.37$; (D) $S = 0.07$, $K = 2.98$. The hypothesis that the amplitude distribution belongs to a normal distribution can be rejected at $P > 0.01$ whenever $S > 0.464$ and/or $2.45 > K > 4.13$ with $N = 160$.

CORRELATION FUNCTIONS AND SPECTRA

In general terms, successive values of a signal, such as an EEG, which result from a stochastic process are not necessarily independent. On the contrary, it is often found that successive discrete values of an EEG signal have a certain degree of *interdependence*. To describe this interdependence, one may compute the signal *joint probability distribution*. As an example, consider the definition of the joint probability applied to a pair of values at two discrete moments, $\underline{x}(t_1)$ and $\underline{x}(t_2)$; assume that one disposes of N realizations of the signal; the number of times that at t_1 a value v and at t_2 a value u are encountered is equal to n_{12} . Thus, the joint probability of $\underline{x}(t_1)$ and $\underline{x}(t_2) = u$ may be defined as follows:

$$p(\underline{x}(t_1) = v, \underline{x}(t_2) = u) = \lim_{N \rightarrow \infty} \frac{n_{12}}{N} \tag{54.3}$$

A complete description of the properties of the signal generated by a random process can be achieved by specifying the *joint probability density function*:

$$\rho(\underline{x}(t_1), \underline{x}(t_2), \dots, \underline{x}(t_n)) \tag{54.4}$$

for every choice of the discrete time samples t_1, t_2, \dots, t_n and for every finite value of n . The computation of this function, however, is rather complex. A simpler alternative to this form of description is to compute a number of *averages* characteristic of the signal, such as *covariance*, *correlations*, and *spectra*. These averages do not necessarily describe a stochastic signal completely, but they may be very useful for a general description of signals such as EEG.

The *covariance* between two random variables at two time samples $\underline{x}(t_1)$ and $\underline{x}(t_2)$ is given by the following expectation:

$$E[(\underline{x}(t_1) - E(\underline{x}(t_1)))(\underline{x}(t_2) - E(\underline{x}(t_2)))] \tag{54.5}$$

Estimating the covariance between any two variables $\underline{x}(t_1)$ and $\underline{x}(t_2)$ requires averaging over a number of realizations of an ensemble. Another way to estimate the covariance, provided that the signal is stationary and ergodic (for a discussion of these concepts see Ref. 14), is by computing a time average, for one realization of the signal, of the product of the signal and a replica of itself shifted by a certain time τ_k along the time axis. This time average is called the *autocorrelation function*:

$$\Phi_{xx}(\tau_k) = \langle \underline{x}(t_i)\underline{x}(t_i + \tau_k) \rangle = \frac{1}{T} \sum_{i=1}^N \underline{x}(t_i)\underline{x}(t_i + \tau_k) \tag{54.6}$$

where $\tau_k = k \cdot \Delta t$.

The following description considers continuous random variables $x(t)$, for the sake of simplifying the formulas. Assuming that every sample function, or realization, is representative of the whole signal being analyzed, it can be shown that for stationary and ergodic processes the time average $\Phi_{xx}(\tau)$ for one realization $\underline{x}(t)$ is an estimate of the ensemble average $R_{xx}(\tau)$:

$$R_{xx}(\tau) = E[\underline{x}(t)\underline{x}(t + \tau)] \tag{54.7}$$

assuming that the signal $\underline{x}(t)$ has mean zero. For the value $\tau = 0$:

$$R_{xx}(0) = E[\underline{x}^2(t)] = \lim_{T \rightarrow \infty} \frac{1}{2T} \int_{-T}^T \underline{x}^2(t) dt \tag{54.8}$$

which is the signal's average power or variance σ . An important property of the autocorrelation function is that its Fourier transform (FT) is:

$$S_{xx}(f) = \int_{-\infty}^{\infty} R(\tau) \exp(-j2\pi f\tau) d\tau = FT(R_{xx}(\tau)) \tag{54.9}$$

$S_{xx}(f)$ is called the power density spectrum, or simply the *power spectrum*, a common method of EEG quantification (Fig. 54.3). The power spectrum $S_{xx}(f)$ is a function of frequency (Hz); it gives the distribution of the squared amplitude of different frequency components. It should be noted that the word *power* does not have the meaning of dissipated power in an RC circuit but is used here in another sense. This discussion deals with a question of time series analysis. In general, a stochastic

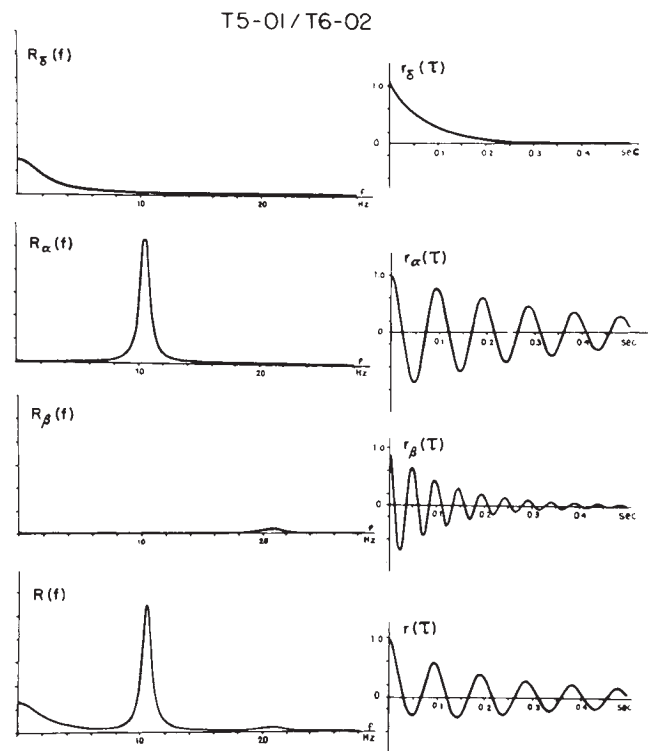


Figure 54.3 The power spectrum of an EEG signal is shown in the lower left plot; vertical axis power indicated here as $R(f)$; horizontal axis frequency, f , in hertz. On the lower right the corresponding autocorrelation function $r(\tau)$ is plotted. The power spectrum and autocorrelation functions are considered to be composed of three components (δ, α, β) corresponding to three EEG frequency bands. (Adapted from Zetterberg LH. Experience with analysis and simulation of EEG signals with parametric description of spectra. In: Kellaway P, Petersén I, eds. *Automation of Clinical Electroencephalography*. New York, NY: Raven; 1973:161-201.)

Copyright © 2010, Wolters Kluwer Health. All rights reserved.

time function may be expressed in one of the several ways, as a voltage, a length, a velocity, a number of occurrences of a certain event, and so forth. The power spectrum or simply the spectral density of the time function is the FT of the autocorrelation function, the dimension of which is the function's amplitude dimension squared. In case the signal dimension is in volts, the power spectrum is in (V²·sec) or (V²/Hz). Of course, if the function's amplitude is in any other dimension, the intensity of the corresponding power spectrum would be yet another dimension. It is useful to keep a clear distinction between electric power dissipated in an electric circuit ($P = 1/T \int_0^T V^2/R dt$ with units [V²·sec/Ω]) and power spectrum.

A function that represents the average correlation between two signals $\underline{x}(t)$ and $\underline{y}(t)$ may be defined in terms equivalent to expression 54.7:

$$R_{xy}(\tau) = E[\underline{x}(t)\underline{y}(t + \tau)] \tag{54.10}$$

where the signals $\underline{x}(t)$ and $\underline{y}(t)$ are assumed to have means of zero. $R_{xy}(\tau)$ measures the correlation between the two signals and is called the *cross-correlation function*. Similarly, one can define the FT of R_{xy} , which is the *cross-power spectrum* between signals \underline{x} and \underline{y} :

$$S_{xy}(f) = FT[R_{xy}(\tau)] \tag{54.11}$$

Fundamental discussions of power spectra and related topics are found in many textbooks on signal analysis, for example, Refs. 15 and 14. This discussion cannot go into details about ways of Bendat and Piersol (16) and Otnes and Enochson (17). Application of the frequency analysis principle to EEG signal analysis has a long history, beginning with the pioneering work of Dietsch (18), Grass and Gibbs (19), Knott and Gibbs (20), Drohocki (21), and Walter (22,23). Brazier and Casby (24) and Barlow and Brazier (25) first computed the autocorrelation functions of EEG signals. The general principles on which this work has been based have remained essentially the same since Wiener proposed these signal analysis methods (for a review, see Ref. 26). An important advance in computing power spectra has been achieved with the introduction of a new algorithm for computing the *discrete Fourier transform*, known as the *fast Fourier transform* (FFT) (27). In this case, it is assumed that one wants to compute the power spectrum of a discrete EEG signal; the epoch $[\underline{x}(t_1)]$ is considered as a signal sampled at intervals Δt , $x(n \Delta t)$ with a total of N samples ($n = 1 \dots N$). By using the discrete FT, the so-called *periodogram* $F(f_i)$ can be computed:

$$F_{xx}(f_i) = \frac{\Delta t}{N} \left| \sum_{n=1}^N x(t_n) \exp(-j2\pi \cdot i \Delta f \cdot n \Delta t) \right|^2 \tag{54.12}$$

where $f_i = i \cdot \Delta f$ with $i = 0, 1, 2, \dots, N$. The periodogram can be smoothed by means of a window $W(f_k)$ in order to obtain $P_{xx}(f_k)$, which is a better estimate of the real power spectrum $S_{xx}(f)$:

$$P_{xx}(f_i) = \sum_{k=-p}^p W(f_k) F_{xx}(f_{i+k}) \tag{54.13}$$

where $W(f_k)$ is the smoothing window with a duration of $(2p + 1)$ samples or data points. Similarly, one can compute a smoothed estimate of the cross-power spectrum (S_{xy}), which might be called $C_{xy}(f)$.

The FFT power spectral analysis and its applications are discussed in more detail below.

The close relationship between the concepts of variance σ^2 , autocorrelation (equations 54.6 and 54.7), and power density spectrum (equation 54.9) has already been made apparent; in fact $R_{xx}(0) = \sigma^2$ and

$$\sigma^2 = \int_{-\infty}^{\infty} S_{xx}(f) df \tag{54.14}$$

The autocorrelation function $R(\tau)$ and the power density spectrum $S(f)$ correspond thus to the second-order moment of the probability distribution of the random process.

In case the signals are not gaussian, higher order spectra moments must be considered. These can be derived as follows. Assuming that the signal has mean = 0, one can write (as in expression 54.7):

$$R_{xx}(\tau_1, \tau_2) = E[\underline{x}(t)\underline{x}(t_1)\underline{x}(t + \tau_2)] \tag{54.15}$$

Similar to expression 54.9, the two-dimensional Fourier transform FT_2 of $R_{xx}(\tau_1, \tau_2)$ can be defined as the *bispectrum* or *bispectral density*:

$$B_{xx}(f_1, f_2) = FT_2[R_{xx}(\tau_1, \tau_2)] \tag{54.16}$$

This discussion cannot go into details about ways of estimating the bispectrum B_{xx} . For a detailed account of bispectral EEG analysis, refer to Huber et al. (28) and to Dumermuth et al. (29). It is, however, interesting to note that high B_{xx} values for a couple of frequencies, f_1 and f_2 , indicate phase coupling within the frequency triplet f_1, f_2 , and $(f_1 + f_2)$. The third moment of the probability distribution, or skewness, is related to the bispectrum. When there exists a sufficiently strong relation between two harmonically related frequency components in a signal, there will exist a significant bispectrum and skewness. The process in such a case is not gaussian; if it were gaussian with mean zero, the bispectrum would be zero. The bispectrum can be used to determine whether the system underlying the EEG generation has nonlinear properties. An example of this form of analysis is given in Figure 54.4.

This section has demonstrated the progression from the basic principles of probability distribution and corresponding moments to the concepts of autocorrelation, power spectra, and high-order spectra. It is also of interest to examine the *moments* of the spectral density $S_{xx}(f)$, because this analysis leads to another set of concepts applicable to EEG analysis, the so-called descriptors of Hjorth (30). Thus, one can define the *n*th spectral moment as follows:

$$a_n = \int_{-\infty}^{\infty} (2\pi f)^n S_{xx}(f) df \tag{54.17}$$

BICOHERENCE CONTOURMAP OF AN AVERAGE OF 4 FILES
CONTOURS AT 0.25 0.35 0.45

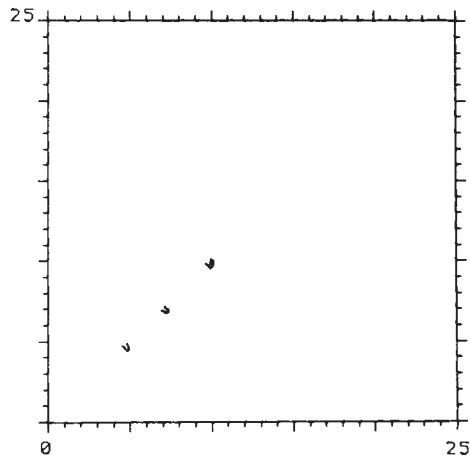


Figure 54.4 Contour map of the normalized bispectrum (also called bicoherence) of an EEG signal recorded from a subject who presented an alpha variant (the corresponding power spectrum is shown in Fig. 54.8). The plot shows three maxima in the value of bicoherence (>0.25). One is at the intersection of approximately 5 and 5 Hz (phase coupling between 5, 5, and 10 Hz); another one is at the intersection of about 7 and 7 Hz (phase coupling between 7, 7, and 14 Hz). Still another is at the intersection of about 10 and 10 Hz (phase coupling between 10, 10, and 20 Hz). This means that the two peaks seen in the power spectrum of Figure 54.8 at 5 and 10 Hz, respectively, are harmonically related, that is, 5 Hz is one-half subharmonic of the dominant alpha frequency. Moreover, there is another component at 20 Hz, difficult to see in the power spectrum, of Figure 54.8, which is also harmonically related to the alpha frequency (i.e., a second harmonic of the alpha component is also present). Another component at about 7 Hz related to 14 Hz can also be identified. (This component may be distinguished as a small notch at the flank of the 10-Hz peak in the power spectrum of Fig. 54.8.)

The zero-order moment is then:

$$a_0 = \int_{-\infty}^{\infty} S_{xx}(f) df \tag{54.18}$$

which is equal to the variance σ^2 .

It can be shown (for derivation, see Ref. 31) that the second-order moment is defined by the following expression:

$$a_2 = \int_{-\infty}^{\infty} (2\pi f)^2 S_{xx}(f) df = - \left. \frac{d^2 R_{xx}(\tau)}{d\tau^2} \right|_{\tau=0} = E \left[\frac{d^2 x(t)}{dt^2} \right]^2 \tag{54.19}$$

and the fourth-order moment is:

$$a_4 = \int_{-\infty}^{\infty} (2\pi f)^4 S_{xx}(f) df = - \left. \frac{d^4 R_{xx}(\tau)}{d\tau^4} \right|_{\tau=0} = E \left[\frac{d^4 x(t)}{dt^4} \right]^2 \tag{54.20}$$

In this way the spectral moments relate to the derivatives of the autocorrelation function $R_{xx}(\tau)$ and of the signal $x(t)$. The

discussion below illustrates how these spectral moments a_0 , a_2 , and a_4 are related to the descriptors proposed by Hjorth.

INTERVAL OR PERIOD ANALYSIS

An alternative method of EEG signal analysis is based on measuring the distribution of intervals between zero and other level crossings, or between maxima and minima.

A level crossing may be defined in general terms as the time at which a signal $x(t)$ passes a certain amplitude level b ; $b = 0$ is a special case referred to as zero crossing (Fig. 54.5). Knowledge of the probability density function of the intervals between successive zero crossings can be useful in characterizing some statistical properties of the signal $x(t)$ (mean value 0). $p_0(\tau)$ can be called the probability distribution density function of the intervals between any two successive zero crossings and $p_1(\tau)$, corresponding to the total time τ between successive zero crossings at which the signal changes in the same direction (i.e., from positive to negative or vice versa). In practice, these functions can be approximated by computing histograms of the interval length between two successive zero crossings or between zero crossings at which the signal has a derivative with the same sign. The moments of the distribution function can also be computed; the simplest case is to compute the average number of zero crossings per time unit (N_0) (e.g., per second) of the signal $x(t)$:

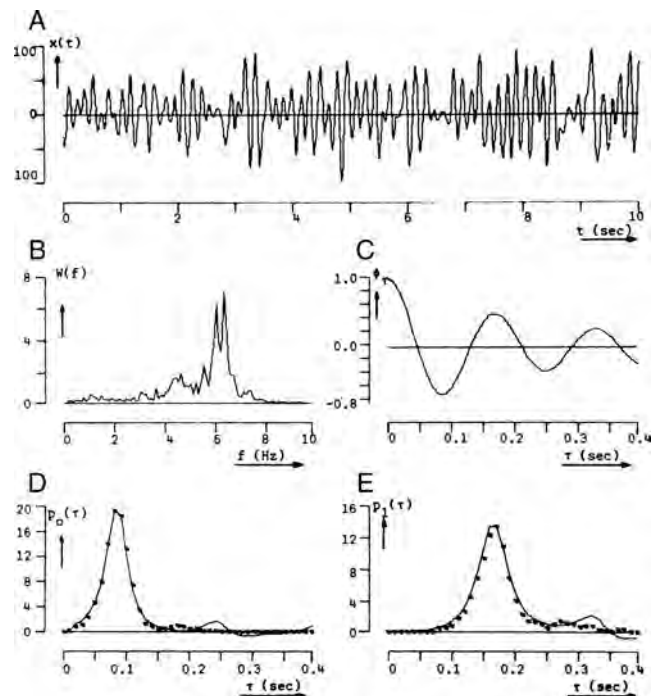


Figure 54.5 A: An EEG signal $x(t)$. B: Plot of the corresponding power spectrum $w(f)$ as function of frequency f in hertz. C: Plot of the autocorrelation function (τ) . D: Plot of $p_0(\tau)$ (i.e., the distribution density function of the intervals between any two successive zero crossing). E: Plot of $p_1(\tau)$ (i.e., the distribution density function of the time between successive zero crossings at which the signal $x(t)$ changes in the same direction, from positive to negative or vice versa). (Illustration courtesy of R.A.F. Pronk.)

$$N_0^{-1} = \bar{\tau} = \int_0^{\infty} \tau p_0(\tau) d\tau \quad (54.21)$$

This means that the number of zero crossings per time unit N_0 equals the reciprocal of the mean interval length τ .

In some cases it is helpful to determine the probability density function of the intervals between two adjacent zero crossings where the sign of $\underline{x}(t)$ changes from negative to positive or vice versa. In this case, it is necessary to compute additionally the zero crossing interval distribution of the first derivative of $\underline{x}(t)$, $\underline{y}(t)$ (i.e., $\underline{y}(t) = d\underline{x}(t)/dt$). If the signal $\underline{x}(t)$ to be analyzed is quasi-stationary and has a gaussian distribution, a mathematical relation between N_k , the average rate of zero crossings of the k th derivative of $\underline{x}(t)$, and the power spectrum $S_{xx}(f)$ can be shown (32–34):

$$N_k = 4 \left[\frac{\int_0^{\infty} f^{2k+2} S_{xx}(f) df}{\int_0^{\infty} f^{2k} S_{xx}(f) df} \right]^{1/2} \quad (54.22)$$

In interval analysis, only the values N_k for $k = 0, 1, 2$ are usually computed. N_0 thus represents the average rate of zero crossings of $d\underline{x}(t)/dt$ (i.e., the rate of intervals between extremes of the signal $\underline{x}(t)$); N_2 represents the average rate of zero crossings of $d^2\underline{x}(t)/dt^2$ (i.e., the rate of intervals of the a nonparametric or a parametric approach that is combined inflection points of $\underline{x}(t)$).

It can be shown (32) that expression 54.22 can separately also be given in terms of the autocorrelation function:

$$\frac{N_0}{2} = \left[(\pi\tau)^2 \left[1 - \frac{R_{xx}(\tau)}{R_{xx}(0)} \right] \right]^{1/2} = f_g \quad (54.23)$$

where f_g is the so-called gyrating frequency (35).

These relations between the number of zero crossings per time unit and either spectral moments or the autocorrelation function for EEG signals have been studied in detail by Saltzberg and Burch (36), who concluded that, when the purpose is to monitor long-term changes in the statistical properties of EEG signals, it is legitimate to use average zero-crossing rates to calculate moments of the power spectral density.

Instead of measuring intervals between zero crossings, one can characterize a signal by determining intervals between successive maxima (or minima), which defines a “wave,” or between a maximum and the immediately following minimum or vice versa, which defines a “half-wave.” The section “Mimetic Analysis” considers some of the variants of interval analysis as applied to EEG signals; the straightforward applications of interval analysis are described in the section “Time–Frequency Analysis.”

EEG SIGNAL PROCESSING METHODS IN PRACTICE

The previous section considered the statistical properties of EEG signals as realizations of random processes, explaining how such signals can be characterized by the corresponding probability distribution and its moments, by the autocorrela-

tion function or the power spectrum, or by distribution of intervals between level crossings. In all cases, the EEG was treated as a stochastic signal without a specific generation model. Therefore, all the previously described methods and related ones are *nonparametric methods*. *Parametric methods* may also be used to analyze EEG signals; in such cases one assumes the EEG signal to be generated by a specific model. For example, assuming that the EEG signal is the output of a linear filter given a white noise input allows characterization of the linear filter by a set of coefficients or parameters (e.g., it may correspond to an autoregressive model as explained below).

Therefore, EEG analysis methods can be divided into two basic categories, *parametric* and *nonparametric*. Such a division is conceptually more correct than the more common differentiation between frequency and time domain methods because, as has been explained, such methods as power spectra in the frequency domain and interval analysis in the time domain are closely related; indeed, they represent two different ways of describing the same phenomena. The methods of EEG analysis described here are classified as shown in Table 54.1.

Not all EEG analysis methods can be assigned to one of the two general categories just described. Those having mixed character (i.e., methods that have, as a starting point, a nonparametric or parametric approach that is combined with pattern recognition techniques) must be considered separately. The latter fall into the category of *pattern recognition* methods. Last, this section shall discuss *topographic analysis* methods, in which the emphasis is on topographic relations between derivations. Not included here are the evoked potentials, which are discussed elsewhere.

A thorough review of the main techniques currently in use in EEG analysis has been edited by Gevins and Remond (37). For more details on methods of analyzing brain electric signals, the reader is referred to this authoritative handbook.

Table 54.1

EEG Analysis Methods

Nonparametric Methods

Amplitude distributions

Interval or period distributions

Amplitude–interval scatter plots

Correlation functions

Auto- and cross-correlation

Complex demodulation

Power spectral analysis

Time-varying spectra

Cross-spectral functions (coherence and phase)

Bispectra

Walsh and Haar transforms

Hjorth slope descriptor

NONPARAMETRIC METHODS

Amplitude Distribution

A random signal can be characterized by the distribution of amplitude and its moments. An example of an amplitude distribution is shown in Figure 54.2. The first question that is asked regarding the amplitude distribution of an EEG epoch is whether the distribution is normal or gaussian. The most common tests of normality are the chi-square goodness-of-fit test (17), the Kolmogorov–Smirnov test, or the values of skewness and kurtosis (7,38). It has been shown (39) that, for the small EEG samples usually analyzed, the Kolmogorov–Smirnov test is more powerful than the chi-square test. It should be emphasized that in order to apply these tests of goodness-of-fit, two requirements must be satisfied: stationarity and independence of adjacent samples. The first requirement was considered in the previous sections. The second requirement is a well-known prerequisite for the application of the statistical tests of the type we consider here. Persson (40) has clearly pointed out the pitfalls of applying goodness-of-fit tests to EEG amplitude distributions. The problem is that the EEG signals are usually recorded at such a sampling rate that, depending on the spectral composition of the signal, adjacent samples are more or less correlated. In this way, the second requirement is commonly violated. This has also been shown clearly by McEwen and Anderson's (5) statistical study of EEG signals. The degree of correlation between adjacent samples can be deduced from the autocorrelation function. Persson found that a correlation coefficient of 0.50 or larger for adjacent samples introduces a considerable error in interpreting a goodness-of-fit test. His experience with EEG signals led to the conclusion that sampling rates in most cases should be restricted to about 20/sec in order to achieve an acceptably small degree of correlation between adjacent samples.

It is of general interest to know an EEG sample's type of amplitude distribution. Several studies have been carried out, mainly investigating whether or not EEG amplitude distributions were gaussian. Saunders (41), using a sample rate of 60/sec, epoch lengths of 8.33 seconds, and the chi-square test, concluded that alpha activity had a gaussian distribution; this confirmed previous results from Lion and Winter (42) and Kozhevnikov (43), who used analog techniques. On the contrary, Campbell et al. (44), using a sample rate of 125/sec, epoch lengths of 52.8 seconds, and the chi-square test, concluded that most EEG signals had non-gaussian distributions; however, it is likely that in this case the dual requirements of stationarity and independence were not met.

The results obtained by Elul (45) are of special interest because he examined EEG time-varying properties using amplitude distributions for epochs of 2 seconds (200 samples/sec, chi-square goodness-of-fit test); this study most certainly failed to meet the requirement of independence. Nevertheless, Elul found that a resting EEG signal could be considered to have a gaussian distribution 66% of the time, whereas, during performance of a mental arithmetic task, this incidence decreased to 32%. Evaluating a small series of waking EEGs in twins, Dumermuth (46,47) found amplitude distribution deviations from gaussianity in the majority of the subjects; he tested the normality hypothesis by way of the third- and fourth-order moments, skewness, and kurtosis. In adult sleep EEG, skewness and

kurtosis also deviated significantly from the values expected for a gaussian distribution depending on sleep stage (48,49). These observations have led to a study of higher order moments of the spectral density function using bispectral analysis.

The method recommended to test whether EEG amplitude distributions are gaussian is that proposed by Gasser (7,38); it involves calculating skewness and kurtosis after correction in view of the possibility that adjacent samples may have a large (e.g., >0.50) degree of correlation. The allowed kurtosis and skewness values can be found in statistical tables. Kurtosis in most cases without paroxysmal activity or artifacts is within the limits allowed to accept the normality hypothesis; skewness different from zero is encountered particularly in those cases in which harmonic components are present in the power spectra. In such instances, the bispectrum exists (see below).

An alternative method of calculating measures of EEG amplitude was developed by Drohocki (50) and is used mainly in psychopharmacologic and psychiatric studies (see review in Ref. 51). This method involves measuring the surface of rectified EEG waves. Its usefulness for routine EEG analysis is limited.

Interval Analysis

Interval or period analysis has been used, as described above, to study the statistical properties of EEG signals in general and in relation to other analysis methods, such as autocorrelation functions and power spectra. This discussion considers a more practical aspect, the simplicity of evaluating EEG signals using interval analysis. The method, as originally applied by Saltzberg et al. (52) and Burch et al. (53), has been shown to be useful primarily in quantifying EEG changes induced by psychoactive drugs (54–57), monitoring long-term EEG changes during anesthesia (58,59), psychiatry (60), and sleep research (see Ref. 35).

When using interval analysis, it is good practice to compute not only the zero crossings of the original EEG signal, but also those of the signal's first and second derivatives, to obtain more information about the spectral properties of the signal. One disadvantage of this method is sensitivity to high-frequency noise in the estimation of zero crossings. This problem can be avoided by introducing hysteresis, that is, by creating a dead band (e.g., between $+a$ and $-a$ μV) so that no zero crossing can be detected when the signal has an amplitude between those limits. In this way, Pronk et al. (58) have found that a dead band between $+3$ and -3 μV is a good practical choice. Another disadvantage is that, when examining histograms of zero-crossing counts, it is easy to underestimate the contribution of low-frequency components, of which there may be very few, and to overestimate fast frequency components. These disadvantages are particularly evident when zero-crossing histograms and power spectra of the same signal are compared as shown in Figure 54.6 (61). Sometimes corrections are made to enhance the number of long intervals in relation to the short ones, but this may complicate the interpretations even more.

Another approach is to compute zero-crossing intervals only within determined frequency bands; this may solve the problem of missing superimposed waves (62,63).

The main advantage of zero-crossing analysis is ease of computation, which makes this method particularly attractive for

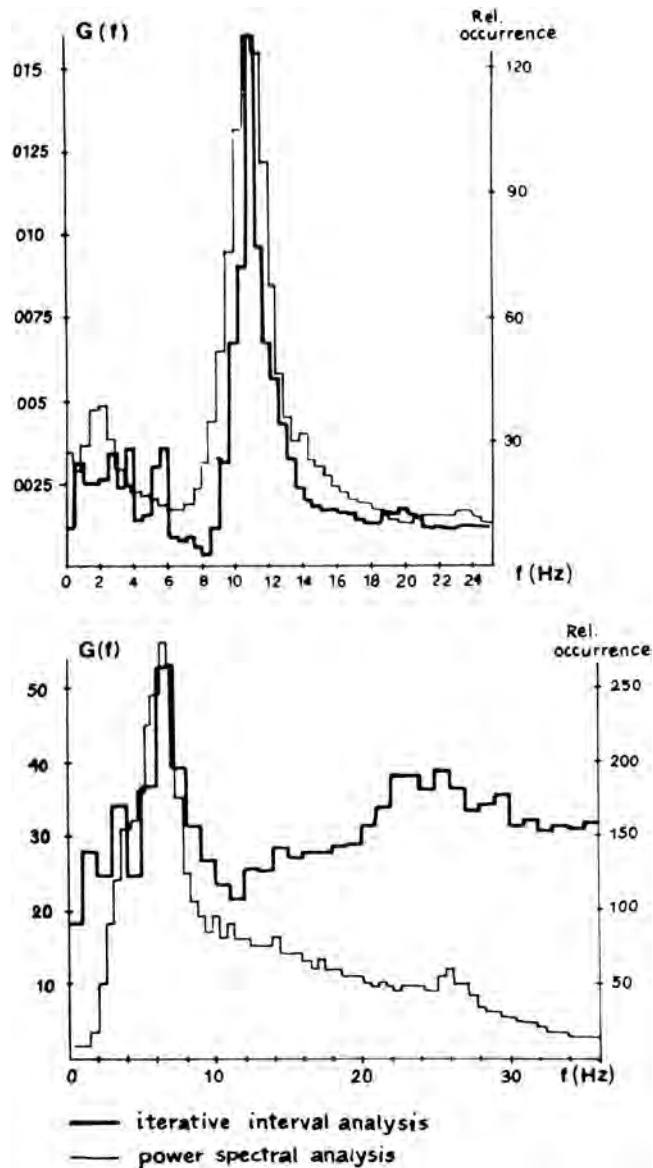


Figure 54.6 Two examples for comparison of iterative interval analysis and power spectra of the same EEG signals. The intervals are plotted as inverse frequencies. The agreement is fairly good in the case presented above; a pronounced rhythmic component (peak at about 11 Hz) is present. However, in the plot below, the interval analysis emphasizes in a marked way the high-frequency components. (Adapted from Matejcek M, Schenk GK. Die iterative Intervall-Analyse—Ein methodischer Beitrag zur Quantitativen Beschreibung des Elektroenzephalogramms in Zeitbereich. In: Schenk GK, ed. *Die Quantifizierung des Elektroenzephalogramms*. Konstanz: AEG Telefunken; 1973:293–306.)

the online quantification of very long EEG records, for example, during sleep or intensive monitoring. To perform interval analysis, it is useful to combine it with prefiltering (31) in the analysis of narrow-band signals.

Interval–Amplitude Analysis

Interval–amplitude analysis is the method by which the EEG is decomposed in waves or half-waves, defined both in time, by

the interval between zero crossings, and in amplitude by the peak-to-trough amplitudes. This hybrid method had been proposed repeatedly in the past by Marko and Petsche (64), Leader et al. (65), Legewie and Probst (62), and Pfurtscheller and Koch (66); it has been applied intensively in a clinical setting by Harner (67) and Harner and Ostergren (68). The latter called this method “sequential analysis” because the amplitude and interval duration of successive half-waves are analyzed, displayed, and stored in sequence in real time. The method used by these authors requires that the sampling rate be at least 250/sec, the zero level be updated continuously by estimating the running mean zero level, and, as just discussed, there be a dead band to avoid the influence of high-frequency noise. The high-frequency sampling is desirable in order to obtain a relatively accurate estimate of the peaks and troughs. The amplitude and the interval duration of a *half-wave* are defined by the peak–trough differences in amplitude and time; the amplitude and the interval duration of a *wave* are defined by the mean amplitude and the sum of the interval durations of two consecutive half-waves. These data are displayed in a scatter diagram as illustrated in Figure 54.7.

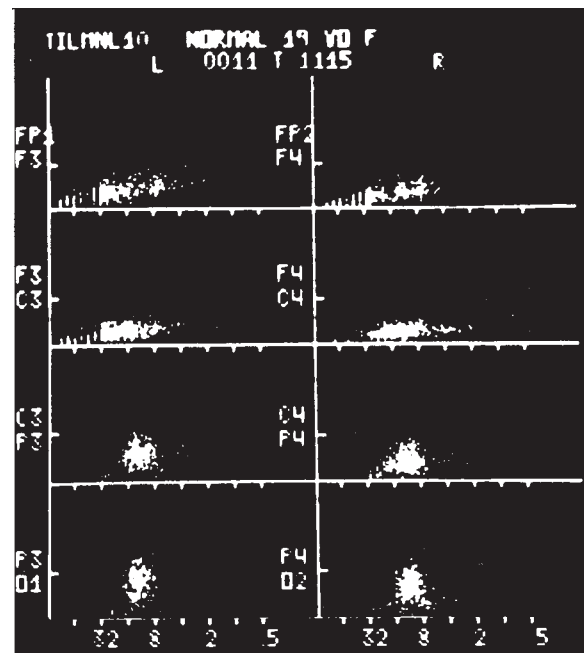


Figure 54.7 A display of sequential analysis obtained in real time. The *dots* represent individual half-waves displayed within 2 msec of their occurrence in each of the eight channels. The distribution of *dots*, for example, in the 8- to 16-Hz range (frequency equivalents of wavelength are used) gives an indication in amplitude and frequency of the alpha rhythm. Side-by-side comparison of homologous areas allows assessment of symmetry. Marking in y-axis indicates 50 μV . (Illustration courtesy of R.N. Harner; also in Lopes da Silva FH, Cooper R, Dumermuth G, et al. Sampling, conversion, and measurement of bioelectrical phenomena. In: Remond A, ed-in-chief; Brazier MA, ed. *Handbook of Electroencephalography and Clinical Neurophysiology*. Vol 4. Part A. Amsterdam: Elsevier; 1976.)

Correlation Analysis

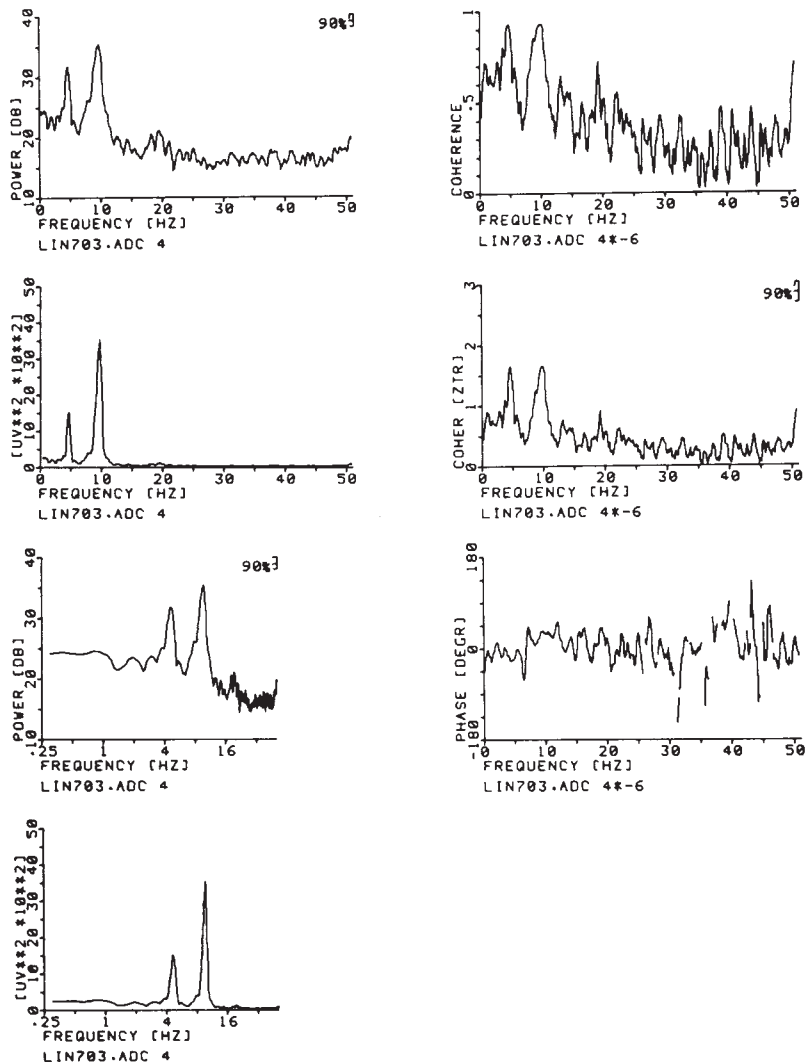
In practical terms, the computation of correlation functions in the 1950s and 1960s constituted the forerunner of contemporary spectral analysis of EEG signals (25,69,70) and provided an impetus to implement EEG quantification in practice. However, the computations were time-consuming and therefore not widely used. A simplified form of correlator was introduced, based on the fact that auto- or cross-correlation functions can be approximated by replacing the signals $\underline{x}(t)$ and $\underline{x}(t + \tau)$ (see equation 54.4) by their signs ($\text{sign } x(t)$ and $\text{sign } x(t + \tau)$), where $\text{sign } x(t) = +1$ for $x(t) > 0$ and $\text{sign } x(t) = -1$ for $x(t) \leq 0$, as demonstrated by McFadden (71). The function thus defined is called the polarity coincidence correlation function, and it has proved useful in EEG analysis (72–74). Another simplified form of EEG analysis that is akin to correlation has been used by Kamp et al. (75) and Lesèvre and Remond (76). It can be called autoaveraging and consists of making pulses at a certain phase of the EEG (e.g., zero crossing, peak, or trough) that are then used to trigger a device that averages the same signal (autoaveraging) or another signal (cross-averaging). In this way, rhythmic EEG phenomena can be detected and some characteristic measures obtained.

However, correlation analysis has lost much of its attractiveness for EEG analysts since the advent of FT computation of power spectra. The latter technique is less time-consuming and therefore more economical, and, in general terms, more powerful. Above all, it is difficult to determine from an autocorrelation function EEG components when the signals contain more than one dominant rhythm, an investigation that can be done simply by using the power spectrum (Fig. 54.8). Nevertheless, it should be noted that the simplified methods of correlation analysis just described and used in the 1960s can still have practical value in simple problems, such as computing an alpha average.

The computation of autocorrelation functions has been revived due to the introduction of such parametric analysis methods as the autoregressive model, which, as described below, implies the computation of such functions. Michael and Houchin (77) have even proposed a method of segmenting EEG signals based on the autocorrelation function.

Related to correlation functions is the method of *complex demodulation* (78). With this method, a particular frequency component (e.g., ~10 Hz) can be detected and followed as a function of time. In this case, a priori knowledge of the component to be

Figure 54.8 Left-hand column: Different ways of plotting the spectrum of the same EEG epoch, the bicoherence of which is shown in Figure 54.4. First plot: y-axis, power in dB, and x-axis, frequency (Hz) along a linear scale; the 90% confidence band of the spectral estimate is indicated. Second plot: y-axis, power in $\mu V^2/Hz$, and x-axis as above. Third plot: y-axis, power in dB, and x-axis, frequency (Hz) logarithmic scale (this way emphasizes somewhat the low-frequency components). Fourth plot: y-axis, power in $\mu V^2/Hz$, and x-axis, frequency (Hz) along a logarithmic scale. **Right-hand column:** First plot: squared coherence (Coh or (γ^2)) between two symmetric EEG signals; the power of one is shown in the plots on the left side. Second plot: the same function as above; along the vertical axis the z transformed coherence is plotted, $z = (1/2)\ln((1 + \gamma)/(1 - \gamma))$; the advantage of this form of presentation lies in the fact that, in this case, the confidence bands are the same for the whole curve and are not dependent on the value of γ . Third plot: phase spectrum corresponding to the coherence spectrum shown above.



Copyright © 2010. Wolters Kluwer Health. All rights reserved.

analyzed is necessary. Assuming, thus, that in an EEG signal a component at about 10 Hz exists and should be followed, one can set an “analysis oscillator” at 10 Hz; the oscillator output and the signal are then multiplied. The product contains components at the sum frequency (~20 Hz) and at the difference frequency (~0 Hz). This product is smoothed so that only the difference components (at about 0 Hz) are considered. In this way, phase and amplitude of EEG frequency components can be detected and their modulation in time determined. Complex demodulation has been used to analyze rhythmic components of visual potentials (79) and sleep spindles (80). This method is similar to a direct Fourier analysis in which an EEG signal is multiplied by sines and cosines at a particular frequency in the study of evoked potentials (81) and also the method of phase-locked loop analysis as used to detect sleep spindles (82,83).

Power Spectra Analysis

A classical way of describing an EEG signal is in terms of frequency as established by the common EEG frequency bands. It is possible to obtain information on the frequency components of EEG signals using interval or period analysis. However, the most appropriate methods in this respect are analog filtering or Fourier analysis, using either expression 54.9 (i.e., the FT of the autocorrelation function) or expressions 54.12 and 54.13 (i.e., the periodogram). Several forms of analog filtering were introduced in the early days of EEG research; that technique reached a technical level appropriate for clinical application mainly due to the work of Walter (22,23). Even in the 1960s banks of active analog filters were used to decompose EEG signals into frequency components (84–87). In 1975, Matousek and collaborators compared analog and digital techniques of EEG spectral analysis and demonstrated clearly the superiority of digital techniques. Digital methods are more accurate and flexible; using digital computers simplifies multichannel analysis.

The crucial landmarks in the development of EEG quantification methods have always followed technical advances: first, banks of active analog filters as just described; second, large digital computers (88,89); and third, a fast algorithm for digital computation of discrete FTs, Cooley and Tukey’s (27) so-called FFT. The latter has since been used extensively in EEG analysis (review in Ref. (90)).

This chapter cannot discuss the technical aspects of applying FFT spectral analysis to EEG quantification; for these aspects, the reader is referred to Matousek et al. (35), Dumermuth (90), and the books of Jenkins and Watts (14), Otnes and Enochson (17), and Gevins and Remond (37). It is sufficient to state here that, when planning to perform FFT spectral analysis, the electroencephalographer should consider the basic issues described in the following sections.

Digitization and Prefiltering

Digitization and prefiltering were discussed in relation to the sampling process. It is necessary to define beforehand the frequency range over which the spectrum should be computed, not only to avoid aliasing, but also to minimize computation time.

Length

The length of the epoch T to be analyzed must be selected. It is important to take into account that the epoch should be short enough to avoid nonstationarity segments but long enough to obtain the desired level of frequency resolution f ; the maximum Δf is, of course, $\Delta f = 1/T$. In many clinical applications one uses $T = 5$ or 10 seconds.

Frequency Smoothing and Ensemble Averaging

The estimate of one frequency point of a periodogram $F_{xx}(f_1)$ of one EEG epoch has a chi-square distribution with only 2 degrees of freedom. The number of degrees of freedom must be increased and the estimate variance reduced either by averaging for a number of equivalent epochs or by smoothing over adjacent frequency components. Sometimes both ensemble averaging and frequency smoothing are used. Generally, the spectral estimate $P_{xx}(f_1)$ (equation 54.13) should correspond to at least 60 degrees of freedom (91), which allows acceptable estimates of spectral values. This implies that an ensemble of at least 30 epochs should be used if only ensemble averaging is carried out. The number of degrees of freedom can also be increased, at the expense of frequency resolution Δf , by using a spectral window $W(f_k)$ (see equation 54.13). A spectral window is defined by its form and duration. The duration at the base is given by the distance between truncation points. Using a window with a large base reduces the variance but increases the bias of the estimator. An excessively large window decreases too greatly the equivalent frequency resolution Δf . In practice, therefore, a complex compromise between all the aforementioned points must be reached. Details about the technicalities of choosing the appropriate form $W(f_k)$ can be found in Jenkins and Watts (14) and Künkel and EEG Project Group (92). A good deal of freedom in the choice of the spectral window is tolerable; the appropriate choice depends on the practical use of spectral analysis. In EEG quantification in the clinical routine, it is common to compute average spectra by making averages of ensembles of 10 epochs of 10 seconds ($N = 1024$) each, using an elliptic window five sample points wide for smoothing; the equivalent bandwidth is thus 0.5 Hz. The resulting estimate corresponds, therefore, to less than 100 (more precisely, 93) degrees of freedom, owing to the fact that for each frequency component the power estimate is based on 2 degrees of freedom; this number must be multiplied by 10 (epochs), by 5 (window width), and by a factor 0.93 that corresponds to the fact that the window is elliptic.

Calibration

The dimension of power spectra in EEG analysis is intensity per bandwidth; the unit of measurement is in V^2/Hz (93). Calibration can be carried out using sine waves, as proposed by Abraham et al. (94), Clusin et al. (95), Dumermuth and Flühler (96), and Matousek et al. (35); Sciarretta G, Erculiani P (97) proposed a simple method, using a single rectangular pulse, that has practical advantages.

Graphic Representation

The graphic representation of power spectra merits special attention. In most instances, the EEG analyst needs a *plot* of power spectra, as shown in Figure 54.8. In most cases, the

vertical scale is simply the spectral density as computed by way of the Fourier coefficients (i.e., in $\mu V^2/Hz$). A preferred alternative is plotting the spectral intensity along a logarithmic scale. The advantage of choosing log power intensity instead of simply power intensity is that the confidence intervals of the former are independent of the values of the spectral intensity. Another technique involves computing the square root of the spectral intensity and plotting it along the vertical axis. Frequency is usually presented along a linear scale calibrated in hertz; however, one may prefer, if the most attention is to be paid to the lower frequencies (delta and theta), to compress the frequency scale in the higher frequency range by plotting log Hz (Fig. 54.8) along the horizontal axis or a more compressed scale for frequencies higher than, for instance, 15 Hz. The presentation of a power spectrum plotting log spectral intensity vertically and frequency horizontally, and where the higher frequency components are plotted in a more compressed way than the lower ones, is useful in routine clinical situations.

Time-Varying Spectra

Time-varying spectra are often computed in order to analyze more or less slowly changing EEG records. Such spectra can be plotted simply by using the so-called compressed spectra array (Fig. 54.9) as introduced by Bickford et al. (98,99). This method is particularly valuable in obtaining an overall view of EEG spectral changes for intraoperative or sleep monitoring (100). Another form of plotting time-varying power spectra is by using contour plots (i.e., plots of frequency against time), as shown in Figure 54.10; in such plots, points corresponding to equal values of power spectra computed from successive epochs are connected by contour lines. These plots provide useful, easily interpretable visual displays of the evolution of power spectra as a function of time.

The computation of time-varying power spectra is particularly important in those studies in which the problem is that

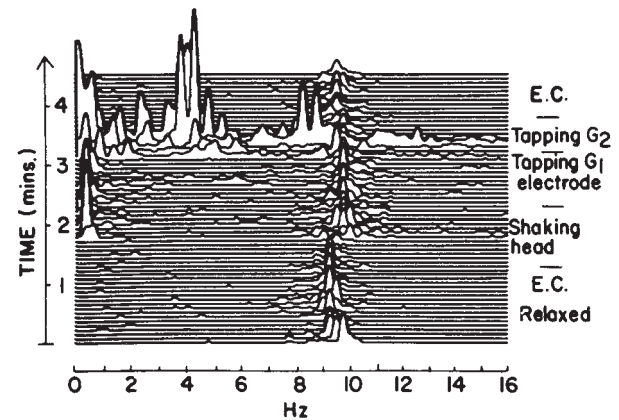
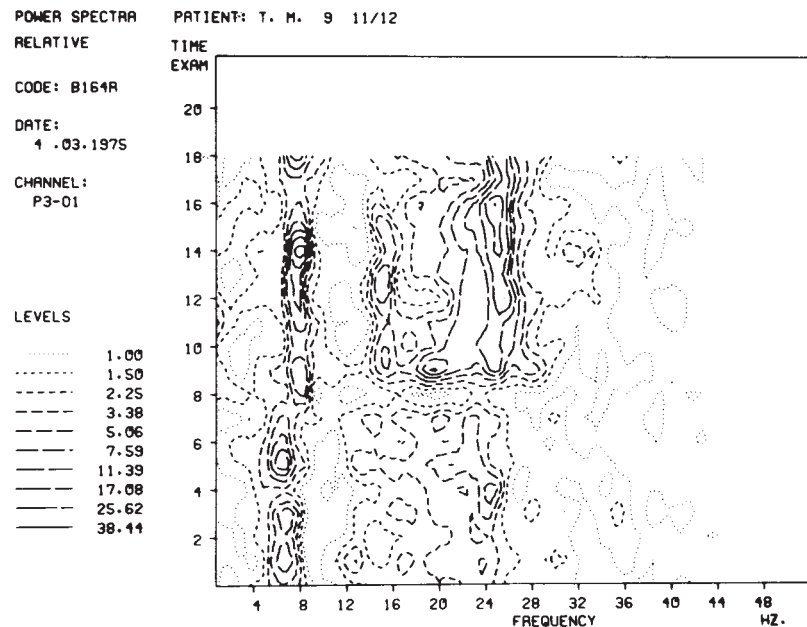


Figure 54.9 Display of a compressed spectral array showing the alpha rhythm and the effects of various artifact-inducing maneuvers on the background activity. Note the change in alpha peak frequency from the eyes-closed situation when shaking occurs. Note also the influence of artifacts in the spectra, particularly at tapping the electrodes; the large peaks at low frequencies are artifactual. (Adapted from Bickford RG. Computer analysis of background activity. In: Remond A, ed. *EEG Informatics. A Didactic Review of Methods and Applications of EEG Data Processing*. Amsterdam: Elsevier; 1977:215–232.)

of characterizing EEG changes in relation to specific events, such as eyes closing/opening (101), fists closing/opening (102), word association tests (103), and similar events. The problem here is to quantify time-locked changes in EEG spectra by way of ensemble averaging, using a particular event as a trigger. Kawabata (101) considered this problem analytically and proposed a formalism to compute time-varying EEG spectra. Using this construct, he could show that initially at eye closure, power within the alpha band increases, with the greatest concentration in the center

Figure 54.10 Contour plot of power spectra: note the frequency shifts and increase in power intensity occurring in the second part of the registration. (Adapted from Dumermuth G. Fundamentals of spectral analysis in electroencephalography. In: Remond A, ed. *EEG Informatics. A Didactic Review of Methods and Applications of EEG Data Processing*. Amsterdam: Elsevier; 1977:83–105.)



frequency; later the center frequency shifts to a lower frequency. When the eyes open, the alpha power decreases and the center frequency increases.

Pfurtscheller and Aranibar (102) designed a method for analyzing EEG changes related to sets of stimuli such as those used to study the phenomenon of contingent negative variation (CNV). According to this method, the 6-second EEG epoch occurring before and after the event of interest is subdivided into 1-second overlapping segments. For each segment, a power spectrum is computed; in the experiment quoted above, the total power (0 to 32 Hz) and the power in the alpha frequency range (7 to 13 Hz) of each segment are averaged over a number of equivalent segments, and mean values and standard errors calculated. In this manner, these authors demonstrated phasic decreases of power in the alpha band related to sensory stimulation and to the interstimulus interval in a CNV paradigm. Pfurtscheller and Aranibar (104) used the same method to study changes in central mu rhythms occurring in relation to opening and closing the fists in normal subjects and patients (Fig. 54.11). A large number of studies where dynamical changes of the ongoing EEG, within different frequency components, were detected and characterized have been revised by Pfurtscheller et al. (105).

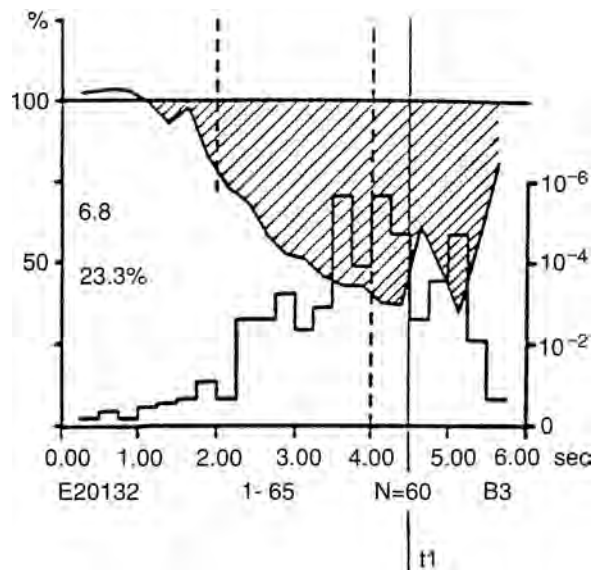


Figure 54.11 Alpha power time course over a 6-second interval calculated during voluntary hand movement (movement onset at 4 seconds). The scale on the left gives the percentage alpha power. Reference interval 0 to 2 seconds with an absolute reference power of $6.8 \mu\text{V}^2$ corresponding to 100% (this reference power corresponds to 23.8% of the total power within the frequency band 0 to 32 Hz). The significance levels for the power decrease (event-related desynchronization [ERD]) are indicated on the right scale (10^{-2} corresponds to $P < 0.01$, etc., sign test). Note that a decrease of alpha power is indicative for ERD. (Adapted from Pfurtscheller G, Klimesch W. Functional topography during a visuo-verbal judgment task studied with event-related desynchronization mapping. *J Clin Neurophysiol.* 1992;9:120-131.)

The fact that EEG baseline values (i.e., pre-event segments) can change from trial to trial makes a statistical analysis based on ensemble averages and standard deviations particularly difficult. Kamp and Vliegenthart (103) proposed resolving this type of difficulty by analyzing EEG epochs immediately before and immediately after the event causing the change. In this way a pre-event epoch of, for instance, 4 seconds and a postevent epoch of, for instance, 4 seconds are analyzed. A relatively large number of trials are recorded, and the degree to which the spectral value within a certain frequency band for each postevent subsegment (e.g., 1-second long) differs from the pre-event epoch evaluated using a nonparametric test (Mann-Whitney test) (106). The end result is given as the number of trials in which a certain frequency band changed significantly at a particular postevent segment. A similar method has been used by Arnolds et al. (107), who compared spectral parameters of EEG segments occurring after a behavioral event with pre-event values of the same parameter simply by using the sign test (106). The advantages of using this type of nonparametric method should be emphasized. Because the baseline values may vary dramatically, one runs the risk of failing to detect real EEG changes related to a particular event that exist if one compares only mean values. Directly comparing within each trial the baseline with the postevent values, particularly by means of a nonparametric statistical test, avoids the difficulty pointed out above.

Statistical Evaluation

Statistical evaluation of spectra is not done only in the analysis of time averaging EEG signals as discussed previously. Frequently, it is helpful to determine whether or not two sets of EEG power spectra differ significantly. The sets might have been obtained under two different behavioral conditions or during administration of two different treatments (e.g., a placebo or a psychotropic drug); they could have been recorded from symmetric derivations over the scalp. The question is a simple one. Given two sets of power spectra, how can one determine whether they belong to the same population? The answer, however, is not so simple. To start with, it is necessary to emphasize that the power spectrum of a certain EEG epoch is an estimate; thus, it also has a variance. A convenient way of presenting estimate variability is to present the corresponding confidence bands simultaneously with the average power spectrum as indicated previously. The question of testing whether the two sets of spectra belong to the same population has been approached using a variety of methods (for references see Ref. 49). Often analysis of variance (F test) and Student t test are applied (108). The F test in principle should be the first test chosen, because power density is a quadratic function. If the number of degrees of freedom increases, the power density distribution tends to normalize so that a t test can be applied.

In general, it is advisable to apply to the power spectrum a logarithmic transformation, because it produces a symmetric distribution. Confidence intervals for $\log P_{xx}(f)$ are given approximately as (35) $\log P_{xx}(f) \neq Z_{\alpha/2}(\sqrt{2/N})$, where $Z_{\alpha/2}$ is the 100 alpha/2 percentage point of the standardized normal distribution and N is the equivalent number of degrees of

freedom (16). Nevertheless, in many applications, especially if the number of degrees of freedom is small, it is preferable to apply nonparametric tests, such as the simple sign test or the more powerful Wilcoxon or Mann–Whitney tests. For a detailed analysis of the questions of statistical inference on EEG data, the reader is referred to Gasser (7,109). This problem has been discussed in detail in relation to those psychopharmacologic investigations in which EEG plays a central role (56,57,60,110), but these aspects are too specialized to be considered here.

Cross-Spectral Analysis

Cross-spectral analysis is an important part of EEG spectral analysis because it allows quantification of the relationships between different EEG signals. The section “Basic Statistical Properties” mentioned the smoothed estimate of the *cross-power spectrum* $C_{xy}(f)$; this quantity is the product of the smoothed discrete FT of one signal and the complex conjugate of the other (see for details Ref. 14). $C_{xy}(f)$ is a complex quantity that therefore has a magnitude and phase:

$$C_{xy}(f) = |C_{xy}(f)| \cdot \exp[j\Phi_{xy}(f)] \quad (54.24)$$

where $j = \sqrt{-1}$. The function of frequency $\Phi_{xy}(f)$ is the *phase spectrum*. It is useful to define a normalized quantity, the *coherence function*, as follows:

$$\text{Coh}_{xy}(f) = \frac{|C_{xy}(f)|^2}{P_{xx}(f)P_{yy}(f)} \quad (54.25)$$

Examples of coherence and phase functions are shown in Figure 54.8. In EEG analysis these functions are computed after the application of cross-correlation functions, which was carried out in a way similar to the autocorrelation function as described previously (see for details Ref. 35). Coherence functions have been used in several investigations of the EEG signal generation and their relation to brain functions, including studies of hippocampal theta rhythms (89,111), on limbic structures in humans (112), on thalamic and cortical alpha rhythms (113), on sleep stages in humans (48), on EEG development in babies (91,114), and on the spatial and temporal structures of dynamical features of local EEG signals (115,116). The latter measured coherence functions between EEG signals recorded using electrodes with 5- to 10-mm spacing from epileptic patients, and found that in both the subdural surface samples and those from temporal lobe depth arrays, coherence declines with distance between electrodes of the pair, on the average quite severely in millimeters. This demonstrates that coherence fluctuations are quite local.

The recommended way to evaluate coherence functions statistically is to apply Fisher’s z transformation (14) as used by Lopes da Silva et al. (113) to analyze EEG signals. Thus, the confidence intervals and bias are dependent on the coherence values (Fig. 54.8).

The use of coherence functions in routine clinical EEG analysis has been rather limited thus far. In one system dedicated to this type of analysis, coherence functions have been

applied with good results (117). The important point is to define clearly which questions one wishes to answer through coherence functions application. In this context, the most relevant points are as follows.

Is it possible to differentiate spectral components with frequencies lying close to each other? For example, alpha and mu rhythms may be difficult to differentiate in plots of power spectra but are readily separated using coherence functions computed between symmetric transversal derivations because the former show large values of transversal coherences, whereas the latter have insignificant values (118).

Is it possible to detect the existence of bilateral synchronous frequency components? Such components may make relatively small contributions to power spectra, whereas they may give rise to large coherence values. Coherences also may be useful in determining the topographic relations of different EEG components.

The counterpart of coherence is the phase function (Fig. 54.8), which provides information on the time relationships between two EEG signals. An explanation of the use of the term *phase* is necessary here. *Phase* is used in the present context as a mathematical notion referring to the proportion of the period of a sine wave component of a signal as obtained through Fourier analysis. The existence of a phase difference between two EEG signals as obtained from the phase function can have different meanings. First, assume that the two signals were recorded from bipolar derivations and that some components, for example, between 0 and 3 Hz, show an inverted polarity (phase opposition, in EEG terms); in this case, the phase function computed from the cross-power spectrum between the two signals will show, for the 0- to 3-Hz components, a phase difference of 180° . In the second case, assuming that some components of the signal recorded from one derivation will be transmitted to the other derivation after a certain delay time Δt (in seconds) the phase difference $\Delta\Phi$ (in degrees) between the two signals will be linear with frequency in the range Δf (in Hz) corresponding to those components; in this case, the following relationship is valid:

$$\Delta t = \frac{\Delta\Phi}{360 \cdot \Delta f} \quad (54.26)$$

Until now, phase functions have been little used in routine clinical EEG practice, probably because phase measurements are generally difficult to interpret in terms of the two models just presented. This is because scalp EEG derivations are a complex representation of underlying cortical activity, so that the potentials recorded at a distance are not easily reduced to clear-cut biophysical processes at the cortical level. Nevertheless, Gotman’s (119) system of EEG analysis included phase function computation in order to detect phase opposition between the slow frequency components of different bipolar derivations. If the phase difference between the two signals is about 180° with a significant coherence between the two signals, one can conclude that a phase reversal exists. In Gotman’s system, the search for phase reversals is performed only in the presence of slow activity. Computing phase functions to determine time delays between EEG signals during epileptic seizures has also been proposed (120). The interpretation of these results,

however, poses a problem. A time delay between two signals can be concluded with certainty only if there is a linear relationship between phase and frequency within a certain frequency band; if the coherence between the two signals is significant over only a very narrow frequency band (around a peak), it may be impossible to define a best fit line to the phase function. In such a case, the result may be impossible to interpret definitively in terms of time delay. Instead of using the simple phase function, it may be recommended to use a weighted phase function, as proposed by Carter (121), in the sort of problems just discussed. A fundamental problem, however, is that very often the relations between EEG signals cannot be considered linear, so that the use of coherence is not justified. Alternative methods have been developed (122) in order to overcome this limitation.

Another approach to identifying the source of EEG seizure activity is use of a generalized form of coherence analysis, the so-called *spectral regression—amount of information analysis* introduced and first applied to EEG analysis by Gersch and Goddard (123). This method has been used not only to analyze seizures (124,125), but also to investigate the process underlying the generation of hippocampal theta rhythms (126) and thalamocortical alpha rhythms (127,128), the organization of infantile EEGs (129), and seizure activity in animals (130). This analytic method involves computing first the coherence between two EEG signals and then the partial coherence based on a third EEG signal. Computing partial coherences implies eliminating from each of the two EEG signals that part that can be regarded as being determined by or predictable on the basis of the third signal, which constitutes a form of regression analysis. If the initial coherence decreases significantly, one can conclude that the coherence between the two initially chosen signals is due to the effect of the third one. As indicated in the references cited earlier, it is possible to thus determine the pattern of interactions between a series of simultaneously recorded EEG signals and, eventually, to find the more likely source of a given EEG phenomenon (e.g., seizure or rhythmic activity).

Bispectra

Equation 54.16 defines the bispectrum. Although the power spectrum is sufficient to describe the statistical characteristics of signals generated by a stationary gaussian process, deviation of amplitude distribution from normality indicates the need to examine spectra of higher orders. This is particularly true for the spectrum corresponding to the second-order autocovariance function $R(\tau_1, \tau_2)$: the bispectrum $B_{xx}(f_1, f_2)$ can be estimated by smoothing the triple product $F_{xx}(f_1)F_{xx}^*(f_2)F_{xx}(f_1 + f_2)$, where $F_{xx}(f)$ represents the complex FT of the signal $x(t)$ and $F_{xx}^*(f)$ represents the complex conjugate (see for details Refs. 28 and 29). Moreover, the bicoherence of signal $x(t)$, which is the normalized bispectrum of $x(t)$, can be defined. (Do not confuse with coherence, which is the normalized magnitude of the cross-spectrum between two signals $\underline{x}(t)$ and $\underline{y}(t)$.) Until now, few studies have put bispectral computation to practical use. Nevertheless, the specific information yielded by bispectra about the relationship between harmonic frequency components in EEG signals can be valuable. For example, Dumermuth et al. (49) have shown that

some rhythmic EEG activities have a significant bispectrum; examples are the mu rhythm, which presents significant relations between harmonics of 10 Hz (5, 20, and 30 Hz), and the psychomotor variant, with relations between 6, 12, 18, and 24 Hz. Lopes da Silva and Storm van Leeuwen (131) found that alpha rhythms recorded from the cortex also may have a significant bispectrum with harmonic components at 10 and 20 Hz. Moreover, alpha rhythms recorded on the human scalp may also show a significant bispectrum; in a few studied cases (Fig. 54.4), the so-called alpha variant has been characterized by a significant relation between the dominant frequency at 10 Hz and the one-half subharmonic at 5 Hz. Under such circumstances, bispectrum computation disproves the alternative hypothesis that the two components at 10 and 5 Hz are independent of each other and thus that low-frequency components would correspond to abnormal occipital activity. Furthermore, bispectral analysis of some forms of visual evoked potentials (132) has permitted putting in evidence some essential properties of the visual system.

Walsh and Haar Transforms

Alternative ways of computing power spectra have been proposed. These include the Walsh and Haar transforms, which can improve computational speed (90). These alternative methods, however, have not yet proved to be of practical interest, particularly because the FFT already provides a satisfactory solution.

Hjorth Slope Descriptors The section “Basic Statistical Properties” defined the n th spectral moment of the power spectrum a_n (equation 54.17). Hjorth (30) and Berglund and Hjorth (133) have developed special hardware to compute in real time the spectral moments a_0 (equation 54.18), a_2 (equation 54.19), and a_4 (equation 54.20). In this way, the spectral moments are not invariant in time as described earlier; rather, spectral moments are allowed to vary as a function of time (i.e., the statistical properties of the signal can vary in time), meaning that this form of analysis can be applied to nonstationary signals.

Based on these quantities, Hjorth derived the following parameters, also called descriptors:

$$\begin{array}{ll} \text{Activity,} & A = a_0 \\ \text{Mobility,} & M = [(a_2/a_0)]^{1/2} \\ \text{Complexity,} & C = [(a_4/a_2)(a_2/a_0)]^{1/2} \end{array} \quad (54.27)$$

Note that $a_0 = \sigma_2$ (equation 54.18), that is, the variance of the signal; a_2 is the variance of the signal's first derivative as shown in equation 54.19; a_4 is the variance of the signal's second derivative (equation 54.20). It should be noted that Hjorth's descriptors give a valid description of an EEG signal only if the signals have a symmetric probability density function with only one maximum (134). This may be true for simple EEG generation models (135,136) but not in general practice. Nevertheless, the ease of computing Hjorth's descriptors makes them attractive in real-time EEG analysis. The required calculations involve the computation of time derivatives only.

It must be noted, however, that computing the descriptor complexity implies taking the ratio between the second and first derivatives, so that the possibility of introducing large errors is considerable. To avoid this, the signal bandwidth must be rather limited. In the author's opinion, Hjorth descriptors can be useful if the EEG patterns to be analyzed have a simple character, a probability density distribution with only one maximum, and change over time is rather gradual. It is, therefore, not surprising that Hjorth's descriptors have demonstrated value in monitoring time-varying EEG signals, for instance, during sleep (137). This method has also been used to quantify multichannel EEG recordings obtained under routing conditions (138).

PARAMETRIC METHODS

It is reasonable to argue that, in general terms, EEG signals may be analyzed by any suitable method regardless of precise knowledge of their biophysical origins. It may be asked, however, whether more appropriate methods of EEG analysis might be developed if more precise models of the biophysical processes underlying the generation of EEG phenomena (e.g., alpha rhythms, delta waves, spike and wave complexes, and so on) were available. In the particular case of alpha rhythm generation, there exist biophysical models that can help in formulating a reply to such questions (136,139,140). These alpha rhythm models have indicated that an EEG with a dominant rhythmic component in the alpha frequency range can be described by a filter network with parameters related to physiologically acceptable variables submitted to a noise input. This filter network can be analyzed in a first approximation as a linear processor. This processor can be realized in terms of a mathematical model. A special case of this model is the mixed autoregressive model as described by Zetterberg (141) and the autoregressive model used by Gersch (142), Fenwick et al. (143), and Bohlin (144). Such methods are called parametric, because in such cases the EEG signals are described in terms of a mathematical model characterized by a set of parameters.

A link may be said to exist between this type of mathematical model and the biophysical model of alpha rhythm generation, but this link is neither specific nor essential. The use of such mathematical models in EEG analysis is yet to be justified through pragmatic arguments. These models provide a practically useful method for quantifying EEG signals, not only in order to compute spectra (142–150), but also to detect EEG transient nonstationarities such as epileptiform spikes and sharp waves (146,151) and to subdivide the EEG into quasi-stationary segments (152,153). Parametric methods allow considerable EEG data reduction. For instance, using an autoregressive model, it is possible to describe an EEG signal using a few coefficients; by following the values of these coefficients, the signal's time-varying properties can be traced. The coefficients can be used to classify EEG spectra using, for instance, cluster analysis; moreover, the model can also be used to help detect nonstationary events. The basic model can be described following the scheme of Figure 54.12, as proposed by Zetterberg (31). In this figure, two cases are shown: the contin-

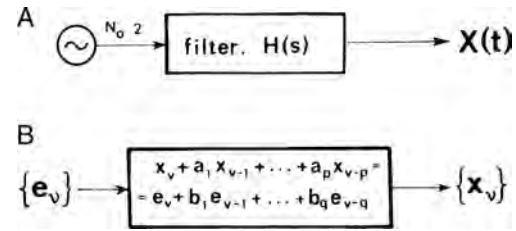


Figure 54.12 Block scheme. **A:** The filtering process on a time continuous signal. **B:** The autoregressive moving average filter model applied to a time discrete signal. (Adapted from Zetterberg LH. Means and methods for processing of physiological signals with emphasis on EEG analysis. In: Lawrence JH, et al. *Advances in Biology and Medical Physics*. Vol 16. New York, NY: Academic Press; 1977:41–91.)

uous case and the discrete case. According to the continuous case, the EEG signal $x(t)$ is assumed to result from the operation of filtering (with a filter having as transfer function $H(s)$) on a noise source with a flat spectrum within the frequency range of interest. In the discrete case, the EEG signal is given as a set of samples $x(k)$ resulting from a filter operation on an input noise signal $e(k)$ with zero mean. The filter, corresponding to the autoregressive moving average (ARMA) model, is described by a linear difference equation of the following form:

$$a_0 x(k) + a_1 x(k-1) + \dots + a_p x(k-p) = b_0 e(k) + b_1 e(k-1) + \dots + b_q e(k-q) \quad (54.28)$$

where $q \leq p$. The relation between $x(k)$ and $e(k)$ is given by the sets of coefficients a_1, \dots, a_p and b_1, \dots, b_q with $a_0 = 1$. In case $b_i = 0$ for $i = 1, \dots, q$, we are left with the so-called autoregressive (AR) model:

$$x(k) + a_1 x(k-1) + \dots + a_p x(k-p) = e(k) \quad (54.29)$$

The computation problem, therefore, is to estimate the coefficients. An important step in this estimation is defining the minimum number of coefficients to be computed.

Fast algorithms exist to enable computation of those coefficients; they are described in detail by Zetterberg (31), Makhoul (154), and Eykhoff (155) among others, and employ several criteria for estimating the order of the model. Using Durbin's algorithm, it was found in a group of EEG recordings of epileptic patients that the minimal order of the model was, in about 70% of the cases, equal to or smaller than 5 (156). However, when one wishes a faithful reproduction of the power spectral density, many coefficients may be needed (31). In most applications it is sufficient to compute the AR model of the EEG signal, so this section need not consider the special problems regarding ARMA model computation.

Computation of Power Spectra

The computation of power spectra using an AR or ARMA model presents no special difficulties. Using a special algorithm (spectral parameter analysis [SPA]) developed at Zetterberg's

(31) laboratory, both an estimation of the model parameters and the best spectral representation can be obtained. In the case of the ARMA model (equation 54.28) spectral density of a signal sampled with sampling interval is given by:

$$P_{xx}(f) = \sigma^2 \frac{\left| \sum_{i=0}^q b_i (\exp(-j2\pi f_i \Delta t)) \right|^2}{\left| \sum_{i=0}^p a_i (\exp(-j2\pi f_i \Delta t)) \right|^2} \quad (54.30)$$

In case of the AR model, the spectral density is as follows:

$$P_{xx}(f) = \frac{\sigma^2}{\left| \sum_{i=0}^p a_i \exp(-j2\pi f_i \Delta t) \right|^2} \quad (54.31)$$

In both cases described, spectral density is estimated using the sets of coefficients. In Zetterberg's original computational procedure, the SPA, the EEG analysis is based on the ARMA model (31). In this form of analysis, Zetterberg not only computes the EEG power spectrum, but also decomposes the spectrum into a number of components to achieve a degree of data reduction; he usually distinguishes three spectral components so that $P_{xx}(f)$ is written as the sum of three components (see also Fig. 54.3):

$$P_{xx}(f) = P_{\delta}(f) + P_{\alpha}(f) + P_{\beta}(f) \quad (54.32)$$

The delta (δ) component is described by a first-order model; both alpha (α) and beta (β) components require second-order models. The δ component is defined by a power parameter G_{δ} and a frequency parameter σ_{δ} , which denotes the corresponding bandwidth; G_{δ} is defined as:

$$G_{\delta} = \int_{-\infty}^{\infty} P_{\delta}(f) df \quad (54.33)$$

The rhythmic components (α and β) require two frequency parameters, the center or resonance frequency f_{α} or f_{β} , and two power parameters, G_{α} or G_{β} , defined as in equation 54.33. An example of the spectral decomposition of an EEG signal calculated in this way is shown in Figure 54.13.

Spectral analysis can be performed much faster with the AR than with the ARMA model. It is also easy to use this model to analyze multidimensional processes so that not only auto, but also cross-power spectra can be computed.

Inverse Autoregressive Filtering

The AR model can also be used in an inverted form, which leads to the *inverse autoregressive filtering* operation. Assuming that an EEG signal results from a stationary process, it is possible to approximate it as a filtered noise with a normal distribution. Consequently, passing such an EEG signal through the inverse of its estimated autoregressive filter should result in a normally distributed noise N with mean zero and variance σ^2 . The null hypothesis is that an EEG signal follows the assumption of stationarity and can be expressed in terms of the prop-

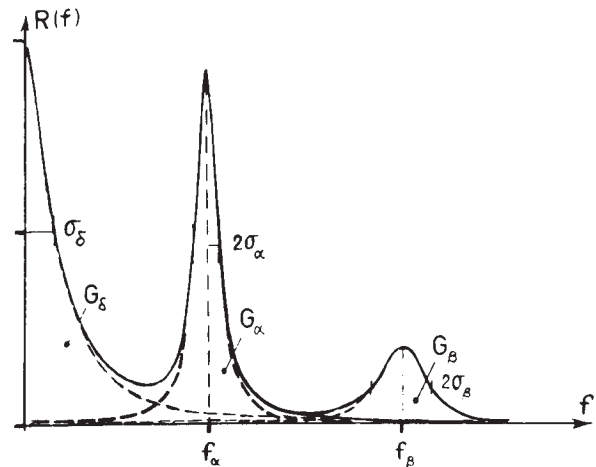


Figure 54.13 Power spectrum of an EEG signal analyzed with a fifth-order model. It consists of a low-frequency component (δ) and two resonance peaks (α and β); the components are described by the parameters G (power), σ (bandwidth), and f (peak frequency). *Dashed lines* denote the individual spectral components; the *solid line* indicates the total spectrum. (Adapted from Isaksson A, Wennberg A. Visual evaluation and computer analysis of the EEG—a comparison. *Electroencephalogr Clin Neurophysiol.* 1975;38:79–86.)

erties of the estimated noise, $\hat{\epsilon}(k)$, resulting from the inverse autoregressive filtering:

$$\hat{\epsilon}(k) = x_k + \sum_{i=1}^p a_i x(k-i) \quad (54.34)$$

The EEG signal is said to be nonstationary for $t = nT$ if the null hypothesis can be rejected (i.e., if $\hat{\epsilon}(k)$ deviates at a certain probability level from a noise with a normal distribution). Thus, nonstationarities in an EEG signal can be detected; this is particularly interesting in the detection of EEG transients of epileptic patients, as shown by Lopes da Silva et al. (146,157,158). A simple test on each sample of the estimated noise can give an indication of the stationarity of the signal at that moment. However, instead of testing $\hat{\epsilon}(k)$, a detection function $d(k)$ is used in order to obtain a certain degree of smoothing; $d(k)$ is defined as follows:

$$d(k) = \sum_{n=k-m}^{k+m} \left[\frac{\hat{\epsilon}(n)}{\hat{\sigma}} \right]^2 \quad (54.35)$$

Because the square of a normally distributed variable (with unity variance) follows a chi-squared distribution, the detection function should also have a chi-squared distribution with a number of degrees of freedom $(2m + 1)$. The null hypothesis can then be tested at a certain level, for example, at $p < 10^{-3}$. An application of this process of inverse filtering for the detection of transient nonstationarities (epileptiform events) in EEG is illustrated in Figure 54.14.

Time-Varying Signals: Kalman Filtering

Parametric models can be extended in order to analyze time-varying signals. A method of analyzing this type of EEG signal

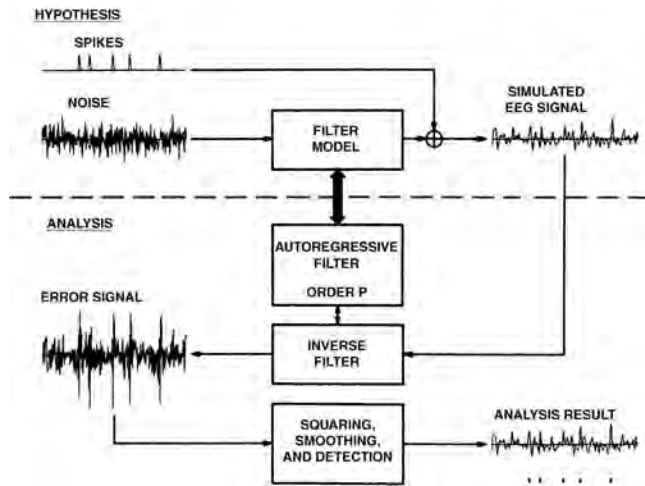


Figure 54.14 Scheme of the principle of automatic spike detection (ASD) analysis method using simulated signals. **Top:** The hypothesis is that the interictal EEG of an epileptic patient results from filtered noise to which spikes have been added. For simplification in this scheme, the spikes are not represented as being the output of a filtering process; this, however, would have been more realistic. **Bottom:** The analysis consists of computing an autoregressive filter model representing the hypothetical process, determining the corresponding inverse filter through which the EEG signal is passed, and squaring and smoothing the resulting error signal. The end result or detection signal is tested using the chi-square statistic; the time samples lying above a certain level are indicated by *thin lines* under the curve. Note that in this example the ASD program detected at the correct time samples the spikes that had been added to the filtered noise. (Adapted from Lopes da Silva FH, van Hulten K, Lommen JG, et al. Automatic detection and localization of epileptic foci. *Electroencephalogr Clin Neurophysiol.* 1977;43:1–13.)

consists of applying the so-called *Kalman estimation method* of tracking the parameters describing the signals (159–161). The input signal to a hypothetical processor responsible for generating the EEG signal is assumed to be a normally distributed noise $\epsilon(k)$. A model is assumed in order to represent the observed signal; the process dynamics are represented by an autoregressive model.

The main objective of this procedure is achieved by means of a recursive algorithm called the Kalman filter to obtain estimates of the model coefficients using earlier estimated data. This involves updating based on new samples of the time series (31). The Kalman filtering procedure is not simple to implement; for an appropriate procedure, it is necessary to choose, properly, the order of the model and the initial conditions. An application of this method in the subdivision of EEG signals (segmentation procedure) is described below. Without entering into the details of different procedures of Kalman filtering, it is of interest to note that a measure of EEG signal stationarity can be derived from the application of this method.

Isaksson (162) has introduced for EEG analysis an algorithm called SPARK, which stands for spectral parameter analysis, based on recursive Kalman filtering. He found that an AR model of order $p^* = p + q$ gave good results as an ARMA

model of order p with $q = p - 1$; a good choice appeared to be a value of $p^* = 11$ or 13.

Segmentation Analysis

The original purpose of segmentation analysis as introduced by Praetorius et al. (153) and Bodenstein and Praetorius (152) was to find in an EEG signal those segments that could be considered to have unvarying statistical properties.

This means that those segments should be considered as being quasi-stationary, and the segments could have variable length. This necessitated the development of criteria for establishing divisions between segments. These authors based their analysis on a parametric model of the EEG, an autoregressive model as defined by equation 54.29. Consult the aforementioned references for details. Duquesnoy (159) proposed an EEG segmentation method related to that just described. A problem in applying this analytic method is the difficulty of defining clinical–neurophysiologic boundaries between segments. Therefore, judgment of whether the method produces segments acceptable on clinical–neurophysiological grounds is rather subjective and depends strongly on personal criteria. Nevertheless, this method may be useful in reducing data in analyses of long EEG records recorded under variable behavioral conditions.

Michael and Houchin (77) proposed a similar method based simply on computing a running autocorrelation function, which ensures a quicker procedure. Barlow (163) used the method devised by Michael and Houchin (77) to compare the performance of automatic adaptive segmentation with those of selective analog filtering and inverse digital filtering in automatic evaluation of significant EEG changes associated with carotid clamping. Of the three methods, the former was clearly the best.

Adaptive segmentation was used to analyze a series of clinical EEGs showing a variety of normal and abnormal patterns (164); the computer method was used based on the autocorrelation function. By means of this algorithm, EEG segments were defined; similar segments were then clustered without supervision. The study concluded that minimal supervision of the clustering process may be necessary. Nevertheless, this adaptive segmentation method is useful for obtaining significant data reduction and has practical value for the clinical neurophysiologist. A review of methods for analyzing nonstationary EEGs has appeared (165).

MIMETIC ANALYSIS

This form of analysis has been developed mainly by Remond and collaborators (166–169) and is based on the general concept that automatic EEG analysis should mirror the visual analysis performed by electroencephalographers in their daily practice. This is why it has been called *mimetic analysis* (168). However, this analytic form uses tools common to other methods, particularly those nonparametric methods based on signal features characterized in the time domain, namely interval–amplitude analysis (68). The peculiar aspect of Remond’s mimetic analysis is that the whole procedure of

extracting EEG features and sets of features follows a syntactic approach: half-waves and minimal descriptors correspond to linguistic characters or letters, significant wave series such as K complexes and spindles to words, segments composed of wave series such as rhythms to paragraphs, and ensembles of segments to chapters or sections.

Based on these features it is possible to construct tables or graphs that demonstrate synoptically the distribution of the different features in an EEG epoch and determine their statistical properties for several epochs and derivations. A similar type of analysis has also been proposed by Schenk (170). These methods, which have as common background an iterative interval analysis, tend to emphasize the high-frequency components of the signal, compared directly to spectral analysis (see also Fig. 54.6) (171). The section “Interval Analysis” stressed the rather intimate relationship between interval analysis based on the signal and its derivatives and the spectral moments (see equation 54.22). Therefore, the methodology used by Remond and collaborators does not differ essentially from spectral analysis. The main difference is that mimetic analysis combines feature extraction with segmentation and logical classification.

MATCHED FILTERING OR TEMPLATE MATCHING

Matched filtering is a form of pattern analysis in which a certain pattern or template (i.e., a set of values in the EEG signal $x(t)$) is detected by using cross-correlation (equation 54.10) between $x(t)$ and a priori defined pattern $m(t)$. (For the sake of simplicity the underscore of the stochastic variable is omitted in the following.) As in equation 54.10, one may write:

$$s(t) = \int_0^\tau x(\tau - t)m(\tau)d\tau \tag{54.36}$$

The efficiency of the estimator $s(t)$ is defined as follows:

$$0 \leq \frac{[s(t)]^2}{\left[\int_{t-T}^t x^2 dt \right] \left[\int_0^T m^2 dt \right]} \leq 1 \tag{54.37}$$

The estimator reaches its maximum value (=1) when $m(t)$ is identical to $x(t)$ and when both signals are aligned perfectly along the time axis. In this case, the template $m(t)$ can best be extracted from the signal $x(t)$. Various algorithms can be used to complete this operation efficiently. Saltzberg and Burch (36), Herolf (172), Zetterberg (173), Lopes da Silva et al. (146), Barlow and Dubinsky (174), and Pfurtscheller and Fischer (175) have all suggested using matched filtering to help epileptiform events (Fig. 54.15).

TIME-FREQUENCY ANALYSIS

Above we have already mentioned that an important problem in EEG analysis is the fact that EEG signals, in general, can only be considered stationary during relatively short epochs. This has led to the development of several ways of analyzing such

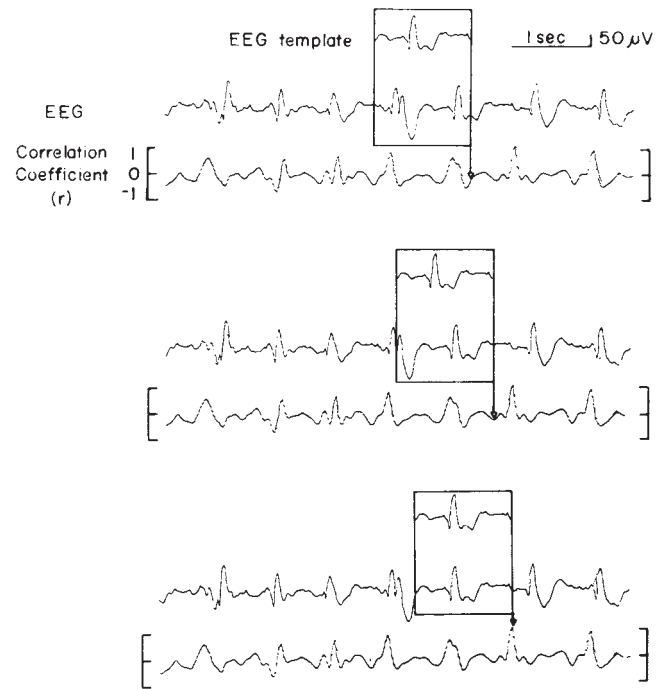


Figure 54.15 Continuous correlation coefficient write-out at three different points in time for an EEG signal and a template. In each record the *rectangle* indicates the time window for comparisons of template and EEG. In the first two instances there is no match, but in the third the template and EEG match exactly (they are identical); hence, the correlation coefficient reaches a peak at 1.0. Sampling rate, 50 Hz; number of points in template, 72; duration of template, 1.24 seconds. (Adapted from Barlow JS, Dubinsky J. Some computer approaches to continuous automatic clinical EEG monitoring. In: Kellaway, P, Petersén I, eds. *Quantitative Analytic Methods in Epilepsy*. New York, NY: Raven; 1976:309-327.)

EEG signals by way of time-varying spectra, namely in the form of spectral arrays, and by applying segmentation methods. A more recent development in this respect is the introduction of methods that can combine analysis both in time and in frequency in an optimal way. Some of these methods use a special class of basis functions, the so-called wavelets. A function can be accepted as a wavelet if it satisfies the following relation:

$$\int_{-\infty}^{\infty} \psi(t)dt = 1 \tag{54.38}$$

This means that wavelets have typically a waveform of a damped oscillation. The essential point of this method consists in decomposing the EEG signal in a set of wavelet functions defined as follows:

$$\psi_{s,u}(t) = \frac{1}{\sqrt{s}} \psi\left(\frac{t-u}{s}\right) \tag{54.39}$$

where s represents the time scale and u is the translation variable. Based on this definition a set of orthogonal wavelets can be constructed that forms an orthonormal basis. A given function, such as an EEG signal, may be characterized by the

corresponding wavelet coefficients. For a basic theoretical treatment of this issue, the reader is referred to Mallat (176). Wavelet analysis was applied to ongoing EEG signals (177,178) and to evoked potentials (179,180) with interesting results. The set of wavelets is limited. To represent nonstationary EEG signals, a wider repertoire of basis functions is desirable. With this aim in view, the method called matching pursuit was developed by Mallat and Zhang (181) and applied to the detection of transients in EEG signals by Durka and Blinowska (182). A large set of basis functions can be obtained by scaling, translating, and modulating a window function $g(t)$:

$$g(t) = \frac{1}{\sqrt{s}} g\left(\frac{t-u}{s}\right) e^{i\xi t} \quad (54.40)$$

where in the time domain the function is concentrated around u with a width proportional to s , and in the frequency domain its energy is concentrated around ξ with a spread proportional to $1/s$.

The minimal time–frequency variance corresponds to the condition that $g(t)$ is gaussian. By means of the matching pursuit algorithm, using a dictionary of such basic functions, a convenient expansion of a given signal can be obtained, as explained in detail by Mallat and Zhang (181) and by Durka and Blinowska (182). In practice, since EEG signals are available as real discrete time series, the basis function has the following form:

$$g_{(\gamma,\phi)}(n) = K_{(\gamma,\phi)} g_j(n-p) \cos\left(2\pi \frac{k}{N} n + \phi\right) \quad (54.41)$$

where the index $\gamma = (j, k, p)$ is the discrete analog of (ξ, s, u) of equation 54.40, $N = 2^L$ represents the number of samples, and

the parameters p and k are sampled at intervals 2^j . The procedure is iterative and it is stopped as the set of waveforms is able to explain a given amount of the signal's variance.

The corresponding results can be visualized by means of the so-called Wigner maps, an example of which is given in Figure 54.16 (183) for the analysis of an epoch of sleep EEG where the detection of different types of sleep spindles is put in evidence.

An alternative way to compute the time evolution of the frequency spectrum is to apply a windowed Fourier transform that gives information about gradual changes in frequency spectra in the course of time. It was shown that this method can be useful in the analysis of ictal activity (184).

EEG signals recorded from several derivations represent large data sets that may give related, or even redundant, information. Multivariate statistical methods can be useful in reducing such large data sets and in determining a small number of statistically independent components. Classically this has been accomplished by factor analysis or principal component analysis. Pioneering studies of Walter et al. (185) showed that alpha rhythms recorded from the posterior cerebral regions could be accounted for by two independent orthogonal components. It should be noted, however, that while these methods are useful in data reduction, they do not give information on the nature and location of physiologic generators of EEG signals (186). An alternative approach consists in applying independent component analysis (ICA), initially proposed by Bell and Sejnowski (187) and Makeig et al. (188–190). ICA is a method that can be used to separate a number of statistically independent signals, or sources, from an equal number of linear mixtures of these sources. The basic

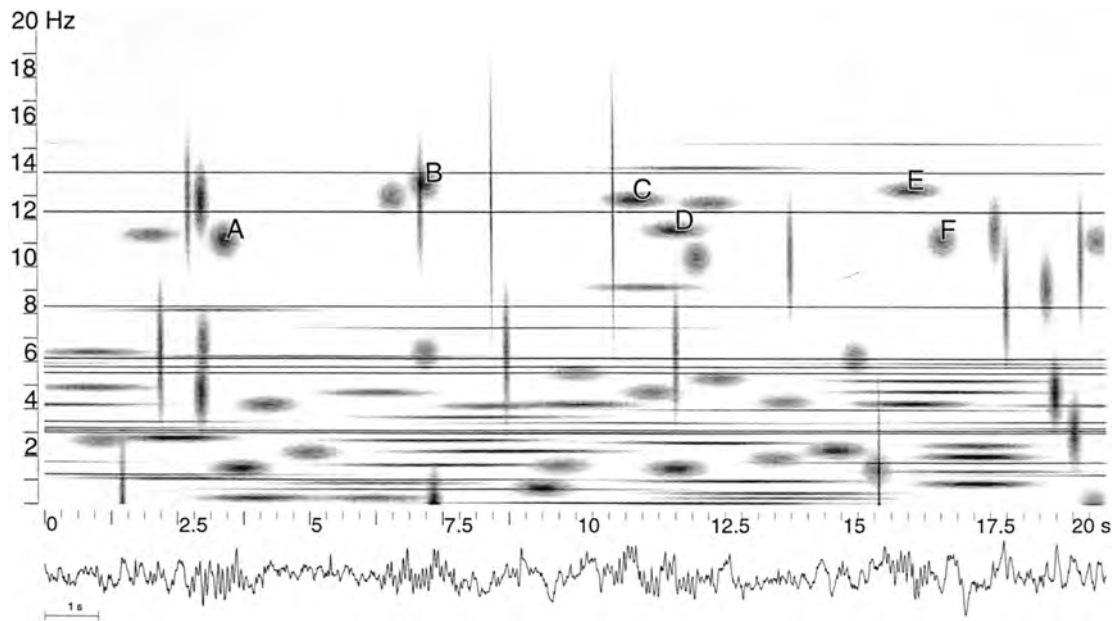


Figure 54.16 Wigner plot of the analysis of an EEG epoch of 20 seconds recorded during light sleep using a matching pursuit algorithm. Here the main objective was to detect sleep spindles automatically and to compare the results with those obtained by visual inspection by experts. The spindles automatically detected are indicated by the letters A to F. Spindles indicated by A and B were also detected by the experts. C, D, and E were classified by the experts as single spindles, but F was outside the section marked by the experts. (Adapted from Durka PJ. *Time Frequency Analyses of EEG* [PhD thesis]. Department of Physics, University of Warsaw; 1996.)

assumption is that EEG/MEG signals recorded at a given site at the level of the scalp result from the sum of the projected activities of a number of multiple brain sources, sometimes contaminated by extracerebral (artifacts) sources. ICA method aims at separating these sources in an optimal way. Mathematically the process of computing ICA consists of a simple transformation of one matrix (containing the sources) to another matrix (containing the mixtures or recorded signals) by multiplication with a mixing matrix. The inverse of the latter can be used to decompose the set of mixtures into the original sources. The problem is that one does not know, a priori, how the sources are combined, that is, the coefficients of the mixing matrix are not known. To estimate these coefficients by way of the ICA method, the set of independent components is estimated by finding the minima of their mutual information. In case this process is done successfully the independent components represent the original sources. It should be realized that the sources should be non-gaussian and that the number of sources should not exceed the number of mixtures. Anemüller et al. (191) presented a generalized method that considers the EEG sources as eliciting spatiotemporal activity patterns, corresponding, for example, to trajectories of active processes, propagating across the cortex. This led them to propose a model of convolutive signal superposition, in contrast to the commonly used instantaneous mixing model. In this way the sources of spatiotemporal dynamics of EEG signals recorded during a visual attention task could be identified. Further ICA has been applied to short-time Fourier transforms of EEG/MEG signals, in order to improve the identification of sources of rhythmic activity (192).

There are many kinds of algorithms to compute ICA. Klemm et al. (193) reported a comparative study of the performance of 22 algorithms, with the objective of applying them in EEG analysis. The results of this comparative study may help to select a task-specific algorithm to analyze a variety of EEG patterns.

A concern about the interpretation of the results of ICA is the question of how reliable the estimated components are. To answer this question Groppe et al. (194) presented a new algorithm for assessing the reliability of ICAs based on applying ICA separately to split-halves of a data set. These authors showed further that ICA reliability is enhanced by removing the mean EEG at each channel for each epoch of data rather than the mean EEG in a prestimulus baseline period.

With the advent of combined fMRI and EEG recording, it has been proposed to apply ICA to decompose EEG and fMRI signals in order to facilitate the integration of the two modalities. This opens interesting possibilities to obtain multimodal integrated images (195). An interesting field of application is in the field of epilepsy. In this respect Marques et al. (196) decomposed EEG signals using ICA and identified the relevant components' time courses to find the regions exhibiting fMRI signal changes related to interictal activity.

A problem that one is faced while interpreting correlations between EEG signals recorded from the scalp is the well-known smearing effect of the volume conductor currents. One method that may help to circumvent this difficulty is to use ICA as a preliminary step in the analysis. With this objective in view a novel methodology based on multivariate autoregressive (MVAR) mod-

eling and ICA was proposed by Gómez-Herrero et al. (197), to estimate the sources of alpha rhythms and their propagation in the brain. The application of this methodology to 20 subjects under resting conditions suggested that the major alpha generator process consists of a strong bidirectional feedback between thalamus and cuneus, while the precuneus appeared to participate also in the generation of the alpha rhythm, which is in accordance with results obtained using other methodologies (see Chapter 5).

SPATIOTEMPORAL DYNAMICAL ANALYSIS OF EEG: THE QUESTION OF PHASE RELATIONSHIPS, SYNCHRONIZATION, AND CAUSALITY

In the past editions of this book we present a historical overview of several aspects regarding methodological approaches applied to the issue of spatial analysis of EEG signals. These are now presented and discussed more extensively in Chapter 55. Here we focus on some general considerations with respect to the analysis of phase relationships between EEG/MEG signals recorded from different sites and the related concepts of phase locking and synchronization.

We must emphasize that the determination of phase relationships between EEG/MEG signals is of great interest to get insight into the dynamics of underlying brain processes. Two main conditions have to be fulfilled in order to estimate relevant phase relations. One is that spatial sampling is optimal for the phenomena of interest; another one is that the influence of volume currents is reduced to a minimum, as mentioned above. It should always be remembered that EEG phenomena with potential fields that have spatial frequencies higher than the spatial sampling frequency may give rise to important errors of interpretation (198).

Synchronization between EEG/MEG signals may be put in evidence in different ways. In EEG literature the terms synchronization and desynchronization are commonly used to refer to changes in power spectra of EEG activities in a given frequency band, such as desynchronization or synchronization of alpha rhythms with respect to a given event, and are expressed by the terms “*event-related desynchronization or ERD*,” and “*event-related synchronization or ERS*” (199). Implicit to this terminology is the assumption that when the activities of the neuronal elements in a population are not phase-locked to each other, the resulting amplitude—or power—in the EEG decreases (desynchronized state), and the reverse happens when the neuronal activities are highly phase-locked (synchronized state). These EEG phenomena are presented in Chapter 45, and thus will not be discussed further in this section.

Here we will focus on the notion of phase with respect to pairs, or multiple, EEG/MEG signals: this means *phase locking* at a distance, and not only locally within a circumscribed neuronal population. In particular, considerable attention has been given to EEG/MEG oscillations within the gamma frequency range occurring in-phase at a certain time, as possibly constituting a general mechanism of transient association between neuronal assemblies underlying sensory perception (200–202). This would constitute the substrate of the “binding” mechanism by

means of which the neuronal representation of different features of a complex sensory stimulus would be bound together to form a unified percept, a “gestalt.” This concept was also generalized to brain systems engaged in memory processing, as the (para)hippocampal system, where synchronized gamma oscillations in the entorhinal–hippocampal circuits may allow distributed neuronal populations to form functional assemblies necessary for the formation of memory traces (203).

The estimation of phase relationships is not trivial. Several algorithms are used in order to estimate phase synchrony. The method used by the Paris group (204) starts by choosing EEG/MEG epochs and applying a band-pass filter to select the frequency band of interest; thereafter, the instantaneous phase of

the filtered signals is computed by means of the Hilbert transform; finally the degree of phase synchrony, called phase-locking value (PLV) by these authors, is estimated by averaging the phase differences on the unit circle in the complex plane. In this way the phase can be displayed separately from the amplitude component for a given frequency range (201,205,206). Using this methodology it was shown, for example, that the scalp EEG/MEG of subjects performing the perceptive task of recognizing human faces induces a long-distance pattern of *phase synchronization* that represents active coupling of the underlying neural populations. This coupling appears to be necessary for the realization of this cognitive task (207). An example is shown in Figure 54.17, which illustrates how the perception of a human

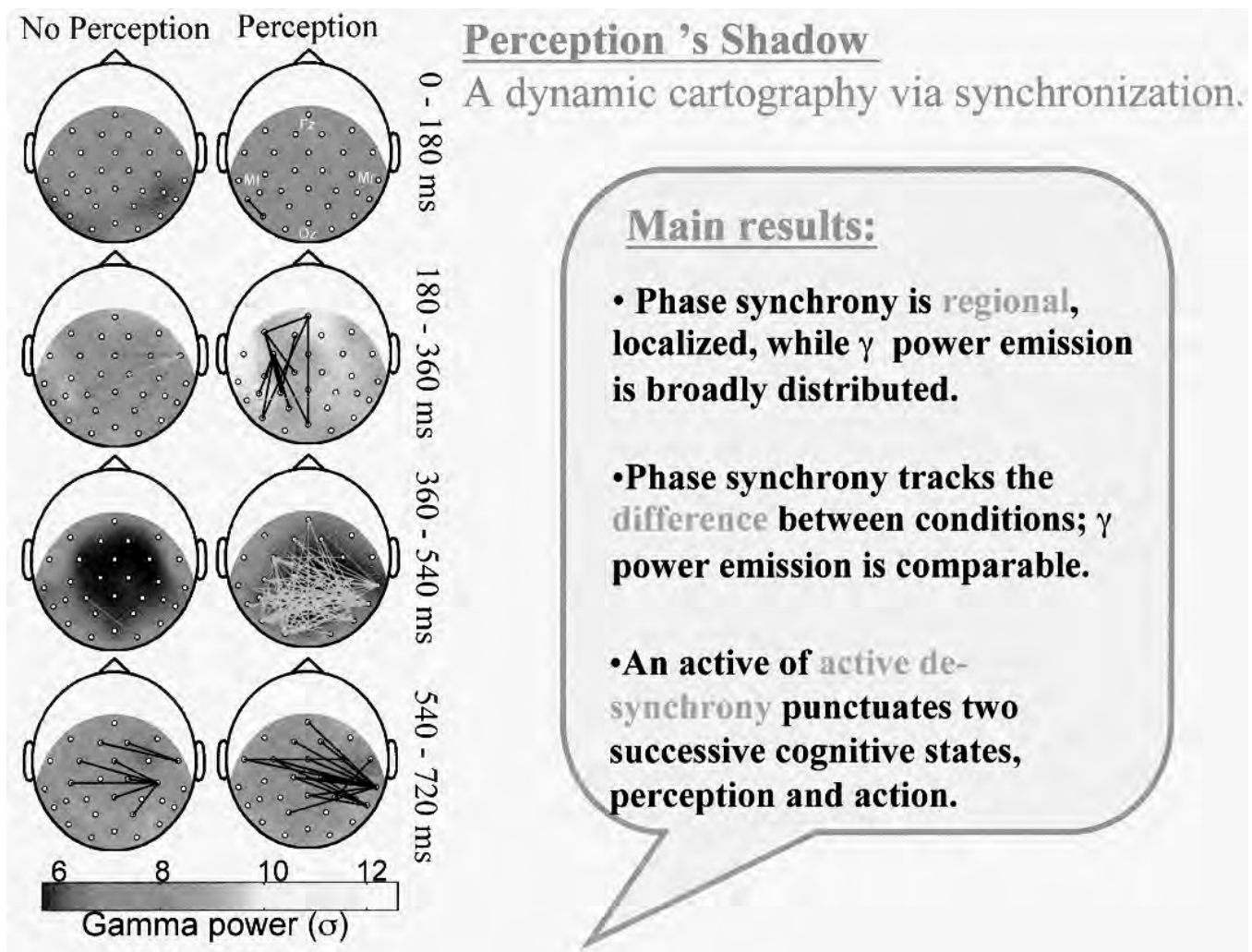


Figure 54.17 Average scalp distribution of gamma EEG activity and phase synchrony. Color coding indicates gamma power (averaged in a 34- to 40-Hz frequency range) over an electrode and during a 180-msec time window, from stimulation onset (0 msec) to motor response (720 msec). Gamma activity is spatially homogeneous and similar between conditions over time. In contrast, phase synchrony is markedly regional and differs between conditions. Synchrony between electrode pairs is indicated by lines, which are drawn only if the synchrony is beyond the distribution of shuffled data sets ($P < 0.01$). Black and green lines correspond to a significant increase or decrease in synchrony, respectively. (Adapted from Rodriguez E, George N, Lachaux JP, et al. Perception's shadow: long-distance synchronization of human brain activity. *Nature*. 1999;397(6718):430–433.) (See color insert)

face (shown in the upright position) induces a long-distance stable pattern of phase synchronization that corresponds to the moment of perception, while this was not the case when the faces were presented in an inverted position, and thus were difficult to identify as faces. Later, this study was replicated by Trujillo et al. (208) who revealed that some other aspects should be taken into account with respect to the analysis of phase relationships. These authors put in evidence the dependency of phase relations on the frequency range at which the phase relationships were estimated, and on the EEG montage used. They were able to replicate Rodriguez et al.'s results but only at the frequency range that exhibited the largest gamma power for the face upright position. Additionally they found, however, substantial phase synchrony in other conditions, but at different frequencies. Furthermore, they showed also that the use of EEG signals recorded using Laplacian "reference-free" derivations (209–211) yields more robust results than using another referential montage. The judicious choice of the EEG montage appears to be essential to obtain reliable EEG phase relationships. It may be noted here that one may use other methods of source estimation with the same purpose, such as low resolution brain electromagnetic tomography (LORETA)

(212,213) or variable resolution electromagnetic tomography (VARETA) (214).

Another novel approach based also on a measure of phase synchronization was introduced for the analysis of visual evoked responses to intermittent light stimulation in photosensitive epileptic patients (215,216). The method consists in estimating the phase dispersion of each frequency component present in the EEG/MEG. In this way a phase clustering index can be defined that differs from that used by Lachaux et al. (205). Applying the *phase clustering index* it was found that the patients who develop epileptiform discharges during the light stimulation present an enhancement of the phase clustering index in the gamma frequency band in comparison to that at the driving frequency, appearing before the occurrence of paroxysmal activity (Fig. 54.18). Thus, the phase clustering index reflects the degree of excitability of the underlying neural system and it suggests the existence of nonlinear dynamics.

In general the interpretation of phase relationships between EEG/MEG signals is not straightforward. Indeed it implies the specification of a biophysical model. The point is to specify how the neuronal sources of the signals communicate one with the

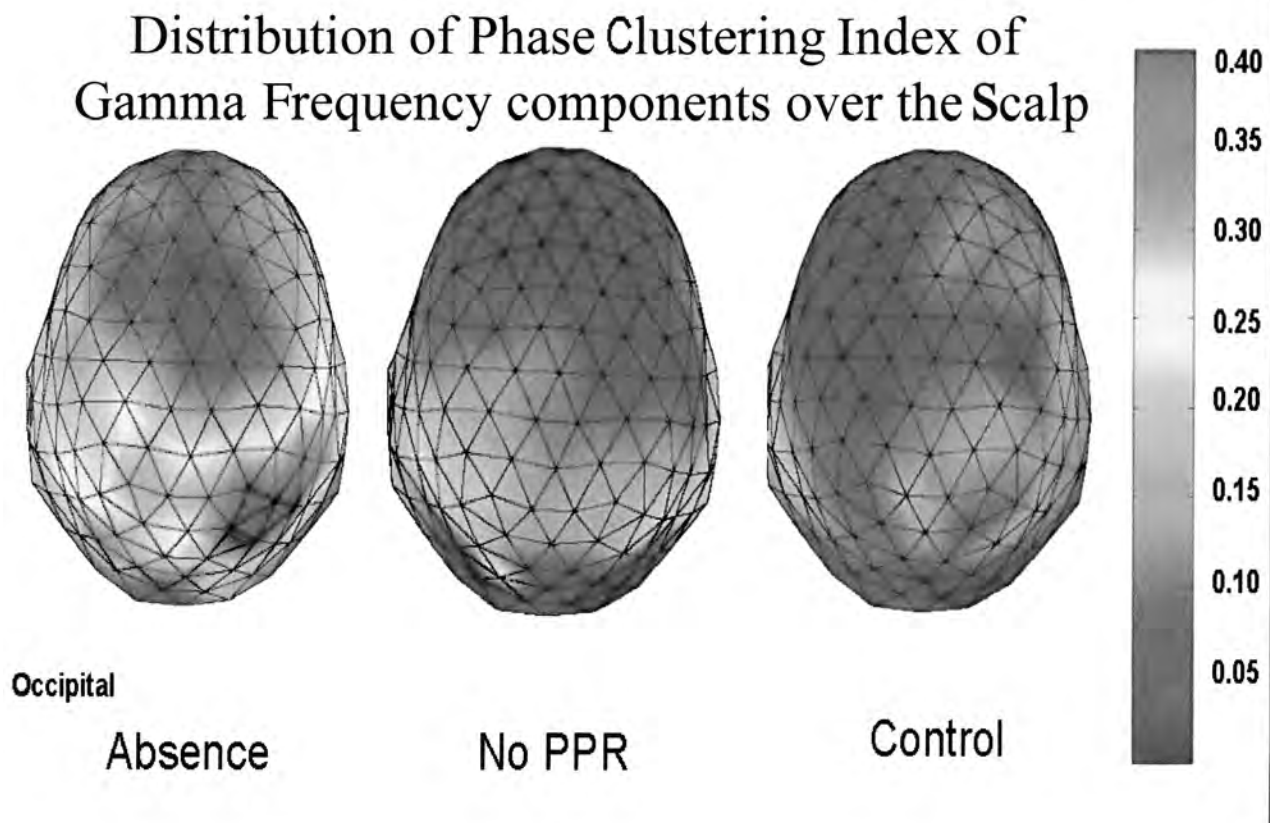


Figure 54.18 Spatial distribution of the relative phase clustering index (rPCI) changes per magnetic sensor over the magnetoencephalography (MEG) helmet. **Left plot:** Average of the means of rPCI from four trials where intermittent light stimulation at 20 Hz was followed by a photoparoxysmal response (PPR), compared with two trials where light stimulation was not followed by PPR (**middle plot**), and with the average of four trials in an age- and sex-matched control subject (**right plot**). (Adapted from Parra J, Kalitzin SN, Iriarte J, et al. Gamma-band phase clustering and photosensitivity: is there an underlying mechanism common to photosensitive epilepsy and visual perception? *Brain*. 2003;126:1164–1172.) ((See color insert))

other, that is, what kind of transfer function relates both sources. A general biophysical model may be defined, as an example, as follows: at a given site in the brain there is a source of neuronal activity, for instance, a generator of signals in the gamma frequency range; this activity propagates to another site but suffers some transformation (amplification or attenuation) in the way; as a first approximation, we may assume that this transformation is linear, and that one signal may be considered as input and the other as output of a linear system; in general for any such system there is a mathematical relationship between the gain, that is, the relation between the amplitudes of the input and output signals, and the phase function. Under certain conditions, the phase function is uniquely determined from the gain function. The class of systems with this property is called minimum phase shift systems. This refers to the smallest possible phase lag that can be obtained for physically realizable systems with a specified gain function. More precisely, the gain and phase of the system's transfer function are related by a set of equations called the Hilbert transform pair (cf., Ref. 217). In the case of EEG signals, one may assume that the phase spectrum between the two signals is composed of two components: one corresponding to the minimum phase component, as described above, and the other to a phase component due to the existence of a time delay. The former can be estimated from the gain function. Then this component can be subtracted from the measured phase spectrum and, if a time delay exists, the difference should be a phase component that is linear with frequency. From the slope of the latter a time delay can be computed. This method was, for example, applied to the beta/gamma activities recorded from the prepyriform cortex and the anterior entorhinal cortex of a cat (218).

We should note, however, that in the analysis of EEG/MEG signals one encounters quite often nonlinear relations, so that methods based on linear assumptions, such as coherence and cross-correlation (70,24), in those cases are not the most appropriate. To estimate the degree of association between two signals and the corresponding time delay in a more general way, the nonlinear correlation coefficient h^2 as a function of time shift between the two signals was first introduced in EEG signal analysis by Pijn and colleagues (219,220) and has also been shown to give reliable measures for the degree and direction of functional coupling between neuronal populations in different types of epilepsy (221–224). This method has some major advantages over other signal analysis methods like coherency, mutual information, and cross-correlation, as it can be applied independently of whether the type of relationship between the two signals is linear or nonlinear. The basic assumption is that if the amplitude of signal y is considered as a function of the amplitude of signal x , the value of y given a certain value of x can be predicted according to a nonlinear regression curve. The variance of y according to this regression curve is called the explained variance, that is, it is explained or predicted on the basis of x . By subtracting the explained variance from the total variance, one obtains the unexplained variance. The nonlinear correlation ratio h^2 expresses the reduction of variance of y that can be obtained by predicting the y values according to the regression curve as follows: $h^2 = (\text{explained variance} - \text{unexplained variance})/\text{total variance}$, which takes values in the range $[0, 1]$.

This nonlinear correlation ratio h^2 can be computed for a number of time delays Δt between x and y ; the estimated time delay between the two signals corresponds to the value of Δt for which h^2 is maximum. Low values of h^2 denote that signals x and y are independent; high values of h^2 mean that signal y may be explained by a transformation (possibly nonlinear) of signal x . Bidirectional associations reflect the invertibility of the nonlinear mapping while highly asymmetric, unidirectional associations indicate noninvertible mapping. This implies that high asymmetric association values may indicate essentially nonlinear, irreversible dynamics of the underlying system (225).

In addition to the estimation of h^2 , a derived quantity was proposed by Guye et al. (226) that gives information about the causality of the association, and was called the direction index D . This quantity takes into account both the estimated time delay between signals x and y (Δt) and the asymmetric nature of the nonlinear correlation coefficient h^2 (values of the h^2 coefficient are different if the computation is performed from x to y or from y to x). Values of parameter D range from -1.0 (x is driven by y) to 1.0 (y is driven by x). More recently Kalitzin et al. (225) presented a general definition of the nonlinear association index h^2 , demonstrating rigorously that the index measures the best dynamical range of any nonlinear map between signals. A further refinement of the nonlinear association analysis is the so-called “partialization” of the association measure between two signals. Indeed in cases where a nonlinear association index h^2 between two signals may be caused by a third one, acting as a common source, the influence of the third one can be removed and the residual signals' correlations may be computed to determine whether the association between them is caused by the common influence of the third signal, or not.

In addition to these nonlinear association methods, some others have been proposed and implemented to detect general types of interactions between EEG/MEG signals based on the theory of nonlinear dynamical systems, such as the concept of *generalized synchronization* that can be applied to any kind of time series (227), based on the theory of nonlinear dynamical systems that was introduced by Rulkov et al. (228). According to this concept synchronization between two dynamical systems X (the driver) and Y (the response) exists when the state of the response system Y is a function of the state of the driving system, $X: Y = F(X)$. Assuming that F is continuous and that two points on the attractor of X , x_i and x_j , are close to each other, the corresponding points on attractor Y , y_i and y_j , will be also close to each other. The probability that embedded vectors are closer to each other than a certain small critical distance is estimated for each discrete time pair (i, j) . This is done for each signal, or channel k of a set of M channels. Thereafter, the number of channels $H_{i,j}$ for which the embedded vectors $X_{k,i}$ and $X_{k,j}$ are closer together than the critical distance can be calculated. Inspired by these theoretical concepts, Stam and van Dijk (227) defined a synchronization likelihood $S_{k,i,j}$ for each EEG/MEG channel k and each discrete time pair (i, j) as:

$$\begin{aligned} \text{If } |X_{k,i} - X_{k,j}| < \varepsilon_{k,i}: S_{k,i,j} &= (H_{i,j} - 1)/(M - 1) \\ \text{If } |X_{k,i} - X_{k,j}| > \varepsilon_{k,i}: S_{k,i,j} &= 0 \end{aligned} \quad (54.42)$$

By averaging over all j , the synchronization likelihood $S_{k,i}$ can be estimated. Thus, $S_{k,i}$ is a measure that describes how strongly signal k at time i is synchronized to all other $M - 1$ signals. The synchronization likelihood is a measure of the dynamical interdependencies of EEG/MEG signals, both linear and nonlinear, as a function of time, and may be used to quantify phase relations of nonstationary time series. A number of applications have been published, as, for example, in a study of EEG changes related to the performance of a visuospatial task (229), and also in clinical study of EEG synchronization in mild cognitive impairment and Alzheimer disease (230).

We may conclude that when brain activities are coupled in time, and when one uses the term “synchrony” in the context of brain signals, one should take into account that synchronous activities do not necessarily occur with time delay equal to zero, but with a consistent time delay compatible with the mechanism of propagation of neural activity. To account for the case where neuronal activities recorded from different cortical areas appear to occur synchronously with zero delay, as in the case of the experiments of Roelfsema et al. (231), where zero time-lag synchrony was found between cortical areas in a visuomotor task in cats, two mechanisms can be proposed: one is that both activities depend on a third source that reaches at the same time both cortical areas where the recordings were made; another is that the two cortical areas have strong bidirectionally re-entrant properties. This was, for example, experimentally demonstrated in the case of epileptiform afterdischarges elicited from a focus in the hippocampus spread to homologous sites in the contralateral hippocampus following commissural systems that may be strong enough to ensure the forming of one bilateral oscillating system with zero interhemispheric delay (232).

Above we have discussed a number of issues with respect to the question of EEG phase synchronization. This question, however, may be considered in the more general context of causal relationships between EEG signals, that is, the question of *causality*. We have already indicated that the nonlinear association index h^2 allows to infer causal relations between two signals and to estimate the corresponding time delays. This property is an example of how to infer causal relations between two time series in a statistical sense. Already in 1956 Wiener proposed that given two time series, one can be considered causal with respect to the other if the second one can be better predicted by adding knowledge about the first one. Later Granger (233) applied this concept to linear regression models particularly in studies of econometrics. These concepts were adapted to the spectral domain by Geweke (234) using MVAR models. Besides many applications of these statistical concepts of causality in different scientific fields, analytic methods based on these concepts have entered the field of neurosciences in the course of the 1980s. A comprehensive review of these early neuroscientific applications can be found in Kamiński et al. (235). Among many others, one example of such methods is the “short-time directed transfer function (SDTF)” that allows estimating the propagation of brain activity as a function of frequency and time (236). This was applied, for example, to a study of the propagation of gamma and beta components

during motor imagery using EEG signals recorded from electrodes overlying cortical sensorimotor areas (237).

An interesting development in this field that was mainly inspired by the need of analyzing multiple images produced in fMRI studies, and further to analyze combined fMRI–EEG recordings. This domain has been called dynamic causal modeling (DCM) (238). This methodology goes beyond functional connectivity analysis as revealed by the statistical methods described above, but it includes explicit biophysical models of the processes that are responsible for the generation of the signals and the causal relationships between them. This is what has been called *effective connectivity*, in contrast with *functional connectivity*. Accordingly, DCM is based on two kinds of models: of neural population dynamics and of the transfer between the neural activity and the signals being recorded, either EEG or fMRI signals (see for details of these models Chapter 4; 239,240). This approach is most challenging for the future because it brings together analytic methodologies with the necessity of constructing biophysical models of the phenomena of interest, be these EEG or fMRI signals or combinations of both.

REFERENCES

1. Isaksson A, Wennberg A. Spectral properties of nonstationary EEG signals, evaluated by means of Kalman filtering: application examples from a vigilance test. In: Kellaway P, Petersén I, eds. *Quantitative Analytic Studies in Epilepsy*. New York, NY: Raven; 1976:389–402.
2. Dumermuth G, Gasser T, Hecker A, et al. Exploration of EEG components in the beta frequency range. In: Kellaway P, Petersén I, eds. *Quantitative Analytic Studies in Epilepsy*. New York, NY: Raven; 1976:533–558.
3. Jansen BH. *EEG Segmentation and Classification* [thesis]. Amsterdam: Free University; 1979:237 pp.
4. Grosveld FM, Jansen BH, Hasman A, et al. La reconnaissance des individus à l'intérieur d'un groupe de seize sujets normaux. *Rev Electroencephalogr Neurophysiol Clin*. 1976;9:295–297.
5. McEwen J, Anderson GB. Modelling the stationarity and Gaussianity of spontaneous electroencephalographic activity. *IEEE Trans Biomed Eng*. 1975;22:361–369.
6. Elul R. The genesis of the EEG. *Int Rev Neurobiol*. 1972;15:227–272.
7. Gasser T. General characteristics of the EEG as a signal. In: Remond A, ed. *EEG Informatics. A Didactic Review of Methods and Applications of EEG Data Processing*. Amsterdam: Elsevier; 1977:37–52.
8. Siebert WM. The description of random processes. In: Communications Biophysics Group, Siebert WM, eds. *Processing Neuroelectric Data*. Cambridge, MA: MIT Press; 1959:66–87.
9. Pijn JP, Van Neerven J, Noest A, et al. Chaos or noise in EEG signals; dependence on state and brain site. *Electroencephalogr Clin Neurophysiol*. 1991;79(5):371–381.
10. Jay F, ed-in-chief. *IEEE Standard Dictionary of Electrical and Electronics Terms*. The Institute of Electrical and Electronics Engineers, Inc. New York, NY: Wiley; 1977.
11. Lopes da Silva FH, ed. Cooper R, Dumermuth G, et al. Sampling, conversion and measurement of bioelectrical phenomena. In: Remond A, ed-in-chief; Brazier MA, ed. *Handbook of Electroencephalography and Clinical Neurophysiology*. Vol 4. Part A. Amsterdam: Elsevier; 1976.

12. Susskind AK, ed. *Notes on Analog–Digital Conversion Techniques*. New York, NY: Wiley; 1957
13. Steineberg CA, Paine LW. Methods and techniques of data conversion. *Ann N Y Acad Sci*. 1964;115/2:614–626.
14. Jenkins GM, Watts DG. *Spectral Analysis and its Applications*. San Francisco, CA: Holden Day; 1968.
15. Blackman RB, Tukey JW. *The Measurement of Power Spectra*. New York, NY: Dover Press; 1958.
16. Bendat JS, Piersol AG. *Measurements and Analysis of Random Data*. New York, NY: Wiley Interscience; 1971.
17. Otne RK, Enochson L. *Digital Time Series Analysis*. New York, NY: Wiley; 1978.
18. Dietsch G. Fourier Analyse von Elektroenzephalogrammen des Menschen. *Pflugers Arch Ges Physiol*. 1932;230:106–112.
19. Grass AM, Gibbs FA. A Fourier transform of the electroencephalogram. *J Neurophysiol*. 1938;1:521–526.
20. Knott JR, Gibbs FA. A Fourier transform of the EEG from one to eighteen years. *Psychol Bull*. 1939;36:512–513.
21. Drohocki Z. L'Électroencéphalographie du cerveau. *C R Soc Biol*. 1938;129:889–893.
22. Walter WG. Automatic low frequency analyzer. *Electron Eng*. 1943;16:9–13.
23. Walter WG. An improved low frequency analyzer. *Electron Eng*. 1943;16:236–240.
24. Brazier MAB, Casby JU. Cross-correlation and autocorrelation of EEG potentials. *Electroencephalogr Clin Neurophysiol*. 1952;4:201.
25. Barlow JS, Brazier MAB. A note on a correlator system for brain potentials. *Electroencephalogr Clin Neurophysiol*. 1954;6:321–325.
26. Wiener N. *Cybernetics*. Cambridge, MA: MIT Press; 1961.
27. Cooley JW, Tukey JW. An algorithm for the machine calculation of complex Fourier series. *Math Comput*. 1965;19:297–301.
28. Huber PJ, Kleiner B, Gasser T, et al. Statistical methods for investigating phase relations in stationary stochastic processes. *IEEE Trans Audio Electroacoust*. 1971;19:78–86.
29. Dumermuth G, Huber PJ, Kleiner B, et al. Analysis of the interrelations between frequency bands of the EEG by means of the bispectrum. *Electroencephalogr Clin Neurophysiol*. 1971;31:137–148.
30. Hjorth B. EEG analysis based on time domain properties. *Electroencephalogr Clin Neurophysiol*. 1970;29:306–310.
31. Zetterberg LH. Means and methods for processing of physiological signals with emphasis on EEG analysis. In: Lawrence JH. *Advances in Biology and Medical Physics*. Vol 16. New York, NY: Academic Press; 1977:41–91.
32. Cohen BA. Period analysis of the electroencephalogram. *Comput Programs Biomed*. 1976;6:269–276.
33. Rice SO. Mathematical analysis of random noise. In: Wax N, ed. *Noise and Stochastic Processes*. New York, NY: Dover; 1954:133–294.
34. Saltzberg B, Edwards RJ, Heath RG, et al. Synoptic analysis of EEG signals. In: Enslein K, ed. *Data Acquisition and Processing in Biology and Medicine*. Vol 5. Oxford: Pergamon Press; 1968:267–307.
35. Matousek M ed., Barlow JS, Dumermuth G, et al. Frequency and correlation analysis. In: Brazier MAB, Walter DO, eds. *Evaluation of Bioelectrical Data from Brain, Nerve and Muscle, II*. In: Remond A, ed-in-chief. *Handbook of Electroencephalography and Clinical Neurophysiology*. Vol 5. Part A. Amsterdam: Elsevier; 1973.
36. Saltzberg B, Burch NR. Period analytic estimates of moments of the power spectrum. A simplified EEG time domain procedure. *Electroencephalogr Clin Neurophysiol*. 1971;30:568–570.
37. Gevins A, Remond A, eds. *Methods of Analysis of Brain Electrical and Magnetic Signals. Handbook of Electroencephalography and Clinical Neurophysiology*. Vol 1. Amsterdam: Elsevier; 1987: 541–582 [new series].
38. Gasser T. Goodness-of-fit tests for correlated data. *Biometrika*. 1975;62:563–570.
39. Lilliefors HW. On the Kolmogorov–Smirnov test for normality with mean and variance unknown. *J Am Stat Assoc*. 1967;67: 399–402.
40. Persson J. Comments on estimations and tests of EEG amplitude distributions. *Electroencephalogr Clin Neurophysiol*. 1974;37: 309–313.
41. Saunders MG. Amplitude probability density studies on alpha and alpha-like patterns. *Electroencephalogr Clin Neurophysiol*. 1963;15: 761–767.
42. Lion KS, Winter DF. A method for the discrimination between signal and random noise of electrobiological potentials. *Electroencephalogr Clin Neurophysiol*. 1961;5:109–111.
43. Kozhevnikov VA. Some methods of automatic measurement of the electroencephalogram. *Electroencephalogr Clin Neurophysiol*. 1958; 10:269–278.
44. Campbell J, Bower E, Dwyer SJ, et al. On the sufficiency of autocorrelation functions as EEG descriptors. *IEEE Trans Biomed Eng*. 1967;BME14:49–52.
45. Elul R. Gaussian behaviour of the electroencephalogram: changes during performance of mental task. *Science*. 1969;164:328–331.
46. Dumermuth G. Variance spectra of electroencephalogram in twins. A contribution to the problem of quantification of EEG background activity in childhood. In: Kellaway P, Petersén I, eds. *Clinical Electroencephalography in Childhood*. Stockholm: Almqvist & Wiksell; 1968:119–154.
47. Dumermuth G. Die Anwendung von Varianzspectra für einen quantitativen Vergleich von EEG bei Zwillingen. *Helv Paediatr Acta*. 1969;24:45–54.
48. Dumermuth G, Walz W, Scollo Lavizzari G, et al. Spectral analysis of EEG activity during sleep stages in normal adults. *Eur Neurol*. 1972;7:265–296.
49. Dumermuth G, Gasser T, Lange B. Aspects of EEG analysis in the frequency domain. In: Dolce G, Künkel H, eds. *Computerized EEG Analysis*. Stuttgart: Fischer; 1975:429–457.
50. Drohocki Z. L'intégrateur de l'Électroproduction cérébrale pour l'Électroencéphalographie quantitative. *Rev Neurol Paris*. 1948;80: 617–619.
51. Goldstein L. Time domain analysis of the EEG. The integrative method. In: Dolce G, Künkel H, eds. *CEAN—Computerized EEG Analysis*. Stuttgart: Fischer; 1975:251–270.
52. Saltzberg B, Burch NR, McLennan MA, et al. A new approach to signal analysis in electroencephalography. *IRE Trans Med Electron*. 1957;8:24–30.
53. Burch NR, Nettleton WJ, Sweeney J, et al. Period analysis of the electroencephalogram on a general purpose digital computer. *Ann N Y Acad Sci*. 1964;115:827–843.
54. Fink M. EEG and human psychopharmacology. *Annu Rev Pharmacol*. 1969;9:241–258.
55. Fink M. EEG profiles and bioavailability measures of psychoactive drugs. In: Itil TM, ed. *Psychotropic Drugs and the Human EEG*. Basel: S. Karger; 1974:76–98.
56. Fink M. Cerebral electrometry—quantitative EEG applied to human psychopharmacology. In: Dolce G, Künkel H, eds. *Computerized EEG Analysis*. Stuttgart: Fischer; 1975:271–288.
57. Itil TM, Shapiro DM, Herrmann WM, et al. HZI systems for EEG parameterization and classification of psychotropic drugs. *Pharmakopsychiatrie*. 1979;12:4–19.
58. Pronk RAF, Simons AJR. Processing of the electroencephalogram in cardiac surgery. *Comput Programs Biomed*. 1984;18(3):181–189.
59. Pronk RAF, de Boer SJ, Cornelissen RCM, et al. Computer assisted patient monitoring during open heart surgery with the aid of the EEG. In: van Eijnsbergen B, Lopes da Silva FH, eds. *Progress Report No. PR6*. Utrecht: Institute of Medical Physics TNO; 1976:224–228.

60. Itil TM. Digital computer period analyzed EEG in psychiatry and psychopharmacology. In: Dolce G, Künkel H, eds. *CEAN—Computerized EEG Analysis*. Stuttgart: Fischer; 1975:289–308.
61. Matejcek M, Schenk GK. Die iterative IntervallAnalyse—Ein methodischer Beitrag zur Quantitativen Beschreibung des Elektroenzephalogramms in Zeitbereich. In: Schenk GK, ed. *Die Quantifizierung des Elektroenzephalogramms*. Konstanz: AEG Telefunken; 1973:293–306.
62. Legewie H, Probst W. Online analysis of EEG with a small computer. *Electroencephalogr Clin Neurophysiol*. 1969;27:533–535.
63. Schwarzer F, Reets H. Machines for EEG analysis. *Electroencephalogr Clin Neurophysiol*. 1966;20:278.
64. Marko H, Petsche H. Ein Gerat zur gleichzeitigen Frequenz und Amplitudenanalyse von EEGKurven bei frei wählbarer Zeitbasis. *Arch Psychiat Nervenkr*. 1957;196:191–195.
65. Leader HS, Cohn R, Wehrer AL, et al. Pattern reading of the clinical electroencephalogram with a digital computer. *Electroencephalogr Clin Neurophysiol*. 1967;23:566–570.
66. Pfurtscheller G, Koch W. Eine maschinelle Methode zur EEG Klassifikation. *Methods Inform Med*. 1972;11:233–237.
67. Harner RN. Computer analysis and clinical EEG interpretation—perspective and application. In: Dolce G, Künkel H, eds. *CEAN—Computerized EEG Analysis*. Stuttgart: Fischer; 1975:337–343.
68. Harner RN, Ostergren KA. Sequential analysis of quasistable and paroxysmal activity. In: Kellaway P, Petersén I, eds. *Quantitative Analytic Studies in Epilepsy*. New York, NY: Raven; 1976:343–361.
69. Barlow JS, Brown RM. *An Analog Correlator System for Brain Potentials*. Research Lab Electronics, Technical Report No. 300. Cambridge, MA: Massachusetts Institute of Technology (MIT); 1955.
70. Brazier MAB, Barlow JS. Some applications of correlation analysis to clinical problems in electroencephalography. *Electroencephalogr Clin Neurophysiol*. 1956;8:325–331.
71. McFadden JA. The correlation function of a sine-wave plus noise after extreme clipping. *IRE Trans Inform Theory*. 1956;2(2):82–83.
72. Kaiser JF, Angell RK. *New Techniques and Equipment for Correlation Computation*. Technical Memo 7668TM2, Servomechanisms Lab. Cambridge, MA: MIT Press; 1957.
73. Lopes da Silva FH. *Dynamic Characteristics of Visual Evoked Potentials* [thesis]. Utrecht, The Netherlands: University of Utrecht; 1970:126 pp.
74. Sologub EB. EEG cross correlation analysis during the formation of motor dynamic stereotype in human. *Zh Vyssh Nerv Deiat*. 1965;15:32–41 [in Russian].
75. Kamp A, Storm van Leeuwen W, Tielen AM. A method for auto- and cross-relation analysis of the EEG. *Electroencephalogr Clin Neurophysiol*. 1965;19:91–95.
76. Lesèvre N, Remond A. Variations in the average visual response in relation to the alpha phase “autostimulation.” *Electroencephalogr Clin Neurophysiol*. 1967;23:578–579.
77. Michael D, Houchin H. Automatic EEG analysis: a segmentation procedure based on the autocorrelation function. *Electroencephalogr Clin Neurophysiol*. 1979;46:232–235.
78. Walter DO. The method of complex demodulation. In: Walter DO, Brazier MAB, eds. *Advances in EEG Analysis*. *Electroencephalogr Clin Neurophysiol*. 1968;(suppl 27):51–57.
79. Childers DG, Pao MT. Complex demodulation for transient wavelet detection and extraction. *IEEE Trans Audio Electroacoust*. 1972;AU20:295–308.
80. Kumar A. The complex demodulation method for detection of a waves and sleep spindles of the human EEG in real time. *Proceedings of International Conference on Advanced Signal Processing Techniques, Lausanne*. 1975:355–361.
81. Regan D. Evoked potentials in basic and clinical research. In: Remond A, ed. *EEG Informatics. A Didactic Review of Methods and Applications of EEG Data Processing*. Amsterdam: Elsevier; 1977:319–346.
82. Broughton R, Healey T, Maru J, et al. A phase locked loop device for automatic detection of sleep spindles and stage 2. *Electroencephalogr Clin Neurophysiol*. 1978;44:677–680.
83. Campbell K, Kumar A, Hofman W. Human and automatic validation of a phase-locked loop spindle detection system. *Electroencephalogr Clin Neurophysiol*. 1980;48:602–605.
84. Kaiser E, Petersén I, Selldin U, et al. EEG data representation in broadband frequency analysis. *Electroencephalogr Clin Neurophysiol*. 1964;17:76–80.
85. Matousek M, Petersén I, Friberg S. Automatic assessment of randomly selected routine EEG records. In: Dolce G, Künkel H, eds. *CEAN—Computerized EEG Analysis*. Stuttgart: Fischer; 1975:421–428.
86. Storm van Leeuwen W. Comparison of EEG data obtained with frequency analysis and with correlation methods. *Electroencephalogr Clin Neurophysiol Electroencephalogr Clin Neurophysiol Suppl*. 1961;20:37–40.
87. Storm van Leeuwen W. Complementary of different analysis methods. *Electroencephalogr Clin Neurophysiol*. 1964;16:136–139.
88. Walter DO. Spectral analysis of electroencephalograms: mathematical determination of neurological relationships from records of limited duration. *Exp Neurol*. 1963;8:155–181.
89. Walter DO, Adey WR. Analysis of brain wave generators as multiple statistical time series. *IEEE Trans Biomed Eng*. 1965;12:8–13.
90. Dumermuth G. Fundamentals of spectral analysis in electroencephalography. In: Remond A, ed. *EEG Informatics. A Didactic Review of Methods and Applications of EEG Data Processing*. Amsterdam: Elsevier; 1977:83–105.
91. Vos JE. Representation in the frequency domain of nonstationary EEGs. In: Dolce G, Künkel H, eds. *CEAN—Computerized EEG Analysis*. Stuttgart: Fischer; 1975:41–50.
92. Künkel H, EEG Project Group. Hybrid computing system for EEG analysis. In: Dolce G, Künkel H, eds. *CEAN—Computerized EEG Analysis*. Stuttgart: Fischer; 1975:365–385.
93. Walter DO. On units and dimensions for reporting spectral intensities. *Electroencephalogr Clin Neurophysiol*. 1968;24:486–487.
94. Abraham F, Brown D, Gardiner M. Calibration of EEG power spectra. *Commun Behav Biol Part A*. 1968;1:31.
95. Clusin W, Trapani G, Roccaforte PA. A numerical approach to matching amplification for the spectral analysis of recorded EEG. *Electroencephalogr Clin Neurophysiol*. 1970;28:639–641.
96. Dumermuth G, Flühler H. Some modern aspects in numerical spectrum analysis of multichannel electroencephalographic data. *Med Biol Eng*. 1967;5:319–331.
97. Sciarretta G, Erculiani P. A proposal for calibrating EFG spectrograms. *Electroencephalogr Clin Neurophysiol*. 1978;5:674–676.
98. Bickford RG. Computer analysis of background activity. In: Remond A, ed. *EEG Informatics. A Didactic Review of Methods and Applications of EEG Data Processing*. Amsterdam: Elsevier; 1977:215–232.
99. Bickford RG, Brimm J, Berger L, et al. Application of compressed spectral array in clinical EEG. In: Kellaway P, Petersén I, eds. *Automation of Clinical Electroencephalography*. New York, NY: Raven; 1973:55–64.
100. Johnson LC, Hanson K, Bickford RG. Effect of flurazepam on sleep spindles and K complexes. *Electroencephalogr Clin Neurophysiol*. 1976;40:67–77.
101. Kawabata N. A nonstationary analysis of the electroencephalogram. *IEEE Trans Biomed Eng*. 1973;20:444–452.

102. Pfurtscheller G, Aranibar A. Event-related cortical desynchronization detected by power measurements of scalp EEG. *Electroencephalogr Clin Neurophysiol*. 1977;42:817–826.
103. Kamp A, Vliegenthart W. Sequential frequency analysis: a method to quantify event related EEG changes. *Electroencephalogr Clin Neurophysiol*. 1977;42:843–846.
104. Pfurtscheller G, Aranibar A. Voluntary movement event-related desynchronization (ERD): normative studies. In: Pfurtscheller G, Buser P, Lopes da Silva FH, et al., eds. *EEG Activities and Cortical Functioning, Developments in Neuroscience*. Vol 10. Amsterdam: Elsevier; 1980:151–177.
105. Pfurtscheller G, Stancak A Jr, Neuper C. Event-related synchronization (ERS) in the alpha band—an electrophysiological correlate of cortical idling: a review. *Int J Psychophysiol*. 1996;24:39–46.
106. Siegel S. *Nonparametric Statistics for the Behavioural Sciences*. Tokyo: McGraw-Hill; 1956.
107. Arnolds DEAT, Lopes da Silva FH, Aitink AW, et al. Hippocampal EEG and behaviour in dog. I. Hippocampal EEG correlates of gross motor behaviour. *Electroencephalogr Clin Neurophysiol*. 1979;46:552–570.
108. Etévenon P, Pidoux B. From biparametric to multidimensional analysis of EEG. In: Remond A, ed. *EEG Informatics. A Didactic Review of Methods and Application of EEG Data Processing*. Amsterdam: Elsevier; 1977:193–214.
109. Gasser T. Statistical handling of EEG data. *Pharmakopsychiatrie*. 1979;12:210–219.
110. Abt K. Statistical problems in the analysis of comparative pharmac-EEG trials. *Pharmakopsychiatrie*. 1979;12:228–236.
111. Walter DO, Adey WR. Spectral analysis of electroencephalograms recorded during learning in the cat. *Exp Neurol*. 1963;8:155–181.
112. Brazier MAB. Studies of the EEG activity of limbic structures in man. *Electroencephalogr Clin Neurophysiol*. 1968;25:309–318.
113. Lopes da Silva FH, van Lierop THMT, Schrijer CF, et al. Organization of thalamic and cortical alpha rhythms: spectra and coherence. *Electroencephalogr Clin Neurophysiol*. 1973;35: 627–639.
114. Prechtel HFR, Vos JE. Verlaufsmuster der Frequenzspektren und Kohärenzen bei schlafenden normalen und neurologisch abnormen Neugeborenen. In: Schenk GK, ed. *Die Quantifizierung des Elektroenzephalogramms*. Konstanz: AEG Telefunken; 1973: 167–188.
115. Bullock TH, McClune MC, Achimowicz JZ, et al. EEG coherence has structure in the millimeter domain: subdural and hippocampal recordings from epileptic patients. *Electroencephalogr Clin Neurophysiol*. 1995;95:161–177.
116. Bullock TH, McClune MC, Achimowicz JZ, et al. Temporal fluctuations in coherence of brain waves. *Proc Natl Acad Sci U S A*. 1995;92:11568–11572.
117. Storm van Leeuwen W, Arntz A, Spoelstra P, et al. The use of computer analysis for diagnosis in routine electroencephalography. *Rev Electroencephalogr Neurophysiol Clin*. 1976;62:318–327.
118. Storm van Leeuwen W, Wieneke GH, Spoelstra P, et al. Lack of bilateral coherence of mu rhythm. *Electroencephalogr Clin Neurophysiol*. 1978;44:140–146.
119. Gotman J. *Experiments in the Automation and Quantification of EEG Interpretation: Localized Brain Lesions and Epilepsy* [thesis]. Montreal: McGill University; 1976.
120. Brazier MAB. Spread of seizure discharges in epilepsy: anatomical and electrophysiological considerations. *Exp Neurol*. 1972;36:263–272.
121. Carter GC. *Time Delay Estimation. Report TR5335*. New London, CT: Naval Underwater Systems Center; 1976.
122. Mars NJI, van Arragon GW. Time delay estimation in nonlinear systems using average mutual amount of information analysis. *IEEE Trans Acoustics, Speech Signal Processing*. 1981;ASSP29(3): 619–621.
123. Gersch W, Goddard G. Locating the site of epileptic focus by spectral analysis methods. *Science*. 1970;169:701–702.
124. Gersch W, Tharp BR. Spectral regression—amount of information analysis of seizures in humans. In: Kellaway P, Petersén I, eds. *Quantitative Analytical Studies in Epilepsy*. New York, NY: Raven; 1976:509–532.
125. Tharp BR, Gersch W. Spectral analysis of seizures in humans. *Comput Biomed Res*. 1975;8:503–521.
126. Etévenon P. *Étude méthodologique de l'Electroencéphalographie quantitative. Application à quelques exemples* [Thèse]. Paris VI: Université Pierre et Marie Curie; 1977.
127. Lopes da Silva FH, Vos JE, Mooibroek J, et al. Partial coherence analysis of thalamic and cortical alpha rhythms in dog. A contribution towards a general model of the cortical organization of rhythmic activity. In: Pfurtscheller G, Buser P, Lopes da Silva FH, et al., eds. *EEG Activities and Cortical Functioning. Developments in Neuroscience*. Vol 10. Amsterdam: Elsevier; 1980:33–59.
128. Lopes da Silva FH, Vos JE, Mooibroek H, et al. Relative contributions of intracortical and thalamocortical processes in the generation of alpha rhythms revealed by partial coherence analysis. *Electroencephalogr Clin Neurophysiol*. 1980;50:449–456.
129. Vos JE, Lammerstsma AA, Van Eykeren LA. Ordinary and partial coherences of bipolar and quasiunipolar derivations of infant electroencephalograms. In: *Random Signal Analysis, IEE Cofn. Publ. No. 159*. London; 1977:154–160.
130. Rappelsberger P, Petsche H, Vollmer R, et al. Rhythmicity in seizure patterns—intracortical aspects. In: Speckmann EJ, Caspers H, eds. *Origin of Cerebral Field Potentials*. Stuttgart: Thieme; 1978:80–97.
131. Lopes da Silva FH, Storm van Leeuwen W. The cortical alpha rhythm in dog: depth and surface profile of phase. In: Brazier MAB, Petsche H, eds. *Architectonics of the Cerebral Cortex. IBRO Monograph Series*. Vol 3. New York, NY: Raven; 1978:319–333.
132. Reits D. *Cortical Potentials in Man Evoked by Noise Modulated Light* [thesis]. Utrecht, The Netherlands: University of Utrecht; 1975.
133. Berglund K, Hjorth B. Normierte SteilheitsBeschreibungparameter und der en physikalischer Sinn hinsichtlich der EEG Deutung. In: Schenk G, ed. *Quantifizierung des EEGs*. Konstanz: AEG Telefunken; 1973:249–257.
134. Denoth F. Some general remarks on Hjorth's parameters used in EEG analysis. In: Dolce G, Künkel H, eds. *CEAN—Computerized EEG Analysis*. Stuttgart: Fischer; 1975:9–18.
135. Hjorth B. Time domain descriptors and their relation to a particular model for generation of EEG activity. In: Dolce G, Künkel H, eds. *CEAN—Computerized EEG Analysis*. Stuttgart: Fischer; 1975:3–8.
136. Lopes da Silva FH, Hoeks A, Smits H, et al. Model of brain rhythmic activity, the alpha rhythm of the thalamus. *Kybernetik*. 1974;15:27–37.
137. Caille EJ, Bassano JL. Value and limits of sleep statistical analysis. Objective parameters and subjective evaluations. In: Dolce G, Künkel H, eds. *CEAN—Computerized EEG Analysis*. Stuttgart: Fischer; 1975:227–235.
138. Lütcke A, Mertins L, Masuch A. Die Darstellung von Grundaktivität, Herd, und Verlaufsbefunden sowie von paroxysmalen Ereignissen mit Hilfe der von Hjorth angegebene nen normierten Steilheitsparameter (vorläufige Mitteilungen). In: Matejcek M, Schenk GK, eds. *Quantitative Analysis of the EEG*. Konstanz: AEG Telefunken; 1973:259–280.
139. Zetterberg LH. *Stochastic Activity in a Population of Neurons. A Systems Analysis Approach. Report No. 2.3.153/1*. Utrecht: Institute of Medical Physics TNO; 1973:23 pp.

140. Zetterberg LH, Kristiansson L, Mossberg K. Performance of a model of a local neuron population. *Biol Cybern.* 1978;31:15–26.
141. Zetterberg LH. Estimation of parameters for a linear difference equation with application to EEG analysis. *Math Biosci.* 1969;5:227–275.
142. Gersch W. Spectral analysis of EEGs by autoregressive decomposition of time series. *Math Biosci.* 1970;7:205–222.
143. Fenwick PBC, Michie P, Dollimore J, et al. Mathematical simulation of the electroencephalogram using an autoregressive series. *Int J Biomed Comput.* 1971;2:281–307.
144. Bohlin T. *Analysis of EEG Signals with Changing Spectra.* Stockholm: IBM New Lab Technology; 1971:118 pp. Paper TP 18.212.
145. Isaksson A, Wennberg A. Visual evaluation and computer analysis of the EEG—a comparison. *Electroencephalogr Clin Neurophysiol.* 1975;38:79–86.
146. Lopes da Silva FH, Dijk A, Smits H. Detection of nonstationarities in EEGs using the autoregressive model. An application to EEGs of epileptics. In: Dolce G, Kunkel H, eds. *CEAN—Computerized EEG Analysis.* Stuttgart: Fischer; 1975:180–199.
147. Pfuertscheller G, Haring G. The use of an EEG autoregressive model for the time saving calculation of spectral power density distribution with a digital computer. *Electroencephalogr Clin Neurophysiol.* 1972;33:113–115.
148. Rappelsberger P, Petsche H. Spectral analysis of the EEG by means of autoregression. In: Dolce G, Kunkel H, eds. *CEAN—Computerized EEG Analysis.* Stuttgart: Fischer; 1975:27–40.
149. Wennberg A, Zetterberg LH. Application of a computer-based model for EEG analysis. *Electroencephalogr Clin Neurophysiol.* 1971;31:457–468.
150. Zetterberg LH. Experience with analysis and simulation of EEG signals with parametric description of spectra. In: Kellaway P, Petersén I, eds. *Automation of Clinical Electroencephalography.* New York, NY: Raven; 1973:161–201.
151. Herolf M. *A Recursive Detector.* Telecommunication Theory, Technical Report No. 99. Stockholm: Royal Institute of Technology; 1975.
152. Bodenstein G, Praetorius HM. Feature extraction from the encephalogram by adaptive segmentation. *Proc IEEE.* 1977;65:642–657.
153. Praetorius HM, Bodenstein G, Creutzfeldt O. Adaptive segmentation of EEG records: a new approach to automatic EEG analysis. *Electroencephalogr Clin Neurophysiol.* 1977;42:84–94.
154. Makhoul J. Linear prediction: a tutorial review. *Proc IEEE.* 1975;63:561–580.
155. Eykhoff P. *System Identification. Parameter and State Estimation.* London: Wiley; 1974.
156. Lopes da Silva FH. Analysis of EEG nonstationarities. *Electroencephalogr Clin Neurophysiol Suppl.* 1978;34:163–179.
157. Lopes da Silva FH, Dijk A, Smiths H, et al. Automatic detection and pattern recognition of epileptic spikes from surface and depth recording in man. In: Schenk GK, ed. *Die Quantifizierung des Elektroenzephalogramms.* Konstanz: AEG Telefunken; 1973:425–436.
158. Lopes da Silva FH, van Hulten K, Lommen JG, et al. Automatic detection and localization of epileptic foci. *Electroencephalogr Clin Neurophysiol.* 1977;43:1–13.
159. Duquesnoy AJ. *Segmentation of EEGs by Means of Kalman Filtering.* Progress Report No. PR5. Utrecht: Institute of Medical Physics TNO; 1976:87–92.
160. Isaksson A. *On Time Variable Properties of EEG Signals Examined by Means of a Kalman Filter Method.* Telecommunication Theory, Technical Report No. 95. Stockholm: Royal Institute of Technology; 1975.
161. Mathieu M. *Analyse de l'electroencephalogramme par prediction lineaire* [Thèse]. Paris: Université Pierre et Marie Curie; 1976: 173 pp.
162. Isaksson A. *SPARK—A Sparsely Updated Kalman Filter with Application to EEG Signals.* Telecommunication Theory, Technical Report No. 120. Stockholm: Royal Institute of Technology; 1974.
163. Barlow JS. Analysis of EEG changes with carotid clamping by selective analog filtering, matched inverse digital filtering and automatic adaptive segmentation: a comparative study. *Electroencephalogr Clin Neurophysiol.* 1984;58:193–204.
164. Creutzfeldt OD, Bodenstein G, Barlow JS. Computerized EEG pattern classification by adaptive segmentation and probability density function classification. Clinical evaluation. *Electroencephalogr Clin Neurophysiol.* 1985;60:373–393.
165. Barlow JS. Methods of analysis of nonstationary EEGs, with emphasis on segmentation techniques: a comparative review. *J Clin Neurophysiol.* 1985;2:267–304.
166. Baillon JF, Bienenfeld G, Findji F, et al. Lecture, mesure et traitement automatique de l'analyse mimétique de l'EEG. *Rev Electroencephalogr Neurophysiol Clin.* 1976;6:255–270.
167. Remond A. An EEGer's approach to automatic data processing. In: Dolce G, Kunkel H, eds. *CEAN—Computerized EEG Analysis.* Stuttgart: Fischer; 1975:128–136.
168. Remond A. From graphoelements to EEG pattern recognition. *Electroencephalogr Clin Neurophysiol Suppl.* 1978;34:141–145.
169. Remond A, Renault B. La theorie des objets electroencephalographiques. *Rev Electroencephalogr Clin Neurophysiol.* 1972;2:241–256.
170. Schenk GK. Die Quantifizierung des EEG mittels vektorieller Iterationstechnik, einer Simulationsmethode der visuellen Analyse. In: Schenk GK, ed. *Die Quantifizierung des Elektroencephalogramms.* Konstanz: AEG Telefunken; 1973:307–343.
171. Ahlblom G, Zetterberg LH. *A Comparative Study of Five Methods for Analysis of EEG.* Technical Report No. 112. Stockholm: Royal Institute of Technology; 1975:56 pp.
172. Herolf M. *Detection of Pulse-shaped Signals in EEG Telecommunication Theory, Technical Report No. 41.* Stockholm: Royal Institute of Technology; 1971.
173. Zetterberg LH. Spike detection by computer and by analog equipment. In: Kellaway P, Petersén I, eds. *Automation of Clinical Electroencephalogr. Clin. Neurophysiol.* New York, NY: Raven; 1973:227–234.
174. Barlow JS, Dubinsky J. Some computer approaches to continuous automatic clinical EEG monitoring. In: Kellaway P, Petersén I, eds. *Quantitative Analytic Methods in Epilepsy.* New York, NY: Raven; 1976:309–327.
175. Pfuertscheller G, Fischer G. A new approach to spike detection using a combination of inverse and matched filter techniques. *Electroencephalogr Clin Neurophysiol.* 1978;44: 243–247.
176. Mallat SG. A theory of multiresolution signal decomposition: the wavelet representation. *IEEE Trans Pattern Anal Machine Intell.* 1989;11:674–693.
177. Blanco S, D'Atellis CA, Isaacson S, et al. Time frequency analysis of electroencephalogram series (II): Gabor and wavelet transform. *Phys Rev E.* 1996;54:6661–6672.
178. Schiff SJ, Aldrouby A, Unser M, et al. Fast wavelet transformation of EEG. *Electroencephalogr Clin Neurophysiol.* 1994;91: 442–455.
179. Bartnik EA, Blinowska KJ. Wavelets: new method of evoked potential analysis. *Med Biol Eng Comput.* 1992;30:125–126.
180. Geva AB, Pratt H, Zeevi YY. Multichannel wavelet-type decomposition of evoked potentials: model-based recognition of generator activity. *Med Biol Eng Comput.* 1997;35(1):40–46.

181. Mallat SG, Zhang Z. Matching pursuit with time frequency dictionaries. *IEEE Trans Signal Processing*. 1993;41:3397–3415.
182. Durka PJ, Blinowska KJ. Analysis of EEG transients by means of matching pursuit. *Ann Biomed Eng*. 1995;23:608–611.
183. Durka PJ. *Time Frequency Analyses of EEG* [PhD thesis]. Department of Physics, Warsaw, Poland: University of Warsaw; 1996.
184. Quian Quiroga R, Blanco S, Rosso OA, et al. Searching for hidden information with Gabor transform in generalized tonic-clonic seizures. *Electroencephalogr Clin Neurophysiol*. 1997;103: 434–439.
185. Walter DO, Rhodes JM, Brown D, et al. Comprehensive spectral analysis of human generators in posterior cerebral regions. *Electroencephalogr Clin Neurophysiol*. 1966;20:224–237.
186. van Rotterdam A. Limitations and difficulties in signal processing by means of the principal components analysis. *IEEE Trans Biomed Eng*. 1970;17:268–269.
187. Bell AJ, Sejnowski TJ. An information-maximization approach to blind separation and blind deconvolution. *Neural Comput*. 1995;7(6):1129–1159.
188. Makeig S, Bell AJ, Jung TP, et al. Independent component analysis of electroencephalographic data. In: Touretzki D, Mozer M, Hasselmo M, eds. *Advances in Neural Information Processing Systems*. Cambridge, MA: MIT Press; 1996:145–151.
189. Makeig S, Jung T-P, Bell A, et al. Blind separation of auditory event-related brain responses into independent components. *Proc Natl Acad Sci U S A*. 1997;94(20):10979–10984.
190. Makeig S, Westerfield M, Jung TP, et al. Dynamic brain sources of visual evoked responses. *Science*. 2002;295(5555):690–694.
191. Anemüller J, Sejnowski T, Makeig S. Complex independent component analysis of frequency-domain electroencephalographic data. *Neural Netw*. 2003;16(9):1311–1323.
192. Hyvärinen A, Ramkumar P, Parkkonen L, et al. Independent component analysis of short-time Fourier transforms for spontaneous EEG/MEG analysis. *Neuroimage*. 2010;49(1):257–271.
193. Klemm M, Hauelsen J, Ivanova G. Independent component analysis: comparison of algorithms for the investigation of surface electrical brain activity. *Med Biol Eng Comput*. 2009;47(4): 413–423.
194. Groppe DM, Makeig S, Kutas M. Identifying reliable independent components via split-half comparisons. *Neuroimage*. 2009;45(4): 1199–1211.
195. Eichele T, Calhoun VD, Debener S. Mining EEG–fMRI using independent component analysis. *Int J Psychophysiol*. 2009;73(1):53–61.
196. Marques JP, Rebola J, Figueiredo P, et al. ICA decomposition of EEG signal for fMRI processing in epilepsy. *Hum Brain Mapp*. 2009;30(9):2986–2996.
197. Gómez-Herrero G, Atienza M, Egiazarian K, et al. Measuring directional coupling between EEG sources. *Neuroimage*. 2008; 43(3):497–508.
198. Ryyanen OR, Hyttinen JA, Malmivuo JA. Effect of measurement noise and electrode density on the spatial resolution of cortical potential distribution with different resistivity values for the skull. *IEEE Trans Biomed Eng*. 2006;53(9):1851–1858.
199. Pfurtscheller G, Lopes da Silva FH. Event-related EEG/MEG synchronization and desynchronization: basic principles. *Clin Neurophysiol*. 1999;110(11):1842–1857.
200. Engel AK, Singer W. Temporal binding and the neural correlates of sensory awareness. *Trends Cogn Sci*. 2001;5(1):16–25.
201. Varela F, Lachaux JP, Rodriguez E, et al. The brainweb: phase synchronization and large-scale integration. *Nat Rev Neurosci*. 2001;2(4):229–239.
202. Fell J, Fernández G, Klaver P, et al. Is synchronized neuronal gamma activity relevant for selective attention? *Brain Res Brain Res Rev*. 2003;42(3):265–272.
203. Fell J, Klaver P, Elfadil H, et al. Rhinal–hippocampal theta coherence during declarative memory formation: interaction with gamma synchronization? *Eur J Neurosci*. 2003;17(5): 1082–1088.
204. Le Van Quyen M, Foucher J, Lachaux J, et al. Comparison of Hilbert transform and wavelet methods for the analysis of neuronal synchrony. *J Neurosci Methods*. 2001;111(2):83–98.
205. Lachaux JP, Rodriguez E, Martinerie J, et al. Measuring phase synchrony in brain signal. *Hum Brain Mapp*. 1999;8:194–208.
206. Tass P, Rosenblum MG, Weule J, et al. Detection of n:m phase locking from noisy data: application to magnetoencephalography. *Phys Rev Lett*. 1998;81:3291–3294.
207. Rodriguez E, George N, Lachaux JP, et al. Perception’s shadow: long-distance synchronization of human brain activity. *Nature*. 1999;397(6718):430–433.
208. Trujillo LT, Peterson MA, Kaszniak AW, et al. EEG phase synchrony differences across visual perception conditions may depend on recording and analysis methods. *Clin Neurophysiol*. 2005;116(1):172–189.
209. Pernier J, Perrin F, Bertrand O. Scalp current density fields: concept and properties. *Electroencephalogr Clin Neurophysiol*. 1988; 69(4):385–389.
210. Nunez PL, Pilgreen KL. The spline-Laplacian in clinical neurophysiology: a method to improve EEG spatial resolution. *J Clin Neurophysiol*. 1991;8(4):397–413.
211. Nunez PL, Silberstein RB, Cadusch PJ, et al. A theoretical and experimental study of high resolution EEG based on surface Laplacian and cortical imaging. *Electroencephalogr Clin Neurophysiol*. 1994;90:40–57.
212. Pascual-Marqui RD, Michel CM, Lehmann D. Low resolution electromagnetic tomography: a new method for localizing electrical activity in the brain. *Int J Psychophysiol*. 1994;18:49–65.
213. Pascual-Marqui RD. Standardized low resolution brain electromagnetic tomography (sLORETA): technical details. *Methods Find Exp Clin Pharmacol*. 2002;24D:5–12.
214. Bosch-Bayard J, Valdés-Sosa P, Virues-Alba T, et al. 3D statistical parametric mapping of EEG source spectra by means of variable resolution electromagnetic tomography (VARETA). *Clin Electroencephalogr*. 2001;32(2):47–61.
215. Kalitzin SN, Parra J, Velis DN, et al. Enhancement of phase clustering in the EEG/MEG gamma frequency band anticipates transitions to paroxysmal epileptiform activity in epileptic patients with known visual sensitivity. *IEEE Trans Biomed Eng*. 2002;49:1279–1286.
216. Parra J, Kalitzin SN, Iriarte J, et al. Gamma-band phase clustering and photosensitivity: is there an underlying mechanism common to photosensitive epilepsy and visual perception? *Brain*. 2003;126:1164–1172.
217. Papoulis A. *Probability, Random Variables, and Stochastic Processes*. 9th ed. Tokyo: McGraw-Hill Kogakusha; 1965.
218. Boeijinga PH, Lopes da Silva FH. Modulations of EEG activity in the entorhinal cortex and forebrain olfactory areas during odour sampling. *Brain Res*. 1989;478(2):257–268.
219. Lopes da Silva F, Pijn JP, Boeijinga PI. Interdependence of EEG signals: linear vs. nonlinear associations and the significance of time delays and phase shifts. *Brain Topogr*. 1989; 2(1–2):9–18.
220. Pijn JP, Vijn PC, Lopes da Silva FH, et al. Localization of epileptogenic foci using a new signal analytical approach. *Neurophysiol Clin*. 1990;20(1):1–11.
221. Wendling F, Bartolomei F, Bellanger JJ, et al. Interpretation of interdependencies in epileptic signals using a macroscopic physiological model of the EEG. *Clin Neurophysiol*. 2001;112 (7):1201–1218.
222. Meeren HK, Pijn JP, Van Luijckelaar EL, et al. Cortical focus drives widespread corticothalamic networks during spontaneous absence seizures in rats. *J Neurosci*. 2002;22(4):1480–1495.

223. Bartolomei F, Wendling F, Régis J, et al. Pre-ictal synchronicity in limbic networks of mesial temporal lobe epilepsy. *Epilepsy Res.* 2004;61(1–3):89–104.
224. Uva L, Librizzi L, Wendling F, et al. Propagation dynamics of epileptiform activity acutely induced by bicuculline in the hippocampal–parahippocampal region of the isolated Guinea pig brain. *Epilepsia.* 2005;46(12):1914–1925.
225. Kalitzin SN, Parra J, Velis DN, et al. Quantification of unidirectional nonlinear associations between multidimensional signals. *IEEE Trans Biomed Eng.* 2007;54(3):454–461.
226. Guye M, Régis J, Tamura M, et al. The role of corticothalamic coupling in human temporal lobe epilepsy. *Brain.* 2006;129(pt 7):1917–1928.
227. Stam CJ, van Dijk BW. Synchronization likelihood: an unbiased measure of generalized synchronization in multivariate data series. *Physica D.* 2002;163:236–251.
228. Rulkov NE, Sushchik MM, Tsimring LS, et al. Generalized synchronization of chaos in directionally coupled chaotic systems. *Phys Rev E Stat Phys Plasmas Fluids Relat Interdiscip Top.* 1995; 51(2):980–994.
229. Micheloyannis S, Vourkas M, Bizas M, et al. Changes in linear and nonlinear EEG measures as a function of task complexity: evidence for local and distant signal synchronization. *Brain Topogr.* 2003;15(4):239–247.
230. Stam CJ, van der Made Y, Pijnenburg YAL, et al. EEG synchronization in mild cognitive impairment and Alzheimer’s disease. *Acta Neurol Scand.* 2003;108:90–96.
231. Roelfsema PR, Engel AK, König P, et al. Visuomotor integration is associated with zero time-lag synchronization among cortical areas. *Nature.* 1997;385(6612):157–161.
232. Granger CWJ. Investigating causal relations by econometric models and cross-spectral methods. *Econometrica.* 1969; 37, 24–39.
233. Fernandes de Lima VM, Pijn JP, Nunes Filipe C, et al. The role of hippocampal commissures in the interhemispheric transfer of epileptiform afterdischarges in the rat: a study using linear and non-linear regression analysis. *Electroencephalogr Clin Neurophysiol.* 1990;76(6):520–539.
234. Geweke J. Measurement of linear dependence and feedback between multiple time series. *J Am Stat Assoc.* 1982;77:304–324.
235. Kamiński M, Ding M, Truccolo WA, et al. Evaluating causal relations in neural systems: granger causality, directed transfer function and statistical assessment of significance. *Biol Cybern.* 2001; 85(2):145–157.
236. Korzeniewska A, Crainiceanu CM, Kuś R, et al. Dynamics of event-related causality in brain electrical activity. *Hum Brain Mapp.* 2008;29(10):1170–1192.
237. Ginter J Jr, Blinowska KJ, Kamiński M, et al. Propagation of EEG activity in the beta and gamma band during movement imagery in humans. *Methods Inf Med.* 2005;44(1):106–113.
238. Friston KJ, Tononi G, Reeke GN Jr, et al. Value-dependent selection in the brain: simulation in a synthetic neural model. *Neuroscience.* 1994;59(2):229–243.
239. David O, Harrison L, Friston KJ. Modelling event-related responses in the brain. *Neuroimage.* 2005;25(3):756–770.
240. Stephan KE, Harrison LM, Kiebel SJ, et al. Dynamic causal models of neural system dynamics: current state and future extensions. *J Biosci.* 2007;32(1):129–144.

EEG Mapping and Source Imaging

CHRISTOPH M. MICHEL AND BIN HE

INTRODUCTION

This chapter is concerned with the use of EEG as a functional imaging method. Great advancements have been made in the past several years in recording and analyzing of high-resolution EEG. Powerful EEG systems have been designed that allow fast and easy recording from hundreds of channels simultaneously, even in clinical settings. Sophisticated pattern recognition algorithms have been developed to characterize the topography of the scalp electric fields and to detect changes in the topography over time and between experimental or clinical conditions. New methods for estimating the sources underlying the recorded scalp potential maps have been constructed and applied to numerous experimental and clinical data. The incorporation of anatomical information, as obtained from magnetic resonance imaging (MRI) in the individual subject, has boosted the use of electrophysiologic neuroimaging and has stimulated clinical interest.

We will here discuss these recent developments and present the current state of the art in electrophysiologic neuroimaging, thereby extending other recent detailed reviews on this topic (1–6).

Neuronal activities in the brain generate current flows in the head volume conductor, reflected as electric potentials over the head surface, where they give rise to a specific topographical map. The proper recording and analysis of these maps are precursors for source localization. A great deal of localization information can already be derived from these maps, but their incorrect interpretation can also lead to a misleading conclusion about the putative generators. The second section of this chapter will deal with the proper recording of the scalp potential fields and the characterization, description, and statistical comparison of scalp potential maps. It will also summarize analysis methods that are based on spatiotemporal characteristics of potential maps, thereby leading to data reduction and a priori constraints for subsequent source localization.

The propagation of the electric potential in the brain that is generated by the active neuronal populations is modulated by the conductivity properties of the different tissues and by the shape of the head. If these parameters are known, the electric potentials that a given current source in the brain produces on the surface electrodes can be calculated. This so-called forward solution is the basis of every source localization method. The third section of the chapter will discuss the different head models and the current knowledge on head conductivities and their influence on the scalp potential maps.

EEG source localization has evolved from single dipole searching methods to distributed source estimation procedures without

any a priori assumption on the number of sources. However, solving the underdetermined inverse problem requires a priori assumptions based on information other than the number of sources, preferentially incorporating physiologic or biophysical knowledge. The correctness of these assumptions determines the correctness of the source estimation. The fourth section will discuss the different source reconstruction algorithms that are currently used and show examples of applications.

The spatial resolution of high-density EEG with sophisticated source localization methods in realistic geometry head models has become very impressive and the images that are produced are as tempting as pictures from other functional imaging methods, particularly because they show direct neuronal signaling rather than indirect metabolic changes. But EEG has a second important attraction: the high temporal resolution. This temporal resolution combined with electrophysiologic neuroimaging leads to the possibility to elucidate the temporal dynamics of neuronal signaling in large-scale neuronal networks and directly estimate network connectivity. The last section will discuss such analysis methods.

The power of EEG as a functional neuroimaging method is largely underestimated and many impressive experimental and clinical studies using these tools have not received the attention they merit. The reason is manifold. First, functional MRI has received a unique status of being able to reduce brain activity to the underlying sources nonambiguously. Second, misinterpretations of EEG and evoked potential waveforms due to a lack of understanding of the properties of electromagnetic fields, of the role of the reference electrode, and of the influence of non-neuronal signals such as myogenic or oculomotor activity resulted in a number of claims that later proved to be wrong. Third, the EEG is somehow harmed by history. The term EEG is still often related to the artistic interpretation of graph elements by some skilled neurophysiologists. The magnetoencephalogram (MEG) that basically measures the same neuronal activity with the same limitations does not suffer from this history and is easily considered as a neuroimaging method by public encyclopedias such as Wikipedia. With this chapter we would like to diminish this incorrect historical view and show that the EEG has considerably matured and can now be considered as a powerful, flexible, and affordable imaging technology.

MAPPING OF THE SCALP ELECTRIC FIELD

Electrophysiologic neuroimaging is based on the recording of the electric potential from a multitude of electrodes distributed over the surface of the head. From these simultaneous recordings a

potential map can be constructed for any single moment in time, depicting the momentary configuration of the potential field (7). The idea to analyze these topographies instead of waveform morphologies has already been formulated some decades ago (8–10) and has been called EEG topographical mapping. EEG mapping is a precursor to source imaging (11), and the proper analysis and interpretation of EEG maps can give a great deal of information with regard to the putative sources in the brain. Most importantly, by physical laws, different map topographies must have been produced by different source configurations in the brain (12). Thus, statistical methods that allow determining significantly different map topographies over time or between conditions or subjects provide important a priori hypotheses about whether and when differences in the source localization algorithms can be expected. Analysis of topographic maps is therefore an important step in electric source imaging (3).

Visualization and proper inspection of topographic maps is also mandatory for source imaging to assure that maps that are clean of artifact enter the algorithms. The quality of the maps determines the goodness of the source imaging procedures. It is therefore of crucial importance that these scalp potential fields are recorded and preprocessed in a reasonable manner, and that they are visualized and carefully inspected before applying source imaging algorithms to them. This particularly concerns EEG that is recorded in noisy environments such as in the MRI scanner. EEG waveforms that look correct after filtering and denoising do not yet necessarily indicate that the EEG maps will be correct and usable for source analysis.

In the following we discuss some practical issues related to the recording and construction of topographic maps. This concerns the number and the distribution of the electrodes on the scalp to provide an adequate spatial sampling of the potential field. It also concerns the parametric description of the map configuration and the comparison of map topographies in a global and reference-independent way. Further details can be found in Ref. 13.

Spatial Sampling

It is clear that proper sampling of the electromagnetic field over the whole scalp needs a large number of sensors. The MEG community has consequently quickly moved from low- to high-resolution systems, and most of the MEG laboratories are nowadays recording from over ~150 channels. Until recently, this was a severe limitation for the EEG, because application of a large number of electrodes was time consuming, uncomfortable, and expensive. However, this is not a limiting factor anymore. EEG systems of up to 256 electrodes are commercially available and are easy and fast applicable, even in clinical settings (Fig. 55.1) (14–17).

The question of how many electrodes are needed for proper EEG mapping and source imaging is not completely answered. It depends on the spatial frequency of the scalp potential field, which is limited by the blurring caused by volume conductor effects, particularly induced by the low conductivity of the skull (18). The maximal spatial frequency has to be correctly sampled to avoid aliasing, which appears when the frequency of the measured signal is higher than the sampling frequency. In the case of discrete sampling of time-varying signals, a sampling

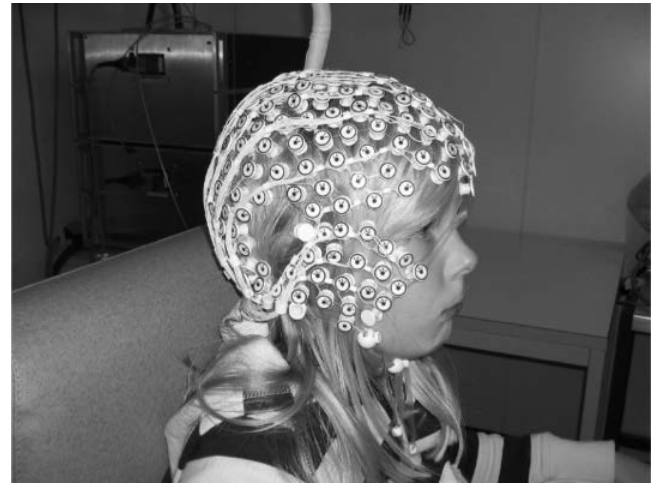


Figure 55.1 High-resolution EEG. Example of an EEG system that allows fast application of 256 electrodes. The electrodes are interconnected by thin rubber bands and each contains a small sponge that touches the subject's head directly (14). The nets are soaked in saline water before put on the subject's head. The whole net is applied at once and needs no skin abrasion and no electrode paste. (HydroCel Geodesic Sensor Net constructed by Electrical Geodesics Inc., Eugene, OR, USA.)

frequency that is twice as high as the highest frequency in the signal is required to avoid aliasing (Nyquist rate) (see also Chapter 54). Similar rules apply to sampling in space, since the potential distribution is only sampled at discrete measurement points (electrodes) (19,20). Spatial frequencies of the potential field that are higher than the spatial sampling frequency (i.e., the distance between electrodes) will distort the map topography (21–24) and will lead to misinterpretation of maps and consequently to mislocalization of the sources.

Already many years ago, researchers tried to estimate the maximal spatial frequency of the scalp electric field based on theoretical considerations and modeling. These works suggested that interelectrode distances of ~2 to 3 cm are preferable (25,26) for proper sampling of the field, which would lead to around 100 required electrodes. Freeman et al. (27) suggested from spatial spectral density calculations that even less than 1-cm spacing of electrodes is needed. Lantz et al. (28) and Michel et al. (3) performed simulations using dipole forward modeling (see section "EEG Forward Problem") to calculate the dipole localization error of different source localization algorithms when different number of electrodes were used. Both studies showed that the localization precision does not increase linearly, but reaches a plateau at about 100 electrodes for fully distributed inverse solution algorithms.

Several experimental studies used subsampling techniques to establish the number of electrodes needed to correctly reconstruct potential maps and localize the sources. Michel et al. (3) demonstrated incorrect lateralization of the source estimated for the P100 component of the visual-evoked potential when down-sampling from 46 to 19 electrodes, and that an incomplete coverage of the scalp surface can lead to complete misplacement of the sources (Fig. 55.2). Luu et al. (29) and Lantz et al. (28) used the

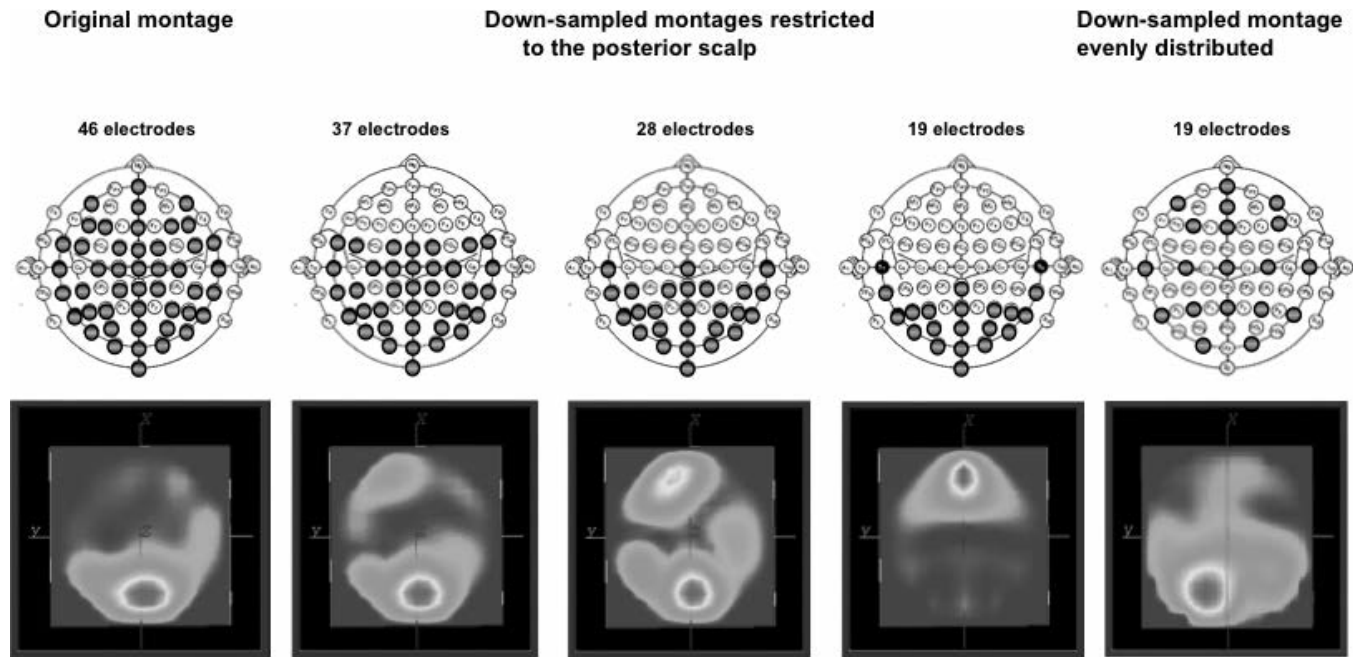


Figure 55.2 Spatial sampling. The figure illustrates the importance of proper sampling of the scalp potential field. Visually evoked potentials were recorded from 46 electrodes positioned according to the scheme on the left. A distributed source localization algorithm (LORETA) was applied to the data at the peak of the P100 component, resulting in a medial occipital source maximum. Data were then downsampled to fewer electrodes that were restricted to the posterior part of the head. The same localization procedure (with the same spherical head model) at the same time point led to incorrect localization, with even a frontal maximum with 19 occipital electrodes. Using again only 19 electrodes, but distributing them equally over the head as illustrated on the scheme on the right, leads to a complete sampling of the electric field and to a more correct localization. (From Michel CM, Lantz G, Spinelli L, et al. 128-Channel EEG source imaging in epilepsy: clinical yield and localization precision. *J Clin Neurophysiol.* 2004;21:71–83.) (See color insert)

downsample method in clinical data to evaluate the correctness of localization of pathologic activity. Luu et al. (29) studied patients with acute focal ischemic stroke recorded with 128 electrodes and downsampled to 64, 32, and 19 channels. Visual comparison of the EEG maps with radiographic images led to the conclusion that more than 64 electrodes were desirable to avoid mislocalizations of the affected region. More objectively was the downsample study of Lantz et al. (28) on 123-electrode recordings from patients with partial epilepsy. Fourteen patients with different focus localization were recorded before successful resective surgery; thus, the location of the epileptic focus was known. Several interictal spikes were manually identified and then downsampled to 63 and 31 electrodes. Source localization was applied to each single spike and the distance of the source maximum to the resected area was determined and statistically compared between the different electrode sets. Significant smaller localization error was found when using 63 instead of only 31 electrodes. Accuracy still systematically increased from 63 to 123 electrodes, but less significantly (Fig. 55.3).

The above-described studies estimate that around 64 or more electrodes are desirable for accurate spatial sampling and reconstruction of the scalp potential field. However, as shown by Ryyänen et al. (23,24) in computer simulation studies, these estimations are only valid if we assume a conductivity ratio of approximately 1:80 between skull and brain, as proposed by Rush

and Driscoll (30). These traditional values were used in the above-described simulation and downsampling studies, but they are most probably incorrect as indicated by several recent studies (31–33). If the conductivity of the skull is lower as it is proposed by these studies, the spatial blurring is smaller and the spatial frequency is higher. Ryyänen et al. (23,24) investigated the relation between the number of electrodes and the resistance values of the different compartments. Their computer simulation results suggest that if the 1:80 ratio is considered as correct, 64 to 128 electrodes are indeed sufficient. However, when more realistic skull conductivity values are used, a higher number of electrodes may be needed. More realistic values for the conductivity ratio are suggested to be between ~20 and 50 (34), depending on the skull thickness. In an experimental study of pediatric patients undergoing intracranial recordings, He and colleagues (35) measured the scalp and subdural potentials simultaneously during cortical current injection, and used them to estimate the brain-to-skull conductivity ratio. The experimental data suggested that the averaged brain-to-skull conductivity ratio is about 25 when using the three-sphere head model (33), and about 20 when using the realistic geometry finite element head model (35). In newborns the skull thickness is approximately seven to eight times lower than in adults, leading to a ratio of approximately 14:1 (20,36). Ryyänen et al. (24) suggested from their computer simulation studies that with this ratio, spatial resolution still increases with

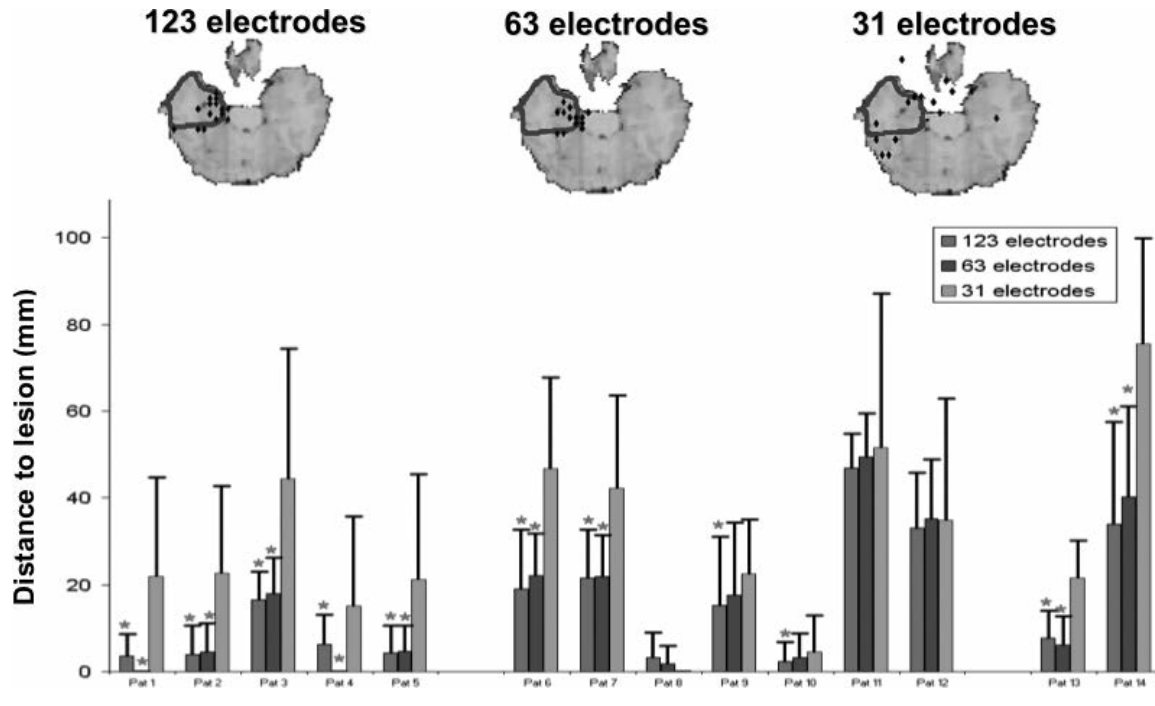


Figure 55.3 Influence of number of electrodes on source localization. Evaluation of source localization precision of interictal discharges in 14 epileptic patients, recorded with 123 electrodes. Single spikes were localized with a linear inverse solution in the individual brain and the distance of the source maximum to the resected area was measured. Mean and standard deviation of the distance were compared between the original high-resolution recording and with downsampling of the same data to fewer channels (but still equally distributed). The top row shows the example of one patient. The diamonds indicate the source maximum; the blue area marks the resected zone. Diamonds outside the brain are actually on another level and projected onto the illustrated slide. The bar graph shows the mean distance to the lesion. Stars indicate significant differences between the different number of electrodes. A clear significant amelioration of the localization precision was observed when increasing the number of recording channels. (From Michel CM, Brandeis D. Data acquisition and pre-processing standards for electrical neuroimaging. In: Michel CM, Koenig T, Brandeis D, et al., eds. *Electrical Neuroimaging*. Cambridge: Cambridge University Press; 2009. Modified after Lantz G, Spinelli L, Seeck M, et al. Propagation of interictal epileptiform activity can lead to erroneous source localizations: a 128 channel EEG mapping study. *J Clin Neurophysiol*. 2003;20:311–319.) (See color insert)

256 as compared to 128 electrodes in realistic noise levels. Grieve et al. (20) also suggested that a 256-electrode array is needed in infants to obtain a spatial sampling error of less than 10%. However, larger electrode arrays are also more influenced by measurement noise, which affects the spatial resolution. As suggested by Ryyänen et al. (23,24), the measurement noise is a critical limiting factor for the spatial resolution of high-density EEG systems. Thus, there is an important interplay between number of electrodes, measurement noise, and conductivity values of the different compartments of the head. Furthermore, it remains for the moment unclear how much an imperfect spatial sampling influences the source imaging. Some data did suggest that even with ~32 electrodes, one gains important insight about the underlying brain electric sources by performing source localization and imaging (37–40). Further studies with direct measurements of the conductivities at different locations on the head through current injection (41) or with the aid of MRI (42) will be needed to definitely answer the question of the head tissue conductivity. Further experimental and clinical studies shall also be needed to systematically investigate the question of optimal

number of electrodes that are needed to recover spatial features of scalp topography and to estimate the underlying brain sources that generate the scalp EEG.

Map Inspection, Artifact Correction, Interpolation

A mandatory requirement in EEG and ERP analysis is the detection and elimination of artifacts, caused by bad electrode contact, muscle or eye movement activity, or other environmental noise. Besides automatic detection of such artifacts using amplitude windows, careful visual inspection of the EEG traces is mandatory. These requirements evidently also hold for EEG mapping and source localization, but in addition to the need for clean EEG traces, the spatial EEG analysis also requires clean maps (13). Even if the EEG traces appear correct, they might be contaminated by noise that destroys the spatial configuration of the maps. Spatial inhomogeneities due to bad electrodes can drastically influence source localization outcome because they can lead to strong local gradients. Figure 55.4 illustrates this problem. In one case, the bad electrode is readily seen in the 256-channel EEG traces, and it is also easily seen in the topographic

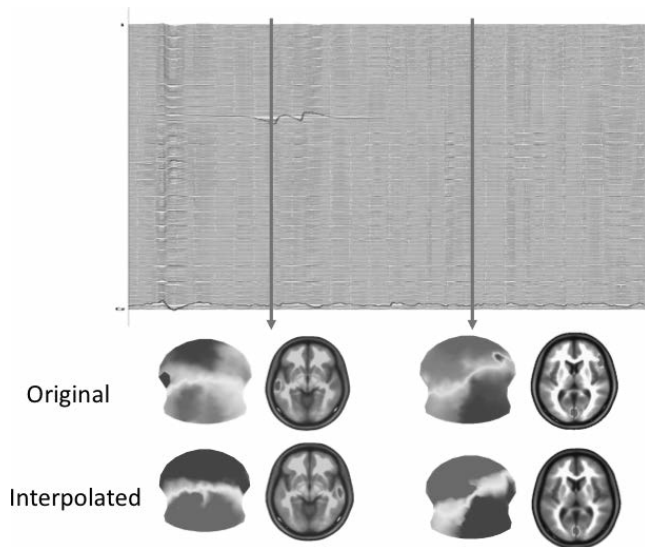


Figure 55.4 Influence of artifacts on source localization. Example of a 256-channel EEG recording and the reconstruction of the scalp potential map and the source estimation for this map using a distributed linear inverse solution (LAURA). The first time point (*left*) includes a clear artifact on a left temporal electrode, easily identifiable on the EEG traces and on the EEG map. This leads to a dominant source under this electrode position in the inverse solution. Excluding (or interpolating) this electrode leads to a dominant source on the contralateral temporal lobe. The artifact channel at the second time point (*right*) is not easily identifiable on the traces (artifact trace shown in red). However, the map clearly identifies this bad right frontal electrode with a negative potential surrounded by otherwise positive electrodes. Elimination of this bad electrode leads to a unique occipital source. Keeping the electrode for the inverse solution calculation leads to an additional right frontal source underlying this electrode. (Modified from Michel CM, Brandeis D. Data acquisition and pre-processing standards for electrical neuroimaging. In: Michel CM, Koenig T, Brandeis D, et al., eds. *Electrical Neuroimaging*. Cambridge: Cambridge University Press; 2009.) (See color insert)

map by a strong and isolated local potential minimum. The second bad channel is not easily seen in the traces and is not detected by an amplitude window. However, it is readily visible on the map by a negative “island” within the otherwise positive potential. Keeping these bad channels in the construction of the potential field leads to an incorrect estimation of a focal source under this electrode, which completely disappears when these electrodes are taken out.

This example illustrates the importance of inspecting not only the EEG traces for abnormal graph elements, but also the potential maps for abnormal topographies. It is thereby important that the recording reference is included in the electrode array for map construction, because also the reference electrode is an active electrode and has to be inspected for abnormal values. The most convincing example has been demonstrated by Yuval-Greenberg et al. (43), showing a map with a very steep potential maximum at the nose reference. This was due to the recording of miniature saccades by this “noncephalic” reference electrode. This becomes readily visible when looking at the map,

but is ignored and misinterpreted as occipital gamma activity when looking at single occipital electrodes that were recorded against this nose reference (43).

When data are averaged over sweeps or over subjects, bad electrodes must be interpolated before averaging. Most of the commonly used interpolation routines belong to the family of spline interpolations. Spline interpolations can be linear (based on a polynomial of first degree), or quadratic, cubic, or of higher order. Using cross-validation tests, it was concluded that higher order spherical spline interpolations perform reasonably well in sufficiently dense electrode arrays (44,45). The estimation of potentials is less reliable when the potentials are located outside of the electrode array and not between some electrodes. Extrapolating potentials beyond the electrode array should thus be avoided.

Efficient algorithms to detect and eliminate artifacts based on “abnormal” spatial configurations are increasingly used in EEG mapping and source localization studies. Most efficient are algorithms based on independent component analysis (ICA) (46). The ICA is particularly useful for eye movement artifact detection and elimination, because the artifact is largely independent from the remaining part of the data.

Topographic Analysis

The traditional analysis of EEG and evoked potentials relies on waveforms. Parameters of interest are thereby changes in amplitude or frequency, or peaks at certain latency time-locked to stimulus presentation. These measures are ambiguous because the EEG is by definition a bipolar signal. Changes of the location of one of the two electrodes will change the values of the above parameters. This ambiguity is well known and has led to a large discussion on the reference-dependency of the EEG and the question of the correct recording reference for a certain experimental or clinical condition (47–51).

This reference problem of the EEG is completely resolved when topographic analysis methods are applied. The potential map topography does not depend on the reference (3,50,52–54). The reference only changes the zero level, but the topographical features of the map remain unaffected (53). Thus, the reference only introduces a DC shift. This shift is eliminated when applying topographic analysis methods including source imaging. Elimination of the DC level can be achieved by calculating the so-called common average reference at each moment in time (9).

One way to sharpen the spatial details of the scalp potential maps is to calculate the scalp current source density, or the surface Laplacian of the potential (21,55,56). The surface Laplacian of the scalp potential is the second spatial derivative of the potential field in the local curvature in $\mu\text{V}/\text{cm}^2$. The surface Laplacian has been mainly derived from unipolar potential recordings on the scalp, using algorithms such as finite difference algorithm (57), spherical spline algorithm (58), or realistic geometry spline algorithm (59). The surface Laplacian has been widely used in applications when one wishes to enhance the sensitivity to local activity. It can be interpreted as an estimation of the current density entering or exiting the scalp. It emphasizes superficial sources because deeper sources produce smaller potentials on the surface. Like the other topographic measures that will be described below,

the surface Laplacian estimates are independent of the position of the recording reference, because the potential common to all electrodes is automatically removed (60).

Scalp potential maps can be characterized by their strength and their topography. A reference-independent measure of map strength is the global field power (GFP) (8). GFP is the standard deviation of the potentials at all electrodes of an average-reference map. It is defined as

$$\text{GFP} = \sqrt{\frac{\sum_{i=1}^N (u_i - \bar{u})^2}{N}} \quad (55.1)$$

where u_i is the voltage of the map u at the electrode i , \bar{u} is the average voltage of all electrodes of the map u , and N is the number of electrodes of the map u . Scalp potential fields with pronounced peaks and troughs and steep gradients, that is, very “hilly” maps, will result in high GFP, while GFP is low in maps that have a “flat” appearance with shallow gradients. GFP is a one-number measure of the map at each moment in time. Displaying this measure over time allows to identify moments of high signal-to-noise ratio, corresponding to moments of high global neuronal synchronization (61).

A reference-independent measure of topographic differences of scalp potential maps is the so-called global map dissimilarity measure (GMD) (8). It is defined as

$$\text{GMD} = \sqrt{\frac{1}{N} \sum_{i=1}^N \left\{ \frac{u_i - \bar{u}}{\sqrt{\sum_{i=1}^N (u_i - \bar{u})^2 / N}} - \frac{v_i - \bar{v}}{\sqrt{\sum_{i=1}^N (v_i - \bar{v})^2 / N}} \right\}^2}$$

where u_i is the voltage of map u at the electrode i , v_i is the voltage of map v at the electrode i , \bar{u} is the average voltage of all electrodes of map u , \bar{v} is the average voltage of all electrodes of map v , and N is the total number of electrodes. In order to assure that only topography differences are taken into account, the two maps that are compared are first normalized by dividing the potential values at each electrode of a given map by its GFP.

The GMD is 0 when two maps are equal, and maximally reaches 2 for the case where the two maps have the same topography with reversed polarity. It can be shown that the GMD is equivalent to the spatial Pearson's product-moment correlation coefficient between the potentials of the two maps to compare (62).

If two maps differ in topography independent of their strength, it directly indicates that the two maps were generated by a different configuration of sources in the brain (4,11,63). The inverse is not necessarily true: infinite number of source configurations may produce the same scalp potential topography (12). The GMD calculation is therefore considered as a first step for defining whether different sources were involved in the two processes that were compared. When comparing subsequent maps in time using the GMD, periods where source configuration changes appeared can be defined. It is interesting to note

that the GMD inversely correlates with the GFP: GMD is high when GFP is low, that is, maps tend to be stable during high GFP and change the configuration when GFP is low (Fig. 55.5). The GMD is itself not a statistical measure. However, if two groups of maps are compared, a statistical statement of the significance of the topographic differences can be made. This is achieved by performing nonparametric randomization tests based on the GMD values as, for example, described in Ref. 54.

Spatiotemporal Decomposition

Source localization procedures can be applied to multichannel EEG and ERP data at any instant in time. With the high sampling rate of modern EEG systems that easily exceed 1000 Hz, this leads to a large amount of data from which the relevant information has to be extracted. Consequently, experimenters typically predetermine relevant events within a continuous time series of data to which source analysis will be applied. This particularly concerns ERP research, where peaks in certain time windows at certain electrodes are identified and spatially analyzed (64). This traditional approach is however less tenable with high-density EEG and ERP recordings, because different scalp sites have different peak latencies, and because the waveforms (and thus the peaks) at certain electrodes change when changing the position of the reference electrode.

An alternative to the traditional preselection of relevant events based on ERP waveforms is to define components on the basis of the topography of the potential field (65). Most commonly, some kind of spatial factor analysis methods are used for this purpose. These methods produce a series of factors that represent a weighted sum of all recorded channels across time. The aim of this factor analysis approach is to find a limited number of optimal factors that best represent a given data set. The load for each of these factors (i.e., the goodness of fit) then varies in time. Each factor represents a certain potential topography, that is, a prototypical map. Source localization applied to these maps results in a limited number of putative sources in the brain that explain a full time series of multichannel EEG data with time-varying strength.

The most commonly used variant of spatial factor analyses is the *principal component analysis* (PCA) (66–69). The first factor of the PCA solution accounts for the maximally possible amount of data variance, and each next orthogonal factor accounts for the maximum possible residual variance. Since factors that contribute little to the explained variance can be neglected, the PCA is a powerful exploratory tool to reduce complex multichannel EEG data in space and time. It has been repeatedly applied to ERP studies with the aim to extract ERP components whose variance is related to a given experimental condition. It can provide useful information on how a given experimental manipulation affects ERP components without any a priori assumption about the shape or number of components in the data set (69–73).

The PCA does not allow for cross-correlations between activities corresponding to separate factors and thus excludes linear dependencies between the factor maps. However, it does not exclude dependencies based on higher order correlations. The factor analysis method that also removes these higher order relations is called independent component analysis (ICA) (74). The

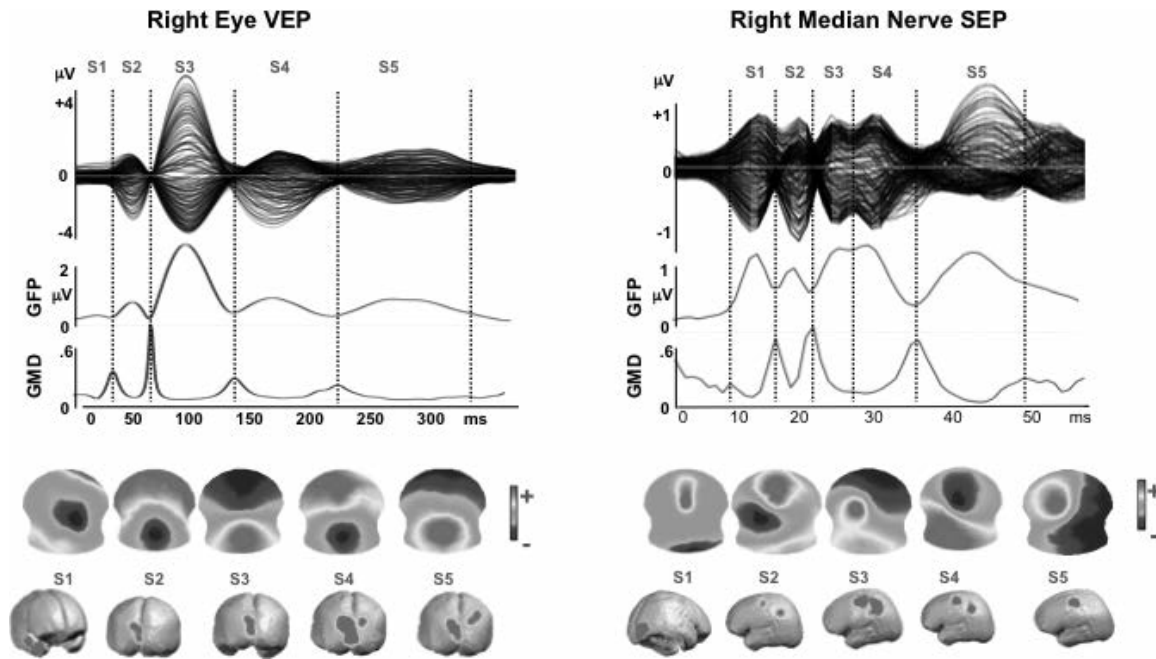


Figure 55.5 Spatial analysis of evoked potentials. Example of 256-channel visual-evoked potential (VEP) and somatosensory-evoked potential (SEP). VEP from full-field checkerboard reversal presented to the right eye only (*left eye covered*). SEP from electric stimulation of the right median nerve. Data represent the grand mean of over 20 subjects. **Top row:** Overlaid traces of all 256 channels against the average reference. **Second row:** Global field power curve (GFP) as a measure of field strength indicates five dominant peaks in both evoked potentials. **Third row:** Global map dissimilarity curve (GMD) measuring topography differences between successive time points. It shows low values during extended periods and sharp peaks at moments of low GFP. **Fourth row:** Potential maps (*seen from top, nose up, left ear left*) that were derived from a *k*-means cluster analysis of the whole data sets. In both EPs, five maps best explained the data. Each one dominated a given period as determined by spatial correlation analysis. Vertical dashed lines mark these periods. **Last row:** Distributed linear inverse solution applied to each of the five maps, revealing activation and propagation of visual and sensor-motor cortex, respectively. Note that the first period represents extracortical activity in both cases (activity in the right retina for the VEP and in the brainstem for the SEP). Both areas were not included in the solution space, consequently leading to incorrect localization in the source estimation. (For more details see Ref. 106.) (See color insert)

objective of the ICA is sometimes illustrated by the so-called “cocktail party problem,” where the ICA allows decomposing a sound record from a party into the independent contributions of the individual persons. Like the PCA, the ICA produces a weight coefficient for each factor. Each factor is supposed to represent a temporally independent component.

As described earlier, the ICA can be very useful for detecting and removing artifacts such as eye blinks (46), or artifacts produced by brain-independent sources such as the ballistocardiogram artifact of the EEG recorded in an MRI scanner (75–77), although negative results have been reported as well (78–80). More critical is the idea of decomposing the brain processes into a number of statistically independent factors (74,81) because it implies that there are indeed a similar number of independent processes in the brain.

An alternative to the above-described component analysis approaches is the so-called microstate segmentation method (82). It is based on the highly reproducible observation that the topography of the EEG or ERP potential maps remains stable for several tens of milliseconds and then abruptly switches to a new configuration in which it remains stable again. This can easily be

seen in the ERP examples in Figure 55.5 by the stable low global dissimilarity (GMD) over extended time periods separated by sharp dissimilarity peaks indicating periods of topographic change. The same observation holds for spontaneous EEG, if polarity inversion caused by the intrinsic oscillatory activity of the generator processes is ignored (Fig. 55.6) (83–86). This fundamental observation led to the proposal to apply cluster analysis to the data set to identify a set of topographies that explain a maximum amount of the variance of the data (87). The difference to the above-described factor analysis approach is that the microstate model allows only one single topography to occur at one moment in time. Evidently, each topography can represent multiple simultaneously active sources, but they are active together for a certain time period, forming a large-scale neuronal network configuration that is expressed as unique stable map topography. During the period of stable topography, the strength of the field varies, indicating different level of synchronization of the simultaneously active areas. In contrast to the ICA-based models of independent brain processes that overlap in time, the microstate model proposes one global brain state per time period, consisting of an interdependent and synchronized

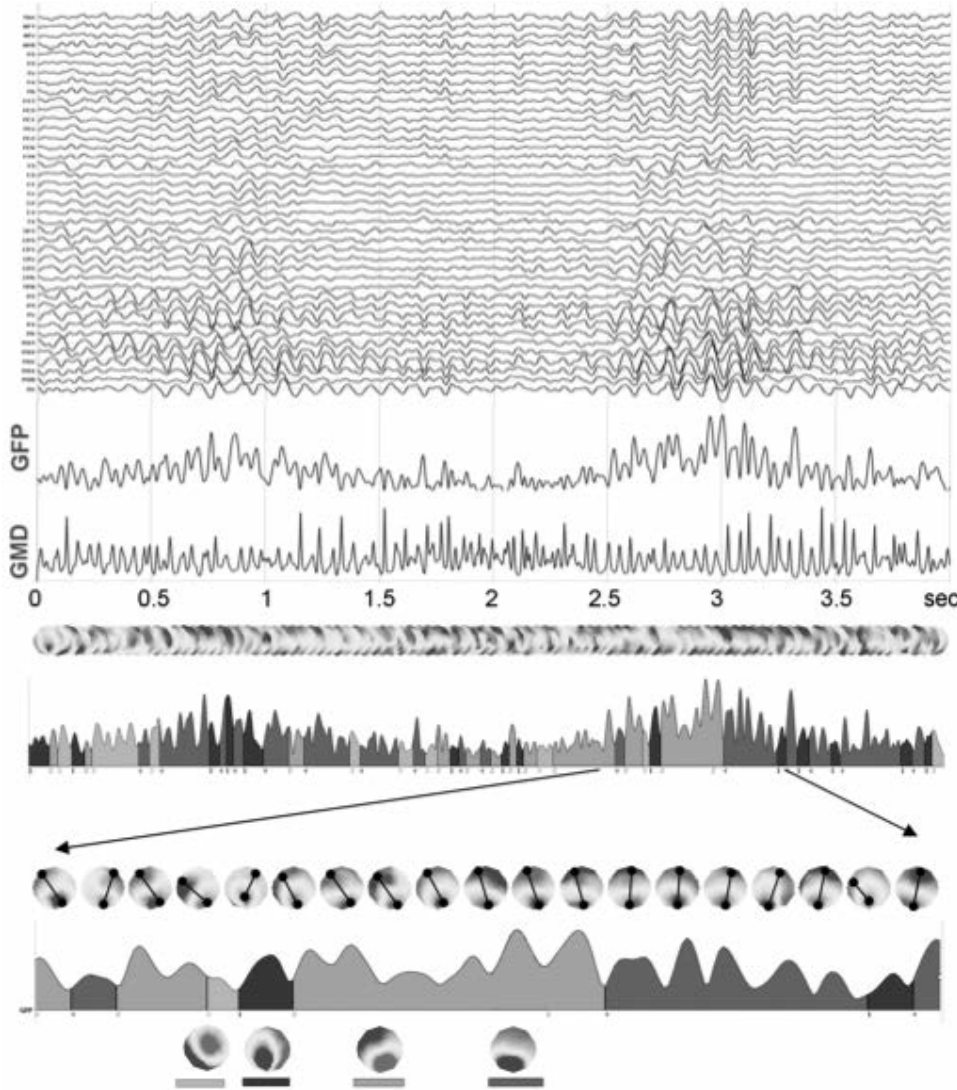


Figure 55.6 Microstate segmentation of spontaneous EEG. Four seconds of eyes-closed EEG measured from 42 electrodes are shown on top. The two blue curves represent the global field power (GFP) and the global map dissimilarity, respectively. A series of potential maps illustrate the data that has been submitted to a k -means cluster analysis with ignoring strength and polarity. Four maps best explained the whole 4 seconds of data. The four maps are illustrated on the bottom. On the GFP curve below the map series, the time periods during which each map was dominant are marked in different colors. A shorter period is zoomed in and all maps during this period are shown. Marking and connecting the extreme potentials illustrates the stability of topography during each period. (From Michel CM, Brandeis D. Data acquisition and pre-processing standards for electrical neuroimaging. In: Michel CM, Koenig T, Brandeis D, et al., eds. *Electrical Neuroimaging*. Cambridge, MA: Cambridge University Press; 2009.) (See color insert)

network (88). This corresponds well to the neuronal workspace model, which suggests that episodes of coherent activity last a certain amount of time (around 100 msec) and are separated by sharp transitions (89,90), as well as to the proposal that neurocognitive networks evolve through a sequence of quasistable coordination states rather than a continuous flow of neuronal activity (91–93). Cross-validation methods following cluster analysis have shown that a very limited number of map topographies are needed to explain extended periods of spontaneous EEG, and that these few configurations follow each other according to certain rules (85,87). Changes in the succession and duration of the microstates have been observed in several pathologic conditions such as depression (94), dementia (95,96), schizophrenia (97,98), and epilepsy (99), as well as after drug intake (100,101). In normal subjects, the duration and frequency of appearance of the four most dominant microstate configurations varies with age (86). Concerning ERPs, the cluster analysis is an efficient way to determine different ERP components exclusively on the basis of their topography (73,87,102,103). Statistical specificity of these component maps for different experimental conditions can then be assessed by spatial fitting procedures using the

global dissimilarity as metric (54,104,105). Such methods can be used for an objective analysis of clinical evoked potentials, for example, in multiple sclerosis (106). They have been used in numerous experimental ERP studies on sensory and cognitive information processing and have allowed creating a microstate dictionary for different brain functions (107–115). Source localization applied to these microstate maps has proven to be an efficient way to describe those brain areas that are crucially implicated in the processing of stimuli and that differ depending on the task demands (Fig. 55.5) (103).

EEG FORWARD PROBLEM

In this section, we introduce the methods for solving the so-called EEG forward problem, which deals with (i) how to model the neuronal excitation within the brain volume and (ii) how to model the head volume conduction process in order to quantitatively link neuronal electric sources with the electric potentials over the scalp. Solving the EEG forward problem can help understand the relationship between neuronal sources and the recorded EEG signals, and is also an integrative part of the EEG

inverse problem, which will be discussed in the section “EEG Inverse Problem.”

Source Models

The primary sources of EEG are considered to be the postsynaptic currents flowing through the apical dendritic trees of cortical pyramidal cells. Such neuronal currents, when viewed from a location on the scalp surface that is relatively remote to where the neural excitation takes place (far field), can be modeled as an electric current dipole composed of a pair of current source and sink with infinitely small interdistance. When the brain electric activity is confined to a few focal regions, each of these focal areas of neuronal excitation may be modeled as an equivalent current dipole (ECD) based on the far field theory (for a theoretical treatment see the appendix in Chapter 5). Such equivalent dipole model has been widely used in source localization analysis of EEG in an attempt to better interpret the origins of the scalp-recorded EEG (116–120). While the ECD is a simplified model and higher order equivalent source models such as the quadrupole have also been studied to represent the neural electric sources (121,122), the dipole model has been so far the most commonly used brain electric source model. A number of experimental and clinical studies have demonstrated its merits in helping interpreting EEG data and localizing sources generating the scalp-recorded EEG.

When the neuronal sources are no longer confined to a few focal regions, the ECD model may not well represent the distributed brain electric activity. Distributed current source models can then be used to represent the whole-brain bioelectric activity. The essence of the distributed current source models is to model the neuronal activities over a small region by a current dipole located at each region. The brain activity with any distribution of neuronal currents can be approximately represented by a source model consisting of a distribution of current dipoles that are evenly placed within the entire brain volume. At each location, three orthogonal dipoles are used in that the weighted combination of them is capable of representing an averaged current flow with an arbitrary direction in the region. Such source model is usually called volume current density (VCD) model, in which current dipoles distribute over the entire brain volume (123). The brain anatomical information can also be used to constrain the current source space to the cortical gray matter due to its dominant presence of large pyramidal cells. Such anatomical constraints can be obtained from existing structural neuroimaging modalities, particularly T1-weighted MRI, which provides high spatial resolution and a great contrast to differentiate the cortical gray matter from the white matter and cerebrospinal fluid (CSF). The current source orientations can be further constrained to be perpendicular to the cortical surface, because the columnar organization of neurons within the cortical gray matter constrains the regional current flow in either outward or inward normal direction with respect to the local cortical patch (124), and the gray matter thickness (about 2 to 4 mm) is much smaller relative to the “source-to-sensor” distance (60). Under such cortical constraints, such source model is usually called cortical current density (CCD) model, in which current dipoles distribute over a surface in parallel to the epicortical surface.

All of the above current source models are often referred to as distributed current density models. Physically, any bioelectric source activity can be represented by a continuous distribution of primary current density. Mathematically, the current density and current dipole share the identical form of equations for computing the extracellular potential, supporting the use of distributed current dipoles to approximate the continuous current density distribution. The dipole distribution may be viewed as discretized version of the continuous current density distribution in the space domain. Each of such current dipoles represents the regional neuronal activity, and the dipole amplitude indicates the amount of synchronized neuronal activity in the local region.

In addition to current dipole-based source models, the current monopole model (125) was also used to equivalently represent brain electric activity. Mathematically, such current monopole model can also represent the source activities in a sense that it produces almost the same electric potentials on the scalp electrodes. However, the biologic interpretation of such monopole source model remains unclear. Another alternative source model is based on the estimation of the three-dimensional (3D) distribution of the intracranial potentials instead of the three components of a dipole, as proposed in the ELECTRA source imaging technique (102,126). It is based on the neurophysiologic consideration that ohmic currents dominate the EEG measurements (127). While such 3D potential estimation more closely resembles intracranial recordings, their biologic interpretation is as difficult as the estimation of current monopoles.

Volume Conductor Models

When the source model is determined, the EEG forward problem consists of obtaining the distribution of electric potential Φ on the scalp surface, given any known distribution of current density \vec{J} inside the brain as well as conductivity values throughout the head volume. Such solution is usually called EEG forward solution for a given head volume conductor model. The head volume conductor model refers to our assumption on the shape and conductivity properties of the tissues of the head. Head volume conductor models include the infinite homogeneous model, single-sphere model, three concentric-sphere model, four concentric-sphere model, realistic geometry homogeneous head model, realistic geometry multicompartiment head model, and realistic geometry inhomogeneous head model.

The simplest EEG forward solution is that in the infinite homogeneous model, where the entire space is assumed to be occupied by a homogeneous conductive medium (4,127). The electric potential over the scalp electrodes can then be given as

$$\Phi = \frac{1}{4\pi\sigma} \int_V \nabla \left(\frac{1}{r} \right) \cdot \vec{J}^i dv \quad (55.3)$$

where the source element $\vec{J}^i dv$ behaves like a dipole source, with a field that varies as $1/r^2$, and ∇ represents the divergence operator (see the appendix in Chapter 5). The impressed current density \vec{J}^i , representing neuronal currents, may be interpreted as an equivalent dipole source density, which behaves as

a fundamental driving force establishing the electric potentials within the head volume conductor with an electric conductivity σ .

A more reasonable representation of head is the series of spherical models, including a single-sphere model (128), three concentric-sphere model (30,55,129), and four concentric-sphere model (130,131). In these spherical models, the shape of the head is approximated by spherical surfaces, including the scalp, the skull surface, the brain surface, etc. In such cases, the electric potentials over the scalp surface (the outer sphere) due to a current dipole can be derived analytically for the single-sphere model, or by use of special function for the multisphere models. Since the low-conductivity skull layer smears significantly the electric potential, the three-sphere model (brain, skull, and scalp), in which the skull layer is incorporated, has been used widely and found to be a good approximation to the head volume conductor when the shape of the head is ignored. Furthermore, the CSF layer can also be incorporated as in the four-sphere model (130), although there is no converging agreement that the CSF layer must be incorporated when modeling the head volume conductor.

We should note that the influence of the inhomogeneities of the tissues of the head as volume conductor affect differently the EEG and the MEG, since the brain and surrounding tissues behave as a medium with constant magnetic permeability. The magnetic field, in contrast to the electric field, is not influenced by the tissue inhomogeneities, for a given primary current density distribution (the current density distribution solely induced by neuronal activation). In particular, for concentric spherical head models, MEG is not influenced by the concentric layers. However, when the realistic geometry of head tissue is taken into consideration, existence of head tissue inhomogeneities introduces secondary current sources, which in turn affect the magnetic field out of the scalp. See also discussion in the appendix of Chapter 5 and in Chapter 42.

A major disadvantage of the spherical head model is that it does not make any distinction between areas that generate electric activity (gray matter) and those that do not (white matter and ventricles). Constraining the source space to the gray matter of the individual brain is an important anatomical constraint that improves the accuracy of the EEG forward solution. A simple straightforward way is to map the individual segmented MRI to a sphere and use the analytical multishell spherical model described above, but with the solution space constrained to the individual gray matter (132).

More advanced EEG forward solutions have used numerical techniques to take both the conductivity inhomogeneity and the geometry of the head into consideration. The most popular EEG forward solution is based on the boundary element method (BEM) (118,133,134). He et al. (118) first reported the use of BEM in solving the EEG forward and inverse problems using a realistic geometry homogeneous head model. The low-conductivity skull layer was incorporated later by the studies of Hämäläinen and Sarvas (133) and Meijs et al. (134). In particular, the numerical treatment of the low-conductivity skull layer developed by Hämäläinen and Sarvas (133) made the BEM forward solution widely used for EEG as well as MEG studies. An

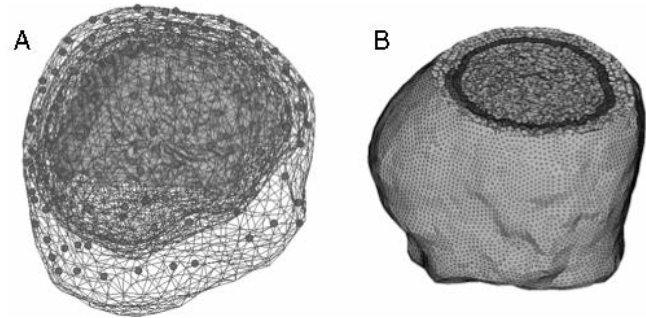


Figure 55.7 A: A realistic geometry multishell boundary element head model as derived from structure MRI of a human subject (207). The scalp, skull, and brain surfaces are represented by a number of surface triangles. Brown and blue surfaces refer to the right and left cortical surfaces. Pink circles refer to the scalp electrodes. B: A realistic geometry inhomogeneous finite element head model as derived from structure MRI and CT of a human subject (139). Green, gray, blue, and brown regions refer to the scalp, skull, CSF, and brain. Red refers to the subdural pad of ECoG electrode array, which has low electric conductivity. The red layer is not displayed continuously in this figure due to the angle of view. (From Liu ZM, He B. FMRI-EEG integrated cortical source imaging by use of time-variant spatial constraints. *NeuroImage*. 2008;39(3):1198–1214 [Panel A], and Zhang Y, van Drongelen W, Kohrman M, et al. Three-dimensional brain current source reconstruction from Intra-cranial ECoG recordings. *NeuroImage*. 2008;42:683–695 [Panel B]). (See color insert)

example of three-shell BEM head model is illustrated in Figure 55.7A, as derived from structural MRI of a human subject.

In addition to the BEM that provides forward solutions when the head can be modeled by multicompartiment model of homogeneous conductivity profiles within each compartment, the finite element method (FEM) has been further used to handle the inhomogeneous conductivity distribution within the head (135–139). Figure 55.7B shows an example of a FEM head model of a patient undergoing subdural recordings. The FEM modeling allows proper handling of inhomogeneity of head tissues including the surgical alteration such as the very low-conductivity subdural pad of ECoG electrodes. The FEM forward solutions enable incorporating the realistic geometries and inhomogeneous conductivities of the head, even allowing inclusion of the anisotropic conductivity distribution of the white matter (140). The challenge of using FEM to solve EEG forward problem is not the FEM algorithm, which has been fairly well developed, but the need to build a FEM mesh model of the head from MRI or CT images. Nowadays this is still a labor-consuming effort to build FEM head models from a subject's MRI. Alternative efforts, such as the finite difference method (FDM), have been reported to solve the EEG forward problem in which the finite difference grids can be reasonably easily built from MRI of a subject. However, it is still not a straightforward procedure to automatically segment and classify head tissues into the FDM model. For recent review of image segmentation for the purpose of solving the EEG forward problem, see Ref. 141. All of these numerical techniques have to utilize the anatomical information provided by other structural imaging modalities, particularly T1- and proton density-weighted MRI, in

order to segment different brain tissues (i.e., the gray matter and the white matter) and head structures (i.e., CSF, skull, and scalp). Sometimes, CT is used together with MRI to obtain structure information of the skull. Image segmentation remains to be an important task in realistic geometry inhomogeneous head modeling regardless of the numerical algorithms to be used.

In addition, recent development of diffusion tensor magnetic resonance imaging (DT-MRI) (142) provides a means to estimate the anisotropic conductivity of the cerebral white matter (137,143,144), which may further improve the accuracy of the EEG forward solution. The white matter anisotropy is caused by the bundled axon fibers that restrict the direction of ionic movements (137). While a computer simulation study (137) suggested that the white matter conductivity anisotropy may have effects to EEG forward and inverse solutions, a recent experimental study suggested otherwise. He and colleagues (140) conducted a human study to localize the sources in primary visual cortex using the single dipole solution and compared with the fMRI activation under the same visual stimuli in the same subjects. Their results indicated that use of the anisotropic white matter model did not return significantly different solution as that using the isotropic white matter model. Further investigation is needed to examine the effects of white matter anisotropy in other brain regions.

EEG INVERSE PROBLEM

The EEG inverse problem shall be considered as to reconstruct brain electric sources from scalp-recorded EEG signals. In experimental and clinical studies, it is desirable to image the neuronal activity that generates recordable scalp EEG signals. When the neuronal activity is localized in few focal regions within the brain, the problem becomes to localize the locations of such activated focal regions, which is usually referred to as source localization. For example, source localization has been found useful in localizing epileptogenic foci in epilepsy patients. On the other hand, when the brain activity is not localized in a few focal areas, one needs to image the distribution of neural electric sources within the brain. Such problem becomes the so-called source imaging, which shall include source localization since focal sources are special cases of distributed sources.

As opposed to the uniqueness of the forward solution, the EEG inverse solution is nonunique if no constraints are given due to the low frequency nature and the limitation of EEG recordings over the scalp surface only. This nonuniqueness issue has represented a great challenge to the field. Over the past two decades, a number of efforts have been made to tackle these challenges and it is encouraging that we have learnt that it is possible to obtain valid estimates of solutions of the EEG inverse problem if reasonable constraints are given on the equivalent source distribution. For example, if the brain electric sources are assumed to consist of few moving ECDs (117,118), or a current dipole distribution over the cortex with orientation being perpendicular to the local curvature of the cortex (124), or a current dipole distribution over the brain volume with smoothness a priori (123), in such cases solutions of the EEG inverse problem can be estimated yielding results that are consistent with other findings of clinical

neurophysiology and neuroscience. Another challenge existing in the EEG inverse problem is that it is ill-posed from the viewpoint of numerical treatment. This ill-posedness of the inverse problem is handled by various signal processing strategies, which has led to great success in the field.

In this section we will discuss the EEG inverse problem in the following aspects: (i) dipole source localization (DSL); (ii) source scanning; (iii) distributed source imaging; and (iv) multimodal imaging integrating EEG source imaging with functional MRI.

Dipole Source Localization

The most classic EEG inverse problem shall be the so-called DSL. Such DSL approach is applicable when the primary generators of scalp-recorded EEG signals are localized to one or few small regions within the brain. Given a specific dipole source model, DSL can yield solutions of the EEG inverse problem by using a nonlinear multidimensional optimization procedure, to estimate the dipole parameters that can best explain the observed scalp potential measurements in a least-square sense (116–118, 120,145–147). Further improvement of the DSL can be achieved by combining EEG with MEG data that may increase information content and improve the overall signal-to-noise ratio (148,149), or integrated with functional MRI (see the section “Multimodal Integration of EEG with fMRI” for details).

The EEG DSL can be solved either from the scalp-recorded EEG at a given time instant or over a time period. The single time-slice source localization estimates the dipole parameters based on the single time “snapshots” of the measured scalp EEG (120). In practice, an initial starting point (also termed seed point) is selected, then using an iterative procedure, the assumed dipole sources are moved around inside the brain volume in an attempt to produce the best match between the measured and dipole-produced scalp electric potentials. This involves solving the forward problem repetitively and calculating the difference between the measured scalp potential vector $\vec{\varphi}$ and the model-predicted scalp potential vector $\vec{\psi}$ at each step. The most commonly used measure is the squared distance between the two vectors, which is given by

$$D = \|\vec{\varphi} - \vec{\psi}\|^2 \quad (55.4)$$

where D is the objective function that is to be minimized (equal to GMD if normalized). The EEG dipole inverse solution is obtained when this objective function is minimized. Due to the effect of measurement noise, usually one can only estimate one or two moving equivalent dipoles by use of the DSL approach. In addition, reciprocal approaches have also been explored in solving the DSL, in an attempt to improve the numerical accuracy of the transfer matrices (150).

The EEG DSL can also be solved from spatiotemporal EEG measurements, which is sometimes termed spatiotemporal source localization (117). In this approach, multiple dipole sources are assumed to have fixed locations inside the brain during a certain time interval, and the variations in scalp potentials are due only to variations in the strengths of these sources. The dipole sources \vec{S} are coupled to the scalp potentials $\vec{\varphi}$ by the lead field matrix A as $\varphi = A\vec{S}$. The task of the spatiotemporal DSL is to determine the magnitudes and

orientations of multiple dipoles, whose parameters could best account for the spatial distribution as well as the temporal waveforms of the scalp EEG measurement. With the incorporation of the EEG temporal information in the model fitting, the spatiotemporal DSL is more robust against measurement noise and artifacts than the single time-slice DSL. However, once the locations of dipoles become unknowns, the problem becomes a nonlinear optimization problem and the number of dipoles that can be estimated reliably is limited.

All equivalent dipole algorithms need an a priori knowledge of the number and class of the underlying dipole sources. If the number of dipoles is underestimated for a given model, then the DSL inverse solution is biased by the missing dipoles. On the other hand, if too many dipoles are specified, then spurious dipoles may be introduced. So while efforts have been made to estimate the number of dipoles based on information criterion theory (151), the prior information with regard to the number of dipoles remains to be the limitation of EEG DSL. Sometimes such information is provided based on the neurophysiology and pathology such as the case when there is a clear focal region of epileptiform activity (152–154), or known physiology such as somatosensory-evoked potentials (118).

The EEG DSL solution can be further improved when prior information is available with regard to the possible solution space. If the observed EEG signals are known to be mainly produced by cortical sources, then the solution space can be restricted to the cortex surface while excluding deep source locations such as the brainstem. In particular situations, when a priori information is known on the possible source region (such as the sensory EP data, or based on preliminary diagnosis of the epilepsy), the solution space can be restricted to only half of the brain or even more focused on a certain lobe. Computer simulation and experimental studies have also demonstrated that the inverse solution of the DSL is more accurate when using the realistic geometry head model than the simplified spherical head model (155–157). Furthermore, by registration with the magnetic resonance images, the coordinates of the estimated dipole sources can be visualized relative to the brain anatomy. Therefore, it has great potential to reveal the electrophysiologically active neural substrate underlying the scalp potential measurements and facilitate comparison with other functional imaging modalities (158,159), and has clinical significance in detecting the epileptic foci (160,161), presurgical localization of sensorimotor cortex (162,163), and some other applications.

Source Scanning

The source localization problem can also be solved by means of a source scanning procedure (164–168). The source scanning technique avoids solving difficult multidimensional nonlinear optimization problems (118,146,152). The scanning results from the subspace source localization approaches will directly provide an estimate of the source distribution in the 3D brain volume. The source scanning approach, which scans each point in the brain volume and returns a metric about how much chance there is a source at the point, may also be used for source imaging. A representative source scanning algorithm is the multiple signal classification (MUSIC) algorithm (164), which has been used to scan

through the 3D brain volume (solution space) to identify sources that produce potential patterns that lie within the signal subspace of the EEG measurements (164). Furthermore, a recursive method (RAP-MUSIC) has been developed in order to overcome the “multiple-peak picking” problem of the original MUSIC scan (166). Recently, another source scanning algorithm (*first principle vectors*, FINE) (167) has been introduced to localize sources with high resolution, and extended to include realistic geometry inhomogeneous head model (168). The applicability of FINE scanning algorithm has been shown in a group of patients of focal interictal epileptogenic activity (38). The FINE algorithm (167,168) is developed under the framework of the subspace source localization approach (164) and solves the spatiotemporal source localization problem using a scanning strategy instead of optimizing a multidimensional cost function. In principle, the subspace source localization approach scans the entire possible source space and calculates the subspace correlation of two subspaces (166). One subspace is spanned by each scanned point and another one is estimated from the scalp EEG, which is known as the noise-only subspace. If the subspace correlation is approximate to zero against the noise-only subspace for one possible source point, this point is regarded as a source. Multiple sources could thus be obtained at multiple extreme values. The FINE algorithm calculates the correlation to a particular subset of the noise-only subspace instead of the entire noise-only subspace, which helps to achieve high spatial resolution. Computer simulation results suggested the enhanced spatial resolution and robustness against source coherence of FINE in comparison to MUSIC or RAP-MUSIC (167,168). Applications to epilepsy source localization demonstrated the ability of FINE in localizing seizure foci (40). Further development of source scanning approach has also been reported (169) in which a higher order source model is used instead of dipole model, enabling imaging of complex activation patterns in humans induced by visual stimulation.

In addition, another technique called beamforming, which is based on linear spatial filtering, can be used to estimate the source activity at a region of interest or every individual location in the source space (170,171). The beamformer for a specific region of interest or source location is derived in an attempt to minimize the interference from other locations.

A source localization that was specifically developed for localization of focal epileptic activity is a method called EPIFOCUS (172). Like the MUSIC method, this technique searches for focal sources in the solution space (which can be restricted to the gray matter). EPIFOCUS is a linear inverse solution and requires no nonlinear optimization procedure to find the best fit. The result of EPIFOCUS can be interpreted as the probability of a focal source (with a certain spatial extent) at any given point in a discrete solution space. The reliability of EPIFOCUS to determine focal epileptic sources has been demonstrated in several studies (15,173,174).

Distributed Source Imaging

Compared with DSL or source scanning approaches, the distributed source imaging approach has received considerable attention in recent years. Such distributed imaging approaches are motivated by the need to image brain electric activity that

may not be a few focal sources, and to minimize the error due to misspecification of the number of dipole sources. The distributed source imaging may be categorized into two groups: distributed current density imaging and equivalent potential imaging, both of which have been studied extensively.

Distributed Current Density Imaging

Unlike the point dipole source models, the distributed source models do not make any ad hoc assumption on the number of brain electric sources. Instead, the equivalent sources are distributed over the source space. For example, the distributed source model may consist of a large number of current dipoles placed over the 3D brain volume (123) or over the gray matter of cortex (124,132). Regardless of the current source models being used, the current dipoles are fixed at preset locations, so they are not movable. The unknown parameters are the dipole moments, which are to be estimated by minimizing the difference between the measure and source model-predicted scalp electric potentials.

Assuming quasistatic condition and the linear properties of the head volume conductor, the brain electric sources and the scalp EEG could be mathematically described by the following linear matrix equation:

$$\vec{\varphi} = A\vec{X} + \vec{n} \quad (55.5)$$

where $\vec{\varphi}$ is the vector of scalp EEG measurements, \vec{X} is the vector of source distribution, \vec{n} is the vector of additive measurement noise, and A is the transfer matrix relating $\vec{\varphi}$ and \vec{X} . So the distributed source imaging is to estimate the source distribution \vec{X} from the noninvasive scalp EEG measurements $\vec{\varphi}$. Mathematically, this is equivalent to design an inverse filter B , which can project the measured data into the solution space:

$$\vec{X} = B\vec{\varphi} \quad (55.6)$$

The above equation indicates that the distributed source imaging is a linear inverse problem, which avoids the difficulty of nonlinear multidimensional optimization problem as in the DSL approach. However, the linear inverse approach is intrinsically underdetermined, because the number of unknown distributed sources is much larger than the limited number of scalp EEG electrodes. Additional constraints have to be imposed in order to obtain unique and well-posed linear inverse solutions. A well-studied solution to this linear inverse problem is the so-called general inverse, which is also termed the minimum norm least-squares (MNLS) inverse, minimizing the least-square error of the estimated inverse solution \vec{X} under the constraint $\vec{\varphi} = A\vec{X}$ in the absence of noise (175). Other variations of the MNLS include the lead field normalized weighted minimum norm (WMN) (176), low-resolution brain electromagnetic tomography (LORETA) (123), local autoregressive average (LAURA) (177), and others. Furthermore, by normalizing the source estimates with respect to the corresponding noise sensitivity, one can assess the statistical significance of the inverse solution and obtain a map of source estimate statistics. Along this line, Dale et al. and Pascual-Marqui et al. have developed two statistical functional mapping techniques,

known as dynamic statistical parametric mapping (dSPM) (178) and standardized LORETA (sLORETA) (179), based on the MNLS and LORETA algorithms, respectively (180).

The EEG linear inverse solutions enjoy the merits of solving a linear inverse problem but end up with low-resolution images of current density or its statistics. One way to improve the spatial resolution is to generate images with focal source distribution by iteratively repeating the linear inverse computation (181,182). For each step during the iteration, the linearly computed inverse solution from the previous step is used as the weighting factors to constrain the linear source estimates in the current step. As such a recursive process continues till convergence, the estimated source distribution tends to shrink to be more focalized. Other than L2 norm estimates that are to minimize the energy function, Lp norm estimates with $P = 1$ or other values have also been explored (147,183–186). A study by Ding and He (186) demonstrates the merits of L1 norm-based distributed current density imaging in imaging focal sources in humans as induced by somatosensory stimulation (Fig. 55.8).

Cortical Potential Imaging

The current density distribution has explicit physical interpretation of neuronal currents, thus being used widely in solving the EEG inverse problem. Another kind of EEG linear inverse

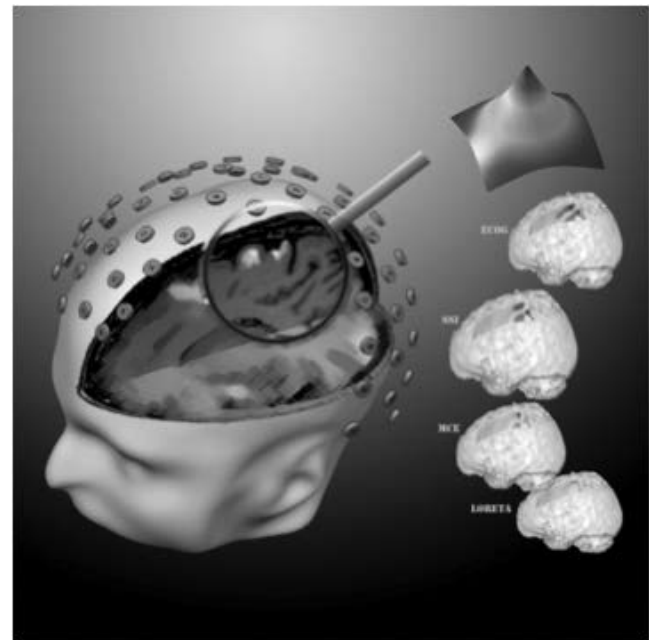


Figure 55.8 Sparse source imaging. The image illustrates the concept of sparse source imaging (SSI) using L1 norm-based generalized minimum norm estimate. The new SSI algorithm corrects inaccurate source field modeling in previously reported L1-norm algorithms and proposes that sparseness a priori should only be applied to the regularization term, not to the data term in the formulation of the regularized inverse problem. The right lower part of the illustration shows that the new SSI is evaluated using somatosensory-evoked potential data with subdural electrocorticographic (ECoG) recordings in a human subject. (Cover image of *Human Brain Mapping*, September 2008 issue for article by Ding and He (186).)

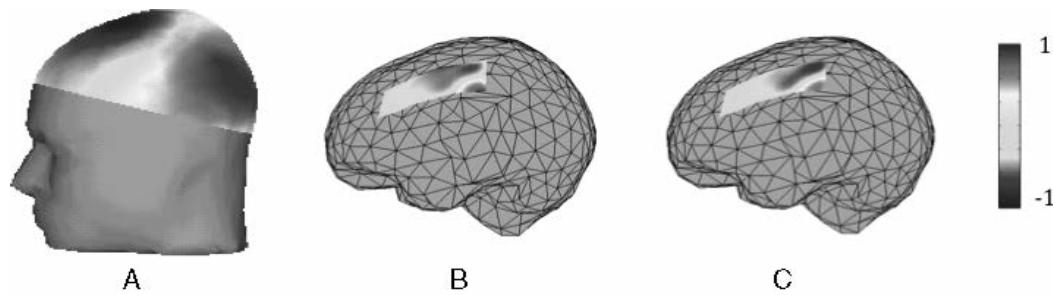


Figure 55.9 At latency of 30 msec after the onset of right median nerve stimuli for a patient: (A) the recorded scalp potential maps, (B) the estimated subdural grid potentials, and (C) the directly recorded subdural grid potentials. All the maps are normalized and the color bars are shown on the right. The CC value between the estimated and recorded subdural grid potentials is 84%. (From He B, Zhang X, Lian J, et al. Boundary element method-based cortical potential imaging of somatosensory evoked potentials using subjects' magnetic resonance images. *Neuroimage*. 2002;16:564–576.) (See color insert)

solution is to estimate the extracellular potential distribution from the scalp EEG. Cortical potential imaging (CPI) has been well studied that aims to reconstruct the distribution of electric potentials over the epicortical surface that can equivalently represent the enclosed brain electric sources (37,56,129,187–195). In this case, the source vector \bar{X} in Eq. (55.5) refers to electric potentials instead of current density. Imaging of electric potential over the epicortical surface has a unique feature that it returns cortical potentials, which are routinely measured by use of subdural electrode arrays in epilepsy patients.

The CPI employs a distributed source model, in which the equivalent sources are distributed in 2D cortical surface, and no ad hoc assumption on the number of source dipoles is needed (37,129,138,139,187–196). Using an explicit biophysical model of the passive conducting properties of a head, the CPI attempts to deconvolve a measured scalp potential distribution into a distribution of the electric potential over the epicortical surface. Because the cortical potential distribution can be experimentally measured (190,195,197) and compared to the inverse imaging results, the CPI approach is of clinical importance. Essentially not affected by the low-conductivity skull layer, CPI offers much-enhanced spatial resolution in assessing the underlying brain activity as compared to the blurred scalp potentials. Figure 55.9 shows an example of cortical potentials estimated from the scalp EEG and directly measured using subdural grids in a human subject, around 30 msec after the onset of right median nerve stimuli. The scalp potential map (Fig. 55.9A) shows dipolar pattern of N/P30, with frontal negativity and parietal positivity over the left scalp. The smearing effect of the scalp potential map was greatly reduced in the inversely estimated cortical potential map (Fig. 55.9B), which shows much more localized areas of positivity and negativity in the posterior edge of the electrode grid. The recorded cortical potential map is shown in Figure 55.9C. Note the estimated and recorded grid potentials have similar distribution patterns, with averaged CC value of 0.84. Moreover, the central sulcus was clearly demarcated in both the estimated and recorded grid potential maps, by the separation of negative and positive potential extrema.

In addition to cortical potential, the extracellular potentials have also been estimated over the entire 3D brain volume in an

approach called ELECTRA (102,126). Although the validation is difficult since the depth electrodes are normally not covering a large volume, this approach theoretically does suggest the possibility of estimating local field potentials in the brain volume.

Multimodal Integration of EEG with fMRI

Integrating electrophysiologic source imaging with functional constraint derived from the hemodynamic imaging modalities has drawn great attention during the past decade (see Ref. 198 for a detailed review). The motivation for integrating EEG/MEG source imaging with fMRI is based on the different strengths and limitations of these two modalities that are precisely the obverse of each other, that is, EEG/MEG enjoys high temporal resolution but limited spatial resolution, and fMRI has high spatial resolution but poor temporal resolution. The fundamental assumption of the multimodal integration approach is that regions in the brain that show increased metabolic activity are also on the average more electrically active over time.

The earliest efforts in the E/MEG–fMRI integrated imaging utilized fMRI statistical parametric maps to obtain a priori information on where brain electric sources are likely located. The spatial information derived from fMRI has been used to constrain the locations of multiple current dipoles (199,200), or to constrain the distributed source distribution (178,201–207). When neural activity is confined to a few small regions, the fMRI activation mapping should yield several hotspots, which can be used to constrain the equivalent dipole locations or as initial locations in the DSL. Once the dipole locations are reconstructed from the EEG data, the time course of dipole moments represents the temporal dynamics of the regional neural activity. Such fMRI-seeded dipole fitting technique is usually used to retrieve the time course of the brain activity at identified fMRI activation foci instead of imaging brain activity. On the other hand, the fMRI-constrained distributed source imaging (i.e., fMRI is used as constraint in the distributed source imaging) can be applied to brain sources that are either focal or extended. The fMRI-constrained current density imaging has been explored, in the framework of Wiener filter (124,178,201) or WMN frameworks (202,203). The major technical limitations of the above-mentioned approaches are primarily due to the

fundamental mismatches between fMRI and EEG (or MEG), owing to different temporal scales in which fMRI and EEG temporal dynamics are generated and collected. The fMRI–EEG/MEG mismatches include fMRI extra sources, fMRI invisible sources, and the fMRI displacement (201,202,206), and it is problematic to constrain the temporally variable current source estimates to “time-invariant” fMRI spatial priors, which may result in fMRI false positives or false negatives.

Efforts have been made to tackle this challenge caused by the different time scales of BOLD fMRI signals and EEG signals, by means of data-driven approaches. For example, the fMRI weighting factor may be selected from data by means of the expectation maximization (EM) algorithm (205,208), or alternatively a two-step estimation algorithm, so-called Twomey regularization, can be used to achieve reasonable estimation of the fMRI weighting factor (206). Recently, a new framework for the fMRI–EEG/MEG integrated neuroimaging has been proposed (207). The system assumes a common neuronal source (i.e., synaptic activity), from which fMRI and EEG signals are generated via a temporal low-pass filter and a spatial low-pass filter, respectively. The EEG inverse problems essentially deal with the spatial deconvolution—the process of reversing the head volume conduction. The EEG inverse solution retains the temporal source evolution even though it may fail to reconstruct the spatial source distribution. In other words, at every source location, the source waveform estimated from EEG is much less distorted than its absolute magnitude, since the

filtering applies to the spatial domain instead of the time domain. This feature is opposed to the temporal regression of fMRI data, which theoretically ends up with high-resolution spatial maps of brain activations but with little or no temporal information. To integrate the EEG and BOLD signals, the BOLD effect size estimated from the fMRI signal in each voxel is set to be proportional to the time integral of the local source power underlying the ERP signals (207). The source estimates are further fitted to the EEG data by means of an adaptive Wiener filter (207). Figure 55.10 shows an experimental example in a human subject exploring the cortical pathway specialized in processing unilateral visual stimuli (207). The experiment included two separate sessions with the identical visual stimuli for the EEG and fMRI data collection. The visual stimulation was a rectangular checkerboard within the lower left quadrant of the visual field; the checkerboard pattern was reversed at 2 Hz. The dynamically integrated EEG–fMRI imaging algorithm (207) revealed a pathway sequentially activating V1/V2, V3/V3a, V5/V7, and intraparietal sulcus, in general agreement with the hierarchical organization of the visual system (209). This pathway was also observed in the low-resolution images reconstructed from the VEP alone. In contrast, a fMRI-weighted source imaging algorithm (178,201) showed a false-positive source region in and around V1/V2 at the latency of 212 msec, whereas a more likely high-tier EEG source around V5, as observed from the EEG data, was missed. This experimental result indicates the promises in dynamic neuroimaging

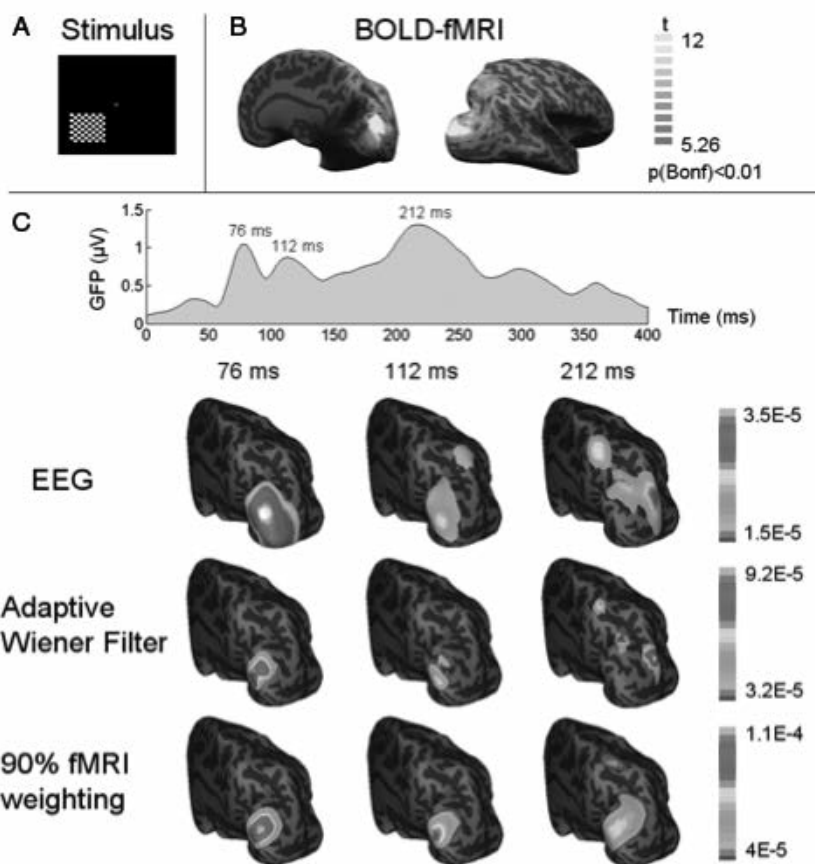


Figure 55.10 fMRI–EEG integration. **A:** The pattern-reversal checkerboard visual stimulation, **(B)** fMRI activation map with a corrected threshold $P < 0.01$, and **(C)** the global field power of VEP and the dynamic cortical source distribution at three VEP latencies (76, 112, 212 msec after the visual onset) imaged from EEG alone (first row), or fMRI–EEG integration using our proposed adaptive wiener filter (second row) and the conventional 90% fMRI-weighted algorithm (third row). Both the source images and the fMRI activation map are visualized on an inflated representation of cortical surface. (From Liu Z, He B. FMRI–EEG integrated cortical source imaging by use of time-variant spatial constraints. *Neuroimage*. 2008;39:1198–1214.) (See color insert)

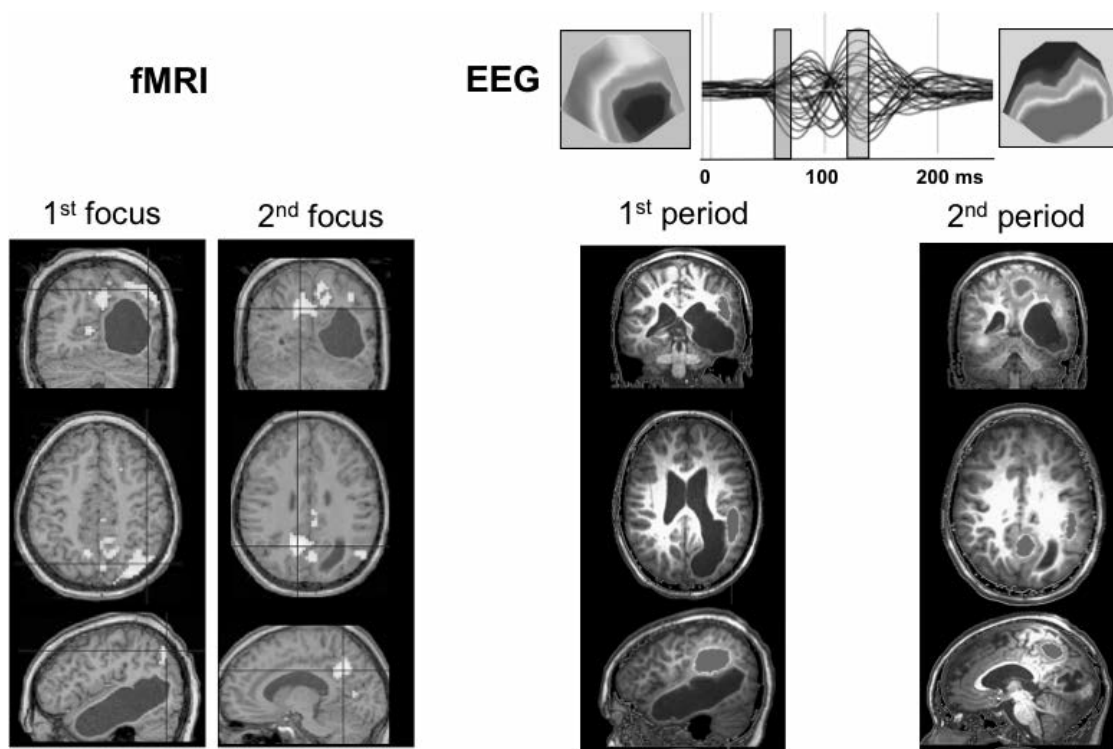


Figure 55.11 Combined EEG–fMRI in epilepsy. Comparison of fMRI and EEG source imaging. A patient with focal epilepsy has been recorded with 32-channel EEG in a 1.5-T MR scanner. Spikes were marked and the significant BOLD responses related to these spikes were determined. Two foci were found around the large lesion: one right lateral parietal and the other mesial parietal. The same spikes recorded in the scanner were cleaned and subjected to EEG source imaging using a distributed linear inverse solution constrained to the gray matter determined from the patient’s MRI. A temporal propagation of the activity was found, with the initial activity in the right parietal lobe, followed by activation in mesial parietal areas. Thus, the foci found in the fMRI were confirmed and temporally resolved. The patient was seizure free after surgical resection of the right lateral parietal focus. (Data collected by M. Siniatchkin, University Hospital of Pediatric Neurology, Kiel, Germany. For details and more examples see Ref. 215.) (See color insert)

by integrating fMRI with EEG using the model-based adaptive Wiener filter (198).

New EEG recording systems together with advanced artifact correction algorithms (79,80) allow recovering the EEG signal that is acquired in the scanner. This opens new possibilities to study the relation between hemodynamic and electric activity, but also to directly combine the temporal resolution of the EEG and the spatial resolution of the fMRI during the same brain state. Several recent studies have used this technique to study the relation between different brain rhythms and the BOLD response (210,211) and the relation between the so-called brain resting state and specific oscillatory activity recorded with the EEG (212–214). With the use of high-density EEG in the scanner, source imaging of this EEG has also become possible. This is particularly interesting in epilepsy where the spike-related fMRI activity can be compared with the source imaging result of the very same spikes. Such studies have recently demonstrated the capability of the EEG source imaging to temporally disentangle the different activated regions seen in the spike-triggered fMRI as illustrated in Figure 55.11 (215,216). This figure also shows that EEG source imaging is also possible in patients with

large brain lesions, indicating that conductivity changes due to such lesions are not as important as one might believe. This has been recently demonstrated in a systematic study in a series of epileptic patients with large brain lesions (217).

CONNECTIVITY ANALYSIS

Static images indicating brain regions responsible for the execution of particular tasks do not convey sufficient information with respect to how these regions communicate with each other. The concept of brain connectivity now plays an important role in neuroscience, as a way to understand the organized behavior of brain regions (218). Previously, some investigators have computed cortical connectivity patterns based on hemodynamic or metabolic measurements such as fMRI (219,220), whereas the sluggishness of the hemodynamic process confounds its interpretation in terms of neuronal interaction (221). The use of EEG data to examine the functional connectivity has a long and rich history (222,223). A variety of techniques have been used, most of which have amounted to evaluating the cross-correlation or phase synchronization of

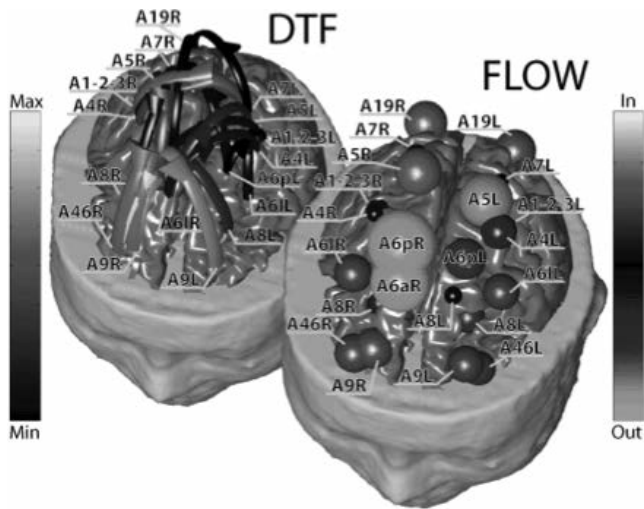


Figure 55.12 Connectivity estimation. **Left panel:** Functional connectivity patterns estimated in a subject during the performance of finger tapping movement, after the EMG onset. Each pattern is represented with arrows moving from one cortical area toward another. The color and size of the arrows code the level of strength of the functional connectivity observed between ROIs. The labels indicate the names of the ROIs employed. **Right panel:** Outflow patterns in all the ROIs obtained for the same connectivity pattern depicted in *top left*. The figure summarizes in red hues the behavior of a ROI in terms of reception of information flow from other ROIs, by adding all the value of the links arriving on the particular ROI from all the others. The information is represented with the size and the color of a sphere, centered on the particular ROI analyzed. The larger the sphere, the higher the value of inflow or outflow for any given ROI. The blue hues code the outflow of information from a single ROI toward all the others. (From Babiloni F, Cincotti F, Babiloni C, et al. Estimation of the cortical functional connectivity with the multimodal integration of high-resolution EEG and fMRI data by directed transfer function. *Neuroimage*. 2005;24:118–131.) (See color insert)

signals between pairs of scalp electrodes or sensors (224). Additionally, it has also been exploited that scalp connectivity patterns can be estimated by other methods (225,226). Graph theory-based tools from the study of complex network have also been developed to describe the connectivity of large-scale networks (227). However, the relation between the observed connectivity pattern in the sensor space and that in the source

space is complicated by the dispersion of electromagnetic signals from the cortex to the sensors.

EEG source imaging techniques have been used in combination with connectivity estimators to noninvasively assess the brain connectivity using methods such as structural equation modeling (SEM) (228,229) and the directed transfer function (DTF) (204). Figure 55.12 shows an example of functional

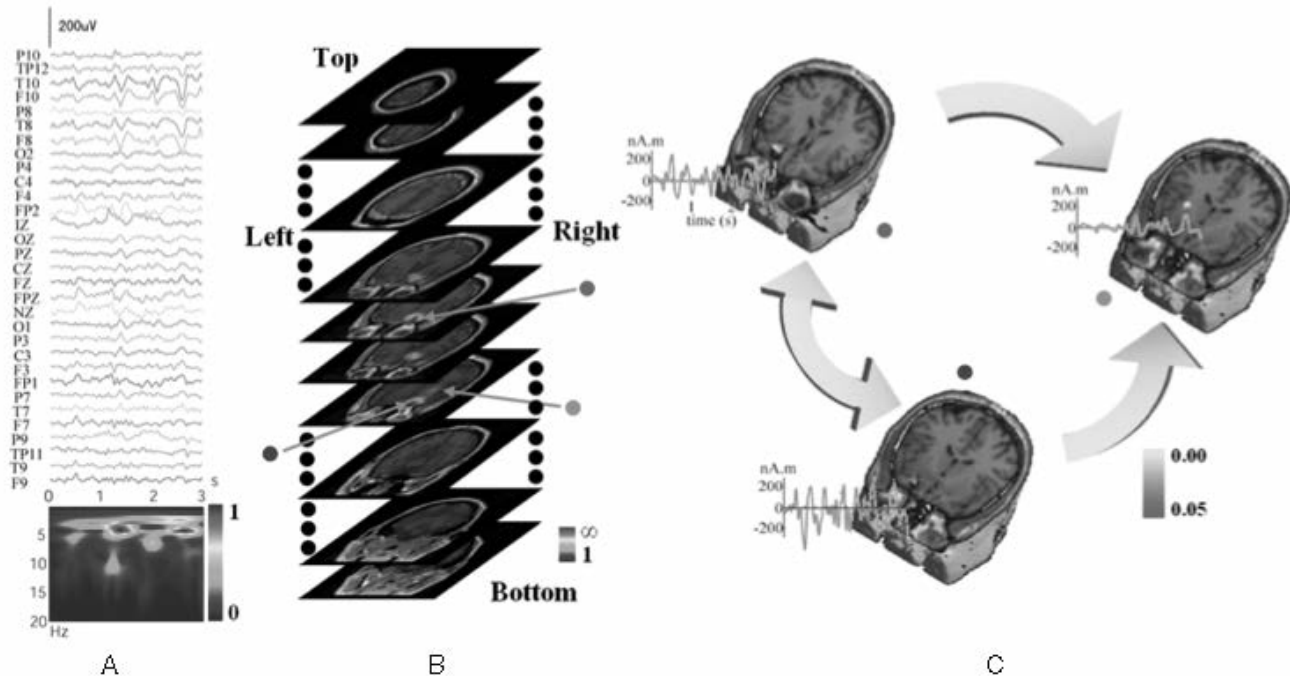


Figure 55.13 Ictal source imaging. **A:** Three second-long 31-channel scalp waveforms for subspace source localization analysis. **B:** Example of a 3D scanning result by FINE for an ictal activity displayed with gray MRI slices. The pseudocolors show the reciprocal of subspace correlation (SC). Red: low SC; blue: high SC. The extent of pseudocolors indicates the coverage of the possible solution space. Three identified sources in the 3D scanning are marked with red, blue, and green dots, respectively. **C:** Locations (pseudocolors on MRI images), waveforms (*green curves*), and causality patterns (*big arrows*) for identified sources from **B**. (From Ding L, Worrell GA, Lagerlund TD, et al. Ictal source analysis: localization and imaging of causal interactions in humans. *Neuroimage*. 2007;34:575–586.) (See color insert)

connectivity patterns as estimated by means of DTF from EEG and functional MRI of a human subject during a motor task (204). It shows connectivity among several regions of interests involved in the motor task.

DTF-based connectivity analysis methods showed promises in localizing epileptogenic foci from interictal spikes (230,231) and from seizures (232) as recorded from ECoG. The functional connectivity in epilepsy patients has also been estimated by applying DTF analysis to 3D current source activity reconstructed from ictal EEG using the FINE source scanning method (40). Figure 55.13 shows an example of the clinical application of connectivity imaging. From ictal EEG data, three putative sources were estimated by means of the FINE source scanning algorithm. The causality among each pair of the three sources, as determined from the source waveforms, was assessed. The causal interactions from the “red” and “green” sources to other sources are deemed significant but not the causal interactions from the “blue” source. Based on this connectivity analysis, it was concluded that the “red” and “green” sources are deemed to be primary seizure sources while the “blue” secondary source. Comparison with MR-visible lesions in the patient supported this conclusion derived by connectivity analysis (40).

CONCLUSION

This chapter focused on modern analysis techniques that convert the EEG to a functional neuroimaging modality. This translation from waveforms to images includes several processing steps that need to be understood and performed properly. It starts with the appropriate spatial sampling of the scalp potential field and ends with proper statistical evaluation of the reconstructed time series of electric activity in the brain.

Concerning the spatial sampling the recent literature strongly suggests that a high number of recording channels are desirable to avoid undersampling of the spatial frequency of the EEG. With modern technology this is not a limiting issue anymore, and 64 to 128 channels of EEG are recorded in many labs. EEG can nowadays easily be sampled from 200 and more electrodes, with electrode nets that allow fast applications even in clinical routine.

Reconstruction and visualization of the scalp potential maps are an important step in EEG source imaging. On the one hand, it serves to detect map distortions due to artifacts that are invisible on the EEG traces. On the other hand, EEG mapping allows to statistically assess time points where map topographies changed over time or between experimental conditions. By physical laws, different map topographies indicate different configurations of the active sources in the brain. Analysis strategies that are based on the topography of the potential field also have the important advantage of being completely reference-free, which is not the case for the analysis of peaks and troughs of EEG or ERP waveforms, and also not for the analysis of coherence or correlations between different electrode sites.

Two main models are involved in EEG source imaging: the head model and the source model. In this chapter we not only

described the historical evolution of these models, but also made clear that a distinction between simple source localization and comprehensive source imaging should be made. The single equivalent dipole fitting approach in a simple spherical head model, which was still state of the art in the last edition of this book, has been largely replaced by imaging of distributed sources in the realistic geometry head model defined by structural MRI. A rapidly growing number of experimental and clinical studies appeared, demonstrating the promising capability of these new techniques. Most impressive are the results in epilepsy where EEG source imaging is used to localize the epileptogenic zone. The fact that the very same methods also allow to localize eloquent cortex with impressive precision renders electric neuroimaging one of the most promising methods in the framework of presurgical evaluation of patients with functional and structural brain lesions.

The temporal resolution is the key advantage of the EEG. However, it also increases the complexity and demands additional analysis steps for electric neuroimaging compared to the other (static) imaging procedures. We here described different methods to deal with the temporal dynamics of the brain electric activity. One of them is based on spatiotemporal decomposition of the topographic maps. It allows to define the most dominant scalp topographies during given time periods and thus permits a reduction of the complex data in time and space. Source imaging procedures can then be applied to this reduced data set only. Since the potential maps represent the real recordings and do not yet rely on models, a preprocessing of the data based on the maps might be more prudent than directly converting the raw data to source images and perform all analysis in the source space. Nevertheless, several interesting studies appeared recently that showed the possibilities of analysis of the source waveforms. Most interesting are the applications of connectivity analysis techniques to these source waveforms. They allow to study causal interactions between different sources in the brain.

In summary, this chapter tried to illustrate that the temporal resolution of the EEG, together with the capability and reliability of modern source imaging algorithms, has converted the EEG to a fully fledged functional neuroimaging method that is not secondary to, but instead is a perfect companion to fMRI and other neuroimaging methods.

REFERENCES

1. Baillet S, Moshier JC, Leahy RM. Electromagnetic brain mapping. *IEEE Signal Processing Mag.* 2001;18:14–30.
2. He B, Lian J. High-resolution spatio-temporal functional neuroimaging of brain activity. *Crit Rev Biomed Eng.* 2002;30:283–306.
3. Michel CM, Murray MM, Lantz G, et al. EEG source imaging. *Clin Neurophysiol.* 2004;115:2195–2222.
4. He B, Lian J. Electrophysiological neuroimaging: solving the EEG inverse problem. In: He B, ed. *Neural Engineering*. Norwell, MA: Kluwer Academic Publishers; 2005:221–261.
5. Sanei S, Chambers J. EEG Source localization. In: Sanei S, Chambers J, eds. *EEG Signal Processing*. New Jersey: Wiley; 2007:197–218.

6. Michel CM, Koenig T, Brandeis D, et al., eds. *Electrical Neuroimaging*. Cambridge, MA: Cambridge University Press; 2009.
7. Lehmann D. Multichannel topography of human alpha EEG fields. *Electroencephalogr Clin Neurophysiol*. 1971;31:439–449.
8. Lehmann D, Skrandies W. Reference-free identification of components of checkerboard-evoked multichannel potential fields. *Electroencephalogr Clin Neurophysiol*. 1980;48:609–621.
9. Lehmann D, Skrandies W. Spatial analysis of evoked potentials in man—a review. *Prog Neurobiol*. 1984;23:227–250.
10. Duffy FH, ed. *Topographic Mapping of Brain Electrical Activity*. Boston, MA: Butterworth; 1986.
11. Fender DH. Source localization of brain electrical activity. In: Gevins AS, Remont A, eds. *Methods of Analysis of Brain Electrical and Magnetic Signals*. Amsterdam: Elsevier; 1987:355–403.
12. Helmholtz HLP. Ueber einige gesetze der vertheilung elektrischer ströme in körperlichen leitern mit anwendung auf die thierisch-elektrischen versuche. *Ann Phys Chem*. 1853;9:211–233.
13. Michel CM, Brandeis D. Data acquisition and pre-processing standards for electrical neuroimaging. In: Michel CM, Koenig T, Brandeis D, et al., eds. *Electrical Neuroimaging*. Cambridge, MA: Cambridge University Press; 2009:79–92.
14. Tucker DM. Spatial sampling of head electrical fields: the geodesic sensor net. *Electroencephalogr Clin Neurophysiol*. 1993;87:154–163.
15. Michel CM, Lantz G, Spinelli L, et al. 128-Channel EEG source imaging in epilepsy: clinical yield and localization precision. *J Clin Neurophysiol*. 2004;21:71–83.
16. Russell GS, Jeffrey EK, Poolman P, et al. Geodesic photogrammetry for localizing sensor positions in dense-array EEG. *Clin Neurophysiol*. 2005;116:1130–1140.
17. Holmes MD. Dense array EEG: methodology and new hypothesis on epilepsy syndromes. *Epilepsia*. 2008;49:3–14.
18. Malmivuo JA, Suikko VE. Effect of skull resistivity on the spatial resolutions of EEG and MEG. *IEEE Trans Biomed Eng*. 2004;51:1276–1280.
19. Li T-H, North G. Aliasing effects and sampling theorems of SRFs when sampled on a finite grid. *Ann Inst Stat Math*. 1996;49:341–354.
20. Grieve PG, Emerson RG, Isler JR, et al. Quantitative analysis of spatial sampling error in the infant and adult electroencephalogram. *Neuroimage*. 2004;21:1260–1274.
21. Srinivasan R, Nunez PL, Tucker DM, et al. Spatial sampling and filtering of EEG with spline Laplacians to estimate cortical potentials. *Brain Topogr*. 1996;8:355–366.
22. Srinivasan R, Tucker DM, Murias M. Estimating the spatial Nyquist of the human EEG. *Behav Res Methods Instrum Comput*. 1998;30:8–19.
23. Ryyänänen OR, Hyttinen JA, Laarne PH, et al. Effect of electrode density and measurement noise on the spatial resolution of cortical potential distribution. *IEEE Trans Biomed Eng*. 2004;51:1547–1554.
24. Ryyänänen OR, Hyttinen JA, Malmivuo JA. Effect of measurement noise and electrode density on the spatial resolution of cortical potential distribution with different resistivity values for the skull. *IEEE Trans Biomed Eng*. 2006;53:1851–1858.
25. Spitzer AR, Cohen LG, Fabrikant J, et al. A method for determining optimal interelectrode spacing for cerebral topographic mapping. *Electroencephalogr Clin Neurophysiol*. 1989;72:355–361.
26. Gevins A, Brickett P, Costales B, et al. Beyond topographic mapping: towards functional–anatomical imaging with 124-channel EEGs and 3-D MRIs. *Brain Topogr*. 1990;3:53–64.
27. Freeman WJ, Holmes MD, Burke BC, et al. Spatial spectra of scalp EEG and EMG from awake humans. *Clin Neurophysiol*. 2003;114:1053–1068.
28. Lantz G, Grave de Peralta R, Spinelli L, et al. Epileptic source localization with high density EEG: how many electrodes are needed? *Clin Neurophysiol*. 2003;114:63–69.
29. Luu P, Tucker DM, Englander R, et al. Localizing acute stroke-related EEG changes: assessing the effects of spatial undersampling. *J Clin Neurophysiol*. 2001;18:302–317.
30. Rush S, Driscoll DA. EEG electrode sensitivity—an application of reciprocity. *IEEE Trans Biomed Eng*. 1969;16:15–22.
31. Oostendorp TF, Delbeke J, Stegeman DF. The conductivity of the human skull: results of in vivo and in vitro measurements. *IEEE Trans Biomed Eng*. 2000;47:1487–1492.
32. Hoekema R, Wieneke GH, Leijten FS, et al. Measurement of the conductivity of skull, temporarily removed during epilepsy surgery. *Brain Topogr*. 2003;16:29–38.
33. Lai Y, van Drongelen W, Ding L, et al. Estimation of in vivo human brain-to-skull conductivity ratio from simultaneous extra- and intra-cranial electrical potential recordings. *Clin Neurophysiol*. 2005;116:456–465.
34. Goncalves S, de Munck JC, Verbunt JP, et al. In vivo measurement of the brain and skull resistivities using an EIT-based method and the combined analysis of SEF/SEP data. *IEEE Trans Biomed Eng*. 2003;50:1124–1128.
35. Zhang Y, van Drongelen W, He B. Estimation of in vivo brain-to-skull conductivity ratio in humans. *Appl Phys Lett*. 2006;89:223903–223905.
36. Fifer WP, Grieve PG, Grose-Fifer J, et al. High-density electroencephalogram monitoring in the neonate. *Clin Perinatol*. 2006;33:679–691, vii.
37. Zhang X, van Drongelen W, Hecox KE, et al. High-resolution EEG: cortical potential imaging of interictal spikes. *Clin Neurophysiol*. 2003;114:1963–1973.
38. Ding L, Worrell GA, Lagerlund TD, et al. 3D source localization of interictal spikes in epilepsy patients with MRI lesions. *Phys Med Biol*. 2006;51:4047–4062.
39. Sperli F, Spinelli L, Seeck M, et al. EEG source imaging in paediatric epilepsy surgery: a new perspective in presurgical workup. *Epilepsia*. 2006;47:981–990.
40. Ding L, Worrell GA, Lagerlund TD, et al. Ictal source analysis: localization and imaging of causal interactions in humans. *Neuroimage*. 2007;34:575–586.
41. Ferree TC, Eriksen KJ, Tucker DM. Regional head tissue conductivity estimation for improved EEG analysis. *IEEE Trans Biomed Eng*. 2000;47:1584–1592.
42. Gao N, Zhu SA, He B. Estimation of electrical conductivity distribution within the human head from magnetic flux density measurement. *Phys Med Biol*. 2005;50:2675–2687.
43. Yuval-Greenberg S, Tomer O, Keren AS, et al. Transient induced gamma-band response in EEG as a manifestation of miniature saccades. *Neuron*. 2008;58:429–441.
44. Perrin F, Pernier J, Bertrand O, et al. Spherical splines for scalp potential and current density mapping. *Electroencephalogr Clin Neurophysiol*. 1989;72:184–187.
45. Fletcher EM, Kussmaul CL, Mangun GR. Estimation of interpolation errors in scalp topographic mapping. *Electroencephalogr Clin Neurophysiol*. 1996;98:422–434.
46. Jung TP, Makeig S, Humphries C, et al. Removing electroencephalographic artifacts by blind source separation. *Psychophysiology*. 2000;37:163–178.
47. Desmedt JE, Tomberg C, Noel P, et al. Beware of the average reference in brain mapping. *Electroencephalogr Clin Neurophysiol Suppl*. 1990;41:22–27.

48. Tomberg C, Noel P, Ozaki I, et al. Inadequacy of the average reference for the topographic mapping of focal enhancements of brain potentials. *Electroencephalogr Clin Neurophysiol*. 1990;77:259–265.
49. Pascual-Marqui RD, Lehmann D. Comparison of topographic maps and the reference electrode: comments on two papers by Desmedt and collaborators. *Electroencephalogr Clin Neurophysiol*. 1993;88:530–531, 534–536.
50. Pascual-Marqui RD, Lehmann D. Topographic maps, source localization inference, and the reference electrode: comments on a paper by Desmedt et al. *Electroencephalogr Clin Neurophysiol*. 1993;88:532–536.
51. Junghofer M, Elbert T, Tucker DM, et al. The polar average reference effect: a bias in estimating the head surface integral in EEG recording. *Clin Neurophysiol*. 1999;110:1149–1155.
52. Lehmann D, Skrandies W. Reference-free identification of components of checkerboard-evoked multichannel potential fields. *Electroencephalogr Clin Neurophysiol*. 1980;48:609–621.
53. Geselowitz DB. The zero of potential. *IEEE Eng Med Biol Mag*. 1998;17:128–132.
54. Murray MM, Brunet D, Michel CM. Topographic ERP analyses: a step-by-step tutorial review. *Brain Topogr*. 2008;20:249–264.
55. Perrin F, Pernier J, Bertrand O, et al. Mapping of scalp potentials by surface spline interpolation. *Electroencephalogr Clin Neurophysiol*. 1987;66:75–81.
56. Nunez PL, Silberstein RB, Cadusch PJ, et al. A theoretical and experimental study of high resolution EEG based on surface Laplacians and cortical imaging. *Electroencephalogr Clin Neurophysiol*. 1994;90:40–57.
57. Hjorth B. An on-line transformation of EEG scalp potentials into orthogonal source derivations. *Electroencephalogr Clin Neurophysiol*. 1975;39:526–530.
58. Perrin F, Bertrand O, Pernier J. Scalp current density mapping: value and estimation from potential data. *IEEE Trans Biomed Eng*. 1987;34:283–288.
59. He B, Lian J, Li G. High-resolution EEG: a new realistic geometry spline Laplacian estimation technique. *Clin Neurophysiol*. 2001;112:845–852.
60. Nunez PL, Srinivasan R. *Electric Fields of the Brain: The Neurophysics of EEG*. 2nd ed. New York: Oxford University Press; 2006.
61. Skrandies W. The effect of stimulation frequency and retinal stimulus location on visual evoked potential topography. *Brain Topogr*. 2007;20:15–20.
62. Brandeis D, Naylor H, Halliday R, et al. Scopolamine effects on visual information processing, attention, and event-related potential map latencies. *Psychophysiology*. 1992;29:315–336.
63. Vaughan HGJ. The neural origins of human event-related potentials. *Ann N Y Acad Sci*. 1982;388:125–138.
64. Picton TW, Bentin S, Berg P, et al. Guidelines for using human event-related potentials to study cognition: recording standards and publication criteria. *Psychophysiology*. 2000;37:127–152.
65. Koenig T, Wackermann J. Overview of analytical approaches. In: Michel CM, Koenig T, Brandeis D, et al., eds. *Electrical Neuroimaging*. Cambridge, MA: Cambridge University Press; 2009:93–109.
66. Skrandies W. Data reduction of multichannel fields: global field power and principal component analysis. *Brain Topogr*. 1989;2:73–80.
67. John ER, Easton P, Prichep LS, et al. Standardized varimax descriptors of event related potentials: basic considerations. *Brain Topogr*. 1993;6:143–162.
68. Wackermann J. Beyond mapping: estimating complexity of multichannel EEG recordings. *Acta Neurobiol Exp (Wars)*. 1996;56:197–208.
69. Kayser J, Tenke CE. Trusting in or breaking with convention: towards a renaissance of principal components analysis in electrophysiology. *Clin Neurophysiol*. 2005;116:1747–1753.
70. Spencer KM, Dien J, Donchin E. Spatiotemporal analysis of the late ERP responses to deviant stimuli. *Psychophysiology*. 2001;38:343–358.
71. Kayser J, Tenke CE. Optimizing PCA methodology for ERP component identification and measurement: theoretical rationale and empirical evaluation. *Clin Neurophysiol*. 2003;114:2307–2325.
72. Kayser J, Tenke CE. Principal components analysis of Laplacian waveforms as a generic method for identifying ERP generator patterns: II. Adequacy of low-density estimates. *Clin Neurophysiol*. 2006;117:369–380.
73. Pourtois G, Deplanque S, Michel C, et al. Beyond the conventional event-related brain potential (ERP): exploring the time-course of visual emotion processing using topographic and principal component analyses. *Brain Topogr*. 2008;20:265–277.
74. Makeig S, Jung TP, Bell AJ, et al. Blind separation of auditory event-related brain responses into independent components. *Proc Natl Acad Sci U S A*. 1997;94:10979–10984.
75. Benar C, Aghakhani Y, Wang Y, et al. Quality of EEG in simultaneous EEG–fMRI for epilepsy. *Clin Neurophysiol*. 2003;114:569–580.
76. Briselli E, Garreffa G, Bianchi L, et al. An independent component analysis-based approach on ballistocardiogram artifact removing. *Magn Reson Imaging*. 2006;24:393–400.
77. Mantini D, Perrucci MG, Cugini S, et al. Complete artifact removal for EEG recorded during continuous fMRI using independent component analysis. *Neuroimage*. 2007;34:598–607.
78. Debener S, Strobel A, Sorger B, et al. Improved quality of auditory event-related potentials recorded simultaneously with 3-T fMRI: removal of the ballistocardiogram artefact. *Neuroimage*. 2007;34:587–597.
79. Grouiller F, Vercueil L, Krainik A, et al. A comparative study of different artefact removal algorithms for EEG signals acquired during functional MRI. *Neuroimage*. 2007;38:124–137.
80. Debener S, Mullinger KJ, Niazy RK, et al. Properties of the ballistocardiogram artefact as revealed by EEG recordings at 1.5, 3 and 7 T static magnetic field strength. *Int J Psychophysiol*. 2008;67:189–199.
81. Makeig S, Westerfield M, Townsend J, et al. Functionally independent components of early event-related potentials in a visual spatial attention task. *Philos Trans R Soc Lond B Biol Sci*. 1999;354:1135–1144.
82. Lehmann D, Ozaki H, Pal I. EEG alpha map series: brain microstates by space-oriented adaptive segmentation. *Electroencephalogr Clin Neurophysiol*. 1987;67:271–288.
83. Lehmann D. Brain electric fields and brain functional states. In: Friedrich R, Wunderlin A, eds. *Evolution of Dynamical Structures in Complex Systems*. Berlin: Springer; 1992:235–248.
84. Strik WK, Lehmann D. Data determined window size and space-oriented segmentation of spontaneous EEG map series. *Electroencephalogr Clin Neurophysiol*. 1993;87:169–174.
85. Wackermann J, Lehmann D, Michel CM, et al. Adaptive segmentation of spontaneous EEG map series into spatially defined microstates. *Int J Psychophysiol*. 1993;14:269–283.
86. Koenig T, Prichep L, Lehmann D, et al. Millisecond by millisecond, year by year: normative EEG microstates and developmental stages. *Neuroimage*. 2002;16:41–48.
87. Pascual-Marqui RD, Michel CM, Lehmann D. Segmentation of brain electrical activity into microstates: model estimation and validation. *IEEE Trans Biomed Eng*. 1995;42:658–665.

88. Lehmann D, Pascual-Marqui R, Michel CM. EEG microstates. *Scholarpedia*. 2009;4:7632.
89. Baars BJ. The conscious access hypothesis: origins and recent evidence. *Trends Cogn Sci*. 2002;6:47–52.
90. Dehaene S, Sergent C, Changeux JP. A neuronal network model linking subjective reports and objective physiological data during conscious perception. *Proc Natl Acad Sci U S A*. 2003;100:8520–8525.
91. Grossberg S. The complementary brain: unifying brain dynamics and modularity. *Trends Cogn Sci*. 2000;4:233–246.
92. Bressler SL, Tognoli E. Operational principles of neurocognitive networks. *Int J Psychophysiol*. 2006;60:139–148.
93. Fingelkurts AA. Timing in cognition and EEG brain dynamics: discreteness versus continuity. *Cogn Process*. 2006;7:135–162.
94. Strik WK, Dierks T, Becker T, et al. Larger topographical variance and decreased duration of brain electric microstates in depression. *J Neural Transm Gen Sect*. 1995;99:213–222.
95. Strik WK, Chiaramonti R, Muscas GC, et al. Decreased EEG microstate duration and anteriorisation of the brain electrical fields in mild and moderate dementia of the Alzheimer type. *Psychiatry Res*. 1997;75:183–191.
96. Koenig T, Prichep L, Dierks T, et al. Decreased EEG synchronization in Alzheimer's disease and mild cognitive impairment. *Neurobiol Aging*. 2005;26:165–171.
97. Koenig T, Lehmann D, Merlo MC, et al. A deviant EEG brain microstate in acute, neuroleptic-naive schizophrenics at rest. *Eur Arch Psychiatry Clin Neurosci*. 1999;249:205–211.
98. Lehmann D, Faber PL, Galderisi S, et al. EEG microstate duration and syntax in acute, medication-naive, first-episode schizophrenia: a multi-center study. *Psychiatry Res*. 2005;138:141–156.
99. Lantz G, Michel CM, Seeck M, et al. Space-oriented segmentation and 3-dimensional source reconstruction of ictal EEG patterns. *Clin Neurophysiol*. 2001;112:688–697.
100. Lehmann D, Wackermann J, Michel CM, et al. Space-oriented EEG segmentation reveals changes in brain electric field maps under the influence of a nootropic drug. *Psychiatry Res*. 1993;50:275–282.
101. Kinoshita T, Strik WK, Michel CM, et al. Microstate segmentation of spontaneous multichannel EEG map series under diazepam and sulpiride. *Pharmacopsychiatry*. 1995;28:51–55.
102. Michel CM, Grave de Peralta R, Lantz G, et al. Spatio-temporal EEG analysis and distributed source estimation in presurgical epilepsy evaluation. *J Clin Neurophysiol*. 1999;16:225–238.
103. Michel CM, Thut G, Morand S, et al. Electric source imaging of human brain functions. *Brain Res Brain Res Rev*. 2001;36:108–118.
104. Pegna AJ, Khateb A, Spinelli L, et al. Unravelling the cerebral dynamics of mental imagery. *Hum Brain Mapp*. 1997;5:410–421.
105. Arzy S, Mohr C, Michel CM, et al. Duration and not strength of activation in temporo-parietal cortex positively correlates with schizotypy. *Neuroimage*. 2007;35:326–333.
106. Lascano AM, Brodbeck V, Lalive PH, et al. Increasing the diagnostic value of evoked potentials in multiple sclerosis by quantitative topographic analysis of multichannel recordings. *J Clin Neurophysiol*. 2009;26:316–325.
107. Murray MM, Michel CM, Grave de Peralta R, et al. Rapid discrimination of visual and multisensory memories revealed by electrical neuroimaging. *Neuroimage*. 2004;21:125–135.
108. Ortigue S, Michel CM, Murray MM, et al. Electrical neuroimaging reveals early generator modulation to emotional words. *Neuroimage*. 2004;21:1242–1251.
109. Overney LS, Michel CM, Harris IM, et al. Cerebral processes in mental transformations of body parts: recognition prior to rotation. *Brain Res Cogn Brain Res*. 2005;25:722–734.
110. Murray MM, Camen C, Gonzalez Andino SL, et al. Rapid brain discrimination of sounds of objects. *J Neurosci*. 2006;26:1293–1302.
111. De Santis L, Spierer L, Clarke S, et al. Getting in touch: segregated somatosensory what and where pathways in humans revealed by electrical neuroimaging. *Neuroimage*. 2007;37:890–903.
112. Schnider A, Mohr C, Morand S, et al. Early cortical response to behaviorally relevant absence of anticipated outcomes: a human event-related potential study. *Neuroimage*. 2007;35:1348–1355.
113. Thierry G, Martin CD, Downing P, et al. Controlling for inter-stimulus perceptual variance abolishes N170 face selectivity. *Nat Neurosci*. 2007;10:505–511.
114. Arzy S, Molnar-Szakacs I, Blanke O. Self in time: imagined self-location influences neural activity related to mental time travel. *J Neurosci*. 2008;28:6502–6507.
115. Spierer L, Murray MM, Tardif E, et al. The path to success in auditory spatial discrimination: electrical neuroimaging responses within the supratemporal plane predict performance outcome. *Neuroimage*. 2008;41:493–503.
116. Kavanagh RN, Darcey TM, Lehmann D, et al. Evaluation of methods for three-dimensional localization of electrical sources in the human brain. *IEEE Trans Biomed Eng*. 1978;25:421–429.
117. Scherg M, von Cramon D. A new interpretation of the generators of BAEP waves I–V: results of a spatio-temporal dipole model. *Electroencephalogr Clin Neurophysiol*. 1985;62:290–299.
118. He B, Musha T, Okamoto Y, et al. Electric dipole tracing in the brain by means of the boundary element method and its accuracy. *IEEE Trans Biomed Eng*. 1987;34:406–414.
119. Cuffin BN, Cohen D, Yunokuchi K, et al. Tests of EEG localization accuracy using implanted sources in the human brain. *Ann Neurol*. 1991;29:132–138.
120. Cuffin BN. A method for localizing EEG sources in realistic head models. *IEEE Trans Biomed Eng*. 1995;42:68–71.
121. Nolte G, Curio G. Current multipole expansion to estimate lateral extent of neuronal activity: a theoretical analysis. *IEEE Trans Biomed Eng*. 2000;47:1347–1355.
122. Jerbi K, Baillet S, Mosher JC, et al. Localization of realistic cortical activity in MEG using current multipoles. *Neuroimage*. 2004;22:779–793.
123. Pascual-Marqui RD, Michel CM, Lehmann D. Low resolution electromagnetic tomography: a new method for localizing electrical activity in the brain. *Int J Psychophysiol*. 1994;18:49–65.
124. Dale AM, Sereno MI. Improved localization of cortical activity by combining EEG and MEG with MRI cortical surface reconstruction: a linear approach. *J Cogn Neurosci*. 1993;5:162–176.
125. He B, Yao D, Lian J, et al. An equivalent current source model and Laplacian weighted minimum norm current estimates of brain electrical activity. *IEEE Trans Biomed Eng*. 2002;49:277–288.
126. Grave de Peralta Menendez R, Gonzalez Andino SL, Morand S, et al. Imaging the electrical activity of the brain: ELECTRA. *Hum Brain Mapp*. 2000;9:1–12.
127. Plonsey R. *Bioelectric Phenomena*. New York, NY: McGraw-Hill; 1969.
128. Wilson FN, Bayley RH. The electric field of an eccentric dipole in a homogeneous spherical conducting medium. *Circulation*. 1950;1:84–92.
129. Wang Y, He B. A computer simulation study of cortical imaging from scalp potentials. *IEEE Trans Biomed Eng*. 1998;45:724–735.
130. Cuffin BN, Cohen D. Comparison of the magnetoencephalogram and electroencephalogram. *Electroencephalogr Clin Neurophysiol*. 1979;47:132–146.
131. Sun M. An efficient algorithm for computing multishell spherical volume conductor models in EEG dipole source localization. *IEEE Trans Biomed Eng*. 1997;44:1243–1252.

132. Spinelli L, Andino SG, Lantz G, et al. Electromagnetic inverse solutions in anatomically constrained spherical head models. *Brain Topogr.* 2000;13:115–125.
133. Hämäläinen M, Sarvas J. Realistic conductor geometry model of the human head for interpretation of neuromagnetic data. *IEEE Trans Biomed Eng.* 1989;36:165–171.
134. Meijs JW, Weier OW, Peters MJ, et al. On the numerical accuracy of the boundary element method. *IEEE Trans Biomed Eng.* 1989;36:1038–1049.
135. Yan Y, Nunez PL, Hart RT. Finite-element model of human head: scalp potentials due to dipole sources. *Med Biol Eng Comput.* 1991;29:475–481.
136. Zhang YC, Zhu SA, He B. A second-order finite element algorithm for solving the three-dimensional EEG forward problem. *Phys Med Biol.* 2004;49:2975–2987.
137. Wolters CH, Anwander A, Tricoche X, et al. Influence of tissue conductivity anisotropy on EEG/MEG field and return current computation in a realistic head model: a simulation and visualization study using high-resolution finite element modeling. *Neuroimage.* 2006;30:813–826.
138. Zhang Y, Ding L, van Drongelen W, et al. A cortical potential imaging study from simultaneous extra- and intracranial electrical recordings by means of the finite element method. *Neuroimage.* 2006;31:1513–1524.
139. Zhang Y, van Drongelen W, Kohrman M, et al. Three-dimensional brain current source reconstruction from intra-cranial ECoG recordings. *Neuroimage.* 2008;42:683–695.
140. Lee WH, Liu Z, Mueller BA, et al. Influence of white matter anisotropic conductivity on EEG source localization: comparison to fMRI in human primary visual cortex. *Clin Neurophysiol.* 2009;120:2071–2081.
141. Withey DJ, Koles ZJ. A review of medical image segmentation: methods and available software. *Int J Bioelectromagnetism.* 2008;10:125–148.
142. Basser PJ, Mattiello J, LeBihan D. MR diffusion tensor spectroscopy and imaging. *Biophys J.* 1994;66:259–267.
143. Tuch DS, Wedeen VJ, Dale AM, et al. Conductivity tensor mapping of the human brain using diffusion tensor MRI. *Proc Natl Acad Sci U S A.* 2001;98:11697–11701.
144. Wang K, Zhu S, Mueller BA, et al. A new method to derive white matter conductivity from diffusion tensor MRI. *IEEE Trans Biomed Eng.* 2008;55:2481–2486.
145. Homma S, Musha T, Nakajima Y, et al. Location of electric current sources in the human brain estimated by the dipole tracing method of the scalp–skull–brain (SSB) head model. *Electroencephalogr Clin Neurophysiol.* 1994;91:374–382.
146. Roth BJ, Ko D, von Albertini-Carletti IR, et al. Dipole localization in patients with epilepsy using the realistically shaped head model. *Electroencephalogr Clin Neurophysiol.* 1997;102:159–166.
147. Bai X, Towle VL, He EJ, et al. Evaluation of cortical imaging techniques based on somatosensory evoked potentials. *Conf Proc IEEE Eng Med Biol Soc.* 2006;1:1000–1001.
148. Diekmann V, Becker W, Jurgens R, et al. Localisation of epileptic foci with electric, magnetic and combined electromagnetic models. *Electroencephalogr Clin Neurophysiol.* 1998;106:297–313.
149. Fuchs M, Wagner M, Wischmann HA, et al. Improving source reconstructions by combining bioelectric and biomagnetic data. *Electroencephalogr Clin Neurophysiol.* 1998;107:93–111.
150. Fletcher DJ, Amir A, Jewett DL, et al. Improved method for computation of potentials in a realistic head shape model. *IEEE Trans Biomed Eng.* 1995;42:1094–1104.
151. Bai X, He B. Estimation of number of independent brain electric sources from the scalp EEGs. *IEEE Trans Biomed Eng.* 2006;53:1883–1892.
152. Ebersole JS. Non-invasive localization of the epileptogenic focus by EEG dipole modeling. *Acta Neurol Scand Suppl.* 1994;152:20–28.
153. Lantz G, Ryding E, Rosén I. Three dimensional localisation of interictal epileptiform activity with dipole analysis: comparison with intracranial recordings and SPECT findings. *J Epilepsy.* 1994;7:117–129.
154. Ebersole JS, Hawes-Ebersole S. Clinical application of dipole models in the localization of epileptiform activity. *J Clin Neurophysiol.* 2007;24:120–129.
155. Cuffin BN. EEG localization accuracy improvements using realistically shaped head models. *IEEE Trans Biomed Eng.* 1996;43:299–303.
156. Waberski TD, Buchner H, Lehnertz K, et al. Properties of advanced headmodelling and source reconstruction for the localization of epileptiform activity. *Brain Topogr.* 1998;10:283–290.
157. Benar CG, Gotman J. Modeling of post-surgical brain and skull defects in the EEG inverse problem with the boundary element method. *Clin Neurophysiol.* 2002;113:48–56.
158. Martinez A, Anllo-Vento L, Sereno MI, et al. Involvement of striate and extrastriate visual cortical areas in spatial attention. *Nat Neurosci.* 1999;2:364–369.
159. Northoff G, Richter A, Gessner M, et al. Functional dissociation between medial and lateral prefrontal cortical spatiotemporal activation in negative and positive emotions: a combined fMRI/MEG study. *Cereb Cortex.* 2000;10:93–107.
160. Lantz G, Holub M, Ryding E, et al. Simultaneous intracranial and extracranial recording of interictal epileptiform activity in patients with drug resistant partial epilepsy: patterns of conduction and results from dipole reconstructions. *Electroencephalogr Clin Neurophysiol.* 1996;99:69–78.
161. Huppertz HJ, Hof E, Klisch J, et al. Localization of interictal delta and epileptiform EEG activity associated with focal epileptogenic brain lesions. *Neuroimage.* 2001;13:15–28.
162. Cakmur R, Towle VL, Mullan JF, et al. Intra-operative localization of sensorimotor cortex by cortical somatosensory evoked potentials: from analysis of waveforms to dipole source modeling. *Acta Neurochir (Wien).* 1997;139:1117–1124 [discussion 1115–1124].
163. Mine S, Oka N, Yamaura A, et al. Presurgical functional localization of primary somatosensory cortex by dipole tracing method of scalp–skull–brain head model applied to somatosensory evoked potential. *Electroencephalogr Clin Neurophysiol.* 1998;108:226–233.
164. Mosher JC, Lewis PS, Leahy RM. Multiple dipole modeling and localization from spatio-temporal MEG data. *IEEE Trans Biomed Eng.* 1992;39:541–557.
165. Sekihara K, Poeppel D, Marantz A, et al. Noise covariance incorporated MEG-MUSIC algorithm: a method for multiple-dipole estimation tolerant of the influence of background brain activity. *IEEE Trans Biomed Eng.* 1997;44:839–847.
166. Mosher JC, Leahy RM. Source localization using recursively applied and projected (RAP) MUSIC. *IEEE Trans Signal Process.* 1999;47:332–340.
167. Xu XL, Xu B, He B. An alternative subspace approach to EEG dipole source localization. *Phys Med Biol.* 2004;49:327–343.
168. Ding L, He B. Spatio-temporal EEG source localization using a three-dimensional subspace FINE approach in a realistic geometry inhomogeneous head model. *IEEE Trans Biomed Eng.* 2006;53:1732–1739.

169. Ding L, Zhang N, Chen W, et al. Three-dimensional imaging of complex neural activation in humans from EEG. *IEEE Trans Biomed Eng.* 2009;56:1980–1988.
170. van Veen BD, van Drongelen W, Yuchtman M, et al. Localization of brain electrical activity via linearly constrained minimum variance spatial filtering. *IEEE Trans Biomed Eng.* 1997;44:867–880.
171. Sekihara K, Nagarajan SS, Poeppel D, et al. Reconstructing spatio-temporal activities of neural sources using an MEG vector beamformer technique. *IEEE Trans Biomed Eng.* 2001;48:760–771.
172. Grave de Peralta R, Gonzalez S, Lantz G, et al. Noninvasive localization of electromagnetic epileptic activity. I. Method descriptions and simulations. *Brain Topogr.* 2001;14:131–137.
173. Lantz G, Spinelli L, Menendez RG, et al. Localization of distributed sources and comparison with functional MRI. *Epileptic Disord.* 2001;(special issue):45–58.
174. Lantz G, Spinelli L, Seeck M, et al. Propagation of interictal epileptiform activity can lead to erroneous source localizations: a 128 channel EEG mapping study. *J Clin Neurophysiol.* 2003;20:311–319.
175. Hämäläinen MS, Ilmoniemi RJ. Interpreting measured magnetic fields of the brain: estimation of current distributions. Helsinki: Helsinki University of Technology; 1984:28 pp.
176. Wang JZ, Williamson SJ, Kaufman L. Magnetic source images determined by a lead-field analysis: the unique minimum-norm least-squares estimation. *IEEE Trans Biomed Eng.* 1992;39:665–675.
177. Grave de Peralta Menendez R, Murray MM, Michel CM, et al. Electrical neuroimaging based on biophysical constraints. *Neuroimage.* 2004;21:527–539.
178. Dale AM, Liu AK, Fischl BR, et al. Dynamic statistical parametric mapping: combining fMRI and MEG for high-resolution imaging of cortical activity. *Neuron.* 2000;26:55–67.
179. Pascual-Marqui RD, Esslen M, Kochi K, et al. Functional imaging with low-resolution brain electromagnetic tomography (LORETA): a review. *Methods Find Exp Clin Pharmacol.* 2002;24(suppl C):91–95.
180. Pascual Marqui RD, Sekihara K, Brandeis D, et al. Imaging the electrical neuronal generators of EEG/MEG. In: Michel CM, Koenig T, Brandeis D, et al., eds. *Electrical Neuroimaging.* Cambridge, MA: Cambridge University Press; 2009;49–78.
181. Gorodnitsky IF, George JS, Rao BD. Neuromagnetic source imaging with FOCUSS: a recursive weighted minimum norm algorithm. *Electroencephalogr Clin Neurophysiol.* 1995;95:231–251.
182. Yao D, He B. A self-coherence enhancement algorithm and its application to enhancing three-dimensional source estimation from EEGs. *Ann Biomed Eng.* 2001;29:1019–1027.
183. Matsuura K, Okabe Y. Selective minimum-norm solution of the biomagnetic inverse problem. *IEEE Trans Biomed Eng.* 1995;42:608–615.
184. Uutela K, Hamalainen M, Somersalo E. Visualization of magnetoencephalographic data using minimum current estimates. *Neuroimage.* 1999;10:173–180.
185. Huang MX, Dale AM, Song T, et al. Vector-based spatial-temporal minimum L1-norm solution for MEG. *Neuroimage.* 2006;31:1025–1037.
186. Ding L, He B. Sparse source imaging in electroencephalography with accurate field modeling. *Hum Brain Mapp.* 2008;29:1053–1067.
187. Sidman RD, Vincent DJ, Smith DB, et al. Experimental tests of the cortical imaging technique—applications to the response to median nerve stimulation and the localization of epileptiform discharges. *IEEE Trans Biomed Eng.* 1992;39:437–444.
188. Le J, Gevins A. Method to reduce blur distortion from EEG's using a realistic head model. *IEEE Trans Biomed Eng.* 1993;40:517–528.
189. Srebro R, Oguz RM, Hughlett K, et al. Estimating regional brain activity from evoked potential fields on the scalp. *IEEE Trans Biomed Eng.* 1993;40:509–516.
190. Gevins A, Le J, Martin NK, et al. High resolution EEG: 124-channel recording, spatial deblurring and MRI integration methods. *Electroencephalogr Clin Neurophysiol.* 1994;90:337–358.
191. He B, Wang Y, Pak S, et al. Cortical source imaging from scalp electroencephalograms. *Med Biol Eng Comput.* 1996;34:257–258.
192. Babiloni F, Babiloni C, Carducci F, et al. High resolution EEG: a new model-potential spatial deblurring method using a realistically-shaped MR-constructed subject's head model. *Electroencephalogr Clin Neurophysiol.* 1997;102:69–80.
193. He B, Wang Y, Wu D. Estimating cortical potentials from scalp EEG's in a realistically shaped inhomogeneous head model by means of the boundary element method. *IEEE Trans Biomed Eng.* 1999;46:1264–1268.
194. He B, Lian J, Spencer KM, et al. A cortical potential imaging analysis of the P300 and novelty P3 components. *Hum Brain Mapp.* 2001;12:120–130.
195. He B, Zhang X, Lian J, et al. Boundary element method-based cortical potential imaging of somatosensory evoked potentials using subjects' magnetic resonance images. *Neuroimage.* 2002;16:564–576.
196. Ollikainen JO, Vauhkonen M, Karjalainen PA, et al. A new computational approach for cortical imaging. *IEEE Trans Med Imaging.* 2001;20:325–332.
197. Towle VL, Cohen S, Alperin N, et al. Displaying electrocorticographic findings on gyral anatomy. *Electroencephalogr Clin Neurophysiol.* 1995;94:221–228.
198. He B, Liu Z. Multimodal functional neuroimaging: integrating functional MRI and EEG/MEG. *IEEE Rev Biomed Eng.* 2008;23–40.
199. Ahlfors SP, Simpson GV, Dale AM, et al. Spatiotemporal activity of a cortical network for processing visual motion revealed by MEG and fMRI. *J Neurophysiol.* 1999;82:2545–2555.
200. Fujimaki N, Hayakawa T, Nielsen M, et al. An fMRI-constrained MEG source analysis with procedures for dividing and grouping activation. *Neuroimage.* 2002;17:324–343.
201. Liu AK, Belliveau JW, Dale AM. Spatiotemporal imaging of human brain activity using functional MRI constrained magnetoencephalography data: Monte Carlo simulations. *Proc Natl Acad Sci U S A.* 1998;95:8945–8950.
202. Wagner M, Fuchs M, Kastner J. fMRI-constrained dipole fits and current density reconstructions. *Proceedings of the 12th International Conference on Biomagnetism, Helsinki, 2000:* 785–788.
203. Babiloni F, Babiloni C, Carducci F, et al. Multimodal integration of high-resolution EEG and functional magnetic resonance imaging data: a simulation study. *Neuroimage.* 2003;19:1–15.
204. Babiloni F, Cincotti F, Babiloni C, et al. Estimation of the cortical functional connectivity with the multimodal integration of high-resolution EEG and fMRI data by directed transfer function. *Neuroimage.* 2005;24:118–131.
205. Phillips C, Mattout J, Rugg MD, et al. An empirical Bayesian solution to the source reconstruction problem in EEG. *Neuroimage.* 2005;24:997–1011.
206. Liu Z, Ding L, He B. Integration of EEG/MEG with MRI and fMRI. *IEEE Eng Med Biol Mag.* 2006;25:46–53.

207. Liu Z, He B. FMRI–EEG integrated cortical source imaging by use of time-variant spatial constraints. *Neuroimage*. 2008;39:1198–1214.
208. Mattout J, Phillips C, Penny WD, et al. MEG source localization under multiple constraints: an extended Bayesian framework. *Neuroimage*. 2006;30:753–767.
209. Felleman DJ, Van Essen DC. Distributed hierarchical processing in the primate cerebral cortex. *Cereb Cortex*. 1991;1:1–47.
210. Laufs H, Holt JL, Elfont R, et al. Where the BOLD signal goes when alpha EEG leaves. *Neuroimage*. 2006;31:1408–1418.
211. Tyvaert L, Levan P, Grova C, et al. Effects of fluctuating physiological rhythms during prolonged EEG–fMRI studies. *Clin Neurophysiol*. 2008;119:2762–2774.
212. Laufs H, Kleinschmidt A, Beyerle A, et al. EEG-correlated fMRI of human alpha activity. *Neuroimage*. 2003;19:1463–1476.
213. Laufs H, Krakow K, Sterzer P, et al. Electroencephalographic signatures of attentional and cognitive default modes in spontaneous brain activity fluctuations at rest. *Proc Natl Acad Sci U S A*. 2003;100:11053–11058.
214. Laufs H, Hamandi K, Salek-Haddadi A, et al. Temporal lobe interictal epileptic discharges affect cerebral activity in “default mode” brain regions. *Hum Brain Mapp*. 2007;28:1023–1032.
215. Groening K, Brodbeck V, Moeller F, et al. Combination of EEG–fMRI and EEG source analysis improves interpretation of spike-associated activation networks in paediatric pharmacoresistant focal epilepsies. *Neuroimage*. 2009;46:827–833.
216. Vulliemoz S, Thornton R, Rodionov R, et al. The spatio-temporal mapping of epileptic networks: combination of EEG–fMRI and EEG source imaging. *Neuroimage*. 2009;46:834–843.
217. Brodbeck V, Lascano AM, Spinelli L, et al. Accuracy of EEG source imaging of epileptic spikes in patients with large brain lesions. *Clin Neurophysiol*. 2009;120:679–685.
218. Ioannides AA. Dynamic functional connectivity. *Curr Opin Neurobiol*. 2007;17:161–170.
219. McIntosh AR, Gonzalez-Lima F. Structural equation modeling and its application to network analysis in functional brain imaging. *Hum Brain Mapp*. 1994;2:2–22.
220. Arthurs OJ, Donovan T, Spiegelhalter DJ, et al. Intracortically distributed neurovascular coupling relationships within and between human somatosensory cortices. *Cereb Cortex*. 2007;17:661–668.
221. Otte A, Halsband U. Brain imaging tools in neurosciences. *J Physiol Paris*. 2006;99:281–292.
222. Adey WR, Walter DO, Hendrix CE. Computer techniques in correlation and spectral analyses of cerebral slow waves during discriminative behavior. *Exp Neurol*. 1961;3:501–524.
223. Gevins AS, Cuttillo BA, Bressler SL, et al. Event-related covariances during a bimanual visuomotor task. II. Preparation and feedback. *Electroencephalogr Clin Neurophysiol*. 1989;74:147–160.
224. Lachaux JP, Rodriguez E, Martinerie J, et al. Measuring phase synchrony in brain signals. *Hum Brain Mapp*. 1999;8:194–208.
225. Urbano A, Babiloni C, Onorati P, et al. Dynamic functional coupling of high resolution EEG potentials related to unilateral internally triggered one-digit movements. *Electroencephalogr Clin Neurophysiol*. 1998;106:477–487.
226. Brovelli A, Ding M, Ledberg A, et al. Beta oscillations in a large-scale sensorimotor cortical network: directional influences revealed by Granger causality. *Proc Natl Acad Sci U S A*. 2004;101:9849–9854.
227. Strogatz SH. Exploring complex networks. *Nature*. 2001;410:268–276.
228. Astolfi L, Cincotti F, Mattia D, et al. Estimation of the effective and functional human cortical connectivity with structural equation modeling and directed transfer function applied to high-resolution EEG. *Magn Reson Imaging*. 2004;22:1457–1470.
229. Astolfi L, Cincotti F, Babiloni C, et al. Estimation of the cortical connectivity by high-resolution EEG and structural equation modeling: simulations and application to finger tapping data. *IEEE Trans Biomed Eng*. 2005;52:757–768.
230. Wilke C, Ding L, He B. Estimation of time-varying connectivity patterns through the use of an adaptive directed transfer function. *IEEE Trans Biomed Eng*. 2008;55:2557–2564.
231. Wilke C, van Drongelen W, Kohrman M, et al. Identification of epileptogenic foci from causal analysis of ECoG interictal spike activity. *Clin Neurophysiol*. 2009;120:1449–1456.
232. Wilke C, van Drongelen W, Kohrman M, et al. Neocortical seizure foci localization by means of a directed transfer function method. *Epilepsia*. 2009;120:1449–1456.

Computer-Assisted EEG Pattern Recognition and Diagnostic Systems

FERNANDO H. LOPES DA SILVA

CHAPTER

56

If someone would compare older editions of this chapter with the present one, he or she would notice how the field of computerized diagnostic systems has rapidly evolved in the last decade that is reflected in the emergence of new algorithms every year, while some older ones have become obsolete. Nonetheless, much of the older literature continues to be valid inasmuch as it illustrates basic concepts and may guide new researchers to find their way in this frontier between clinical neurophysiology and the technology of applied signal analysis. This kind of review of relatively old literature may help to avoid each generation trying to invent the wheel again. Here we pay attention also to recent developments and new trends. We should note that some new algorithms are simple variants of previous approaches. Very often the performance of the new ones is not assessed with respect to the older versions that leads to some lack of transparency in this field.

A common denominator of the field of computer-assisted EEG diagnostic systems is the application of pattern recognition methods. The latter constitute a general class of procedures applicable in a variety of scientific areas. The first operation in EEG analysis is to define a pattern, that is, to choose a set of features that are potentially important in identifying the phenomena of interest. This set of features constitutes a pattern. The second operation may be the *classification* or *clustering of the set of features*. According to the former one must assume a priori that there exists a number of classes (e.g., clinical normal/abnormal) to which the objects must be allocated; according to the clustering approach, however, it is not necessary to define a predetermined number of classes. Rather, in this case the aim is to find clusters of objects based on a given statistical criterion. In the classification approach one chooses a group of EEGs, the so-called *learning set*, to determine the set of features that gives the best possible discrimination between the classes, for example, applying Fisher's *linear discriminant analysis*. Thereafter, the best set of features can be used to classify any other group of EEGs that constitute the *test sets*.

Clustering requires little or no specific a priori knowledge; the objects are grouped in clusters applying a clustering algorithm. The user must determine, however, the most convenient level at which clustering must be stopped, according to the specific problem being analyzed. Thereafter, the relevance of the clusters obtained with respect to the specific clinical application, or any other application of interest, must be evaluated.

Since in EEG analysis, most methods of analysis follow a pattern recognition approach, explicitly or not, we consider here the most important aspects of such an approach in relation to general problems of automatic EEG diagnosis. For a thorough

treatment of pattern recognition theories, the reader is referred to the classic books of Duda and Hart (1), Mendel and Fu (2), and Tou and Gonzalez (3), and to the review of Demartini and Vincent-Carrefour (4) that deals with the specific field of EEG.

FEATURE EXTRACTION: SPECIFIC PROBLEMS

The usefulness of any EEG analysis method depends, to a large extent, on the choice of the set of features that is relevant to answer the question being investigated. In this section we consider, first, the main types of features used in EEG analysis in general terms; then we examine how these features can be incorporated into EEG classification systems in specialized cases.

Time-Domain Analysis Methods

Methods aiming at extracting *time-domain* EEG features were used in the early period of EEG quantification but are less used recently. The main features used in this context are derived from EEG *amplitude analysis*: the features ordinarily chosen are mean (m), standard deviation (σ), skewness, kurtosis, and coefficient of variation [$(\sigma/m) \times 100$] of EEG signals; these are computed from the original signal as discussed in Chapter 54. Furthermore, one can also define similar features for the rectified signal: mean, standard deviation, and coefficient of variation. Furthermore, *interval analysis* of EEG signals yields a number of other features: average frequency of zero crossings of the original signal and also of its first and second derivatives. The combination of amplitude and interval analysis (see Chapter 54) yields a set of features that can characterize EEG signals; in addition to those described above, a few others may be chosen such as the signal half-wave length and its derivatives (mean, standard deviation, and range), peak-to-peak values per wave (mean and standard deviation), and amplitude range (i.e., the difference between the largest and the smallest amplitude value within a certain time epoch). Other features that have been included in this kind of analyses are Hjorth's parameters: activity, mobility, and complexity, and parameters extracted using time–frequency analyses, for example, those obtained by wavelet decomposition, as explained in Chapter 54.

Spectral Analysis Using Nonparametric Methods

The most common features extracted from EEG, however, are derived by way of spectral analysis, such as the spectral intensity within the classic frequency bands, namely the mean *spectral intensity* (power or amplitude) and the average *frequency*. Although this may be rather trivial, it is important to consider

Table 56.1

EEG Features Obtained from Spectral Analysis

Frequency Bands			Factor Analysis			
Classical Definition (Hz)	Matousek and Petersén (5)	Gotman (6)	Weighting Factors, K		Hermann et al. (7)	Wieneke (<i>personal communication</i>)
			Frontal Channels	Other Channels		
$0 \leq \delta_1 \leq 1.9$		0.4–1.2	1.5	2		
$2 \leq \delta_2 \leq 3.4$	1.5–3.5	1.6–4.0	4	4	1.5–5.5	1.5–6.0
$3.5 \leq \theta_1 \leq 5.4$		4.4–6.4	3	5		
$5.4 \leq \theta_2 \leq 7.4$	3.5–7.5	6.8–7.2	3	1	5.5–8.5	6.0–9.0
$7.4 \leq \alpha_1 \leq 9.9$	7.5–9.5				8.6–10.5	9.0–10.5
$9.9 \leq \alpha_2 \leq 12.4$	9.5–12.5	7.6–12.8	1	1.5	10.5–12.0	10.5–12.5
$12.5 \leq \beta_1 \leq 17.9$	12.5–17.5				12.0–18.0	12.5–15.5
$18.0 \leq \beta_2 \leq 23.9$		13.2–30.0	1	0.5	18.0–21.0	15.5–18.5
$24.0 \leq \beta_2$	17.5–25.0				21.0–30.0	18.5–28.0
Ratios used for discrimination	$\frac{\theta}{\alpha + cs1}$		$\frac{k_1\delta_1 + k_2\delta_2 + k_3\theta_1 + k_4\theta_2}{k_3 - \alpha + k_6\beta}$			
	(θ and α in V), asymmetry Q		Asymmetry ratios $\left\{ \begin{array}{l} \alpha + \theta \\ \alpha + \beta \end{array} \right.$			

the fundamental question of how to define the EEG frequency bands. According to the generally accepted empirical definitions, one may use the subdivision indicated in Table 56.1. A question that should be asked is whether the activities in different frequency bands are independent, or not. This question can be answered by means of multivariate statistical analysis of EEG spectral values. This issue has been investigated thoroughly in the 1970s when the first computerized systems were started to be developed. Hermann et al. (7) using factor analysis chose 57 relative power values in frequency bands between 1.5 and 30 Hz with frequency resolution $f = 0.5$ Hz, as well as absolute power values. In this way, it was found that the power spectrum could be broken down into the frequency bands indicated in Table 56.1. Dymond et al. (8) also performed factor analysis of power spectra (log transformed) of bilateral centro-occipital leads and extracted four main factors having high loadings within the following frequency bands: 0 to 8, 6 to 12, 12 to 20, and 20 to 30 Hz; they also extracted factors associated with EEG asymmetry.

It should be noted, however, that applying factor analysis to sets of power spectra is not simple. The results depend on (i) whether the spectra are expressed in power or in root mean square (RMS) values, (ii) the way the spectra have been normalized, (iii) the derivations that were included, and (iv) the subject population. The results of an investigation of the

University Hospital of Utrecht (Wieneke, *personal communication*), which factorized frequency bands of power spectra (logarithmic values) obtained from eight symmetrical derivations in 89 patients, are shown in Table 56.1; in this case, normalization was performed using the band from 5 to 20 Hz as reference. The distribution of the most important frequency factor loadings obtained in this way for different derivations is given in Figure 56.1. We should emphasize that this type of analysis is sensitive to normalization and scaling. It is remarkable, however, that the different methods presented in Table 56.1 yield results that display a considerable degree of overlapping with respect to the different frequency bands. The frequency bands calculated in this way are also clearly compatible with those used in classical EEG; therefore, it may be said that a subdivision in frequency bands as used by Matousek and Petersén (5) or Gotman et al. (9) is acceptable for routine clinical EEG analysis. If one deals with a completely defined group of EEGs (e.g., in psychopharmacologic studies where one has a group of subjects receiving a drug and a control group), factor analysis may preferably be applied to such a specific group in order to define the optimal frequency bands that should be used in that specific study. Within the defined frequency bands, several primary spectral features, such as absolute power intensity in μV^2 or in dB, relative power, square root of power, and average

Copyright © 2010, Wolters Kluwer Health. All rights reserved.

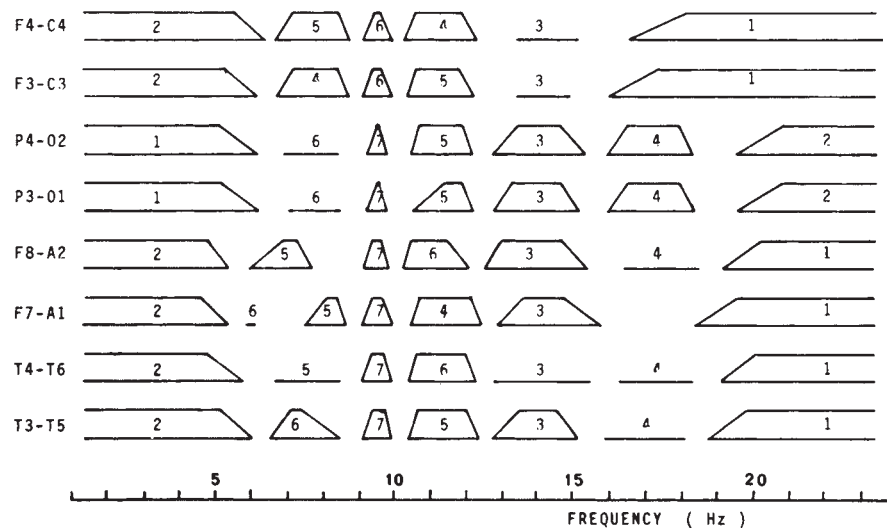


Figure 56.1 Factors found using factor analysis of EEG power spectra. Factor analysis of logarithmic power spectra for several derivations was done; power spectra were normalized in relation to the power within the frequency band between 5 and 20 Hz. Each factor is represented either by a *parallelogram* or simply by a *horizontal line*. The latter or the base of the *parallelogram* indicates the frequency interval within which the factor accounts for more than 50% of the variance; the *top line* of the *parallelogram* indicates the frequency interval within which more than 70% of the variance is accounted for by the corresponding factor. The factors are numbered in the order of decreasing eigenvalues from 1 to 6 or 7. A varimax rotation was used. The data were obtained from EEGs of 243 patients, each consisting of 100-second epochs recorded with eyes closed. (Courtesy of G. Wieneke.)

frequency within a band, can be computed. Secondary spectral features can also be derived. Several types of secondary features have been proposed based on empirical criteria; clinical application has validated those proposed by Matousek and Petersén (5) and by Gotman et al. (9). Matousek and Petersén (5) investigated 20 features extracted from the frequency spectrum of each EEG derivation. This study was based on the authors' claim that an increased amount of slow frequency in the EEG in abnormal cases might be considered analogous to the relatively large amount of slow activity seen in the normal but immature EEG. Initially, the EEG score chosen as being the most clearly age-related was the ratio between theta-band activity (3.5 to 7.5 Hz) and the alpha-band activity (7.5 to 12.5 Hz) added with a constant factor.

The same group later reinvestigated this problem (10). They used as normative data the RMS of the spectral values computed within the frequency bands, indicated in Table 56.1, for a number of derivations (FT-T3, C3-C0, T3-T5, P3-O1, and the symmetrical ones) of 562 EEG recordings from healthy individuals aged 1 to 21 years. A number of ratios between RMS values were also computed. In total, 20 spectral features per derivation were calculated, as follows: $x(1)$ = delta activity, $x(2)$ = theta, $x(3)$ = alpha 1, $x(4)$ = alpha 2, $x(5)$ = beta 1, $x(6)$ = beta 2, $x(9)$ = alpha 1/alpha 2, $x(10)$ = beta 1/(alpha 1 + alpha 2), $x(11)$ = beta 2/(alpha 1 + alpha 2), $x(12)$ = beta 1/beta 2, $x(13)$ = delta/theta, and $x(14)$ = sum of delta, theta, alpha 1, alpha 2, beta 1, and beta 2; features from 15 through 20 are normalized amplitudes in relation to $x(14)$ for the following bands: $x(15)$ = normalized delta, $x(16)$ = normalized theta, $x(17)$ = norma-

lized alpha 1, $x(18)$ = normalized alpha 2, $x(19)$ = normalized beta 1, and $x(20)$ = normalized beta 2.

Friberg et al.'s (10) model is defined by the following linear equation: calculated EEG age = $a(0) + a(1)x(1) + \dots + a(20)x(20)$. The coefficients $a(i)$, with $i = 0$ to 20, were estimated by minimizing the sum of squares of the differences between the subject's actual age and the calculated EEG age. The correlation coefficients between actual and calculated EEG age varied between 0.88 for derivations C3-C0 and C0-C4 and 0.86 for derivations F7-T3 and F8-T4. Those authors found that, according to their model, the calculated EEG age tended to be greater than zero when the line was extrapolated down to an actual age of zero. To avoid this, they introduced two new variables: the *calculated EEG maturity* and the *actual EEG maturity*; the former is linearly related to the calculated EEG age and the latter to the actual age. The ratio between calculated and actual EEG maturity is called the *ratio of EEG normality*, because the authors found that this ratio is closely related to the degree of EEG (ab)normality. To calculate such a ratio, the maximal actual EEG maturity of any individual is fixed to correspond to 22 years (age-related EEG changes are considered to be small beyond that age). The clinical implications of this form of feature extraction and data reduction are discussed below.

Gotman and his collaborators based their procedure for extracting spectral features on the widely accepted assumption that some kind of relation between slow and fast EEG activity should characterize the degree of EEG abnormality. Moreover, they pointed out that a relative measure of spectral intensity is preferable to an absolute measure because the latter depends on

a number of spurious factors (e.g., skull thickness). Therefore, these investigators analyzed the potential of several ratios, for example, $(\delta + \theta)/(\alpha + \beta)$, using different weighing factors and frequency band subdivisions, to discriminate the EEG between normal and abnormal subjects (slow-wave type of abnormality). The best weighing factors for different frequency bands and areas are given in Table 56.1. The same investigators introduced still another important spectral feature, a degree of *asymmetry*. To compute this feature, the scalp was subdivided into four symmetrical regions: frontal (Fp1-F3, Fp1-F7, Fp2-F4, Fp2-F8), temporal (F7-T3, T3-T5, F8-T4, T4-T6), central (F3-C3, C3-P3, F4-C4, C4-P4), and occipital (P3-O1, T5-O1, P4-O2, T6-O2). For each region, two asymmetry coefficients were calculated, one for the slow frequencies (weighted delta and theta values as given in Table 56.1) and one for the higher frequencies (weighted alpha and beta values). The value corresponding with the most active hemisphere was always placed in the numerator. Gotman et al. (9) called the display of these ratios extracted from spectral values *canonograms* (*canon* is Greek for “ratio”) (Fig. 56.2); the clinical validation of these features is discussed later in this chapter.

Other spectral features of interest are the spectral peak *frequencies* and corresponding *bandwidths*. There are several algorithms used to calculate peak frequencies: these involve computing a local maximum of the curve defining the spectral density. A peak is said to exist when it rises significantly above its surroundings. The bandwidth is usually calculated as the frequency interval between the 3-dB points at both sides of the peak.

A comprehensive analysis methodology that combines quantitative EEG and EP features is the approach introduced by John and collaborators and reviewed extensively in John et al. (11,12) and Prichep and John (13), under the name of *neurometrics*. This approach is based on the use of standardized data acquisition techniques, computerized feature extraction, statistical transformations in order to achieve approximately Gaussian distributions, age regression equations, and multivariate statistical methods, namely discriminant and cluster

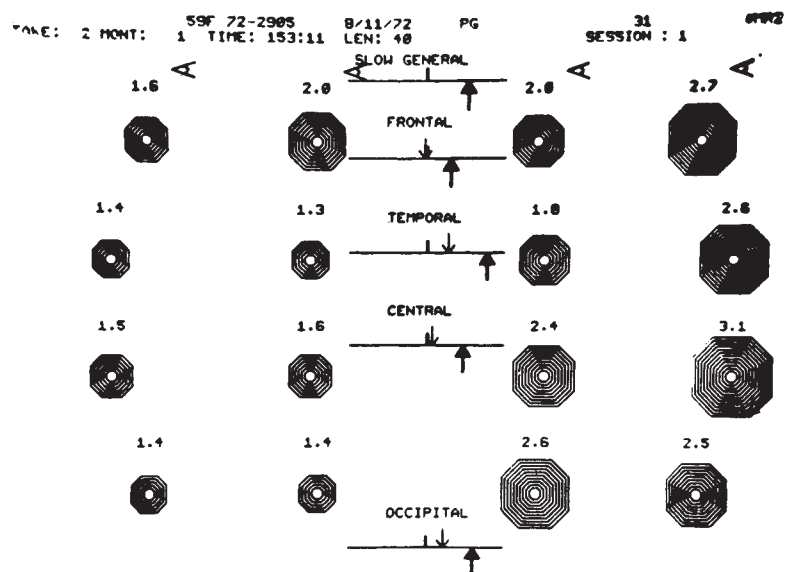
analyses to achieve differential diagnosis between patients’ (sub)populations. In this way, neurometric test batteries were constructed and applied to several clinical problems. A general battery consists typically of the following features: spectral composition, coherence, and symmetry indices of the spontaneous resting EEG; in addition, brainstem auditory evoked potential (BAEP) and brainstem somatosensory evoked potential (BSEP) to unilateral stimuli, checkerboard pattern reversal or flash visual EPs, and cortical EPs to different modalities both to predictable and unpredictable stimuli, are also included. This approach can be implemented in a personal computer.

Profiles of neurometric features that deviate from age-matched normal subjects have been obtained in several categories of patients suffering from cognitive disorders (e.g., dementias), psychiatric illnesses (e.g., different types of depressions and of schizophrenia), and neurologic dysfunctions, for example, compromised cerebral blood flow (14), as discussed by John et al. (12) and Prichep et al. (15). The clinical relevance of neurometrics is controversial and has led to publications presenting opposite points of view by John (16) and Fisch and Pedley (17). A special effort was made by John and collaborators to apply the neurometrics approach of quantitative EEG analysis to distinguish subgroups of patients with psychiatric disorders also with the aim of identifying potential responders to pharmacologic treatments (18). This was applied to patients suffering from obsessive-compulsive disorder (OCD) who received treatment with selective serotonin reuptake inhibitors (SSRIs) with the interesting result that the responders and non-responders presented distinct neurometric profiles (19,20).

Spectral Analysis Using Parametric Methods

In Chapter 54 we discussed the general theory of spectral analysis employing ARMA or AR models. One of the main advantages of these parametric methods of computing power spectra, as proposed initially by Zetterberg (21), is precisely the fact that the use of spectral parameter analysis (SPA) avoids having to subdivide the spectrum in distinct frequency bands

Figure 56.2 Canonogram from subject with multiple metastases in right hemisphere. The size of each *polygon* is proportional to a slow/fast EEG activity ratio, indicator of abnormality for a channel. They are arranged in a topographical pattern corresponding to the position of the derivations on the subject’s head: frontal on *top* and occipital on *bottom*. Arrows under *horizontal lines* indicate the asymmetry in slow EEG activity; *arrows above* indicate the asymmetry in fast EEG activity. Sixteen channels, anteroposterior bipolar montage covering parasagittal and temporal regions; EEG epoch, 40 seconds. (Adapted from Gotman J. Problems of presentation of analytical results. *Electroencephalogr Clin Neurophysiol Suppl.* 1978;34:191–197.)



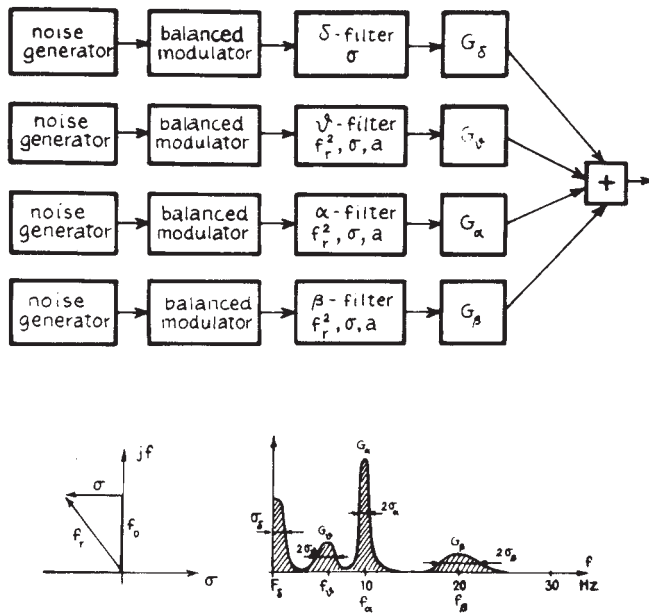


Figure 56.3 Block diagram of the EEG simulator; the δ filter represents a first-order active RC network; the δ , α , and β filters are of second order; potentiometers independently control the parameters $f(2/r)$ (which determine the resonance frequency f_0), σ (which determine the bandwidth), and α (which determine the zero of the transfer function); the power parameter is G . (Adapted from Zetterberg LH. Experience with analysis and simulation of EEG signals with parametric description of spectra. In: Kellaway P, Petersen I, eds. *Automation of Clinical Electroencephalography*. New York, NY: Raven Press; 1973:161–201.)

beforehand. The SPA method describes the EEG as resulting from noise sources passed through a set of parallel first- or second-order filters, as illustrated in Figure 56.3. As demonstrated by Isaksson and Wennberg (22), the relevant spectral features can be derived simply. The first-order filter describing the low-frequency band is characterized by two features: the total power G and the total bandwidth (interval from zero to the frequency corresponding to the 3-dB point); each of the second-order filters describing theta, alpha, and beta components is characterized by the three features: G (power), σ (bandwidth), and f (resonance frequency).

Isaksson and Wennberg (22) concluded that, for most practical applications, a SPA model of the fifth order, at the highest, is sufficient, although using this order model only the first-order delta component and the second-order alpha and beta components can be described. In a few cases, it may be necessary to use a model of the seventh order to include a second-order theta component. In a study comparing the degree of visually evaluated slow activity in a large number of artifact-free EEG epochs with the features identified through SPA of the same epochs, Isaksson and Wennberg (23) concluded that, for most derivations, there was a significant linear correlation between the degree of slow activity encountered with visual inspection and the value of the features G_δ (positive correlation) and σ_δ (negative correlation); in a few cases, there was also correlation with G_α (negative correlation) and σ_α (positive

correlation). The computation of an ARMA or AR model yields an important degree of data reduction. The relevant information is thus condensed in the coefficients of the model; the number of coefficients corresponds to the order of the model. As shown by Mathieu et al. (24) and Jansen (25), the coefficients can be used to characterize the EEG directly. The importance of this approach for EEG pattern classification is discussed later.

The Recognition and Elimination of Artifacts: Eye Movements and Muscle Artifacts

Physiologic and technical artifacts are the outstanding enemies of automatic EEG analysis. They must be eliminated if computer EEG analysis is to be used in clinical practice. It is a general requirement of EEG recording in any clinical laboratory that the records have a minimum of technical artifacts, a requirement that is even more critical in automatic analysis. One way to control the quality of EEG signals while performing analog-to-digital conversion in the clinical laboratory is by simply deleting those epochs that are below acceptable standards due to technical or to physiologic (e.g., ocular or muscular) artifacts. For example, the technician responsible for this operation may delete the series of digitized samples immediately preceding an identified artifact. Nevertheless, there will always be situations in which artifacts, particularly those of a physiologic nature, are unavoidable. This is particularly important during long-lasting EEG monitoring in several clinical (e.g., EEG-video monitoring of epileptic patients) and experimental (e.g., sleep studies) conditions and when computer-assisted quantification is applied (see also Chapter 35).

Eye movements and *muscle potentials* occur in most records of a few minutes' duration; they can distort power spectra and lead to detection of transient nonstationarities that may be difficult to distinguish from epileptiform events. *Eye blinks* can be reduced by recording with eyes closed; *slow eye movements*, however, are more difficult to avoid. These are bilaterally synchronous with a maximum in frontal derivations and represent an important contribution to the power in the delta band in these derivations. In the early days of EEG quantification, Gotman (6) discussed several methods of avoiding this type of artifact at the very first stage, for example, by subtracting the electro-oculogram (EOG). This matter has been reviewed by Jervis et al. (26) and by Brunia et al. (27). However, the technique of EOG subtraction may give rise to distortion of the EEG signals, since the EOG recording also contains brain signals (28) that may be partially eliminated by filtering first the EOG with a low pass of about 8 Hz. The transfer of EOG activity to the EEG can be analyzed using a frequency domain approach. Eye blinks and slow eye movements have different spectral properties and are transferred in different ways to the skull. Gain functions for transferring both types of eye movements to the skull were computed by Gasser et al. (29). These authors obtained average gain functions that they found to be of practical use in correcting EOG artifacts. In other studies, a frequency domain approach to correcting EOG artifacts has been proposed (30,31). Similarly, Jervis et al. (32) found that a computerized correlation technique provides results superior to analog techniques for removing eye movement artifacts. Elbert et al. (33) also stressed that the best correction for these

types of artifacts is obtained in the frequency domain, but indicated that the correction procedure should be based on more than one EOG derivation, and preferably on three. Fortgens and de Bruin (34) also obtained good results using the method of least squares based on four EOG derivations.

Other important physiologic artifacts are *muscle potentials*. Here also it is important to note that electromyographic (EMG) signals affect the EEG power spectrum not only at relatively high frequencies (30 to 60 Hz) but also even down to 14 Hz (35). Under normal conditions, there is very little EEG power at the scalp in the 30- to 50-Hz band; if the power is significantly large, however, one must suspect contamination with EMG signals. Gotman (6) proposed dealing with this problem by introducing a reduction factor with which the activity in the beta band should be multiplied; this factor depends on the spectral intensity integrated over the 30- to 50-Hz band. If this is below 1.5 $\mu\text{V}/\text{Hz}$, the reduction factor is equal to unity; if the activity is larger than 1.5 $\mu\text{V}/\text{Hz}$, the reduction factor decreased linearly to 0.1 as the spectral activity increases up to 5.0 $\mu\text{V}/\text{Hz}$.

An alternative way to deal with artifacts is that used by Gevins et al. (36), who determined thresholds for head and body movement artifacts (under 1 Hz), high-frequency artifacts mainly caused by EMG (34 to 50 Hz), and eye movements (below 3 Hz in frontal derivations) based on a short segment that includes those artifacts; thereafter, EEG epochs exceeding the aforementioned thresholds were simply discarded (37).

The need to avoid the contamination with artifacts of relevant EEG features is so pressing that this area of EEG signal analysis has been, for decades, in constant evolution. Here we briefly review the most relevant approaches.

Rather elaborate methods are based on decomposing a set of EEG signals into components that should represent the artifact and the EEG signals, respectively. One of these is the spatial filtering approach (38,39). According to this method, the topography of the artifact is first estimated on the basis of a specific recording where the artifact is clearly evident, since this is, in general, easier to model than the EEG. Thus, the artifact can be described as the product of the corresponding topography vector and time waveforms. This can be then subtracted from the EEG signals contaminated with artifact to yield the corrected signals.

Other methods have been proposed that differ in the way of separating EEG and artifact signals. With this objective Lagerlund et al. (40) used principal component analysis (PCA), but this method has the drawback that PCA yields uncorrelated components while the EEG signals and the artifacts may be correlated. An important step forward in this context has been the introduction of independent component analysis (ICA) (see Chapter 54) that is very effective in separating EEG signals from artifacts as shown in a number of applications (41–44). The application of ICA, however, needs some form of postprocessing to identify the components corresponding to the EEG signals and to the artifacts. Several strategies and combinations of approaches particularly with respect to their practical implementation are discussed by Ille et al. (38) and by Makeig et al. (42). Particularly useful is the software package developed by Makeig's group (45,46) that they called EEGLAB. This is an interactive Matlab toolbox for processing continuous and event-related EEG, magnetoencephalogram (MEG), and other

electrophysiologic data using ICA, time/frequency analysis, and other methods including artifact rejection, as indicated below.

Transient Nonstationarities: Epileptiform Events

The detection of epileptiform events is a typical example of the application of a pattern recognition approach in EEG analysis. In this case, the epileptiform events (spikes, sharp waves, and spike-and-waves) are considered to constitute the “signal,” whereas the background activity constitutes the “noise.” The difficulty here lies in defining the epileptiform transients, that is, the “signals” that one wants to identify. In 1949, Jasper and Kershman (47) classified these events into *spikes* (duration 10 to 50 milliseconds) and *sharp waves* (duration 50 to 500 milliseconds). The Terminology Committee of the International Federation of EEG Societies defined spikes as waves with a duration of 1/12 second (83 milliseconds) or less, and sharp waves as waves with a duration of more than 1/12 second and less than 1/5 second (200 milliseconds) (48). Later, this Federation Committee gave somewhat different duration limits for these phenomena, with spikes having a duration from 20 to under 70 milliseconds and sharp waves having a duration of 70 to 200 milliseconds (49). A few other characteristics have been identified. Spikes and sharp waves should be clearly distinguishable from background activity and have a pointed peak; their main component should be generally negative relative to other scalp areas, and their amplitude variable. A distinction between spikes and sharp waves has descriptive value only. The parameter characteristics of spikes found in the human EEG have been studied by Celesia and Chen (50).

One problem is the difficulty of defining a learning set that may be unambiguous. A pioneering investigation in this respect was carried out by Gose et al. (51); this study revealed considerable intra- and interrater variability. In practical terms several methods have been used to identify the epileptiform events by increasing the signal-to-noise ratio. Most of them are akin to the classic approach of Carrie (52), who used as a criterion the ratio between the amplitude of the second derivative of the EEG signal and the moving average of similar measurements from a number of preceding and consecutive waves; a ratio of 4 or 5 was said to indicate an epileptiform event. Most other relevant studies have proposed similar types of measures (53–57). All these methods involve a preprocessing stage that constitutes a form of high-pass filtering (e.g., computing the signal's second derivative).

The method used by Lopes da Silva et al. (58–62) is based on an essentially more general form of preprocessing. In this method, an EEG epoch is described by way of an AR model that provides the best fit to the background activity. The basic operation to improve the signal-to-noise ratio consists of passing the EEG signal through the inverse filter of this estimated AR model; this inverse filtering operation yields a new signal that ideally should have the properties of uncorrelated white noise. The statistical properties of this new signal are then determined; deviation of the new signal resulting from inverse filtering from a normal distribution at a certain probability level is thought to identify a transient nonstationarity (see Fig. 54.14). The essential feature of this method is that inverse filtering of the EEG epoch eliminates in an optimal way the background activity, allowing the transient nonstationarities to emerge clearly.

Not all transient nonstationarities, however, are necessarily epileptiform events; some may be physiologic artifacts or other kinds of EEG transients (e.g., lambda waves or sharp bursts of alpha waves). After detecting transient nonstationarities, one must apply a form of pattern recognition to select those that can be accepted as being epileptiform in nature. This constitutes the “two-stage analysis approach” proposed by Guedes de Oliveira and Lopes da Silva (63) and Guedes de Oliveira and Lopes da Silva (64). Two main pattern recognition methods have been proposed; one is based on a matched filtering approach and the other on piecewise characterization of the transient. Matched filtering using as template a spike-and-wave pattern has been used (65) to detect epileptiform transients even without preprocessing. Barlow and Dubinsky (66) used a comparable method, computing the running correlation coefficient between the EEG signal and a template (see Fig. 54.15). However, the variability of the waveforms characteristic of such transients presents a serious difficulty in dealing with this problem in practice. Pfurtscheller and Fischer (67) combined a preprocessing stage using inverse autoregressive filtering and a template matching stage for postselection of relevant epileptiform events. An alternative method is to apply a piecewise analysis to the transient nonstationarities, to identify those that belong to the epileptiform class. Smith (68) and Ktonas and Smith (69) proposed such a piecewise analysis method based on five features (Fig. 56.4): S_1 and S_2 , the maximum slopes, respectively, before and after reaching the peak of the spike; S_3 , the time taken by the spike to reach the peak after it attains maximum slope; and S_4 , the time taken by the spike to reach maximum slope after the peak. The sum ($S_3 + S_4$) of the time intervals corresponds to the duration of the epileptiform spike (S_5). The interval between two consecutive zero crossings of the same polarity of the first derivative (S_6) is also a relevant feature.

Frost (70) considered the problem in a simpler form, proposing the following characteristic features. Assuming that an epileptiform spike is a triangular wave with a point of origin M at the base, an apex S , and a point of termination P , Frost defined *amplitude* as the largest value of the segments MS or SP , and *duration* as the interval MP . Furthermore, he used as a measure of sharpness D , an estimate of the signal's second derivative. The initial processing step involves comparing the value of D with a threshold, so that, whenever D is larger than a certain value, a candidate spike is detected. Extracting the features described here requires a relatively high rate of EEG sampling—at least 200/sec.

The next section considers the practical implications of these methods in assessing the EEGs of epileptiform patients. According to the method of Gotman and Gloor (55), at the end of an analysis session the computer displays all transients detected, whether true or false. The distinction between these two types is made off-line in an interactive way. This form of analysis represents a considerable data reduction and provides a reliable account of the main types of epileptiform transients present in a given record.

The methods of analysis described in this section not only are useful in detecting the presence of epileptiform events, but also provide *quantitative information* on the morphology of such events, on their distribution over long periods of time, and

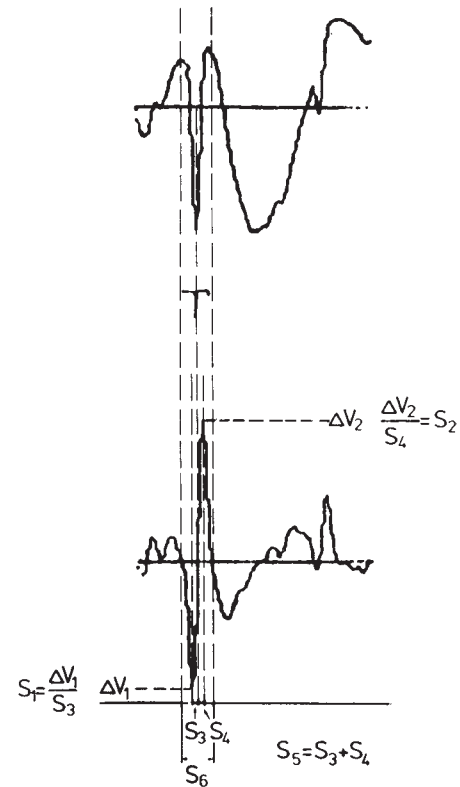


Figure 56.4 Top: An epileptiform spike; bottom: the corresponding first derivative. The parameters proposed by Ktonas and Smith (69) are shown: S_1 and S_2 , the maximal spike slopes, respectively, before and after reaching the peak; S_3 , the time taken by the spike to reach the peak after it attained maximal slope; S_4 , the time taken by the spike to reach maximal slope after the peak. The sum $S_3 + S_4$ is a measure of the duration of the sharp part of the peak. The time interval between two zero crossings of the same polarity of the first derivative is S_6 . The time duration of the signal shown is 1 second. (Adapted from Lopes da Silva FH. Analysis of EEG nonstationarities. *Electroencephalogr Clin Neurophysiol Suppl.* 1978;34:163–179.)

on their spatial distribution. Using this methodology, Ktonas and Smith (69), Lopes da Silva et al. (1978), and Gotman (71) observed that most epileptiform spikes, at the scalp, present a second slope that is steeper than the first, contrary to the qualitative description of Gloor (72). However, Lemieux and Blume (73) found that the spikes recorded directly from the cortex presented a first slope that was equal or steeper than the second. Another interesting analysis that can be realized using these methods consists of the quantification of the distribution of epileptiform spikes in relation to the occurrence of seizures. Gotman and Marciani (74) found that the level of spiking is not related to the probability of seizure occurrence, but they reported an increase in spiking in the days following seizures.

Very much as in the case of the detection of artifacts, the analysis of epileptiform events has attracted the interest of many researchers and new approaches are often being introduced. In most cases, new methods are published without a comprehensive comparison with older methods, which make it difficult to evaluate the performance of new approaches with respect to previous ones. An interesting exception is the study

of Dimpelmann and Elger (75), which we discuss in detail below (see the section “CADS and Epileptiform Events”).

Very often several categories of spikes can be distinguished in the EEG or MEG of patients with epilepsy that may differ considerably in waveform and may even be associated with different sources in the brain. Therefore, the population of spikes recorded in a given patient should preferably be grouped into distinct categories before being averaged. This is especially relevant if source reconstruction is going to be performed. This implies that a form of clustering of spikes has to be carried out. In the simplest case, this may be done by visual inspection by an experienced electroencephalographer. Such an operation becomes rather complex and time consuming if the number of spikes and of channels in the EEG/MEG is quite large. This has led to the development of computer algorithms to automate the identification of clusters of spikes (76). We should add that if the purpose of the analysis of epileptiform spikes includes the estimation of the localization of the corresponding sources in the brain, it is preferable to use MEG than EEG recordings because solutions of the inverse problem are more accurate with MEG (see also Chapter 5). One of these studies is that of Van't Ent et al. (77) who performed cluster analysis of MEG epileptiform spikes, grouping spikes according to the similarity between magnetic field characteristics. Thereafter, the spikes within one cluster are averaged to improve the signal-to-noise ratio such that the quality of equivalent dipole source estimates is enhanced. Similarly Abraham-Fuchs et al. (78) showed that averaging of similar spike events, recorded in the MEG, substantially improves the signal-to-noise ratio (a more general discussion of clustering algorithms is presented in the next section).

Classification and Clustering in EEG Analysis

The previous section considers different ways to find sets of features that can characterize EEG signals. In this section, we consider very briefly the next phase in pattern recognition, *classification* and/or *clustering*. For a detailed account of this problem, the reader is referred to Duda and Hart (1) as indicated above. It is necessary to consider this question here in order to be able to evaluate quantitative EEG analysis methods in the clinical laboratory. The essential problem is one of diagnosis; given a set of EEG epochs that have been analyzed and characterized by a number of features, it is necessary to determine what is the performance of the algorithm regarding the classification of the EEG epochs in a given number of diagnostic categories (e.g., normal/abnormal, sleep stages) or to label EEG transients (e.g., spikes) as epileptiform.

One way to solve this problem is to use *discriminant analysis*, which is possible only if one knows a priori that the EEG signals belong to a defined number of classes. Assuming that the analysis involves classifying EEG signals into two classes, normal and abnormal, and using a set of features, the feature vector defines a point in n -dimensional space.

In discriminant analysis, the space where all objects (e.g., EEG epochs characterized by a vector set) are contained must be subdivided into a number of regions; the objects within a region form one class. The functions that generate the surface separating the regions are called *discriminant functions*. An

object is assigned to a certain region or class by several types of *decision* rules; these are described in detail by Demartini and Vincent-Carrefour (4), among others.

To develop and test a classifier, it is important to dispose of a sufficiently large *learning set* (i.e., a set of N objects that have been classified a priori using independent criteria); in the case of EEG analysis, the independent criteria ought to be clinically valid. This implies that the objects must be classified by expert raters (electroencephalographers) using generally accepted criteria, possibly based on visual inspection, and making use of all relevant clinical information. The learning set should contain a sufficient number of objects (4). One way to develop an automatic method of EEG analysis is to divide the experimental set into two parts. Thus, the first part (*learning set*) is used to develop the classifier and the second to test its performance (*test set*). A useful alternative if the experimental set is too small is the “hold-one-out” strategy, which involves removing one object from the learning set and then resynthesizing the classifier and trying to recognize the selected object. This operation should be repeated for each object. The resulting error rate is a good estimate of the classifier’s performance.

The quality of the learning set is of primary importance. To start with, it is necessary to have knowledge about rater *reproducibility* (intrarater agreement) and *validity* (interrater agreement) as regards evaluation of the EEG records constituting the *learning set*. A few studies have addressed electroencephalographers’ overall classification of EEG records as normal or abnormal; in such cases, the validity of the visual assessment is usually about 80% to 90%. Although most raters generally agree on the division of the EEG into two classes globally (normal or abnormal), classification of short segments or of epileptiform transients is much less consistent. The same applies to intrarater agreement. In the assessment of EEG patterns corresponding to different sleep stages, however, a good degree of interrater agreement can be expected; thus, it is not surprising that methods of automatically classifying sleep stages have been those more often evaluated in a quantitative way. In assessing epileptiform events (spikes, sharp waves, spikes-and-waves), a large degree of interrater variability is also encountered. Gose et al. (51) found considerable variability in the human detection of spikes; a total of 948 events were marked as spikes by one or more electroencephalographers, but only 104 events were marked by five raters. However, disagreement between raters on individual spikes is not very important; a comparison on a patient basis (30 records seen by five raters) is more important; seen from this viewpoint, the average error rate was only 4%.

For the classification of EEG records in the learning set, it is important to utilize a *structural report* such as used by Volavka et al. (79), Rose et al. (80), Gotman et al. (81), Gotman and Gloor (55), and Gevins (82). In other words, EEG classes should be defined unambiguously; the abnormal EEG can be classified as paroxysmal or irritative, hypofunctional (cortical or centrencephalic) or mixed; the location of the abnormality (focal: frontal, temporal, central, occipital, lateralized, or diffuse) should also be specified. Furthermore, one may use a complementary second-order classification into diagnostic types related to the global medical diagnosis: space-occupying lesions, metabolic disorders, cerebrovascular insufficiency, seizure disorders, or psychiatric disorders.

EEG SEGMENTATION AND CLUSTERING

We should emphasize that EEG records are generally nonstationary. Although in the clinical laboratory it is usually possible to obtain representative EEG epochs by tightly controlling the subject's behavioral state, it is often desirable to distinguish in an EEG signal segment, characterized by different properties, that can be separated automatically. This is particularly important in the case of EEGs recorded under intensive care conditions, such as during anesthesia, or in other long-duration records. Ideally equivalent segments thereafter could be grouped together, thus defining a number of classes. An early effort in this direction was made by Bodenstern and Praetorius (83), who proposed a general method of EEG segmentation; they assumed that an EEG should be considered as a sequence of quasi-stationary segments of varying duration. They used an AR model as described in Chapter 54.

By setting appropriate thresholds, Bodenstern and Praetorius (83) have been able to formulate explicit criteria for EEG segmentation. The problem, however, is that the validity of this segmentation procedure in relation to clinically clearly defined states is difficult to demonstrate. Jansen (25) made an interesting effort along a similar line by using an algorithm akin to that discussed above but based on a Kalman filter and following a different strategy; this method is called Kalman–Bucy (KB) clustering. Defining segments of variable length based on statistical criteria proved to be too difficult because a good learning set could not be constructed. An alternative method followed by Jansen (25) was to divide the EEG into a large number of segments with a fixed duration of 1.28 seconds each, and classified them using an *unsupervised learning clustering* approach. In other words, he used a clustering algorithm to group segments with similar properties into a number of classes that were not defined a priori. Each 1.28-second segment is characterized by a feature vector consisting of the five coefficients of the corresponding AR model estimated using a Kalman filter, often complemented by a measure of amplitude. The statistical approach used in this case is a form of clustering (see review in Ref. 84). Clustering can be partitional or hierarchical; the former is based on a priori knowledge of the place occupied by some objects, which are then used as “seed points” around which clusters grow. The latter can have two forms, agglomerative or divisive, depending on whether one starts from an assembly of as many clusters as objects or from one cluster encompassing all objects. Jansen (25) used the agglomerative hierarchical clustering approach to group EEG segments of a number of types. This type of clustering involves an iterative process through which the two most similar clusters of the previous step are merged into a new cluster. The user can stop the process at any point, depending on the application. Using statistical criteria, it is possible to delimit the number of classes in such a way that the distance between their centroids does not fall below a certain value.

Hierarchical clustering of epileptiform spike events has also been used in the analysis of interictal EEGs. Guess and Wilson (85) presented an application by means of which spike events are separated into groups, based on topology and morphology, which yields an efficient method of performing detailed

analysis of long time series. Van't Ent et al. (77) reported a spike clustering analysis that yields meaningful results in neocortical localization-related epilepsy, in MEG.

This type of analysis may be criticized similarly to the segmentation method described earlier. Here also the number and types of classes are arbitrary; an advantage of clustering methods, however, is their flexibility; the same data may be clustered in several ways. This is feasible because all information necessary to characterize the EEG segments is stored in the form of a small number of coefficients (e.g., five coefficients of an AR model). Some applications of this method are discussed in the following section.

NEURAL NETWORK-BASED EEG CLASSIFICATION

Neural networks have been employed to classify EEG features. Several research groups have successfully explored this approach. This appears particularly interesting for the classification of single-EEG epochs. Three types of neural network–based classifications of EEG data were reported: classification of single-EEG trials for selective averaging (86); classification of averaged and nonaveraged multichannel EEG data; and classification of single-trial, multichannel EEG data (87). For these classifications, different types of neural networks were applied. A back-propagation network was used by Gevins and Morgan (86). Self-organizing feature maps followed by a learning vector quantizer (LVQ), both introduced by Kohonen (see review, Ref. 88), were used by Pfurtscheller et al. (87). The latter authors used a neural network approach to analyze and classify nonaveraged multichannel EEG data from an experiment where the subject had to press a microswitch with either the left or right hand, whereby the side of movement was indicated by a cue stimulus. On the basis of the spatiotemporal alpha event-related desynchronization (ERD) prior to movement, this method of automatic classification was able to predict the side of the hand movement. One part of the data was used for training the neural network, the other part to test the performance of the network as classifier. Peters et al. (89), using autoregressive modeling of EEG time series and artificial neural networks (ANNs), developed a classifier that can tell which movement is performed based on information taken from a segment of the EEG signal of a single trial. The classifier's rate of recognition of EEGs not seen before was 92% to 99% on the basis of a 1-second segment per trial. Thus, the classifier was considered suitable for a so-called brain–computer interface, a system that allows one to control a computer, or another device, by means of EEG signals (see also Chapter 57).

SEGMENTATION AND CLASSIFICATION IN SLEEP EEG ANALYSIS

Several attempts have been made to develop an automatic sleep analyzer based on EEG records, in combination with EOG and EMG or independently (see a review of classic studies by Johnson (90)). The development of an automatic processor has been preceded by a thorough quantitative study of the EEG characteristics during different stages of sleep. These studies

have been directed mainly to quantitative analysis of EEG signals recorded from C3-A1 and C4-A2, of EOGs recorded from the outer canthus of each eye referenced to the ipsilateral mastoid, and of EMGs from the submental muscle (see also Chapter 10). Three main characteristics of the sleep EEG have been identified by computer analysis.

Sleep spindles have been shown (91) to range in frequency from 12.4 to 14.6 Hz in young adults. Gondeck and Smith (92), however, found that frequency can vary about 2 Hz between different spindles; spindle duration varies between 0.5 and 0.8 seconds. Based on a model of the generation of sleep spindles, Kemp et al. (93) have introduced an optimal detector for this type of activity. *Delta activity* is the primary feature distinguishing waking and sleep stages; Johnson et al. (91) concluded that the most consistent peak in the spectrum during different sleep stages lies between 0.8 and 1.8 Hz. The delta activity increases between stage 1 (and rapid eye movement [REM]) and stages 2 to 4. With age, delta activity decreases in amplitude but not in incidence (94). In addition, a very slow oscillation, at 0.5 to 1 Hz, during sleep, was described by Steriade et al. (95) in cats, which differs from delta waves (see also Chapter 3). This very slow sleep oscillation was recorded during natural sleep in the EEG (96) and MEG (97) in humans. *K complexes* have been difficult to analyze automatically, probably because of their large variability. Bremer et al. (98) developed a hybrid pattern recognition method for detecting K complexes. Rosa et al. (99) proposed a method for the automatic detection of K complexes that yields good practical results. The method of Rosa et al. is based on a simple model of the neuronal network that is responsible for background EEG signals according to the proposal of Kemp (100). In the model, the main pathway is represented by a frequency-selective feedback loop. The central frequency of the network depends on the time constants of the neuronal elements in the network. Rosa et al. constructed a model that represents the delta activity typical of slow-wave sleep (SWS). The K complex is represented as the impulse response of such a delta model.

This section discusses some of the attempts to analyze automatically EEG signals in relation to sleep stages. The learning sets have been classified according to visual inspection, usually on the basis of criteria proposed by Dement and Kleitman (101) and Rechtschaffen and Kales (102). Künkel (103) summarized the results obtained by several investigators who used as the first extraction procedure a form of spectral or hybrid frequency analysis (104–106) or period analysis alone or combined with analog filtering (107,108). The mean rate of correct recognition of sleep stages varied for the different studies between 60% and 79%, depending largely on the visual classification method used and on the learning set. Martin et al. (109) and Viglione and Martin (110) reanalyzed this problem using a comprehensive methodology; they used power spectra combined with a time-domain technique to detect delta waves (period 0.55 seconds) exceeding 75 μ V amplitude, and two EOGs to detect horizontal eye movements. Interval analysis of delta waves was necessary because the power in the delta frequency band (0 to 2 Hz) was shown not to be proportional to the number of delta waves counted by human observers. EOG recordings were considered necessary in order to help distinguish between REM and waking

states. These authors validated their automatic sleep analyzer on sleep recordings of nine young subjects. Data from four subjects were used as learning sets and those of the other five as test sets. The sleep stages were classified visually by three human raters. For the five subjects, the average agreement between raters ranged from 85.8% to 91.4%; the agreement between the program and raters ranged from 77.7% to 86.2% and the agreement between the program and the consensus of raters (majority decision) ranged from 78.8% to 86.4%. Using hybrid systems, Smith and Karacan (106), Gaillard et al. (111), and Gaillard and Tissot (112) reported similar figures. Poppl (113) used as the first feature extraction method a time-domain amplitude and interval analysis procedure, which allowed considerable data reduction; by mapping the feature space to maximize the variance ratio between classes (in relation to the variance within classes) and using linear discriminant analysis, a very good (91%) recognition rate for a test run was obtained using the hold-one-out strategy. Mathieu et al. (24) obtained EEG features using an autoregressive model of order 9, fitted to a large number of 30-second epochs from five sleep EEG recordings of three different subjects. They found for the three subjects a recognition rate of 81% in a test run; when applied to a single patient's EEG, the recognition rate was 91%. The lower recognition rate obtained when using different subjects is a consequence of the relatively large intersubject variability. Mathieu et al. pointed out that grouping subjects by age classes might reduce variability. In any case, the most difficult operation of the automatic classifier was discriminating, on the one hand, between REM sleep and wakefulness and, on the other, between sleep stages 3 and 4. This would probably be facilitated if the AR model features had been combined with EOG data and with a supplementary method of detecting delta waves, as described above. This technique may be improved still further by incorporating a more accurate detection of EOG data during REM. Regarding the distinction between stages 3 and 4, the difficulty of the automatic methods is shared by the human raters; thus, many observations combine stages 3 and 4 into one stage called, simply, SWS. The usefulness of computer analysis in sleep analysis is still unconfirmed; data reduction is an obvious advantage, but the purpose of the effort being carried out must be clearly defined. A possible interesting application is in psychopharmacologic studies. Probabilistic models describing the statistical properties of the hypnogram (i.e., the transitions between stages and their duration) have been developed (114–116). Kemp and Kamphuisen (117) introduced a model combining probabilistic and deterministic aspects of sleep. Such models, based on a Markov chain process, may be useful for computerized analysis of hypnograms. An account of several classic computerized methods of sleep analysis has been published by Hermann and Kubicki (118). We should note that sleep staging is a rather fuzzy process. Indeed it is not an easy task to perform a computer-assisted analysis since the standards are not well defined. This is a caveat that should be taken into consideration. Most likely this is the reason why many ingenious algorithms developed in the past decades have not gained wide acceptance in practice. One general feature of these algorithms is that they are rule-based, and in general their performance depends very much on the learning population for

which they were developed. When they are tested in other populations and other laboratories, many problems arise. More recently Agarwal and Gotman (119,120) attempted to solve these limitations by developing an automatic sleep staging method that is based on the use of evolving schemes that can be adjusted depending on the type and quality of polysomnographical recordings. This algorithm adapts the sleep staging rules to the user preferences and the record being analyzed. A method based on advanced adaptive time–frequency analysis was developed by Malinowska et al. (121). This method uses Gabor functions that provide optimal definition jointly of frequency and time. This group pursued the development of automatic parametric sleep staging and tested the performance of the system in comparison with visual scoring of sleep stages by experts. The automatic system showed agreement with visual staging close to the interexpert concordance (122). Systems for sleep staging in ambulatory conditions have also been developed and tested (123) including EEG, EMG, and EOG signals; ICA was applied. Compared to a standard sleep analysis system, this system yields a concordance of 67.2%. Methods were also developed with the specific aim of assisting in the diagnosis of sleep apnea syndrome but not including EEG recordings, which falls outside the scope of this chapter. The fact that traditional sleep staging involves a subjective evaluation of EEG and other physiologic signals according to the classic Rechtschaffen and Kales rules has led to discussing the possibility of substituting these rules by an objective classification based on parameters extracted using automatic signal analysis of sleep. This discussion is spurred by the fact that there is considerable interrater variability and the scoring process is time consuming and subjective as discussed by Nieuwenhuijs (124). This discussion, however, is still ongoing.

QUANTITATIVE EEG IN INTENSIVE MONITORING DURING SURGERY

Automatic intensive monitoring of the EEG is of great importance when the cerebral circulation is in acute danger, such as during open heart or carotid surgery, in states of recovery or worsening of cerebral function after brain damage, in coma, or during hemodialysis. Monitoring of cerebral function during extended anesthesia is also of interest. EEG changes during anesthesia are well known (see review of early literature in Ref. 125); in this situation, a complex number of factors may affect neuronal function, cerebral circulation, and the general acid–base equilibrium in blood and tissues. Disturbances of these physiologic functions are reflected in EEG changes. Therefore, compressed spectral arrays (126) have been used in monitoring these conditions. Because significant data reduction is desired in order to implement real-time EEG monitoring at a reasonable cost, it is not surprising that systems have been developed based on drastic simplification of the EEG signal, for example, in the cerebral function monitor (CFM) developed by Maynard (127), Prior (128), and Prior et al. (129). Pronk (130) has published a review of computerized methods in perioperative monitoring. More recently the digital

techniques used in continuous EEG monitoring in the intensive care unit were reviewed by Scheuer (131), including conditions such as cerebral ischemia, acute severe head injury, and coma. It is interesting to note that the main EEG frequency ranges that represent ischemic changes in the brain, in a clinical setting, were examined in detail by Visser et al. (132), who determined EEG spectral changes as a function of time in the course of brain ischemia caused by short periods of circulatory arrest during surgery. After onset of circulatory arrest, the log spectral changes of three-epoch moving averages were calculated relative to the baseline spectrum. Factor analysis was carried out; 17 EEG periods were selected that showed changes progressing to an isoelectrical period. This analysis revealed four factors that represented the spectral EEG changes occurring during circulatory arrest and recovery. The frequency intervals of these factors were 0 to 0.5, 1.5 to 3, 7.5 to 9.5, and 15 to 20 Hz for all channels. The sequence of events was similar for all derivations. The first EEG change after circulatory arrest was an initial increase in alpha power and a decrease in beta power. On average, after approximately 15 seconds alpha power started to decrease, beta power decreased further, delta-1 power started to increase, and delta-2 power started to decrease. After approximately 25 seconds, the delta-1 power increase appeared to plateau or to decrease. Thus, to detect intraoperative cerebral ischemia, monitoring of changes in these four frequency ranges is preferable to monitoring changes in the classically defined frequency bands. Some special uses of EEG computer analysis in clinical environments, with particular emphasis on long-term EEG monitoring, are discussed in detail in Chapter 35, including long-term monitoring in intensive care units during cerebral ischemia and coma, but also during anesthesia in general, and particularly when neuromuscular blockade is used.

Many departments of anesthesia investigated the possibility of using a *simplified index* of EEG activity for this purpose. Thus, a quantified EEG measure was sought to assist the anesthesiologist in interpreting the changes in EEG signals. EEG power spectral analysis was explored; in particular the spectral edge frequency and the median power frequency were EEG parameters applied but were not found to be reliable in practice (133). The search for EEG variables that are valid indices of depth of anesthesia led to finding that EEG bispectra can yield useful results. Bispectra quantify the nonlinear phase coupling between various frequency components of the EEG signals as presented in Chapter 54 (Expression 54.16 and Fig. 54.4). Investigations of the behavior of EEG bispectra and other spectral variables were performed using EEG signals recorded continuously from a bifrontal montage (FP1-Cz and FP2-Cz). EEG parameters were correlated with the Observers' Assessment of Alertness/Sedation (OAA/S) scale (134). The bispectra presented the strongest correlation with OAA/S scores. With increasing sedation a progressive decrease in the magnitude of the bispectrum was found. The EEG bispectral magnitude was found to be a reliable measure for several anesthetics (135,136). Monitoring devices based on quantified EEG in this way appeared in the 1990s. These devices entered the field of EEG monitoring during anesthesia, such as the BIS monitor system (137), but the results must be interpreted carefully taking into

account the specific EEG of a patient, the anesthetic drugs, and other coadjuvant drugs used (e.g., a baseline EEG recording should always be made before administration of any drug). Indeed a multicenter study of bispectral EEG analysis for monitoring anesthetic effects has shown that BIS is a significant predictor of patient response to a surgery incision, but the utility of the BIS depends on the anesthetic technique used (138).

One clinical situation where quantitative EEG monitoring can be indicated is in those cases where barbiturates are used to lower intracranial pressure or to control epileptic seizures that may occur after traumatic brain injury and during convulsive status epilepticus. It is not easy to control the desired doses of barbiturate. Barbiturates are usually administered until EEG burst suppression appears. Monitoring of barbiturate effects on EEG is necessary to establish the lowest useful dose in real time. A prospective study performed at a pediatric intensive care unit (139), including children with barbiturate-induced coma after traumatic brain injury or generalized convulsive status epilepticus, showed that the BIS monitor can help to monitor barbiturate-induced coma, but it should be used with caution.

Quantitative EEG, whether or not along with auditory evoked potentials, should be considered in order to monitor brain functions during a variety of surgical procedures, particularly with respect to cardiac surgery with cardiopulmonary bypass and hypothermic circulatory arrest to detect awareness and indirect memory function, as well as to assess the adequacy of anesthesia (140).

COMPUTER-ASSISTED DIAGNOSTIC SYSTEM

For descriptive reasons it is useful to distinguish two types of computer-assisted diagnostic systems (CADS), because they are based on rather different designs. One pertains to the diagnosis of what might be called *hypofunctional states* of brain function, commonly characterized by some slowing of the dominant EEG frequency components or the appearance of extra-slow components; the other pertains to the diagnosis of so-called *irritative states* or different manifestations of epilepsy.

CADS and Hypofunctional States

Most systems currently used in clinical laboratories include subroutines designed to detect and evaluate hypofunctional states. In this field, several systems combine a high degree of sophistication with considerable clinical practicality and include comprehensive data reduction and specific displays for clinician's use. Thanks to the increased availability of relatively simple computer systems, many dedicated CADS algorithms were developed in the 1970s, such as those of Matousek et al. (141,142), Friberg (143), Friberg et al. (10), Gotman (6,144), Gotman et al. (9,81), Gevins et al. (145), Künkel and EEG Project Group (146), Storm van Leeuwen et al. (147), Mausby et al. (148), McGillivray and Wadbrook (149), Binnie et al. (150), Harner and Ostergren (151), Ebe et al. (152), and Bickford et al. (153). The practical success of the available systems depends not only on the exact method of EEG analysis, but also on (i) the system's capacity to avoid and/or eliminate artifacts, (ii) the degree of data reduction

possible without distortion of information, (iii) the graphical potential to convey adequate communication to the user, and (iv) operating ease and flexibility. In this respect, it is of paramount importance that the CADS allows interactive operation, in order to avoid an overflow of information and thus speed up the computations. At the same time, it should enable users to adopt their own strategies of selecting analytic facilities to give information on the most interesting features in a particular EEG. Because a generally accepted CADS does not yet exist, only a few indications of the most relevant points that one should take into consideration when implementing such a system in the clinical laboratory will be given here. To evaluate the basic method of EEG analysis and the possible *degree of data reduction*, a comparative statistical study of different EEG analysis techniques, available at the time, has been carried out in the same database (142). The database, however, was limited; it consisted of 57 EEG records obtained from patients with renal insufficiency (2), hepatic coma (5), brain injury (3), and patients without organic disease, but under psychotropic treatment (3); moreover, only EEGs recorded from derivation T3-T5 were analyzed. The EEG records were visually assessed by two independent raters; a structured report was used. The EEG records were sampled at 204.8 Hz. The correlation between a number of EEG features and the visually assessed degree of abnormality was computed and the following features were extracted: the RMS value as indicator of mean amplitude; mean frequency number of delta and theta waves calculated using zero-crossing interval analysis; power content in the delta and theta frequency bands calculated using fast Fourier transform (FFT) and the subdivision of frequency bands indicated in Table 56.1 (5); power content in the delta and theta frequency bands as percentage of total power; the ratio between power in the theta and alpha bands (theta/alpha); the ratio between power in the delta plus theta bands and that in the alpha plus beta bands (Power[delta + theta/alpha + beta]); and the so-called EEG age quotient (5) mentioned previously. All measures defined in terms of power were recomputed in terms of amplitude because amplitude is the unit used when employing analog frequency analysis. A few conclusions can be drawn from this early study. Time-domain features give, in general terms, worse results than features obtained using spectral analysis; the two most revealing features that emerged from this study were the relative power in "delta plus theta band" (normalized to total power) and the EEG age quotient. Friberg et al. (10) continued this research line, using mainly the so-called *ratio of EEG normality*, mentioned earlier, in order to obtain an automatic EEG assessment in a wider group of subjects. The overall agreement rate between automatic and visual EEG interpretation in several groups of patients was about 80%. Two types of EEG were difficult to classify: those with an alpha activity of 7 to 8 Hz, which the program tended to classify as abnormal (contrary to the visual assessment), and those with very low amplitudes. In terms of both informative display and interactive operation, the most attractive system proposed at about the same time is that of Gotman et al. (9,55,81). A typical output of the original system is shown in Figure 56.2. The

striking advantages of this form of display are the comprehensive presentation of topographical information and the degree of information compression achieved. Furthermore, it is possible to obtain, using such a system in an interactive way, other outputs of spectral analysis, such as plots of spectra of the EEG channels, plots of coherence and phase functions, as well as an output indicative of the variability of the four main frequency bands. Many of these early basic systems became more sophisticated in the course of time. The relevance of EEG features giving information about changes in symmetry in CADS dedicated to hypofunctional states should be stressed. In this context, a study carried out in order to investigate clinical relevance of quantitative EEG parameters in ischemic cerebrovascular disease should be mentioned. Sheorajpanday et al. (154) studied EEGs of patients suffering from subacute ischemic cerebrovascular disease. They used a pairwise derived brain symmetry index (pdBSI) as important EEG feature for this analysis and determined correlations between EEG parameters, clinical status, and volume of ischemia on diffusion-weighted imaging (DWI). The main conclusion was that pdBSI could reliably discriminate between stroke and TIA patients or control subjects, and correlated significantly with clinical and radiologic status.

CADS and Epileptiform Events

In contrast to the systems used to analyze EEG patterns in hypofunctional states, those that have been derived for automatic recognition and display of epileptiform events have received a good deal of attention in the past decade. Major interest with respect to these systems is in laboratories directly involved in the diagnosis and care of a population of epileptic patients, particularly in those locations where extensive EEG investigations using intracranial electrodes are performed as a guide for neurosurgery and where routine long-term EEG recording is carried out in combination with the determination of plasma levels of antiepileptic drugs. In the section “Transient Nonstationarities: Epileptiform Events,” we discussed already the main features characteristic of these transients and the problem of finding a consensus among raters about the identification of such transients by visual inspection; here we consider this issue at the more general level of the computer-assisted systems (CADS) dedicated to the diagnosis in epilepsy. CADS in epilepsy may have different objectives, such as detecting *interictal epileptiform transients*, detecting *epileptic seizures*, or *localizing an epileptogenic area* in the brain. In the last decade the development of methods that may permit the automatic *anticipation of epileptic seizures* generated wide interest (this specialized issue is presented in Chapter 30).

The principal aims of developing CADS for detecting *interictal epileptiform transients* are to quantify long-term variations in transient occurrence rates, especially in relation to antiepileptic drug therapy, and to determine the topographical distribution of such events. The basic methodologies used have been described in Chapter 54. The criteria mentioned above are imprecise and open to subjective interpretation. Nevertheless, experience has shown that they have pragmatic value. Furthermore, it is also important to consider the problem of

rejecting artifacts that may have characteristics similar to epileptiform transients, such as EMG, lambda waves, vertex waves, or K complexes in sleep, and positive occipital sharp transients.

Taking into consideration the above discussion, it seems desirable to develop CADS in which users can choose whether they want to have detected those events classified with a high probability by a consensus of electroencephalographers as epileptiform or all events that any electroencephalographer would accept as epileptiform (64,155). The strategic choice would depend on the clinical setting in which the analysis takes place. For instance, in routine clinical EEGs, one would probably prefer a stringent criterion in order to minimize the chance of false positives, whereas the investigator monitoring long EEG and plasma levels of antiepileptic drugs in known epileptic patients might be inclined to follow less stringent criteria. The rule-based algorithms developed by Gotman (156,157) and collaborators (158,159), and implemented in software packages, have practical value, especially when the objective is to detect epileptiform transients in long EEG recordings, such as during a whole night (see Chapter 35 for details of long-term monitoring). In this respect, the fact that the performance of these algorithms takes into account the well-known influence of the state of the ongoing EEG, namely of sleep stages on the occurrence of epileptiform events, is particularly valuable. In general, these automatic methods yield a relatively large number of false positives, and thus it is always necessary to perform a secondary visual reevaluation of the detected events. Nevertheless, this automatic CADS achieves a very comprehensive data reduction. Other algorithms have been proposed that may yield smaller rates of false positives (155,160–163). A practical conclusion of such studies is that visually corrected (a posteriori) automatic analysis of epileptiform events is a cost-effective procedure for the presurgical evaluation of epileptic patients associated with video-EEG monitoring (164).

No matter which detection method is chosen, it is always necessary to provide a comprehensive display of the results so that topographical interpretation may be made, particularly with regard to the existence of an irritative area.

To validate the clinical relevance of CADS, it is important to compare different methods according to a comprehensive protocol. Such a study was carried out by Dumpelmann and Elger (75), who reported the results of a comparison of the performance of two specialist reviewers and of three spike-detection approaches with respect to the detection of epileptiform spikes in intracranial recordings from subdural and intrahippocampal depth electrodes in seven patients. The systems analyzed were (i) the “rule-based system” of Gotman’s group, (ii) the “two-stage system” consisting of an inverse autoregressive filter and a second rule-based stage of Lopes da Silva’s group (64), and (iii) a “wavelet detector” using wavelet coefficients of the intracranial EEG (iEEG) data developed by the authors. The results are quite revealing: the agreement between the two human reviewers with respect to spike identification was less than 50%. The automatic systems achieved agreements of 24% (“rule-based system”), 26% (“wavelet detector”), and 32% (“two-stage system”) with the individual human reviewers. In spite of the small

proportion of agreements, the same anatomical regions were identified by human and automatic EEG analysis as generators for the majority of spikes. This led the authors to conclude that the poor agreement between the human EEG reviewers suggests that the definition of spikes and spike-like episodes in intracranial electrodes is far from unequivocal, although the localizing information is highly consistent by either visual or automatic spike detection, independent of the algorithm used for automatic spike detection. These conclusions are not really surprising since in our experience (64) there is considerable variability in how experienced reviewers score epileptiform transients, while the performance of the automatic methods described above does not differ appreciably from a consensus of a panel of eight reviewers. Wilson et al. (165) made a larger reliability study of the performance of human experts in detecting epileptiform spikes and concluded that the average interrater correlation was 0.79. These authors proposed that this database could serve as a “gold standard” for testing computer algorithms or other readers. The same group (166) developed later a neural network approach that performed automatic grouping of spikes via hierarchical clustering (using topology and morphology), the performance of which was close to that of human experts. Appropriately noting that in spite of the many algorithms that have been developed in the past decades dedicated to the detection of epileptiform spikes, an ideal system continues to be illusive, Harner (167) proposes a spike/nonspike database as a tool for assessing parameters and methods for automatic epileptiform spike detection that is available from the author.

Since the advent of the MEG, it has been assumed that this new methodology would be useful for the *localization of epileptiform events* (168). The early literature has been reviewed by Sutherling and Barth (169), Ricci (170), and Engel and Ojeman (171). In the 1990s, the development of large arrays of sensors for MEG recordings combined with advanced realistic models of the brain and surrounding tissues based on magnetic resonance imaging (MRI) scans has led to a number of interesting investigations with the aim of improving spike source localization (172–182). A conclusion that can be derived from these and similar studies is that the localization of epileptiform sources based on MEG data, especially if combined with EEG data, using realistic models of the head based on MRI scans, can provide valuable diagnostic information of particular interest in the evaluation of candidates for epilepsy surgery. The investigation of Van't Ent et al. (77), introduced above with respect to clustering methodologies, is an example; after clustering epileptiform spikes the spikes within one cluster were averaged and the underlying sources were estimated using a single equivalent current dipole model (see Fig. 5.4). A dipole was estimated at each time sample during the same time window as used in the clustering procedure. For the forward computations, a segmentation of the brain from MRI of each subject was used as volume conductor. Dipole solutions were accepted only when the residual error was less than 10%. The MEG data were transformed to the MRI coordinate system by matching fiducial markers. The estimated dipole locations are presented on MRI, as shown in Figure 56.5. Some of these clusters are very close to

the lesion visualized in the MRI. In an interesting study a comparison between the performance of MEG and EEG recordings of epileptiform spikes was performed using intracranial EEG recordings as reference. Tanaka et al. (183) investigated the accuracy of spatiotemporal source analysis of MEG and scalp EEG with respect to the propagation of frontotemporal spikes in patients with partial epilepsy, using a cortically constrained minimum norm estimate. Furthermore, iEEGs were recorded from temporal and frontal lobes in the context of presurgical evaluation. These authors concluded that the spatiotemporal analysis of MEG spikes models the time course of frontotemporal spikes as observed on iEEG more adequately than the EEG.

In *clinical practice* epileptiform spike detectors are currently used in digital acquisition software applied on-line. Although these methods may differ in detail, they all derive from the results obtained in the previous studies described above (for review see Ref. 184). In general terms they are based on the identification of the features described above, namely sharpness, duration, slopes, and relative amplitudes. Furthermore, a measure of EEG background state is very important since detection is always a process of extracting a signal (the spike) from the background, and the changes of the latter necessarily affect the performance of the detector, as shown by Gotman and Wang (159). In addition, information about the distribution in space of the detected events is commonly used (63,77,184–186). As pointed out by Flanagan et al. (185), the computation of equivalent dipole models, using appropriate detection and preprocessing methods, as indicated above, provides a spatial parameter for each detected epileptiform event, and this may constitute valuable information that may be readily combined with MRI and other relevant data, for the clinical assessment of a patient. A critical review of spike-detection methods in scalp EEG has recently been published by Halford (187).

A new development in this area of endeavor is the exploration of the possibilities offered by the combination of EEG and functional MRI (fMRI) recordings (188) in search for ways of improving the localization of sources of epileptiform events. Al-Asmi et al. (189) studied patients with focal epilepsy and frequent spikes who were subjected to spike-triggered or continuous fMRI with simultaneous EEG. The activated regions in fMRI were concordant with EEG localization in almost all studies and confirmed by intracerebral EEG in some patients. Bursts of spikes were more likely to generate an fMRI response than were isolated spikes. The authors concluded that combining EEG and fMRI in focal epilepsy yields regions of activation that are presumably the source of spiking activity. These regions are highly linked with epileptic foci and epileptogenic lesions in a significant number of patients. This research area is most promising since the quality of simultaneously recording of EEG and fMRI in epileptic patients is becoming practically reliable (190).

Automatic *detection of seizures* presents another kind of problems, as discussed in more detail in Chapter 35. In the initial phase of computer-assisted detection of seizures, the recognition of *petit mal absences* characterized by 3/sec spike-and-wave complexes was one main area of investigation.

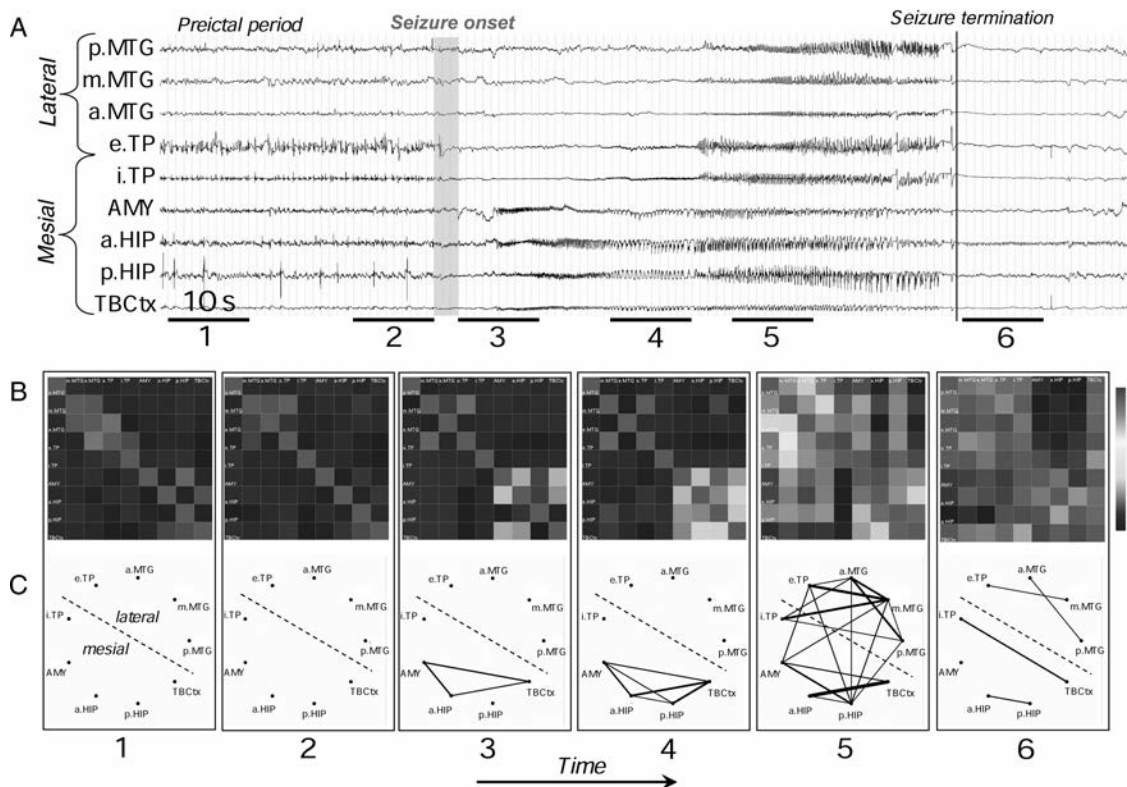


Figure 56.5 Characterization of epileptogenic networks in the temporal lobe during the transition from preictal to seizure activity. **A:** Intracerebral EEG recording performed in a patient with mesial TLE. **B:** Color-coded nonlinear correlation matrices obtained from the pairwise computation of nonlinear correlation coefficient h^2 over six different 10-second intervals chosen during the preictal period (1,2), the ictal period (3 to 5), and after seizure termination (6). **C:** Graphical representation in which the lines indicate “abnormally strong” couplings between the two considered structures (graph nodes). Only significantly high interdependencies are represented (i.e., h^2 values greater than 0.32; this value corresponds to the average h^2 value computed over the interictal period C2 standard deviations). Line thickness is proportional to h^2 values. (Adapted from Wendling F, Bartolomei F, Senhadji L. Spatial analysis of intracerebral electroencephalographic signals in the time and frequency domain: identification of epileptogenic networks in partial epilepsy. *Phil Trans R Soc A*. 2009;367:297–316.) (See color insert)

This is understandable considering that these seizures are relatively simple to detect in the EEG, while they are of clinical interest in order to investigate correlations between such phenomena and behavior. The technique proposed by Ehrenburg and Penry (191) was designed to recognize generalized spike-and-wave patterns whose main component, the *absence spike*, should be detected by way of a procedure based on zero-crossing analysis. The EEG records were classified visually by three raters; the consensus of all three was employed as a criterion for assigning the program’s correct responses. In a test population of 12 patients, the program agreed with the consensus in 85% of the cases, and it had 1% overrecognitions, which correspond to “false positives.” The program’s agreement with the consensus improved to 92% when all sleep sections were eliminated from the analyzed EEG. This particularly well-designed study led the authors to conclude that clinical applications of this CADs will lead to reduced costs over visual EEG assessment. Other CADs with the same main objective as the one described above have been developed (52,70,192,193). The advantages of

this type of CADs in petit mal epilepsy are already widely appreciated by researchers interested in quantitative clinical studies.

Quite another sort of problem is the automatic recognition of other types of epileptic seizures, mainly of *partial complex seizures* characteristic of temporal lobe epilepsy. The interest in automatic detection of this type of seizures stems from the fact that the central objective of EEG in epilepsy is recording an electroclinical seizure. In the early phases of computer-assisted diagnosis in epilepsy, technical and computer facilities enabled recording EEG continuously for further off-line analysis (194,195). Babb et al. (196) proposed an analog device with the objective of performing automatic seizure detection, based on the recognition of high-frequency activity occurring over several seconds. In this system, false alarms were quite frequent (30%). Currently, there is software available for the detection of seizures in clinical settings that provides reliable results, although it is not perfect. In a few laboratories these systems are being used in combination with methods of stimulation to

influence the development of seizures. Peters et al. (197) described an integrated bedside system for real-time seizure detection and automated delivery of electrical stimulation directly to the brains of subjects undergoing invasive epilepsy surgery evaluation. These authors conclude that this network system is proof of the concept of a portable or implantable device that could serve identical functions. Viglione et al. (198) and Viglione (199) attempted earlier to develop miniature automatic seizure recognition and warning systems that could be carried by patients; this system was successful in some cases but led to too many false alarms.

A related question is how to estimate the *localization of an epileptogenic area*, that is, where within the brain epileptic seizures originate. There have been some efforts to localize possible sources of seizures on the basis of scalp recordings, and using dipole fitting methods, however, with much difficulty (200). This is not surprising since it is not likely that the neuronal networks involved in the initiation of an epileptic seizure may be anatomically restricted to an area that might correspond to a discrete dipolar configuration. Nevertheless, this was attempted by Kobayashi et al. (201), who developed a noninvasive method of analysis to localize the source and visualize the time course of seizures, and to provide the location and orientation of the equivalent dipole generating this activity. This method was applied to scalp seizures in three patients with temporal lobe epilepsy and single-focus seizures confirmed by intracerebral recordings. A realistic head model based on MRI was used for computation of field distributions. When seizure activity was still not visually identifiable on the scalp, the method demonstrated in all scalp seizures a source in the temporal neocortex corresponding to the region of seizure activity in intracerebral recordings. More experience with this kind of methodology is needed to validate this approach. More recent and elaborated methods aiming at providing an automatic warning system for epileptic seizures using intracerebral electrodes (202) and at the detection of the onset of seizures in scalp recordings (203) have been developed and are being used in clinical practice (see Chapter 35 for details).

The problem of detecting seizures has been also approached applying ANNs providing an interesting way to seizure detection (163,204). The study of Wilson et al. (205) is particularly interesting because these authors applied the “Reveal algorithm” to the detection of a large number of seizures from 426 epilepsy patients combining three methods, novel in their application to seizure detection: matching pursuit, small neural network rules, and a new connected object hierarchical clustering algorithm. They found a sensitivity of 76% with a false-positive rate of 0.11/h, what was a better performance than of other comparable methods.

The objective of localizing an epileptogenic area, or better an *epileptogenic network*, is particularly important in patients with complex partial seizures resistant to pharmacologic therapy who are candidates for temporal lobectomy. On the basis of iEEG recordings, useful results have been obtained by computing *time relations* between EEG signals recorded from different sites. In this respect, the pioneer work of Brazier (206,207) was particularly influential. She computed cross-power spectra

(*coherence* and *phase*) between EEG seizure records from different derivations. By determining the phase (φ in degrees) between pairs of derivations at a frequency (f in Hz) with pronounced coherence, estimated time delays were computed. Although interesting results have been obtained, mainly in cases of seizures recorded using electrodes implanted in limbic structures, it should be noted that this method can give ambiguous results. To decide that there is a time delay depends on finding a linear relation between phase and frequency over a sufficiently wide frequency band. A difference in phase ($\Delta\varphi$) corresponding linearly to a difference in frequency (Δf) represents a time delay computed as $\Delta t = (\Delta\varphi/\Delta f \times 360^\circ)$. Alternative methods were proposed by Gersch and Goddard (208), Gersch and Tharp (209), and Tharp and Gersch (210). The latter were able to interpret the origin and spread of seizure activity within the brain of a patient carrying chronically indwelling electrodes, a conclusion that was not possible on the basis of visual inspection of the records. Gotman (211) applied the same principles to the analysis of some iEEG records and was able to show that at a contralateral site the seizure activity is delayed by a few milliseconds compared with the seizures at the focal area. In the same way Gotman and Levtova (212) were able to determine the relationships between amygdala and hippocampus in temporal lobe seizures.

From these studies, it became clear that the coherence of, and time delays between, different EEG channels during an epileptic seizure usually change rapidly in the course of time. This implies that such seizures must be analyzed using short EEG segments. An interesting method, also aiming at determining the time relations between different EEG signals in such a way that it is possible to estimate the flow of information between different brain sites, has been proposed by Kaminski and Blinowska (213), based on autoregressive models. This method can yield interesting results with respect to how epileptiform seizure activities may spread in the brain from a focal area (214).

To circumvent the limitations of linearity of the methods described above, new approaches were pursued. In this context Mars and van Arragon (215) proposed to compute a measure of the average amount of mutual information (AAMI), in the sense of Gelfand and Yaglom (216), between pairs of EEG signals as a function of the delay time introduced between both signals. It should be noted that this method is related to the cross-correlation as defined by Equation 54.10, but is more general, since AAMI is not constrained by a linear relation between both signals. The AAMI method of analysis was used for focus localization in animals having a kindled epileptogenic focus (217). In this way, time delays could be found for certain phases of epileptic seizures and the spread pattern of these seizures obtained. The same method was also applied to human seizures (218). The algorithms based on AAMI, however, proved to be rather cumbersome to apply in practice. This led to the creation of a new method of nonlinear regression analysis (the h^2 method of Refs. 219–221). This consists of computing a general coefficient of nonlinear fit between any pair of signals. The applications of this nonlinear regression coefficient to EEG signals recorded during seizures in animals (222) revealed that a

large number of EEG signals recorded from different, but functionally related, brain areas present clear nonlinear relations. The same applies to EEG signals recorded from intracranial electrodes in patients (220,223) and in rats with absence-like seizures (224). Thus, this method offers perspectives for the determination of the site of an epileptogenic focus, based on a set of simultaneously recorded EEG signals. In a recent study of Wendling et al. (225) several methods to assess functional brain connectivity based on signals recorded from different brain areas during partial complex epileptic seizures (Fig. 56.5) were applied, namely linear and nonlinear regression, phase synchronization, and generalized synchronization, using a model-based methodology. This comparison revealed that there was no “ideal” method, that is, none of the methods performed better than the other ones in all studied situations. Nevertheless, regression methods (linear or nonlinear) showed sensitivity to the coupling parameter in all tested models with average or good performances, which leads to the conclusion that it is advisable to first apply these regression methods in order to characterize functional brain connectivity, under normal or pathologic conditions, before using more sophisticated methods that require specific assumptions about the underlying model of relationship. In addition, these authors recommend to use time–frequency methods when it is interesting to determine functional coupling in specific frequency subbands (“frequency-locking”) as in epilepsy. In this context, it should be noted that the choice of frequency bands is critical (226). This was approached by Ansari-Asl et al. (227) using a linear estimator based on the computation of the Pearson product–moment correlation between EEG signals filtered in narrow and overlapping frequency bands.

An exciting novel development is the possibility of detecting changes in the EEG that may occur before an epileptic seizure is manifest in the EEG, that is, to be able to *anticipate a seizure*. Chapter 30 is dedicated to this issue.

BRAIN MAPPING: METHODOLOGY

Brain mapping is the current term used for the methodology of representing the EEG activity, either spontaneous or evoked, in the spatial domain as a topographical map projected onto the scalp. This field has developed very much in the last decade so that the present edition includes a specialized chapter (Chapter 55) concerned with the use of EEG as a functional imaging method.

COMPUTER SYSTEMS FOR ROUTINE APPLICATION IN EEG LABORATORY

Computer technology has advanced very rapidly with the generalized use of microprocessor technology. Thus, nowadays, there is a wide choice of computer systems that can be used in the clinical routine EEG laboratory. These systems offer the possibility of data acquisition, editing and processing the data, artifact rejection, statistical analysis, and brain mapping. An example is the very comprehensive software package developed by Makeig and collaborators (45,46): EEGLAB that is freely available (<http://www.sccn.ucsd.edu/eeglab/>) under a public

license for noncommercial use and open-source development, together with a user tutorial and extensive documentation. Besides this package several other open-source software tools are now available in the public domain that have been developed to analyze multichannel biomedical signals including neurophysiologic data, such as low-resolution brain electromagnetic tomography (LORETA; standard and exact) developed by Pascual-Marqui et al. (228,229). Commercially available since 1996, the ASA software has become rather popular among clinical and cognitive researchers (230). BioSig is an open-source software library for brain–computer interfaces, where an overview of other open-source software tools for biomedical signal processing is available (231).

CONCLUDING REMARKS

The field of computer-assisted diagnosis based on EEG/MEG signals with the aim of automatic analysis of such signals in clinical situations has developed considerably in the past decades. In the 1970s in the early stages of this field, many individual groups proposed their own algorithms that were almost always tested only in the own environment. These algorithms became more sophisticated and more powerful with the advances in computer facilities and software possibilities. Nonetheless, most of these algorithms did not reach a wide acceptance in practice. One weakness is that very few studies made comprehensive comparisons of the performance of different algorithms on the same test set and using identical criteria. Two interesting contributions that carried out such studies are that of Dumpelmann and Elger (75), who compared the performance of two specialist reviewers and three spike-detection approaches with respect to the detection of epileptiform spikes, and that of Wendling et al. (225,226) who compared the performances of several methods to assess functional brain connectivity, as described above. More of such studies are necessary. In the last two decades new possibilities emerged with the enhanced availability of comprehensive software packages that can be used in the clinical routine EEG laboratory, as mentioned already. With respect to the latter we may also stress the need for comparative performance assessment under well-controlled laboratory conditions, particularly regarding their potentiality as valuable tools to enhance EEG/MEG evaluation in clinical settings.

REFERENCES

1. Duda RO, Hart PE. *Pattern Classification and Scene Analysis*. New York, NY: John Wiley & Sons; 1973.
2. Mendel JM, Fu KS, eds. *Adaptive Learning and Pattern Recognition Systems*. New York/London: Academic Press; 1970.
3. Tou JT, Gonzalez RC. *Pattern Recognition Principles*. Reading, MA: Addison-Wesley; 1974.
4. Demartini J, Vincent-Carrefour A. Topics on pattern recognition. In: Remond A, ed. *EEG Informatics. A Didactic Review of Methods and Applications of EEG Data Processing*. Amsterdam: Elsevier; 1977:107–126.
5. Matousek M, Petersén I. Frequency analysis of the EEG in normal children and adolescents. In: Kellaway P, Petersen I, eds.

- Automation of Clinical Electroencephalography*. New York, NY: Raven Press; 1973:75–102.
6. Gotman J. *Experiments in the Automation and Quantification of EEG Interpretation: Localized Brain Lesions and Epilepsy* [PhD thesis]. Montreal, Canada: McGill University; 1976.
 7. Hermann WM, Fichte K, Kubicki S. Mathematische rationale für die klinische EEG-Frequenzbanden. I. Faktorenanalyse mit EEG Powerspektralschätzungen zur Definition von Frequenzbandern. *EEG-EMG*. 1978;9:146–154.
 8. Dymond AM, Coger RW, Serafetinides EA. Preprocessing by factor analysis of centro-occipital EEG power and asymmetry from three subject groups. *Ann Biomed Eng*. 1978;6:108–116.
 9. Gotman J, Skuce DR, Thompson CJ, et al. Clinical applications of spectral analysis and extraction of features from electroencephalograms with slow waves in adult patients. *Electroencephalogr Clin Neurophysiol*. 1973;35:225–235.
 10. Friberg S, Matousek M, Petersen I. *A Mathematical Model for the Age Development of the Background Activity in the Human Electroencephalogram. Technical Report, 2:80*. Gothenburg, Sweden: Research Laboratory of Medical Electronics, Chalmers University of Technology; 1980.
 11. John ER, Prichep LS, Easton P. Normative data banks and neurometrics: basic concepts, methods and results of norm construction. In: Gevins AS, Remond A, eds. *Handbook of Electroencephalography and Clinical Neurophysiology (Revised Series). Vol I: Methods of Analysis of Electrical and Magnetic Signals*. Amsterdam: Elsevier; 1987.
 12. John ER, Prichep LS, Fridman J, et al. Neurometrics: computer-assisted differential diagnosis of brain dysfunctions. *Science*. 1988;239:162–169.
 13. Prichep LS, John ER. Neurometrics: clinical applications. In: Lopes da Silva FH, Storm van Leeuwen W, Remond A, eds. *Clinical Applications of Computer Analysis of EEG and Other Neurophysiological Signals. Handbook of Electroencephalography and Clinical Neurophysiology. Vol 2*. Amsterdam: Elsevier; 1986:153–170.
 14. Jonkman EJ, Poortvliet DCJ, Veering HM, et al. The use of neurometrics in the study of patients with cerebral ischemia. *Electroencephalogr Clin Neurophysiol*. 1985;61:333–341.
 15. Prichep LS, John ER, Mas F. Neurometric functional imaging: 1. Subtyping of schizophrenia. In: John ER, ed. *Machinery of the Mind*. Boston, MA: Birkhauser; 1990:460–471.
 16. John ER. The role of quantitative EEG topographic mapping or ‘neurometrics’ in the diagnosis of psychiatric and neurological disorders: the pros. *Electroencephalogr Clin Neurophysiol*. 1989;73(1):2–4.
 17. Fisch BJ, Pedley TA. The role of quantitative topographic mapping or ‘neurometrics’ in the diagnosis of psychiatric and neurological disorders: the cons. *Electroencephalogr Clin Neurophysiol*. 1989;73:5–9.
 18. Prichep LS, John ER. QEEG profiles of psychiatric disorders. *Brain Topogr*. 1992;4(4):249–257.
 19. Hansen ES, Prichep LS, Bolwig TG, et al. Quantitative electroencephalography in OCD patients treated with paroxetine. *Clin Electroencephalogr*. 2003;34(2):70–74.
 20. Prichep LS, Mas F, Hollander E, et al. Quantitative electroencephalographic subtyping of obsessive-compulsive disorder. *Psychiatry Res*. 1993;50(1):25–32.
 21. Zetterberg LH. Experience with analysis and simulation of EEG signals with parametric description of spectra. In: Kellaway P, Petersen I, eds. *Automation of Clinical Electroencephalography*. New York, NY: Raven Press; 1973:161–201.
 22. Isaksson A, Wennberg A. An EEG simulator—a means of objective clinical interpretation of EEG. *Electroencephalogr Clin Neurophysiol*. 1975;39:313–320.
 23. Isaksson A, Wennberg A. Visual evaluation and computer analysis of the EEG—a comparison. *Electroencephalogr Clin Neurophysiol*. 1975;38:79–86.
 24. Mathieu M, Tirsch W, Poppl SJ. Multichannel online EEG analysis by means of an autoregressive model with applications. In: Matejcek M, Schenk GK, eds. *Die Quantifizierung des Elektroenzephalogramms*. Konstanz: AEG-Telefunken; 1975: 475–486.
 25. Jansen BH. *EEG Segmentation and Classification* [PhD thesis]. Amsterdam: Free University; 1979.
 26. Jervis BW, Ifeachor EC, Allen EM. The removal of ocular artefacts from the electroencephalogram: a review. *Med Biol Eng Comp*. 1988;26:2–12.
 27. Brunia CHM, Mšcks J, van den Berg-Lenssen MMC, et al. Correcting ocular artifacts in the EEG: a comparison of several methods. *J Psychophysiol*. 1989;3:1–50.
 28. Berg P, Scherg M. A multiple sources approach to the correction of eye artifacts. *Electroencephalogr Clin Neurophysiol*. 1994;90:229–241.
 29. Gasser T, Sroka L, Mocks J. The transfer of EOG activity into the EEG for eyes open and closed. *Electroencephalogr Clin Neurophysiol*. 1985;61:181–193.
 30. Whitton JL, Lue F, Moldofsky H. A spectra method for removing eye movement artifacts from the EEG. *Electroencephalogr Clin Neurophysiol*. 1978;44:735–741.
 31. Woestenburg JC, Verbaten MN, Slangen JL. The removal of the eye-movement artifact from the EEG by regression analysis in the frequency domain. *Biol Psychol*. 1983;16:127–147.
 32. Jervis BW, Nichols MJ, Allen EM, et al. The assessment of two methods for removing eye movement artifact from the EEG. *Electroencephalogr Clin Neurophysiol*. 1985;61:444–452.
 33. Elbert T, Lutzenberger W, Rockstroh B, et al. Removal of ocular artifacts from the EEG—a biophysical approach to the EOG. *Electroencephalogr Clin Neurophysiol*. 1985;60:455–463.
 34. Fortgens C, de Bruin MP. Removal of eye movement and EOG artifacts from the non-cephalic reference EEG. *Electroencephalogr Clin Neurophysiol*. 1983;56:90–96.
 35. O’Donnell RD, Berkhout J, Adey WR. Contamination of scalp EEG spectrum during contraction of craniofacial muscles. *Electroencephalogr Clin Neurophysiol*. 1974;37:145–151.
 36. Gevins AS, Yeager CL, Zeitlin GM, et al. On-line computer rejection of EEG artifact. *Electroencephalogr Clin Neurophysiol*. 1977;42:267–274.
 37. Barlow JS. Artifact processing in EEG data processing. In: Lopes da Silva FH, Storm van Leeuwen W, Remond A, eds. *Clinical Application of Computer Analysis of EEG and Other Neurophysiological Signals. Handbook of Electroencephalography and Clinical Neurophysiology (New Series) Vol 2*. Amsterdam: Elsevier; 1986:15–64.
 38. Ille N, Berg P, Scherg M. Artifact correction of the ongoing EEG using spatial filters based on artifact and brain signal topographies. *J Clin Neurophysiol*. 2003;19:113–124.
 39. Scherg M, Ille N, Bornfleth H, et al. Advanced tools for digital EEG review: virtual source montages, whole head mapping, correlation and phase analysis. *J Clin Neurophysiol*. 2002;19:91–112.
 40. Lagerlund TD, Sharbrough FW, Busacker NE. Spatial filtering of multichannel electroencephalographic recordings through principal component analysis by single value decomposition. *J Clin Neurophysiol*. 1997;14:73–82.

41. Jung TP, Makeig S, Westerfield M, et al. Removal of eye activity artifacts from visual event-related potentials in normal and clinical subjects. *Clin Neurophysiol.* 2000;111:1745–1758.
42. Makeig S, Bell AJ, Jung TP, et al. Independent component analysis of electroencephalographic data. In: Touretzky D, Mozer M, Hasselmo M, eds. *Advances in Neural Information Processing.* Cambridge, MA: MIT Press; 1996:145–151.
43. Vigário RN. Extraction of ocular artefacts from EEG using independent component analysis. *Electroencephalogr Clin Neurophysiol.* 1997;103:395–404.
44. Vigário RN, Jousmäski V, Härmäläinen M, et al. Independent component analysis for the identification of artefact in magnetoencephalographic recordings. In: Jordan MI, Kearns MJ, Solla SA, eds. *Advances in Neural Information Processing Systems.* Vol 10. Cambridge, MA: MIT Press; 1998:229–235.
45. Delorme A, Makeig S. EEGLAB: an open source toolbox for analysis of single-trial EEG dynamics including independent component analysis. *J Neurosci Methods.* 2004;134(1):9–21.
46. Delorme A, Fernsler T, Serby H, et al. *EEGLAB Tutorial.* San Diego, CA: University of San Diego; 2006.
47. Jasper H, Kershman J. Classification of the EEG in epilepsy. *Electroencephalogr Clin Neurophysiol Suppl.* 1949;2:123–131.
48. Storm van Leeuwen W, Bickford R, Brazier MAB, et al. Proposal for an EEG terminology by the Terminology Committee of the International Federation for Electroencephalography and Clinical Neurophysiology. *Electroencephalogr Clin Neurophysiol.* 1966;20:293–320.
49. Chatrian GE, Bergamini L, Dondey M, et al. A glossary of terms most commonly used by electroencephalographers. *Electroencephalogr Clin Neurophysiol.* 1974;31:538–548.
50. Celesia GG, Chen R. Parameters of spikes in human epilepsy. *Dis Nerv Syst.* 1976;37:277–281.
51. Gose EE, Werner S, Bickford RG. Computerized spike detection. *Proc San Diego Biomed Symp.* 1974;13:193–198.
52. Carrie JRG. Computer-assisted EEG sharp transient detection and quantification during overnight recording in an epileptic patient. In: Kellaway P, Petersen I, eds. *Quantitative Analytic Studies in Epilepsy.* New York, NY: Raven Press; 1976:225–235.
53. Gevins AS, Yeager CL, Diamond SL, et al. Sharp-transient analysis and thresholded linear coherence spectra of paroxysmal EEGs. In: Kellaway P, Petersen I, eds. *Quantitative Analytical Studies in Epilepsy.* New York, NY: Raven Press; 1976:463–482.
54. Goldberg P, Samson-Dollfus D, Gremy F. An approach to an automatic pattern recognition of the electroencephalogram: background rhythm and paroxysmal elements. *Methods Inf Med.* 1973;12:155–163.
55. Gotman J, Gloor P. Automatic recognition and quantification of interictal epileptic activity in the human scalp EEG. *Electroencephalogr Clin Neurophysiol.* 1976;41:513–529.
56. Harner RN, Ostergren KA. Sequential analysis of quasi-stable and paroxysmal activity. In: Kellaway P, Petersen I, eds. *Quantitative Analytic Studies in Epilepsy.* New York, NY: Raven Press; 1976:343–353.
57. Saltzberg B, Lustick LS, Heath RG. Detection of focal spiking in the scalp EEG of monkeys. *Electroencephalogr Clin Neurophysiol.* 1971;31:327–333.
58. Lopes da Silva FH, Dijk A, Smits H, et al. Automatic detection and pattern recognition of epileptic spikes from surface and depth recording in man. In: Schenk GK, ed. *Die Quantifizierung des Elektroenzephalogramms.* Konstanz: AEG-Telefunken; 1973:425–436.
59. Lopes da Silva FH, Dijk A, Smits H. Detection of nonstationarities in EEGs using the autoregressive model—an application of EEGs of epileptics. In: Dolce G, Kunkel H, eds. *CEAN—Computerized EEG Analysis.* Stuttgart: Fischer; 1975:180–199.
60. Lopes da Silva FH, ten Broeke W, van Hulten K, et al. EEG nonstationarities detected by inverse filtering in scalp and cortical recordings of epileptics: statistical analysis and spatial display. In: Kellaway P, Petersen I, eds. *Quantitative Analytic Studies in Epilepsy.* New York, NY: Raven Press; 1976:375–387.
61. Lopes da Silva FH, van Hulten K, Lommen JG, et al. Automatic detection and localization of epileptic foci. *Electroencephalogr Clin Neurophysiol.* 1977;43:1–13.
62. Lopes da Silva FH. Analysis of EEG nonstationarities. *Electroencephalogr Clin Neurophysiol Suppl.* 1978;34:163–179.
63. Guedes de Oliveira PHH, Lopes da Silva FH. A topographical display of epileptiform transients based on a statistical approach. *Electroencephalogr Clin Neurophysiol.* 1980;48:710–714.
64. Guedes de Oliveira Q, Lopes da Silva FH. Spike detection based on a pattern recognition approach using a microcomputer. *Electroencephalogr Clin Neurophysiol.* 1983;56(1):97–103.
65. Zetterberg LH. Spike detection by computer and by analog equipment. In: Kellaway P, Petersen I, eds. *Automation of Clinical Electroencephalography.* New York, NY: Raven Press; 1973:227–242.
66. Barlow JS, Dubinsky J. Some computer approaches to continuous automatic clinical EEG monitoring. In: Kellaway P, Petersen I, eds. *Quantitative Analytical Methods in Epilepsy.* New York, NY: Raven Press; 1976:309–327.
67. Pfurttscheller G, Fischer G. A new approach to spike detection using a combination of inverse and matched filter techniques. *Electroencephalogr Clin Neurophysiol.* 1978;44:243–247.
68. Smith JR. Automatic analysis and detection of EEG spikes. *IEEE Trans Biomed Eng.* 1972;BME-21:1–7.
69. Ktonas PY, Smith JR. Quantification of abnormal EEG spike characteristics. *Comput Biol Med.* 1974;4:157–163.
70. Frost JD Jr. Microprocessor-based EEG spike detection and quantification. *Int J Biomed Comput.* 1979;10:357–373.
71. Gotman J. Quantitative measurements of epileptic spike morphology in the human EEG. *Electroencephalogr Clin Neurophysiol.* 1980;48:551–557.
72. Gloor P. The EEG and differential diagnosis of epilepsy. In: van Duijn H, Donker DN, van Huffelen AC, eds. *Current Concepts in Clinical Neurophysiology.* The Hague: Trio; 1977:9–21.
73. Lemieux JF, Blume WT. Automated morphological analysis of spikes and sharp waves in human electrocorticograms. *Electroencephalogr Clin Neurophysiol.* 1983;55:45–50.
74. Gotman J, Marciani MG. EEG spiking activity, drug levels and seizure occurrence in epileptic patients. *Ann Neurol.* 1985;17:597–603.
75. Dumpelmann M, Elger CE. Visual and automatic investigation of epileptiform spikes in intracranial EEG recordings. *Epilepsia.* 1999;40(3):275–285.
76. Wahlberg P, Lantz G. Methods for robust clustering of epileptic EEG spikes. *IEEE Trans Biomed Eng.* 2000;47:857–868.
77. Van't Ent D, Manshanden I, Ossenblok P, et al. Spike cluster analysis in neocortical localization related epilepsy yields clinically significant equivalent source localization results in magnetoencephalogram (MEG). *Clin Neurophysiol.* 2003;114(10):1948–1962.
78. Abraham-Fuchs K, Harer W, Schneider S, et al. Pattern recognition in biomagnetic signals by spatio-temporal correlation and application to the localisation of propagating neuronal activity. *Med Biol Eng Comput.* 1990.

79. Volavka J, Matousek M, Feldstein S, et al. The reliability of EEG assessment. *EEG-EMG*. 1973;4:123–130.
80. Rose SW, Penry JK, White BG, et al. Reliability and validity of visual EEG assessment in third grade children. *Clin Electroencephalogr*. 1973;4:197–205.
81. Gotman J, Gloor P, Schaul N. Comparison of traditional reading of the EEG and automatic recognition of interictal epileptic activity. *Electroencephalogr Clin Neurophysiol*. 1978;44:48–60.
82. Gevins AS. Quantitative aspects of electroencephalography. In: Aminoff MJ, ed. *Electrophysiological Approaches to Neurological Diagnosis*. London: Churchill Livingstone; 1979.
83. Bodenstern G, Praetorius HM. Feature extraction from the encephalogram by adaptive segmentation. *Proc IEEE*. 1977;65:642–652.
84. Anderberg MR. *Cluster Analysis for Application*. New York, NY: Academic Press; 1973.
85. Guess MJ, Wilson SB. Introduction to hierarchical clustering. *J Clin Neurophysiol*. 2002;19:144–151.
86. Gevins AS, Morgan NH. Classifier-directed signal processing in brain research. *IEEE Trans Biomed Eng*. 1986;BME-33(12):1054–1068.
87. Pfurtscheller G, Flozinger G, Mohl W. *Prediction of the Side of Hand Movements from Single-trial Multi-channel EEG Data using a Neural Network; Preliminary Results. Report 299*. Graz: Institutes for Information Processing; 1991:1–11.
88. Kohonen T. *Self-organizing Maps. Springer Series in Information Sciences*. Vol 30. 3rd ed. Berlin/Heidelberg/New York: Springer; 2001:501 pp.
89. Peters BO, Pfurtscheller G, Flyvbjerg H. Mining multi-channel EEG for its information content: an ANN-based method for a brain–computer interface. *Neural Netw*. 1998;11(7–8):1429–1433.
90. Johnson LC. The EEG during sleep as viewed by a computer. In: Remond A, ed. *EEG Informatics. A Didactic Review of Methods and Applications of EEG Data Processing*. Amsterdam: Elsevier; 1977:385–406.
91. Johnson L, Lubin A, Nautoh P, et al. Spectral analysis of the EEG of dominant and non-dominant alpha subjects during waking and sleeping. *Electroencephalogr Clin Neurophysiol*. 1969;26:361–370.
92. Gondeck AR, Smith JR. Dynamics of human sleep sigma spindles. *Electroencephalogr Clin Neurophysiol*. 1974;37:293–297.
93. Kemp B, Jaspers P, Franzen JM, et al. An optimal monitor of the electroencephalographic sigma sleep state. *Biol Cybern*. 1985;51:263–270.
94. Smith JR, Karacan I, Yang M. Ontogeny of delta activity during human sleep. *Electroencephalogr Clin Neurophysiol*. 1977;43:229–237.
95. Steriade M, Contreras D, Curro Dossi R, et al. The slow (<1 Hz) oscillation in reticular thalamic and thalamocortical neurons: scenario of sleep rhythm generation in interacting thalamic and neocortical networks. *J Neurosci*. 1993;13(8):3284–3299.
96. Achermann PA, Borbély A. Low-frequency (<1 Hz) oscillations in the human sleep. *Neuroscience*. 1997;81:213–222.
97. Simon NR, Manshanden I, Lopes da Silva FH. A MEG study of sleep. *Brain Res*. 2000;860(1–2):64–76.
98. Bremer G, Smith JR, Karacan I. Automatic detection of the K complex in sleep electroencephalograms. *IEEE Trans Biomed Eng*. 1970;BME-17:314–323.
99. Rosa AC, da Kemp B, Paiva T, et al. A model-based detector of vertex waves and K complexes in sleep electroencephalogram. *Electroencephalogr Clin Neurophysiol*. 1991;78:71–79.
100. Kemp B. *Model-based Monitoring of Human Sleep Stage* [PhD thesis]. Enschede, the Netherlands: University of Twente; 1987.
101. Dement W, Kleitman N. Cyclic variations in EEG during sleep and their relation to eye movements, body motility dreaming. *Electroencephalogr Clin Neurophysiol*. 1957;9:673–690.
102. Rechtschaffen A, Kales A. *Manual of Standardized Terminology, Techniques and Scoring System for Sleep Stages of Human Subjects*. National Institutes of Health Publication No. 204. Washington, DC: U.S. Government Printing Office; 1968.
103. Künkel H. Die Spektraldarstellung des EEG. *EEG-EMG*. 1972;3:15–24.
104. Larsen LE, Walter DO. On automatic methods of sleep staging by EEG spectra. *Electroencephalogr Clin Neurophysiol*. 1970;28:459–467.
105. Lubin A, Johnson LC, Austin NT. Discriminations among states of consciousness using EEG spectra. *Psychophysiology*. 1969;6:122–132.
106. Smith JR, Karacan I. EEG sleep stage scoring by an automatic hybrid system. *Electroencephalogr Clin Neurophysiol*. 1971;31:231–237.
107. Itil TM, Shapiro DM, Fink M, et al. Digital computer classifications of EEG sleep stages. *Electroencephalogr Clin Neurophysiol*. 1969;27:76–83.
108. Rossler R, Collins R, Rostman A. A period analysis, classification of sleep stages. *Electroencephalogr Clin Neurophysiol*. 1970;29:358–362.
109. Martin WB, Johnson LC, Viglione SS, et al. Pattern recognition of EEG–EOG as a technique for all-night sleep stage scoring. *Electroencephalogr Clin Neurophysiol*. 1972;32:417–427.
110. Viglione SS, Martin WB. Automatic analysis of the EEG for sleep staging. In: Kellaway P, Petersen I, eds. *Automation of Clinical Electroencephalography*. New York, NY: Raven Press; 1973:269–285.
111. Gaillard JM, Krassvievitch M, Tissot R. Analyse automatique du sommeil par un système hybride. *Electroencephalogr Clin Neurophysiol*. 1972;33:403–410.
112. Gaillard JM, Tissot R. Principles of automatic analysis of sleep records with a hybrid system. *Comput Biomed Res*. 1973;6:1–13.
113. Poppl SJ. Computer allocation rules for automatic EEG classification. In: Dolce G, Kunkel H, eds. *CEAN—Computerized EEG Analysis*. Stuttgart: Fischer; 1975:202–215.
114. Bowe TR, Anders TF. The use of the semi-Markov model in the study of the development of sleep–wake states in infants. *Psychophysiology*. 1979;16:41–48.
115. Yang MCK, Hirsch CJ. The use of a semi-Markov model for describing sleep pattern. *Biometrics*. 1973;29:667–676.
116. Zung WWK, Naylor TH, Gianturco D, et al. A Markov chain model of sleep EEG pattern. *Electroencephalogr Clin Neurophysiol*. 1965;19:105.
117. Kemp B, Kamphuisen HAC. Simulation of human hypnograms using a Markov chain model. *Sleep*. 1986;9:405–414.
118. Hermann WM, Kubicki S. Various techniques of computer analysis in nocturnal sleep. In: Degen R, Niedermeyer E, eds. *Epilepsy, Sleep and Sleep Deprivation*. Amsterdam: Elsevier; 1984:207–229.
119. Agarwal R, Gotman J. Computer-assisted sleep staging. *IEEE Trans Biomed Eng*. 2001;48:1412–1423.
120. Agarwal R, Gotman J. Digital tools in polysomnography. *J Clin Neurophysiol*. 2002;19:136–143.
121. Malinowska U, Durka PJ, Blinowska KJ, et al. Micro- and macrostructure of sleep EEG: a universal adaptive time–frequency parameterization. *IEEE Eng Med Biol Mag*. 2006;25(4):26–31.

122. Malinowska U, Klekowicz H, Wakarow A, et al. Fully parametric sleep staging compatible with the classical criteria. *Neuroinformatics*. 2009;7(4):245–253.
123. Porée F, Kachenoura A, Gauvrit H, et al. Blind source separation for ambulatory sleep recording. *IEEE Trans Inf Technol Biomed*. 2006;10(2):293–301.
124. Nieuwenhuijs DJ. Processed EEG in natural sleep. *Best Pract Res Clin Anaesthesiol*. 2006;20(1):49–56.
125. Brechner VL, Walter RD, Dillon JB. *Practical Electroencephalography for the Anesthesiologist*. Springfield, IL: Charles C. Thomas; 1962.
126. Bickford RG, Billinger TW, Fleming NI, et al. The compressed spectral array (CSA). A pictorial EEG. *Proc San Diego Biomed Symp*. 1972;11:365–370.
127. Maynard DE. The cerebral function analysis monitor (CFAM). *Electroencephalogr Clin Neurophysiol*. 1977;43:479.
128. Prior P. *Monitoring Cerebral Function: Long-term Recordings of Cerebral Electrical Activity*. Amsterdam: Elsevier; 1979.
129. Prior PF, Maynard DE, Sheaff PC, et al. Monitoring cerebral function: clinical experience with new device for continuous recording of electrical activity of brain. *Br Med J*. 1971;2:736.
130. Pronk RAF. Peri-operative monitoring. In: Lopes da Silva FH, Storm van Leeuwen W, Remond A, eds. *Clinical Applications of Computer Analysis of EEG and Other Neurophysiological Signals. Handbook of Electroencephalography and Clinical Neurophysiology*. Vol 2. Amsterdam: Elsevier; 1986:93–130.
131. Scheuer ML. Continuous EEG monitoring in the intensive care unit. *Epilepsia*. 2002;43(suppl 3):114–127.
132. Visser GH, Wieneke GH, Van Huffelen AC, et al. The development of spectral EEG changes during short periods of circulatory arrest. *J Clin Neurophysiol*. 2001;18(2):169–177.
133. Rampil IJ. A primer for EEG signal processing in anesthesia. *Anesthesiology*. 1998;89:980–1002.
134. Liu J, Singh H, White PF. Electroencephalogram bispectral analysis predicts the depth of midazolam-induced sedation. *Anesthesiology*. 1996;84(1):64–69.
135. Kears LA Jr, Manberg P, Chamoun N, et al. Bispectral analysis of the electroencephalogram correlates with patient movement to skin incision during propofol/nitrous oxide anesthesia. *Anesthesiology*. 1994;81(6):1365–1370.
136. Sigl JC, Chamoun NG. An introduction to bispectral analysis for the electroencephalogram. *J Clin Monit*. 1994;10:392–404.
137. Bard JW. The BIS monitor: a review and technology assessment. *AANA J*. 2001;69(6):477–483.
138. Sebel PS, Lang E, Rampil IJ, et al. A multicenter study of bispectral electroencephalogram analysis for monitoring anesthetic effect. *Anesth Analg*. 1997;84(4):891–899.
139. Prins SA, de Hoog M, Blok JH, et al. Continuous noninvasive monitoring of barbiturate coma in critically ill children using the bispectral index monitor. *Crit Care*. 2007;11(5):R108.
140. Sebel PS. Central nervous system monitoring during open heart surgery: an update. *J Cardiothorac Vasc Anesth*. 1998;12(2 suppl 1):3–8.
141. Matousek M, Petersén I, Friberg S. Automatic assessment of randomly selected routine EEG records. In: Dolce G, Kunkel H, eds. *CEAN—Computerized EEG Analysis*. Stuttgart: Fischer; 1975:421–428.
142. Matousek M, Arvidsson A, Friberg S. Implementation of analytical methods in daily clinical EEG routine. *Electroencephalogr Clin Neurophysiol Suppl*. 1978;34:199–204.
143. Friberg S. *A Program System for the Automatic Evaluation of the Background Activity in the Human Electroencephalogram. Technical Report, 3:80*. Gothenburg, Sweden: Research Laboratory of Medical Electronics, Chalmers University of Technology; 1980.
144. Gotman J. Problems of presentation of analytical results. *Electroencephalogr Clin Neurophysiol Suppl*. 1978;34:191–197.
145. Gevins AS, Yeager CL, Diamond SL, et al. Automated analysis of the electrical activity of the human brain (EEG): a progress report. *Proc IEEE*. 1975;63:1382–1399.
146. Kunkel H, EEG Project Group. Hybrid computing system for EEG analysis. In: Dolce G, Kunkel H, eds. *CEAN—Computerized EEG Analysis*. Stuttgart: Fischer; 1975:365–383.
147. Storm van Leeuwen W, Arntz A, Spoclastra P, et al. The use of computer analysis for diagnosis in routine electroencephalography. *Rev EEG Neurophysiol*. 1976;6(2):318–327.
148. Mausby RL, Saltzberg B, Lustick LS. Toward an EEG screening test: a simple system for analysis and display of clinical EEG data. In: Kellaway P, Petersen I, eds. *Automation of Clinical Electroencephalography*. New York, NY: Raven Press; 1973:45–53.
149. McGillivray BB, Wadbrook DG. A system for extracting a diagnosis from the clinical EEG. In: Dolce G, Kunkel H, eds. *CEAN—Computerized EEG Analysis*. Stuttgart: Fischer; 1975:344–364.
150. Binnie CD, Batchelor BG, Bawring PA, et al. Computer-assisted interpretation of clinical EEGs. *Electroencephalogr Clin Neurophysiol*. 1978;44:575–585.
151. Harner RN, Ostergren KA. Computed EEG topography. *Electroencephalogr Clin Neurophysiol Suppl*. 1978;34:151–161.
152. Ebe M, Homma I, Ishiyama Y, et al. Automatic analysis of clinical information in EEG. *Electroencephalogr Clin Neurophysiol*. 1973;34:706.
153. Bickford RG, Brimm J, Berger L, et al. Application of compressed spectral array in clinical EEG. In: Kellaway P, Petersen I, eds. *Automation of Clinical Electroencephalography*. New York, NY: Raven Press; 1973:55–64.
154. Sheorajpanday RV, Nagels G, Weeren AJ, et al. Reproducibility and clinical relevance of quantitative EEG parameters in cerebral ischemia: a basic approach. *Clin Neurophysiol*. 2009;120(5):845–855.
155. Webber WRS, Harner RN, Duffy FH, et al. Spike detection. I. Correlation and reliability of human experts. *Electroencephalogr Clin Neurophysiol*. 1996;98:186–198.
156. Gotman J. Automatic seizure detection: improvements and evaluation. *Electroencephalogr Clin Neurophysiol*. 1990;76:317–324.
157. Gotman J. Automatic detection of seizures and spikes in the EEG. In: Ljders H, ed. *Epilepsy Surgery*. New York, NY: Raven Press; 1991:307–316.
158. Gotman J, Wang LY. State-dependent spike detection: concepts and preliminary results. *Electroencephalogr Clin Neurophysiol*. 1991;79:11–19.
159. Gotman J, Wang LY. State-dependent spike detection: validation. *Electroencephalogr Clin Neurophysiol*. 1992;83:12–18.
160. Hosteler W, Doller HJ, Homan RW. Assessment of a computer program to detect epileptiform spikes. *Electroencephalogr Clin Neurophysiol*. 1992;83:1–11.
161. Webber WRS, Litt B, Lesser RP, et al. Automatic EEG spike detection: what should the computer imitate? *Electroencephalogr Clin Neurophysiol*. 1993;87:364–373.
162. Webber WRS, Litt B, Wilson K, et al. Practical detection of epileptiform discharges in the EEG using an artificial neural network: a comparison of raw and parameterized EEG data. *Electroencephalogr Clin Neurophysiol*. 1994;91:194–204.
163. Webber WRS, Lesser RP, Richardson RT, et al. An approach to seizure detection using an artificial neural network. *Electroencephalogr Clin Neurophysiol*. 1996;98:250–272.

164. Spatt J, Pelzi G, Mamoli B. Reliability of automatic and visual analysis of interictal spikes in lateralizing an epileptic focus during video-EEG monitoring. *Electroencephalogr Clin Neurophysiol*. 1997;103:421–425.
165. Wilson SB, Harner RN, Dufy FH, et al. Spike detection. I. Correlation and reliability of human experts. *Electroencephalogr Clin Neurophysiol*. 1996;98:186–198.
166. Wilson SB, Turner CA, Emerson RG, et al. Spike detection II: automatic, perception-based detection and clustering. *Clin Neurophysiol*. 1999;110(3):404–411.
167. Harner R. Automatic EEG spike detection. *Clin EEG Neurosci*. 2009;40(4):262–270.
168. Rose DF, Smith PD, Sato S. Magnetoencephalography and epilepsy research. *Science*. 1987;238:329–335.
169. Sutherling WW, Barth DS. Magnetoencephalography in clinical epilepsy studies: the UCLA experience. *Magnetoencephalogr Adv Neurol*. 1990;54:231–246.
170. Ricci GB. Italian contributions to magnetoencephalographic studies on the epilepsies. *Magnetoencephalogr Adv Neurol*. 1990;54:247–260.
171. Engel J, Ojeman GA. The next step. In: Engel J, ed. *Surgical Treatment of the Epilepsies*. 2nd ed. New York, NY: Raven Press; 1993.
172. Ebersole JS, Squires KC, Eliashiv SD, et al. Applications of magnetic source imaging in evaluation of candidates for epilepsy surgery. *Funct Imaging*. 1995;5:267–287.
173. Hari R, Ahonen A, Forss N, et al. Parietal epileptic mirror focus detected with a whole-head neuromagnetometer. *Neuroreport*. 1993;5:45–48.
174. Kettenmann B, Hummel C, Stefan H, et al. Multichannel magnetoencephalographical recordings: separation of cortical responses to different chemical stimulation in man. *Electroencephalogr Clin Neurophysiol Suppl*. 1996;46:271–274.
175. Knowlton RC, Laxer KD, Aminoff MJ, et al. Magnetoencephalography in partial epilepsy: clinical yield and localization accuracy. *Ann Neurol*. 1997;42(4):622–631.
176. Lewine JD, Orrison WW Jr. Magnetoencephalography and magnetic source imaging. In: *Functional Brain Mapping*. St. Louis: Mosby-Year Book; 1995:369–417.
177. Merlet I, Garcia-Larrea L, Grégoire MC, et al. Source propagation of interictal spikes in temporal lobe epilepsy. Correlation between spike dipole modelling and [18F]fluorodeoxyglucose PET data. *Brain*. 1996;119:377–392.
178. Paetau R, Kajola M, Karhu J, et al. Magnetoencephalographic localization of epileptic cortex—impact on surgical treatment. *Ann Neurol*. 1992;32:106–109.
179. Paetau R, Hamalainen M, Hari R, et al. Magnetoencephalographic evaluation of children and adolescents with intractable epilepsy. *Epilepsia*. 1994;35:275–284.
180. Roth BJ, Ko D, von Albertini-Carletti IR, et al. Dipole localization in patients with epilepsy using the realistically shaped head model. *Electroencephalogr Clin Neurophysiol*. 1997;102:159–166.
181. Smith JR, Schwartz BJ, Gallen Ch, et al. Utilization of multichannel magnetoencephalography in the guidance of ablative seizure surgery. *J Epilepsy*. 1995;8:119–130.
182. Stephan H, Schuler P, Abraham-Fuchs K, et al. Magnetic source localization and morphological changes in temporal lobe epilepsy: comparison of MEG/EEG, ECoG and volumetric MRI in presurgical evaluation of operated patients. *Acta Neurol Scand Suppl*. 1994;152:83–88.
183. Tanaka N, Hämäläinen MS, Ahlfors SP, et al. Propagation of epileptic spikes reconstructed from spatiotemporal magnetoencephalographic and electroencephalographic source analysis. *Neuroimage*. 2010;50(1):217–222.
184. Gotman J. Automatic detection of seizures and spikes. *J Clin Neurophysiol*. 1999;16:130–140.
185. Flanagan D, Agarwal R, Gotman J. Computer-aided spatial classification of epileptic spikes. *J Clin Neurophysiol*. 2002;19:125–135.
186. Glover JR Jr, Raghavan N, Ktonas PY, et al. Context-based automated detection of epileptogenic sharp transients in the EEG: elimination of false positives. *IEEE Trans Biomed Eng*. 1989;36:519–527.
187. Halford JJ. Computerized epileptiform transient detection in the scalp electroencephalogram: obstacles to progress and the example of computerized ECG interpretation. *Clin Neurophysiol*. 2009;120(11):1909–1915.
188. Ives JR, Warach S, Schmitt F, et al. Monitoring the patient's EEG during echo planar MRI. *Electroencephalogr Clin Neurophysiol*. 1993;87(6):417–420.
189. Al-Asmi A, Benar CG, Gross DW, et al. fMRI activation in continuous and spike-triggered EEG–fMRI studies of epileptic spikes. *Epilepsia*. 2003;44(10):1328–1339.
190. Salek-Haddadi A, Lemieux L, Merschhemke M, et al. EEG quality during simultaneous functional MRI of interictal epileptiform discharges. *Magn Reson Imaging*. 2003;21(10):1159–1166.
191. Ehrenburg BL, Penry JK. Computer recognition of generalized spike-wave discharges. *Electroencephalogr Clin Neurophysiol*. 1976;41:25–36.
192. Carrie JRG. A hybrid computer technique for detecting sharp EEG transients. *Electroencephalogr Clin Neurophysiol*. 1972;33:336–338.
193. Carrie JRG, Frost JD. Clinical evaluation of a method for quantification of generalized spike-wave EEG patterns by computer during prolonged recordings. *Comput Biomed Res*. 1977;10:449–457.
194. Ives JR, Thompson CJ, Gloor P. Seizure monitoring: a new tool in electroencephalography. *Electroencephalogr Clin Neurophysiol*. 1976;41:422–427.
195. Kamp A, Mars NJI, Wisman T. Long term monitoring of the electroencephalogram in epileptic patients. In: Amlaner CJ Jr, MacDonald DW, eds. *Handbook on Biotelemetry and Radio Tracking*. Oxford: Pergamon Press; 1979:499–503.
196. Babb TL, Mariani E, Crandall PH. An electronic circuit for detection of EEG seizures recorded with implanted electrodes. *Electroencephalogr Clin Neurophysiol*. 1974;37:305–308.
197. Peters TE, Bhavaraju NC, Frei MG, et al. Network system for automated seizure detection and contingent delivery of therapy. *J Clin Neurophysiol*. 2001;18(6):545–549.
198. Viglione SS, Ordon VA, Risch F. *A Methodology for Detecting Ongoing Changes in the EEG Prior to Clinical Seizures*. West Huntington Beach, CA: McDonnell Douglas Astronautics Co; 1970. MDAC Paper WD 1399.
199. Viglione SS. *Validation of Epilepsy Seizure Warning System*. West Huntington Beach, CA: McDonnell Douglas Astronautics Co; 1974. MDAC Paper APA 74133.
200. Gotman J. Noninvasive methods for evaluating the localization and propagation of epileptic activity. *Epilepsia*. 2003;44(suppl 12):21–29.
201. Kobayashi K, James CJ, Yoshinaga H, et al. The electroencephalogram through a software microscope: non-invasive localization and visualization of epileptic seizure activity from inside the brain. *Clin Neurophysiol*. 2000;111(1):134–149.

202. Grewal S, Gotman J. An automatic warning system for epileptic seizures recorded on intracerebral EEGs. *Clin Neurophysiol.* 2005;116(10):2460–2472.
203. Saab ME, Gotman J. A system to detect the onset of epileptic seizures in scalp EEG. *Clin Neurophysiol.* 2005;116(2):427–442.
204. Gabor AJ, Leach RR, Dowla FU. Automated seizure detection using a self-organising neural network. *Electroencephalogr Clin Neurophysiol.* 1996;99:257–266.
205. Wilson SB, Scheuer ML, Emerson RG, et al. Seizure detection: evaluation of the Reveal algorithm. *Clin Neurophysiol.* 2004;115(10):2280–2291.
206. Brazier MAB. Spread of seizure discharges in epilepsy: anatomical and electrophysiological considerations. *Exp Neurol.* 1972;36:263–272.
207. Brazier MAB. Electrical seizure discharges within the human brain: the problem of spread. In: Brazier MAB, ed. *Epilepsy, Its Phenomena in Man.* New York, NY: Academic Press; 1973:155–171.
208. Gersch W, Goddard G. Locating the site of epileptic focus by spectral analysis methods. *Science.* 1970;169:701–702.
209. Gersch W, Tharp BR. Spectral regression—amount of information analysis of seizures in humans. In: Kellaway P, Petersen I, eds. *Quantitative Analytic Studies in Epilepsy.* New York, NY: Raven Press; 1976:509–532.
210. Tharp BR, Gersch W. Spectral analysis of seizures in humans. *Comput Biomed Res.* 1976;8:503–521.
211. Gotman J. Interhemispheric relations during bilateral spike-and-wave activity. *Epilepsia.* 1981;22:453–466.
212. Gotman J, Levtova V. Amygdala–hippocampus relationships in temporal lobe seizures: a phase-coherence study. *Epilepsy Res.* 1996;25:51–57.
213. Kaminski MJ, Blinowska KJ. A new method of the description of the information flow in the brain structures. *Biol Cybern.* 1991;65:203–210.
214. Franaszczuk PJ, Bergey GK, Kaminski MJ. Analysis of mesial temporal seizure onset and propagation using the directed transfer function method. *Electroencephalogr Clin Neurophysiol.* 1994;91(6):413–427.
215. Mars NJI, van Arragon GW. Time delay estimation in nonlinear systems using average mutual amount of information analysis. *IEEE Acoustics Speech Signal Processing.* 1981;29(3):619–621.
216. Gelfand IM, Yaglom AM. Calculation of the amount of information about a random function contained in another such function. *Am Math Soc Transact.* 1959;12:199–246.
217. Mars NJI, Lopes da Silva FH. Propagation of seizure activity in kindled dogs. *Electroencephalogr Clin Neurophysiol.* 1983;56:194–209.
218. Mars NJI, Thompson PM, Wilkus RJ. The spread of epileptic seizures activity in humans. *Epilepsia.* 1985;26:85–94.
219. Lopes da Silva FH, Pijn JPM, Boeijinga PH. Interdependence of EEG signals: linear versus nonlinear association and the significance of time delays and phase shifts. *Brain Topogr.* 1989;2:9–18.
220. Pijn JPM. *Quantitative Evaluation of EEG Signals in Epilepsy. Nonlinear Associations, Time Delays and Nonlinear Dynamics* [PhD thesis]. University of Amsterdam; 1990.
221. Pijn JPM, Vijn PCM, Lopes da Silva FH, et al. The use of signal analysis for the localization of an epileptic focus: a new approach. *Adv Epileptol.* 1989;17:272–276.
222. Fernandes de Lima VM, Pijn JPM, Filipe CN, et al. The role of hippocampal commissures in the interhemispheric transfer of epileptiform after-discharges in the rat: a study using linear and nonlinear regression analysis. *Electroencephalogr Clin Neurophysiol.* 1990;76:520–540.
223. Pijn JP, Lopes da Silva FH. Propagation of electrical activity: nonlinear associations and time delays between EEG signals. In: Zschocke S, Speckmann E-J, eds. *Basic Mechanisms of the EEG.* Boston, MA: Birkhauser; 1993:41–61.
224. Meeren HK, Pijn JP, Van Luijckelaar EL, et al. Cortical focus drives widespread corticothalamic networks during spontaneous absence seizures in rats. *J Neurosci.* 2002;22(4):1480–1495.
225. Wendling F, Ansari-Asl K, Bartolomei F, et al. From EEG signals to brain connectivity: a model-based evaluation of interdependence measures. *J Neurosci Methods.* 2009;183(1):9–18.
226. Wendling F, Bartolomei F, Senhadji L. Spatial analysis of intracerebral electroencephalographic signals in the time and frequency domain: identification of epileptogenic networks in partial epilepsy. *Phil Trans R Soc A.* 2009;367:297–316.
227. Ansari-Asl K, Bellanger JJ, Bartolomei F, et al. Time–frequency characterization of interdependencies in nonstationary signals: application to epileptic EEG. *IEEE Trans Biomed Eng.* 2005;52:1218–1226.
228. Pascual-Marqui RD, Esslen M, Kochi K, et al. Functional imaging with low-resolution brain electromagnetic tomography (LORETA): a review. *Methods Find Exp Clin Pharmacol.* 2002;24(suppl C):91–95.
229. Pascual-Marqui RD. *Discrete, 3D Distributed, Linear Imaging Methods of Electric Neuronal Activity. Part 1: Exact, Zero Error Localization.* arXiv:0710.3341 [math-ph], <http://arxiv.org/pdf/0710.3341>. Accessed October 17, 2007.
230. Zanol F, Knösche TR. ASA—advanced source analysis of continuous and event-related EEG/MEG signals. *Brain Topogr.* 2004;16(4):287–290.
231. Schlögl A, Keinrath C, Zimmermann D, et al. A fully automated correction method of EOG artifacts in EEG recordings. *Clin Neurophysiol.* 2007;118(1):98–104.
232. Harner RN. Computer analysis and clinical EEG interpretation—perspective and application. In: Dolce G, Kunkel H, eds. *CEAN—Computerized EEG Analysis.* Stuttgart: Fischer; 1975:337–343.
233. Rappelsberger P. The reference problem and mapping of coherence: a stimulation study. *Brain Topogr.* 1989;2:63–72.
234. Teschan PE. Electroencephalographic and other neurophysiological abnormalities in uremia. In: *Proceedings of the Conference on Adequacy of Dialysis, Monterey, CA, 1974.*
235. Ursin R, Moses J, Naitoh P, et al. REM–NREM cycle in the cat may be sleep-dependent. *Sleep.* 1983;6:1–9.
236. Walter WG, Shipton HW. A new toposcopic display system. *Electroencephalogr Clin Neurophysiol.* 1951;3:281–292.
237. Williamson SJ, Kaufman L. Advances in neuromagnetic instrumentation and studies of spontaneous brain activity. *Brain Topogr.* 1989;2:129–140.

EEG-Based Brain-Computer Interfaces

GERT PFURTSCHELLER AND CHRISTA NEUPER

CHAPTER

57

INTRODUCTION AND BASIC PRINCIPLES

A relatively recent development in applied neurophysiology is an approach called EEG-based brain-computer interface (BCI). A BCI translates specific features, automatically extracted from EEG signals, into signals able to operate computer-controlled devices in order to assist patients who have highly compromised motor functions, such as tetraplegic patients. This novel approach became possible due to advances both in methods of EEG analysis and in information technology, along with a better understanding of the psychophysiological correlates of certain EEG features. Therefore, it is interesting to take notice of the emerging field of direct brain-computer communication.

A BCI provides the brain with a new nonmuscular communication channel that can be used to convey messages and commands directly from the brain to the external world without using any muscle activity (1). Here, we expand this definition to emphasize that any BCI must have the following four components:

1. Direct: The signals must be recorded directly from the brain. If a device records signals after they pass through peripheral nerves or muscles, it is not a BCI.

2. Intentional control: At least one directly recordable brain signal, which can be intentionally modulated, must provide input to the BCI (electrical potentials, magnetic fields, or hemodynamic changes).
3. Real-time processing: The signal processing must occur online and yield a communication or control signal.
4. Feedback: The user must obtain feedback about the success or failure of his/her efforts to communicate or control.

It follows from these definitions that each BCI is a closed-loop system with two adaptive controllers: the user's brain, which produces the signals and provides the input to the BCI; and the BCI itself, which analyses the brain signals and transforms them to a control signal as the BCI output (Fig. 57.1).

Any BCI contains components to extract features and classify (detect) EEG events. The goal of the feature extraction component is to find a suitable representation of the EEG signal that simplifies the subsequent classification or detection of specific patterns of electrical brain activity. That is, the signal features should encode the commands sent by the user but should not contain noise and other signal components that can impede the classification process. There is a variety of feature extraction methods used in current BCI systems. A nonexhaustive list of

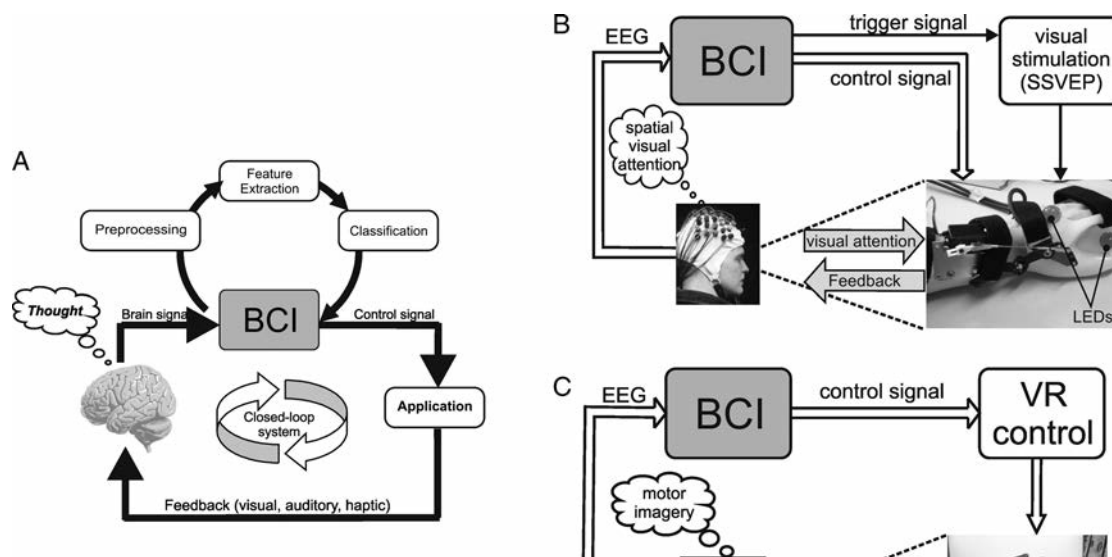


Figure 57.1 Principle of a BCI system with the major internal processing steps (A), visual attention-based BCI used to control a hand orthosis by focusing on one of two flickering lights (LEDs) (B), and motor imagery-based BCI used to control a virtual reality (VR) hand (C). Motor imagery is the most common mental strategy in BCIs and does not rely on external stimulation to generate the necessary brain activity (C). BCIs that do rely on external stimulation to elicit brain activity typically involve spatial visual attention (B).

these methods includes amplitude and band power measures, Hjorth parameters, autoregressive parameters, and wavelet coefficients (2–4).

The task of the classifier is to use the signal features provided by the feature extractor to assign the recorded samples of the signal to a given category of EEG patterns. In the simplest form, detection of an EEG pattern may be made, for instance, by means of a threshold method (5,6). More sophisticated classification algorithms of different EEG patterns depend on the use of linear or nonlinear classifiers (2,7,8).

The classifier output, which can be a simple on-off signal or a signal that encodes a number of different classes, is transformed into an appropriate signal that can then be used to control a variety of devices. For most current BCI systems, the output device is a computer screen and the desired output consists of the selection of certain targets. Advanced applications include controlling of spelling systems or other external apparatuses such as prosthetic devices and multimedia applications.

Feedback of performance is usually obtained by visualization of the classifier output on a computer screen or by presentation of an auditory, tactile, or visual feedback signal. Feedback is an integral part of the BCI system because the users observe, for example, selected letters or certain movements simultaneously with the brain responses they produce.

EEG PATTERNS USED AS INPUT FOR A BCI

The EEG is the most widely used brain signal in BCIs. Two types of changes can be extracted from the ongoing EEG signals:

1. Event-related potentials (ERPs) display time and phase-locked changes (evoked) to an externally or internally paced event. Evoked signals include slow cortical potential (SCP) changes, P300 components, and steady-state-evoked potentials (SSVEPs) (9).
2. Event-related changes in ongoing EEG activity in specific frequency bands. These changes are also time-locked but not phase-locked (induced). Event-related desynchronization (ERD) defines an amplitude (power) decrease of a rhythmic component, whereas event-related synchronization (ERS) characterizes an amplitude (power) increase (10).

Depending on the phenomena analyzed and classified, the following EEG-based BCI systems can be differentiated:

The SCP BCI: Beginning in 1979, Birbaumer and coworkers published a series of experiments demonstrating operant control of SCPs (see Ref. 11 for review). Operant conditioning is a learning process with the goal of the self-regulation of brain potentials (e.g., SCP shifts) or brain waves (e.g., sensorimotor rhythms) with the help of suitable feedback. This process does not require continuous feedback, but a reward for achieving the desired brain potential (wave) change is necessary. Operant conditioning was used in communication systems for completely paralyzed (locked-in) patients (12,13).

The P300 BCI: The P300 is the positive component of the evoked potential that may develop about 300 msec after an item is flashed. The user focuses on one flashing item while ignoring other stimuli. Whenever the target stimulus flashes,

it yields a larger P300 than the other possible choices. P300 BCIs are typically used to spell (14–16) but have been validated with other tasks such as control of a mobile robot (17) or a smart home (18).

The SSVEP BCI: Steady-state evoked potentials (SSEPs) occur when sensory stimuli are repetitively delivered rapidly enough that the relevant neuronal structures do not return to their resting states. In a BCI application, the user focuses on one of several stimuli, each of which flickers at a different rate and/or phase. Gao et al. (19) described a BCI with 48 flickering lights and a high information transfer rate (ITR) of 68 bits/min. Like P300 BCIs, SSVEP BCIs require no training and can facilitate rapid communication (9,20,21). SSVEP BCIs have also recently expanded to tasks beyond spelling, such as controlling an avatar in a computer game (22–24) or controlling an orthosis (25). Some BCI articles argued that the SSVEP can only be used for communication when users have some conscious control of eye muscles and is therefore not applicable for patients in the late stages of amyotrophic lateral sclerosis (ALS) (1,19). Later work showed that this assumption is incorrect; in some cases, SSVEP BCIs can function even when users do not shift gaze (9,26).

The ERD BCI: Brain rhythms can either display an event-related amplitude decrease or desynchronization or an event-related amplitude increase or synchronization (10). The term ERD BCI describes any BCI system that relies on the detection of amplitude changes in sensorimotor (mu and central beta rhythms) and/or other brain oscillations, also including short-lasting postimagery beta bursts (beta ERS, beta rebound) (8,27–29).

One of the first papers reporting on online classification of different motor-imagery-induced ERD/ERS patterns were published by Pfurtscheller et al. (30) and Kalcher et al. (31). At this time, beside others, the Wadsworth BCI (1,32), the Berlin BCI (8), the Graz BCI (33), and variants of the Tübingen BCI (34) use the ERD/ERS as features for single trial EEG classification. The bit rates reported are between approximately 2 and 17 bit/min (35,36) up to 35 bits/min (8).

The ERD BCI can be operated in two different modes which determine when the user performs a mental task and, therefore, intends to transmit a message. The first mode is externally paced (cue-based, computer-driven synchronous BCI) and the second mode is internally paced (noncue-based, uncued, user-driven asynchronous BCI). In the case of a synchronous BCI, a fixed, predefined time window is used. After a visual or auditory cue stimulus, the subject has to act and produce a specific brain pattern. Nearly all known BCI systems work in such a cue-based mode (1,2,37). An asynchronous protocol requires a continuous analysis and feature extraction of the recorded brain signal. Thus, such BCIs are generally even more demanding and more complex than BCIs operating with a fixed timing scheme.

MOTOR IMAGERY AS CONTROL STRATEGY

Several EEG studies indicate that primary sensorimotor areas are activated when subjects imagine the execution of a hand movement. Klass and Bickford (38) and Chatrian et al. (39)

observed blocking or desynchronization of the central mu-rhythm with motor imagery. By means of quantification of the temporal-spatial ERD pattern, it was clearly shown that one-sided hand motor imagery can result in a lateralized activation of sensorimotor areas, similar to that found in the preparatory phase of a self-paced hand/finger movement (40,41). Such a pattern of sensorimotor EEG activity related to motor imagery can also be found in patients with impaired motor function (42,43). To date, a number of more recent electrophysiological studies support motor cortex participation in motor imagery (e.g., EEG: 44–48; MEG: 49).

An example is shown in Figure 57.2 in the form of band power time courses of 11- to 13-Hz EEG activity. The ERD/ERS curves show different reactivity patterns during right and left motor imagery, displaying a significant band power decrease (ERD) over the contralateral hand area. It is of interest to note, first, that contralateral to the side of motor imagery an ERD and ipsilaterally an ERS were present and, second, that feedback enhanced the difference between both patterns, and therewith the classification accuracy (see also Ref. 50).

The enhancement of oscillatory EEG activity (ERS) during motor imagery is a very important aspect in BCI research. For example, foot motor imagery can induce long-lasting beta oscillations during imagery (peri-imagery ERS; Fig. 57.3A) and/or short-lasting beta bursts after the end of the imagery process (postimagery ERS; Fig. 57.3B) over the foot representation area close to the vertex (29,51). The post-imagery ERS is dominant in the beta band with a maximum ~2.5 seconds after brisk cue-paced imagery, can be detected with great accuracy (high rate of true positives, TP; see Fig. 57.3C) in the ongoing EEG and is therefore a good candidate to realize a one-channel EEG-based BCI (29,51).

Summarizing, it can be stated that motor imagery can modify sensorimotor rhythms in a similar way to that observed in the preparatory phase of an executed movement. Since motor imagery results in a somatotopically organized activation patterns, mental imagination of different movements (e.g., left vs. right hand; hand vs. foot) can be an efficient strategy to operate a BCI based on oscillatory EEG activity. The challenge is to detect the imagery-related changes in ongoing EEG recordings.

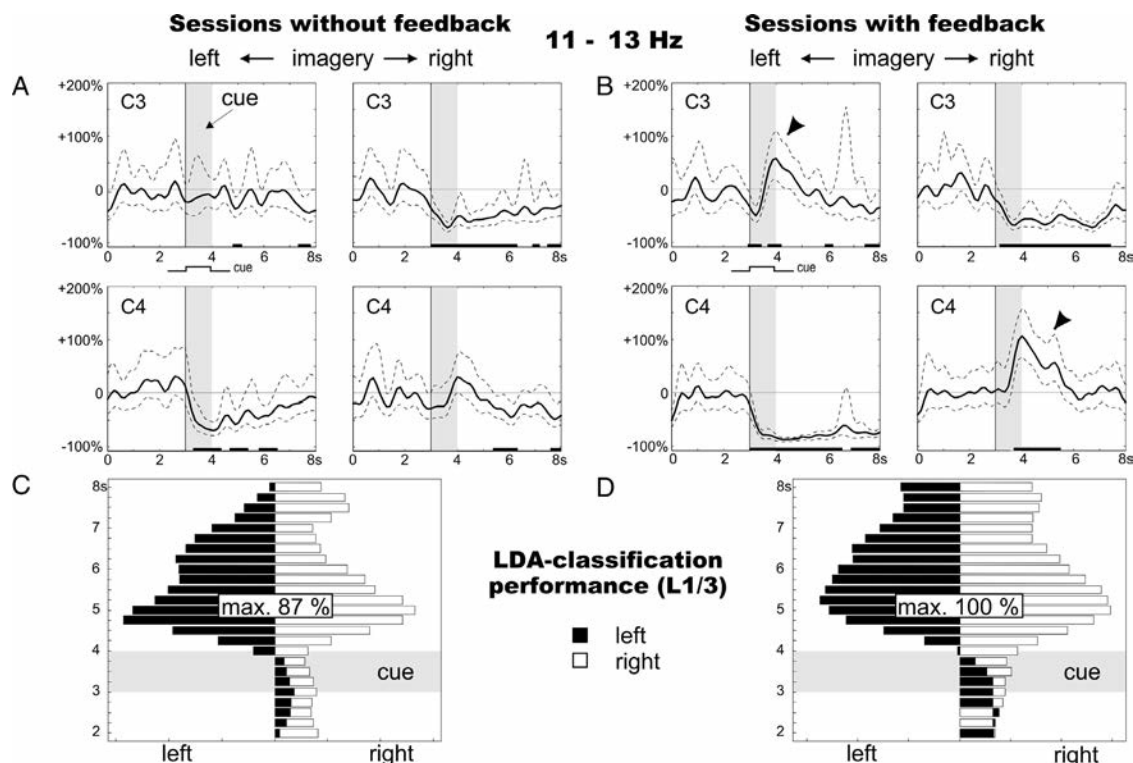


Figure 57.2 Event-related desynchronization (ERD)/event-related synchronization (ERS) curves (11 to 13 Hz; 95% confidence intervals indicated) of one representative subject during imagined movements of the left versus right hand in sessions without feedback (**A**) and in sessions with continuously present feedback (**C**). Data were recorded from the sensorimotor cortex (C3, C4). The time period of cue presentation is indicated by a gray vertical bar. Examples of classification results of single trials (based on linear discriminant analysis, LDA) of two selected sessions: one without (**B**) and one with feedback (**D**). The x-axis denotes the average size of the distance function (resulting from LDA) for all left and right trials of one session (for details, see Ref. 69). In the session with feedback, the average distance corresponds to the average length of the feedback bar presented on the screen. Black bars indicate bar movements to the left side of the screen, white bars indicate bar movements to the right side. The y-axis displays the time points used for classification. The best classification accuracy for each session is indicated.

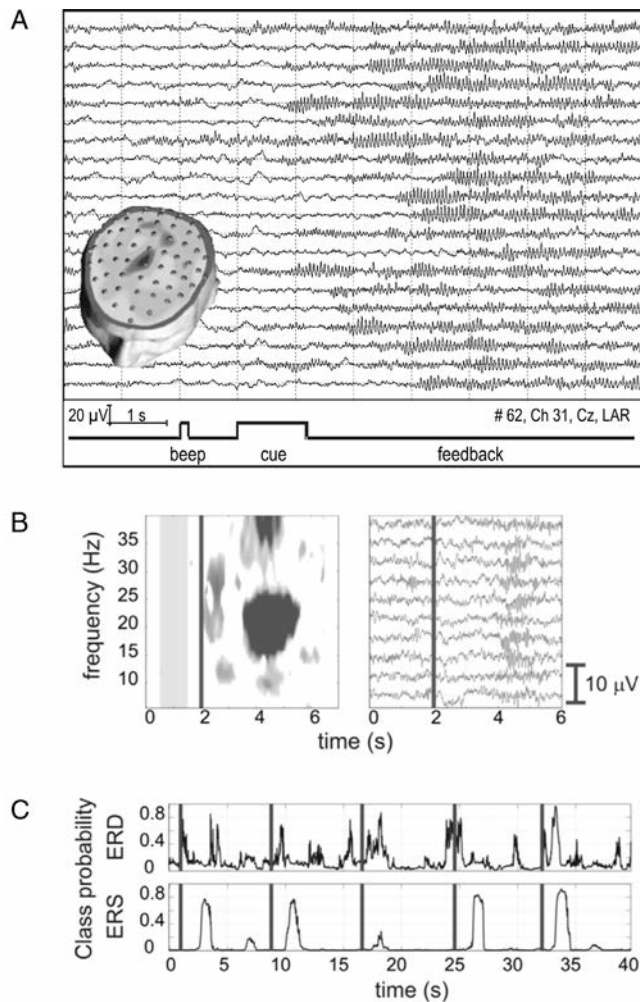


Figure 57.3 Examples of single EEG trials during foot motor imagery recorded at electrode position Cz and topographic map indicating the localized 10-Hz ERS at Cz (A), examples of EEG trials during cue-paced (second 2) brisk foot motor imagery with postimagery beta ERS recorded at Cz (B, right panel), time-frequency map displaying periimagery ERD and postimagery ERS at Cz (B, left panel), and single trial classification of peri-imagery ERD and postimagery ERS with indicated true positives (C).

TRAINING PARADIGM AND IMPACT OF FEEDBACK

Before such a motor-imagery-based BCI can be efficiently used, the participants have to undergo training in order to obtain some control of their brain signals and to maximize the classification accuracy of different brain states. Prior to starting online feedback sessions with an individual, their brain patterns (e.g., related to different types of motor imagery) must be known. To this end, in the first session of an imagery-based BCI standard protocol, users have to imagine repeatedly different kinds of movement (e.g., hand, feet, or tongue movement) in a cue-based mode while their EEG is being recorded (Fig. 57.4A). Optimally, this would entail a full-head recording of their EEG, with topographical and time-frequency analyses of ERD/ERS

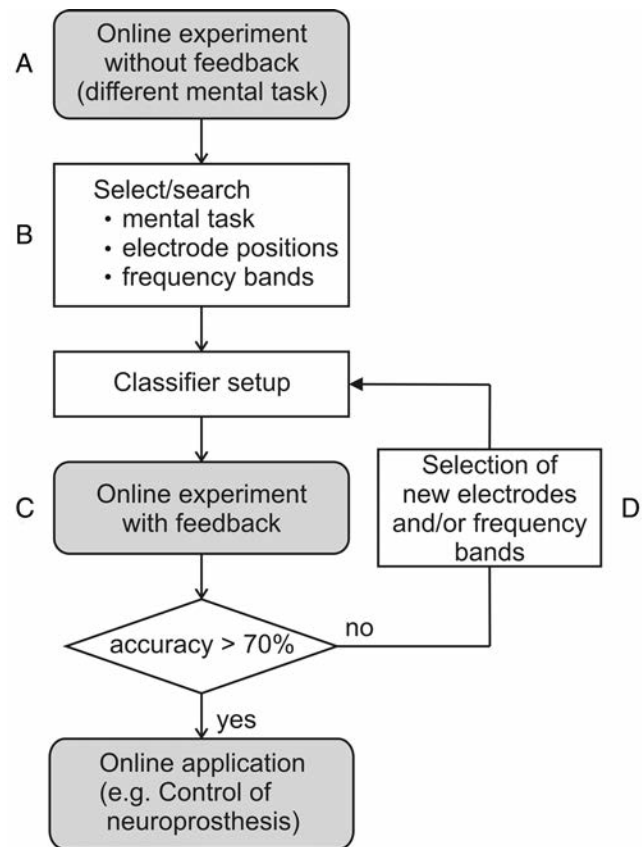


Figure 57.4 Schema for the workflow of an imagery-based BCI with EEG recording (A), feature selection (B), experiment with feedback (C) and classifier update if necessary (D).

patterns, and classification of the individual's brain activity in different imagery conditions. By applying, for example, the distinction-sensitive learning vector quantization (DSLQV) (52) to the screening data, the most important frequency components and electrode locations that best discriminate between different imagery tasks may be identified for each participant, as well as the accuracy of classification (Fig. 57.4B). After setting up the initial classifier, subsequent training sessions can start, where the user receives online feedback of motor imagery-related changes in the EEG (Fig. 57.4C). Depending on the classification accuracy, an update of the classifier and further feedback experiments may be recommended (Fig. 57.4D). This adaptation process between brain and computer can last for many days or weeks in patients. To keep the training period as short as possible, an efficient training strategy is necessary. One example for this could be the so-called basket game.

In the “basket-game” paradigm, for example, the user has to mentally move a falling ball into the correct goal (“basket”) marked on the screen (Fig. 57.5A). If the ball hits the correct basket, it becomes highlighted and points are earned. The horizontal position of the ball is controlled via the BCI output signal and the velocity can be adjusted by the investigator. The speed of the ball can be increased run by run until the person considers it too fast. This approach can find the optimal speed for a maximum ITR. Experiments with two bipolar EEG

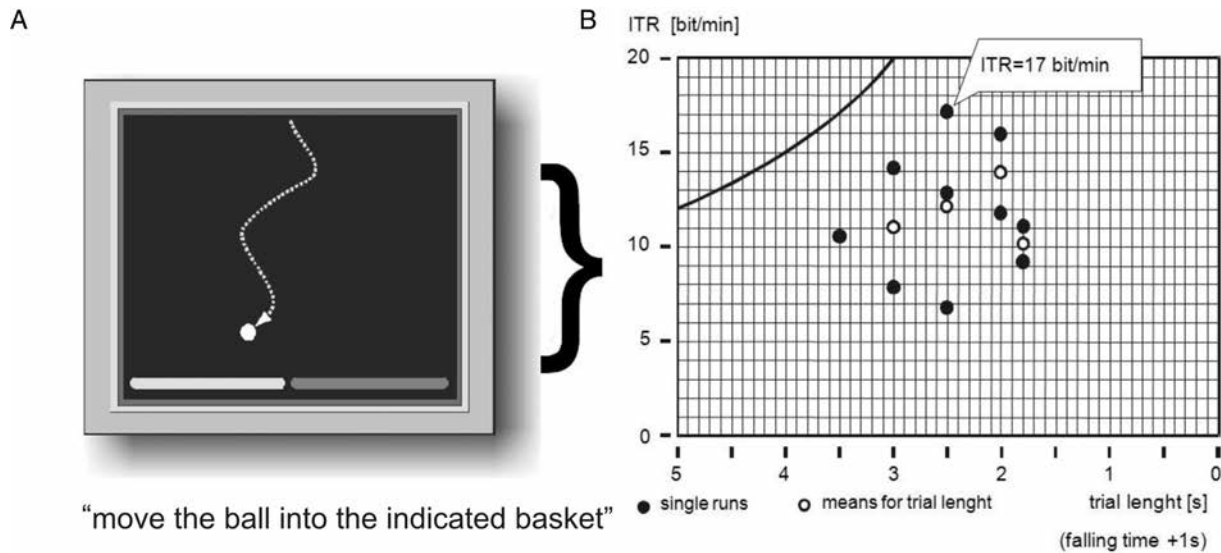


Figure 57.5 Graphical display of the “basket-paradigm” (A). The subject has to direct the ball to the indicated goal (“basket”). The trial length varies across the different runs. Information transfer rate (ITR) for one subject in relation to trial length. The black line represents the maximum possible ITR for an error-free classification (B) Modified from Krausz G, Scherer R, Korisek G, et al. Critical decision-speed and information transfer in the “Graz Brain-Computer Interface.” *Appl Psychophysiol Biofeedback*. 2003;28:233–240.

channels and two motor imagery tasks performed by volunteers with spinal cord injuries revealed a maximal ITR of 17 bits/min with a trial length (falling time of the ball) of 2.5 seconds (36, see also Fig. 57.5B).

To keep the training period as short as possible, a well-thought-out training protocol and helpful feedback signals are essential. The feedback provides the user with information about the efficiency of his/her strategy and enables learning. In this context, two aspects are crucial: (i) the exact manner of how the brain signal is translated into the feedback signal (i.e., information content of the feedback; for advantages of providing continuous or discrete feedback, see Refs. 41 and 50) and (ii) the type of feedback presentation. In any case, the influence of the feedback on the capacity for attention, concentration, and motivation of the user, all aspects which are closely related to the learning process, should be considered (see also Ref. 53).

BCI studies can use different feedback modalities. In the auditory modality, Hinterberger et al. (54) and Pham et al. (55) coded SCP amplitude shifts in the ascending and descending pitches on a major tone scale. Further studies showed that P300 BCIs could also be implemented with auditory rather than visual feedback (56,57). A BCI using only auditory (rather than visual) stimuli would be of importance providing communication support for severely paralyzed patients with visual impairment (58). Although the mentioned studies could show that BCI communication using auditory stimuli only is possible, visual feedback turned out to be superior to auditory feedback. Recently, Chatterjee et al. (59) presented an ERD BCI using a motor imagery paradigm and haptic feedback provided by vibrotactile stimuli to the upper limb. Although further work will be needed to determine how the neural correlates of

vibrotactile feedback affect the modulation of the mu rhythm, haptic information may become a critical component of BCIs, especially if they are designed to control an advanced neuro-prosthetic device (60).

Despite successful approaches to the development of nonvisual BCI systems, visual presentation of stimuli is the most frequently used feedback modality in BCI research (1). Typical visual feedback stimuli comprise cursor movement (8,61), a moving bar of varying size (50,59), and the trajectory of a moving object like in the basket game (8,36). Other interesting variants include color signaling (62) and complex virtual reality environments (28,63).

There is some evidence that a rich visual representation of the feedback signal, for example, in the form of a three-dimensional video game or virtual reality environment, may enhance the learning progress in a BCI task (53,64). Combining BCI and virtual reality technologies could lead to highly realistic and immersive feedback scenarios. As an important step in this direction, Pfurtscheller et al. (28) could show that EEG recording and single-trial processing with sufficiently good classification results are possible in an immersive multi-projection-based stereo and head-tracked virtual reality system (CAVE), and that the obtained signals are even suitable to control events within a virtual environment in real time.

SOME EEG-BASED BCI APPLICATIONS

Currently, the most important applications of a BCI include the restoration of communication for patients with a locked-in-syndrome and the control of neuroprostheses in patients with spinal cord injuries (1,12,65). In addition to these, there is the

important field of neurofeedback to support feedback training in people suffering from epilepsy or stroke (66). Today, the world of BCI application is expanding and new fields are opening. One emerging opportunity is to use the BCI to control multimedia applications (67,68), another is to use the BCI for user authentication (69,70). Some applications are explained in more detail below.

Control of Spelling Systems in Severely Paralyzed Patients

Spelling systems are communication aids that allow users to express themselves by selecting letters or items of an alphabet and thus form words and sentences. The simplest case involves a binary control signal requiring two distinctive mental activities. Patients suffering from ALS can learn to control their own SCP BCI and so to operate the thought translation device spelling device (5,12). By using the same dichotomous selection strategy an ALS patient and a patient suffering from severe cerebral palsy (71) learned to operate the virtual keyboard spelling application (72). The spelling rates in these studies varied from 0.15 to approximately 1 letter/min. An example for such a spelling system with an ERD BCI is displayed in Figure 57.6B.

The Wadsworth speller, based on mu and beta activity for example, divides the alphabet into four parts (73). In Millán and Mouriño (74) an average spelling rate of ~3 letters/min was reported by using a 3-class BCI. A novel spelling concept, possible due to the asynchronous protocol, was introduced by Scherer et al. (75). Another efficient selection strategy was

introduced recently by Müller and Blankertz (76). The Hex-O-Spell application combines asynchronous 2-class ERD BCI control and divides the alphabet into six parts. This raised the average spelling rate up to ~6 letter/min.

Control of Neuroprosthesis to Restore Grasp Function

In general, systems for functional electrical stimulation (FES)—the so-called neuroprostheses—are able to restore lost control/motor functions of body parts after spinal cord injury (SCI) with the use of electrical impulses. The control signal generated by the BCI switches the FES on/off. In a project with a tetraplegic patient, FES resulting in hand grasp was controlled by ongoing EEG activity based on an asynchronous BCI. The patient underwent a large number of BCI training sessions with varying types of motor imagery over a period of several months (77). At the end, he was able to induce trains of 17-Hz beta oscillations focused on the electrode position near the vertex (Cz) by foot motor imagery. These mentally induced 17-Hz oscillations were used as a simple asynchronous brain switch to generate a control signal for the operation of the FES using surface electrodes (Fig. 57.6D). With this method the patient was able to grasp a glass at “free will” (for a detailed description of the procedure see Ref. 78). Müller-Putz et al. (79) reported on an implantable neuroprostheses, known as the Freehand system (80), coupled with an ERD BCI and used in a tetraplegic patient to perform a grasp sequence (Fig. 57.6C).



Figure 57.6 Two students playing table tennis (A), ALS patient operating a spelling system at home (B), motor-imagery-based control of a neuroprosthesis through implanted functional electrical stimulation (FES) of hand muscles (C), motor-imagery-based control of a neuroprosthesis through FES of hand muscles using surface electrodes (D), wheel chair control in a virtual environment (E), and control of virtual hand movement (F). (See color insert)

Rehabilitation after Stroke

Typically, physical therapy aimed at poststroke motor recovery focuses on active movement training. Some patients, however, are so severely disabled that they cannot engage in movement without assistance. Newly developed protocols based on mentally rehearsing movements (motor imagery) represent an intriguing backdoor approach to accessing the motor system, because they can induce an activation of sensorimotor networks that the lesions affected (81).

It is known that unilateral hand motor imagery can result in a contralateral ERD and simultaneously in an ipsilateral ERS after some training sessions (40). Hence, an ERD BCI based on movement imagery can provide some measure of attempted activity in the motor regions and reinforce a patient's sensorimotor experience during poststroke motor recovery. Feedback from the BCI can be solely visual, as in the movement of a virtual hand (Figs. 57.1C and 57.6F) or it can occur through a prosthetic device like an orthotic hand attached to the patient's own (64,82). In both cases, not only can positive feedback reinforce the motor imagery process, but the act of observing the hand movement can itself activate sensorimotor areas.

PERSPECTIVES FOR THE FUTURE

BCI technology is a fast growing field of research and applications with the potential to improve the quality of life in severely disabled people. To date, several BCI prototypes exist and most of them work in a laboratory environment only. Before a BCI can be used for communication and control at home or work, several problems have to be solved, such as how to (i) automatically select electrode positions and frequency components in a motor imagery task, (ii) use the fewest number of recording electrodes possible (the optimum is one EEG channel), (iii) minimize the training time through game-like feedback, and

(iv) automatically detect artefacts. It can be expected that making BCIs useful to a wider group of users will open up new fields of applications such as entertainment in the next several years.

We recently reported on a one-channel EEG-based BCI that detects the postmotor imagery beta rebound (29,51). This beta rebound is a relatively stable EEG phenomenon (47) that can be detected in single trial EEG during foot motor imagery and used to realize a "brain switch." Such a brain switch is a BCI system designed to detect only one brain state (brain pattern) in the ongoing EEG signal (83). One important feature of such a brain switch is that unintended activations should not occur in the output signal. That is, the false-positive rate should be zero or close to zero. An imagery-based brain switch can be used to turn on/off the flickering lights of an SSVEP-controlled hand orthosis (25). This type of BCI, composed of two sequentially operating BCIs, can be seen as an example of a "hybrid BCI."

A clear challenge is to develop more effective BCI control paradigms, offering, for instance, three-dimensional control over a neuroprosthesis or the operation of a spelling device with a speed of at least 5 to 10 characters/minute. Such an improvement of speed and accuracy is possible by analyzing cortical potential changes recorded with subdural electrode strips or grids or the detection of firing patterns in intracortical recordings. Figure 57.7 shows the three types of potential recording with EEG, subdural electrodes (ECoG), and microelectrode array. The advantage of the ECoG over the EEG is the better signal-to-noise ratio, which includes easier detection of gamma activity. Recently, bursts of gamma activity between 60 and 90 Hz in ECoG recordings during self-paced limb and tongue movements were reported (84,85). These gamma bursts are short lasting, display a high somatotopic specificity, and are embedded in the alpha and beta ERD lasting for some seconds. Patient-oriented work with subdural electrodes and ECoG single-trial classification have shown first promising results (3,86).

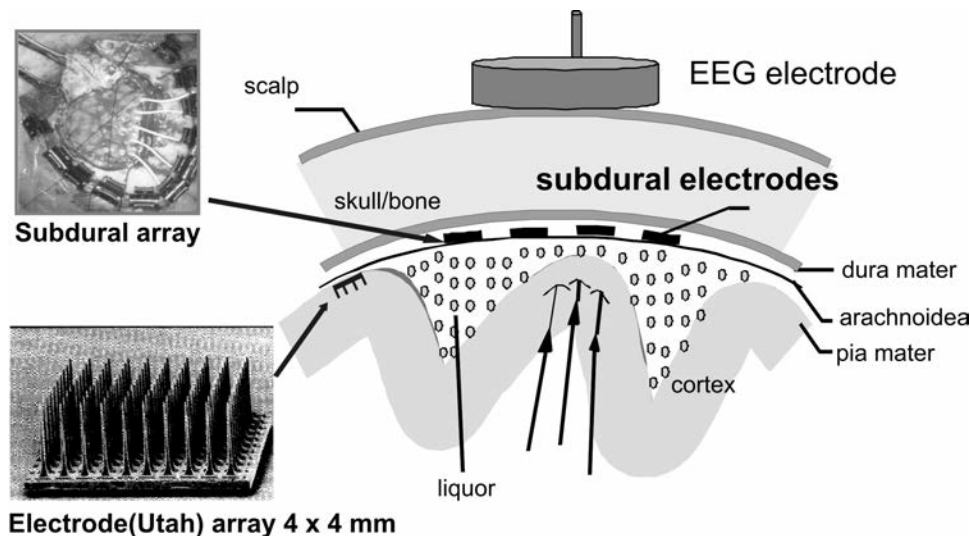


Figure 57.7 Schema of electrical potential recording in BCI research with non-invasive EEG electrodes, invasive subdural electrode strip (array), or highly invasive microelectrode array in the cortex.

Studies in monkeys have shown that three-dimensional control is possible when multiunit activity is recorded in cortical areas. Between 32 and 96 microwires were implanted in different cortical motor areas. After a training period with distinct motor tasks, the monkeys were able to achieve three-dimensional control over the movement of a robotic device by real-time transformation of neuronal multiunit neuronal activity (87). The feasibility of a prosthetic device control in a tetraplegic patient based on recording of neural ensemble activity through a 96-microelectrode array (Fig. 57.7) was reported by Hochberg et al. (88). These early results suggest that recording of intracortical neuronal multiunit activity could provide a new neurotechnology to restore independence for humans with paralysis.

REFERENCES

1. Wolpaw JR, Birbaumer N, McFarland DJ, et al. Brain-computer interfaces for communication and control. *Clin Neurophysiol*. 2002;113:767–791.
2. Pfurtscheller G, Neuper C. Motor imagery and direct brain-computer communication. *Proc IEEE*. 2001;89:1123–1134.
3. Graimann B, Huggins JE, Schlögl A, et al. Detection of movement-related desynchronization patterns in ongoing single-channel electrocorticogram. *IEEE Trans Neural Syst Rehabil Eng*. 2003;11:276–281.
4. Obermaier B, Neuper C, Guger C, et al. Information transfer rate in a five-classes brain-computer interface. *IEEE Trans Neural Syst Rehabil Eng*. 2001;9:283–288.
5. Birbaumer N, Kübler A, Ghanayim N, et al. The thought translation device (TTD) for completely paralyzed patients. *IEEE Trans Rehabil Eng*. 2000;8:190–193.
6. Levine SP, Huggins JE, BeMent SL, et al. A direct brain interface based on event-related potentials. *IEEE Trans Rehabil Eng*. 2000;8:180–185.
7. Millán J, Mouriño J, Franzé M, et al. A local neural classifier for the recognition of EEG patterns associated to mental tasks. *IEEE Trans Neural Netw*. 2002;13:678–686.
8. Blankertz B, Dornhege G, Krauledat M, et al. The non-invasive Berlin brain-computer interface: fast acquisition of effective performance in untrained subjects. *Neuroimage*. 2007;37:539–550.
9. Allison BZ, McFarland DJ, Schalk G, et al. Towards an independent brain-computer interface using steady state visual evoked potentials. *Clin Neurophysiol*. 2008;119:399–408.
10. Pfurtscheller G, Lopes da Silva FH. Event-related EEG/MEG synchronization and desynchronization: basic principles. *Clin Neurophysiol*. 1999;110:1842–1857.
11. Birbaumer N, Elbert T, Canavan AG, et al. Slow potentials of the cerebral cortex and behavior. *Physiol Rev*. 1990;70:1–41.
12. Birbaumer N, Ghanayim N, Hinterberger T, et al. A spelling device for the paralyzed. *Nature*. 1999;398:297–298.
13. Kübler A, Birbaumer N. Brain-computer interfaces and communication in paralysis: extinction of goal directed thinking in completely paralyzed patients? *Clin Neurophysiol*. 2008; 119:2658–2666.
14. Allison BZ, Pineda JA. Effects of SOA and flash pattern manipulations on ERPs, performance, and preference: implications for a BCI system. *Int J Psychophysiol*. 2006;59:127–140.
15. Donchin E, Spencer KM, Wijesinghe R. The mental prosthesis: assessing the speed of a P300-based brain-computer interface. *IEEE Trans Rehabil Eng*. 2000;8:174–179.
16. Farwell LA, Donchin E. Talking off the top of your head: toward a mental prosthesis utilizing event-related brain potentials. *Electroencephalogr Clin Neurophysiol*. 1988;70:510–523.
17. Bell CJ, Shenoy P, Chalodhorn R, et al. Control of a humanoid robot by a noninvasive brain-computer interface in humans. *J Neural Eng*. 2008;5:214–220.
18. Guger C, Daban S, Sellers E, et al. How many people are able to control a P300-based brain-computer interface (BCI)? *Neurosci Lett*. 2009;462:94–98.
19. Gao X, Xu D, Cheng M, et al. A BCI-based environmental controller for the motion-disabled. *IEEE Trans Neural Syst Rehabil Eng*. 2003;11:137–140.
20. Allison BZ, Wolpaw EW, Wolpaw JR. Brain-computer interface systems: progress and prospects. *Expert Rev Med Devices*. 2007;4:463–474.
21. Krusienski D J, Sellers EW, Cabestaing F, et al. A comparison of classification techniques for the P300 speller. *J Neural Eng*. 2006;3:299–305.
22. Faller J, Müller-Putz G, Schmalstieg D, et al. An application framework for controlling an avatar in a desktop based virtual environment via a software SSVEP brain-computer interface. Special Issue of *Presence: Teleoperators and Virtual Environments*. 2010; 19(1):25–34.
23. Lalor EC, Kelly SP, Finucane C, et al. Steady-state VEP-based brain-computer interface control in an immersive 3D gaming environment. *EURASIP J Appl Signal Processing*. 2005; 19:3156–3164.
24. Martinez P, Bakardjian H, Cichocki A. Fully online multicommand brain-computer interface with visual neurofeedback using SSVEP paradigm. *Comput Intell Neurosci*. 2007; Article ID 94561.
25. Pfurtscheller G, Solis-Escalante T, Ortner R, et al. Self-paced operation of an SSVEP-based orthosis with and without an imagery-based “brain switch”: a feasibility study towards a hybrid BCI. *IEEE Trans Neural Syst Rehabil Eng*. in press.
26. Kelly SP, Lalor EC, Finucane C, et al. Visual spatial attention control in an independent brain-computer interface. *IEEE Trans Neural Syst Rehabil Eng*. 2005;52:1588–1596.
27. Pfurtscheller G, Brunner C, Schlögl A, et al. Mu rhythm (de)synchronization and EEG single-trial classification of different motor imagery tasks. *Neuroimage*. 2006;31:153–159.
28. Pfurtscheller G, Leeb R, Keinrath C, et al. Walking from thought. *Brain Res*. 2006;1071:145–152.
29. Pfurtscheller G, Solis-Escalante T. Could the beta rebound in the EEG be suitable to realize a “brain switch”? *Clin Neurophysiol*. 2009;120:24–29.
30. Pfurtscheller G, Kalcher J, Flotzinger D. A new communication device for handicapped persons The Brain-Computer Interface. In: Ballabion E, Placencia-Porrero I, Puig de la Bellacasa R, eds. *Rehabilitation Technology*. Vol 9. Amsterdam: IOS Press; 1993: 123–127.
31. Kalcher J, Flotzinger D, Neuper C, et al. Graz brain-computer interface II: towards communication between humans and computers based on online classification of three different EEG patterns. *Med Biol Eng Comput*. 1996;34:382–388.
32. Sellers EW, Krusienski DJ, McFarland DJ, et al. Noninvasive brain-computer interface research at the Wadsworth Center. In: Dornhege G, Millán J del R, Hinterberger T, et al., eds. *Toward Brain-Computer Interfacing*. Cambridge, Massachusetts: MIT Press; 2007:31–42.
33. Pfurtscheller G, Müller-Putz GR, Schlögl A, et al. Graz-brain-computer interface: state of research. In: Dornhege G, Millán J del R, Hinterberger T, et al., eds. *Toward Brain-Computer Interfacing*. Cambridge, Massachusetts: MIT Press; 2007:65–84.

34. Hinterberger T, Nijboer F, Kübler A, et al. Brain-computer interfaces for communication in paralysis: a clinical experimental approach. In: Dornhege G, Millán J del R, Hinterberger T, et al., eds. *Toward Brain-Computer Interfacing*. Cambridge, Massachusetts: MIT Press; 2007:43–64.
35. McFarland DJ, Sarnacki WA, Wolpaw JR. Brain-computer interface (BCI) operation: optimizing information transfer rates. *Biol Psychol*. 2003;63:237–251.
36. Krausz G, Scherer R, Korisek G, et al. Critical decision-speed and information transfer in the “Graz Brain-Computer Interface”. *Appl Psychophysiol Biofeedback*. 2003;28:233–240.
37. Kübler A, Neumann N, Kaiser J, et al. Brain-computer communication: self-regulation of slow cortical potentials for verbal communication. *Arch Phys Med Rehabil*. 2001;82:1533–1539.
38. Klass SG, Bickford RG. Observations on the rolandic arceau rhythm. *Electroencephalogr Clin Neurophysiol*. 1957;9:570.
39. Chatrian GE, Petersen MC, Lazarte JA. The blocking of the rolandic wicket rhythm and some central changes related to movement. *Electroencephalogr Clin Neurophysiol*. 1959;11:497–510.
40. Pfurtscheller G, Neuper C. Motor imagery activates primary sensorimotor area in humans. *Neurosci Lett*. 1997;239:65–68.
41. Neuper C, Scherer R, Wriessnegger S, et al. Motor imagery and action observation: modulation of sensorimotor brain rhythms during mental control of a brain-computer interface. *Clin Neurophysiol*. 2009;120:239–247.
42. Neuper C, Pfurtscheller G. Motor imagery and ERD. In: Pfurtscheller G, Lopes da Silva FH, eds. *Event-Related Desynchronization: Handbook of Electroencephalography and Clinical Neurophysiology*. Revised Edition, Vol 6. Amsterdam: Elsevier; 1999:303–325.
43. Neuper C, Müller-Putz GR, Scherer R, et al. Motor imagery and EEG-based control of spelling devices and neuroprostheses. In: Neuper C, Klimesch W, eds. *Event-Related Dynamics of Brain Oscillations*. Amsterdam: Elsevier; 2006:393–409.
44. McFarland DJ, Miner LA, Vaughan TM, et al. Mu and beta rhythm topographies during motor imagery and actual movements. *Brain Topogr*. 2000;12:177–186.
45. Caldara R, Deiber MP, Andrey C, et al. Actual and mental motor preparation and execution: a spatiotemporal ERP study. *Exp Brain Res*. 2004;159:389–399.
46. Neuper C, Scherer R, Reiner M, et al. Imagery of motor actions: differential effects of kinaesthetic versus visual-motor mode of imagery on single-trial EEG. *Brain Res Cogn Brain Res*. 2005;25:668–677.
47. Pfurtscheller G, Neuper C, Brunner C, et al. Beta rebound after different types of motor imagery in man. *Neurosci Lett*. 2005;378:156–159.
48. Carrillo-de-la-Pena MT, Lastra-Barreira C, Galdo-Alvarez S. Limb (hand vs. foot) and response conflict have similar effects on event-related potentials (ERPs) recorded during motor imagery and overt execution. *Eur J Neurosci*. 2006;24:635–643.
49. Mellinger J, Schalk G, Braun C, et al. An MEG-based brain-computer interface (BCI). *Neuroimage*. 2007;36:581–593.
50. Neuper C, Schlögl A, Pfurtscheller G. Enhancement of left-right sensorimotor EEG differences during feedback-regulated motor imagery. *J Clin Neurophysiol*. 1999;16:373–382.
51. Solis-Escalante T, Müller-Putz GR, Brunner C, et al. Analysis of sensorimotor rhythms for the implementation of a brain switch for healthy subjects. *Biomed Signal Process Control*. 2010;5:15–20.
52. Pregonzer M, Pfurtscheller G, Flotzinger D. Automated feature selection with a distinction sensitive learning vector quantizer. *Neurocomputing*. 1996;11:19–29.
53. Pineda JA, Silverman DS, Vankov A, et al. Learning to control brain rhythms: making a brain-computer interface possible. *IEEE Trans Neural Syst Rehabil Eng*. 2003;11:181–184.
54. Hinterberger T, Neumann N, Pham M, et al. A multimodal brain-based feedback and communication system. *Exp Brain Res*. 2004;154:521–526.
55. Pham M, Hinterberger T, Neumann N, et al. An auditory brain-computer interface based on the self-regulation of slow cortical potentials. *Neurorehabil Neural Repair*. 2005;19:206–218.
56. Furdea A, Halder S, Krusienski DJ, et al. An auditory oddball (P300) spelling system for brain-computer interfaces. *Psychophysiology*. 2009;46:1–9.
57. Klobassa DS, Vaughan TM, Brunner P, et al. Toward a high-throughput auditory P300-based brain-computer interface. *Clin Neurophysiol*. 2009;120:1252–1261.
58. Kübler A, Furdea A, Halder S, et al. A brain-computer interface controlled auditory event-related potential (P300) spelling system for locked-in patients. *Ann N Y Acad Sci*. 2009;1157:90–100.
59. Lebedev MA, Nicolelis MAL. Brain-machine interfaces: past, present and future. *Trends Neurosci*. 2006;29:536–546.
60. Chatterjee A, Aggarwal V, Ramos A, et al. A brain-computer interface with vibrotactile biofeedback for haptic information. *J Neuroeng Rehabil*. 2007;4:40.
61. McFarland DJ, McCane LM, Wolpaw JR. EEG-based communication and control: short-term role of feedback. *IEEE Trans Rehabil Eng*. 1998;6:7–11.
62. Kaplan AY, Lim JJ, Jin KS, et al. Unconscious operant conditioning in the paradigm of brain-computer interface based on color perception. *Int J Dev Neurosci*. 2005;115:781–802.
63. Leeb R, Keinrath C, Friedman D, et al. Walking by thinking: the brainwaves are crucial, not the muscles! *Presence* 2006;15:500–514.
64. Ron-Angevin R, Diaz-Estrella A, Reyes-Lecuona A. Development of a brain-computer interface based on virtual reality to improve training techniques. *Cyberpsychol Behav*. 2005;8:353–354.
65. Pfurtscheller G, Müller-Putz G, Scherer R, et al. Rehabilitation with brain-computer interface systems. *IEEE Comput Mag*. 2008;41:58–65.
66. Birbaumer N, Cohen LG. Brain-computer interfaces: communication and restoration of movement in paralysis. *J Physiol*. 2007;579:621–636.
67. Scherer R, Lee F, Schlögl A, et al. Toward self-paced brain-computer communication: navigation through virtual worlds. *IEEE Trans Biomed Eng*. 2008;55:675–682.
68. Nijholt A, Tan D, Pfurtscheller G, et al. Brain-computer interfacing for intelligent systems. *IEEE Intell Syst*. 2008;23:72–79.
69. Pfurtscheller G, Neuper C. Future prospects of ERD/ERS in the context of brain-computer interface (BCI) developments. In: Neuper C, Klimesch W, eds. *Event-Related Dynamics of Brain Oscillations, Progress in Brain Research*. Vol 159. Amsterdam: Elsevier; 2006:19–27.
70. Marcel S, Millán J del R. Person authentication using brainwaves (EEG) and maximum a posteriori model adaptation. *IEEE Trans Pattern Anal Mach Intell*. 2007;29:743–748.
71. Neuper C, Müller GR, Kübler A, et al. Clinical application of an EEG-based brain-computer interface: a case study in a patient with severe motor impairment. *Clin Neurophysiol*. 2003;114:399–409.
72. Obermaier B, Müller GR, Pfurtscheller G. “Virtual keyboard” controlled by spontaneous EEG activity. *IEEE Trans Neural Syst Rehabil Eng*. 2003;11:422–426.
73. Wolpaw JR, McFarland DJ, Vaughan TM, et al. The Wadsworth Center brain-computer interface (BCI) research and development program. *IEEE Trans Neural Syst Rehabil Eng*. 2003;11:204–207.

74. Millán J, Mourinho J. Asynchronous BCI and local neural classifiers: an overview of the adaptive brain interface project. *IEEE Trans Neural Syst Rehabil Eng.* 2003;11:159–161.
75. Scherer R, Müller GR, Neuper C, et al. An asynchronously controlled EEG-based virtual keyboard: improvement of the spelling rate. *IEEE Trans Neural Syst Rehabil Eng.* 2004;51:979–984.
76. Müller K-R, Blankertz B. Toward noninvasive brain computer interfaces. *IEEE Signal Process Mag.* 2006;23:125–128.
77. Pfurtscheller G, Guger C, Müller G, et al. Brain oscillations control hand orthosis in a tetraplegic. *Neurosci Lett.* 2000;292:211–214.
78. Pfurtscheller G, Müller GR, Rupp R, et al. “Thought”-control of functional electrical stimulation to restore hand grasp in a tetraplegic. *Neurosci Lett.* 2003;351(1):33–36.
79. Müller-Putz GR, Scherer R, Pfurtscheller G, et al. EEG-based neuroprosthesis control: a step into clinical practice. *Neurosci Lett.* 2005;382:169–174.
80. Keith MW, Peckham PH, Thrope GB, et al. Implantable functional neuromuscular stimulation in the tetraplegic hand. *J Hand Surg Am.* 1989;14:524–530.
81. Sharma N, Pomeroy VM, Baron J-C. Motor imagery: a backdoor to the motor system after stroke? *Stroke.* 2006;37:1941–1952.
82. Birbaumer N. Brain-computer interface research: coming of age clinical. *Neurophysiology.* 2006;117:479–483.
83. Mason SG, Birch GE. A brain-controlled switch for asynchronous control applications. *IEEE Trans Biomed Eng.* 2000;47:1297–1307.
84. Crone NE, Miglioretti DL, Gordon B, et al. Functional mapping of human sensorimotor cortex with electrocorticographic spectral analysis. II. Event-related synchronization in the gamma band. *Brain.* 1998;121:2301–2315.
85. Pfurtscheller G, Graimann B, Huggins JE, et al. Spatiotemporal patterns of beta desynchronization and gamma synchronization in corticographic data during self-paced movement. *Clin Neurophysiol.* 2003;114:1226–1236.
86. Schalk G, Miller KJ, Anderson NR, et al. Two-dimensional movement control using electrocorticographic signals in humans. *J Neural Eng.* 2008;5:75–84.
87. Wessberg J, Stambaugh CR, Kralik JD, et al. Real-time prediction of hand trajectory by ensembles of cortical neurons in primates. *Nature.* 2000;408:361–365.
88. Hochberg LR, Serruya MD, Friehs GM, et al. Neuronal ensemble control of prosthetic devices by a human with tetraplegia. *Nature.* 2006;442:164–171.

Multimodal Monitoring of EEG and Evoked Potentials

GERT PFURTSCHELLER

CHAPTER

58

GENERAL ASPECTS

The most comprehensive form of monitoring of cerebral functioning is obtained when electroencephalograph (EEG) and different modality-evoked potentials (EPs) are recorded and analyzed continuously and simultaneously. This means that EEG spectra, brainstem auditory-evoked potentials (BAEPs), and cervical and cortical somatosensory-evoked potentials (SEPs) are computed at intervals of seconds to minutes and displayed in a compressed form. In addition to EEG and EPs, other physiological signals, such as heart rate (HR), ventilation, temperature, oxygen saturation, and blood pressure, may be useful, depending on the particular condition. This monitoring can be performed in the operating room, in the intensive care unit (ICU), in the sleep laboratory, or in the outpatient clinic. For extensive literature on this subject, see Nuwer (1) and Chapters 39, 40, and 41 of this book.

TECHNICAL ASPECTS OF CONTINUOUS MONITORING OF EEG SPECTRA COMBINED WITH EPs

The techniques necessary for long-term monitoring of EEG and BAEPs were established in normal subjects by Maresch et al. (2). They used two EEG channels (Cz-A1 and Cz-A2) with broadband amplifiers (1.5 Hz to 1.5 kHz); after amplification the signals were divided into low-frequency (EEG; lower cut-off frequency 30 Hz) and high-frequency (BAEP; upper cut-off frequency 250 Hz) branches. In other studies these responses were complemented with recordings of SEPs (3,4). The main technical considerations in this type of analysis are that (a) different sampling frequencies must be used because of the rather different frequency contents of the signal, for example, EEG and BAEP; and (b) the number of samples should be minimized to save memory storage, since the analysis must be done over long periods of time. A way to solve these technical problems is introduced in Figure 58.1 by the sampling schema.

Measurements in the operating room or ICU may be easily affected by noise. To avoid main artifacts (50 or 60 Hz), the interstimulus interval between auditory and somatosensory stimulation should be variable. More specifically, intervals should be alternatively small or large (e.g., to cancel 50 Hz: auditory stimulation 110/90 msec; somatosensory stimulation 210/190 msec). In addition, the stimuli should be applied either on the positive or negative peak of the main frequency EEG component. With this technique, fairly good results are obtained in unshielded rooms and with electrical equipment nearby.

LONG-TERM MONITORING IN THE INTENSIVE CARE UNIT

A great number of patients in the ICU are comatose or recovering from coma, since coma can be caused by many disorders including severe head injury, vascular lesions, encephalitis, posthypoxic or postischemic events, and drug intoxication, among others. The monitoring of ICU patients is important to detect critical situations as fast as possible, to facilitate therapeutic decisions, to monitor the level of impaired consciousness, and to predict the clinical outcome. Another important feature in the ICU is the determination and documentation of brain death, which is a prerequisite for most organ transplantations. The following case report of a patient with unfavorable outcome underlines the importance of monitoring of comatose patients:

A 57-year-old woman with hypernephroma suffered from hypertension for several years. She was admitted with a left hemisphere hemorrhage and was soporous. She had a right hemiplegia and responded appropriately to painful stimuli on the left side. The dominant EEG frequency was 5 to 6/sec, and there was a delta-wave focus over the left hemisphere. On the first day, a ventricular drainage of cerebrospinal fluid was performed. In the following 6 days, the patient's condition deteriorated. After 2 days, she developed anisocoria. One day later, respiration was insufficient. The patient showed extensor responses to painful stimuli. After 5 days, pupillary light reaction and ciliospinal, cornea, and oculocephalic reflexes were negative, and there was no longer any reaction to painful stimulation. The cranial computed tomography (CT) scan showed an enlargement of the hemorrhage and signs of an increased intracerebral pressure (ICP).

Figure 58.2 shows the various parameters registered from the time of admission, throughout the critical rise of ICP, and until brain death was clinically determined. Five days after admission, at 6:20 AM, the intracranial pressure rose to a critical level of 56 mm Hg, in spite of the ventricular drainage. Amplitudes of the cortical SEPs decreased and finally disappeared 30 minutes later. The peak of the EEG spectra shifted to lower frequencies. Pathological HR and heart rate variability (HRV) were observed. Seven hours later, BAEP components IV/V vanished; another 30 minutes later, wave III disappeared, and 60 minutes later, all BAEP components were abolished.

This example provides evidence that monitoring of only one signal gives incomplete information. From the SEPs alone, it can be seen that the cortical component disappeared at 6:50 AM, whereas the cervical component remained unchanged for about 8 additional hours. The cortical component N20 is very sensitive to

Figure 58.1 Sampling scheme of EEG, somatosensory-evoked potential (SEP), and brainstem auditory-evoked potential (BAEP) during computer-controlled click (C) and electrical (E) median nerve stimulation as used for the data displayed in Figures 60.2 and 60.3B; sampling and electrical and auditory stimulation are indicated. BAEP sampling lasts for 10 msec, SEP sampling for 50 msec, the SEP sampling window is variable in a range of 90 msec. Computer-controlled SEP stimulation in intervals of 210/190 msec and BAEP stimulation in intervals of 111/89 msec.

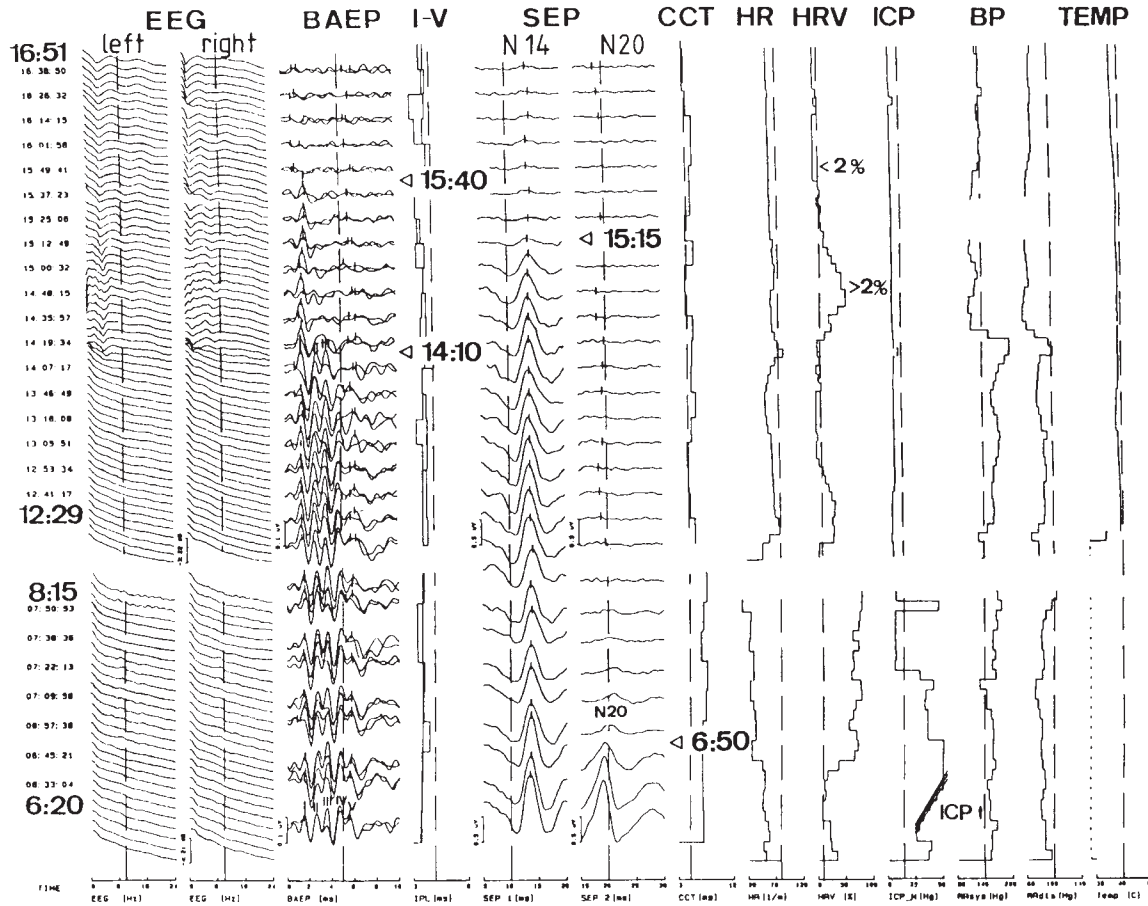
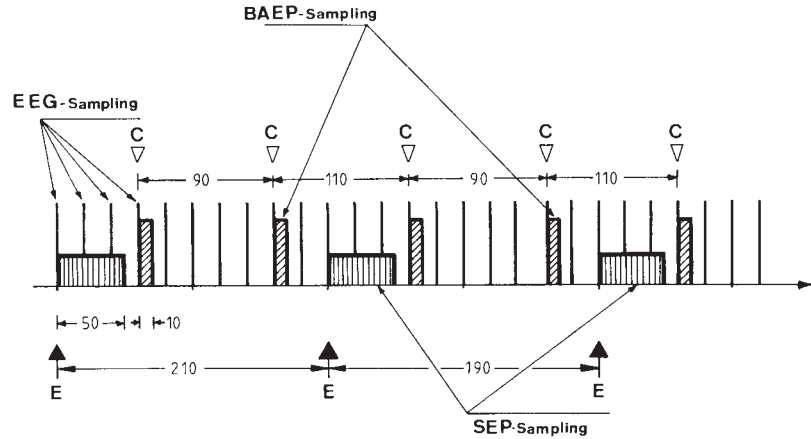


Figure 58.2 Protocol from a 57-year-old patient with a left hemispheric hemorrhage during deterioration of the comatose state and ending with brain death. From left to right: compressed EEG spectra from left and right hemispheres; brainstem auditory-evoked potential (BAEP) to ipsi- and contralateral ear stimulation; BAEP interpeak latency (I-V); cervical (N14) and cortical (N20) SEPs; central conduction time (CCT); heart rate (HR); heart rate variability (HRV); intracranial pressure (ICP); systolic (Bpsys) and diastolic (Bpdia) blood pressure; and rectal body temperature (TEMP). Important events are indicated by arrows. For further explanation, see text. Modified from Hilz MJ, Litscher G, Weis M, et al. Continuous multivariable monitoring in neurological intensive care patients—preliminary reports on four cases. *Intensive Care Med.* 1991;17:857–893.

Copyright © 2010, Wolters Kluwer Health. All rights reserved.

ischemia (6), and its disappearance signals that cortical damage occurred early in the morning. BAEPs show gradual deterioration of the waves V, IV, III, and II in the time between the disappearance of the cortical and cervical SEP components. This can be interpreted to mean that the brainstem function deteriorated during that time (starting from the midbrain level). In summary, it is clear that the most comprehensive picture of the cerebral state in comatose patients can be obtained only by monitoring different neuronal systems and signals with use of EEG, SEPs, and BAEPs.

The importance of multimodality EP measurements in patients with severe head injury was documented by Anderson et al. (7), Greenberg et al. (8), and others. EPs can be even more reliable than intracranial pressure measurements in predicting the clinical outcome (7). Combined EEG and EP monitoring can also be used to differentiate comas due to structural lesions from those of metabolic origin (9).

Besides EEG and EPs, the HR and HRV are displayed in Figure 58.2. The HRV was initially high, dropped at 1:00 p.m., and remained depressed, with an exceptional increase during the disappearance of the cervical component of the SEP. The HRV indicates the spontaneous physiological variations in the HR modulated by the parasympathetic and sympathetic activity of the cardiac nerves. This activity originates mainly in the medullary circulatory center but is also influenced by higher centers (10). HRV in normal subjects and in brain death was reported by Schwarz et al. (11) and in newborns by Mehta et al. (12). Strong correlations exist between EEG and HRV during sleep (13). The measurement of HRV, therefore, is a sensitive parameter to monitor brainstem functions in parallel with or instead of BAEPs (BAEP measurements are not always possible in patients with severe head injury). A decrease of HRV, therefore, can also indicate deterioration of brainstem function.

MONITORING IN THE OPERATING ROOM

In the operating room, there are two different applications for cerebral monitoring systems. One is to provide the surgeon with continuous information and warnings about potential damage to the spinal cord and other neuronal structures. Monitoring, therefore, is indicated in spinal cord operations involving risk of ischemia from compression of feeding blood vessels, aneurysm surgery, cerebrovascular procedures, and posterior fossa operations (1,14). The prognostic significance of SEP, BAEP, and serum S-100B monitoring after aneurysm injury was documented by Schick et al. (15). The second reason for cerebral monitoring is to assist the anesthetist in avoiding brain damage caused by hypoxic and/or ischemic events (16), to control the depth of anesthesia, and to avoid intraoperative wakefulness (17). Further details on intraoperative monitoring are presented in Chapter 39.

Because of the different neuronal systems involved in the generation of EEG, SEPs, and BAEPs and their different sensitivity to the effect of drugs, particularly anesthetics, it is very understandable that combined monitoring of all brain signals together gives more information on neuronal signals than the monitoring of one signal alone.

An example of multiparametric monitoring of EEG spectra combined using different modality EPs under halothane

anesthesia is demonstrated in Figure 58.3. The recordings were taken from a 31-year-old patient during the initial phase of an orthopedic surgical intervention without neurological complications. Collection of the biological data started before anesthesia. Approximately 1 minute after administration of etomidate (Hypnomidate) (23 mg), the expected EEG changes occurred (Fig. 60.3; marked with A). The cardiovascular effects intensified after intubation (B) and after application of pancuronium (4 mg) (C). With increasing concentration of halothane, changes in EEG spectra and cortical SEPs were accentuated (E). The patient was monitored for more than 90 minutes. Despite the massive changes in the EEG as demonstrated in the band power trend curves due to the individual concentration, the BAEPs remained nearly unchanged. The cervical SEP showed an increase in latency of 1 msec, and the cortical N20 component was not identifiable with deeper levels of anesthesia. Synchronous systolic blood pressure measurements displayed a decrease from 135 to 85 mm Hg.

The protocol of Figure 58.3 is a good example of the influence of the level of anesthesia on different neuronal systems. EEG and cortical SEPs are heavily changed, while BAEPs and cervical SEPs are only slightly modified during high levels of halothane. It is of interest to see the different behavior of power trend curves dependent on the frequency band used. Blood pressure and HR measurements give additional information on the cardiovascular system and should be also recorded.

SLEEP MONITORING IN INFANTS AT RISK

In polysomnography, a great number of different signals must be recorded and analyzed. One goal of the sleep polygraphy in infants is to study babies at risk for sudden infant death syndrome (SIDS), that is, babies with sleep apnea and near-miss SIDS (18,19). In this type of monitoring, in addition to the EEG, different physiological signals such as HR electro-oculogram (EOG), electromyogram (EMG), pO_2 , and pCO_2 must be recorded and analyzed to reliably classify sleep stages and to differentiate between rapid eye movement (REM) (active sleep) and non-REM (NREM) (quiet sleep) state. Additional recording of BAEPs is technically possible and allows for monitoring of the brainstem at the same time. Monitoring of BAEPs during nocturnal sleep cycles was reported by Bastuji et al. (20). They found that the latency of wave V was increased and related to physiological hypothermia during the night. This gives evidence of how sensitive BAEP measurements are and that brainstem signals are affected not only by pathophysiological but also by physiological variations.

An example demonstrating the simultaneous recordings of EEG and BAEPs in a 4-month-old baby is shown in Figure 58.4. EEG power trend curves, HR, pO_2 , and pCO_2 show characteristic patterns in active sleep and quiet sleep. Slow EEG waves, spindle activity (10–12 Hz), and pCO_2 increased during quiet sleep, and HR and HRV decreased. In active sleep, HR and HRV increased, and slow-wave activity and spindles decreased. A period of arousal is indicated by HR increase. This example again demonstrates the usefulness of simultaneous monitoring of various cardiovascular and cerebral parameters, as, for example, HR, oxygen saturation, EEG spectra, SEPs, and BAEPs.

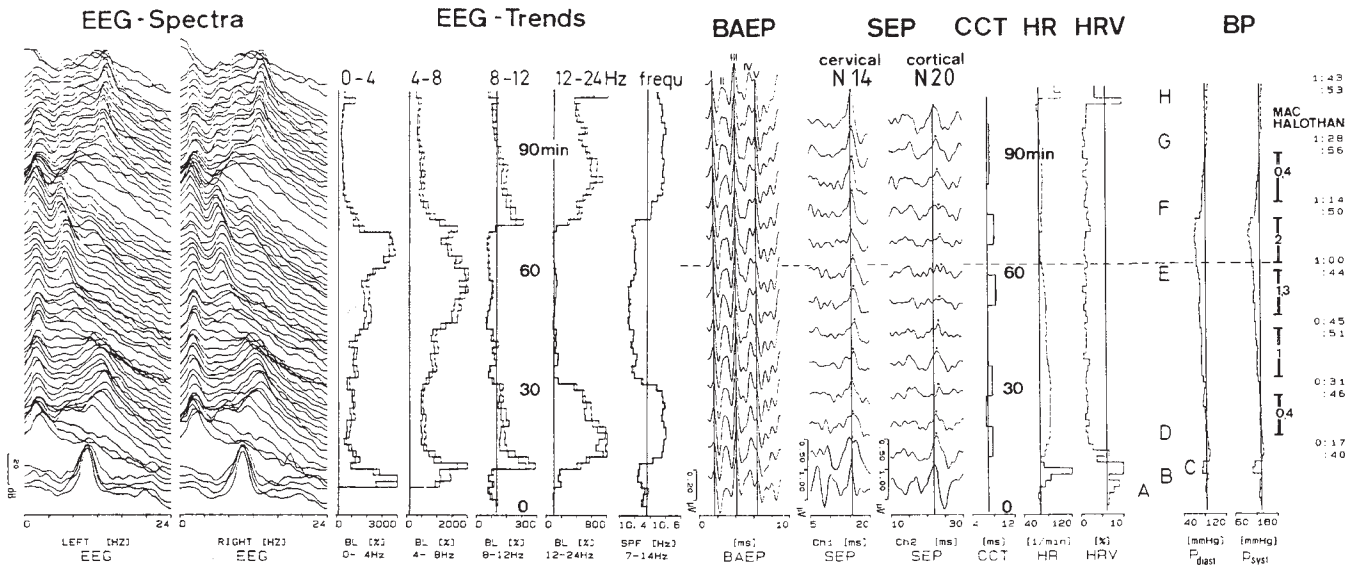


Figure 58.3 Protocol from a case under halothane anesthesia. From left to right: compressed EEG spectra, power trend curves (0 to 4, 4 to 8, and 12 to 24 Hz), mean frequency (7 to 14 Hz), BAEPs, cervical and cortical SEPs, CCT, HR, HRV, and diastolic and systolic blood pressure (BP). On the right side, the level of anesthesia is marked. See text for further explanation.

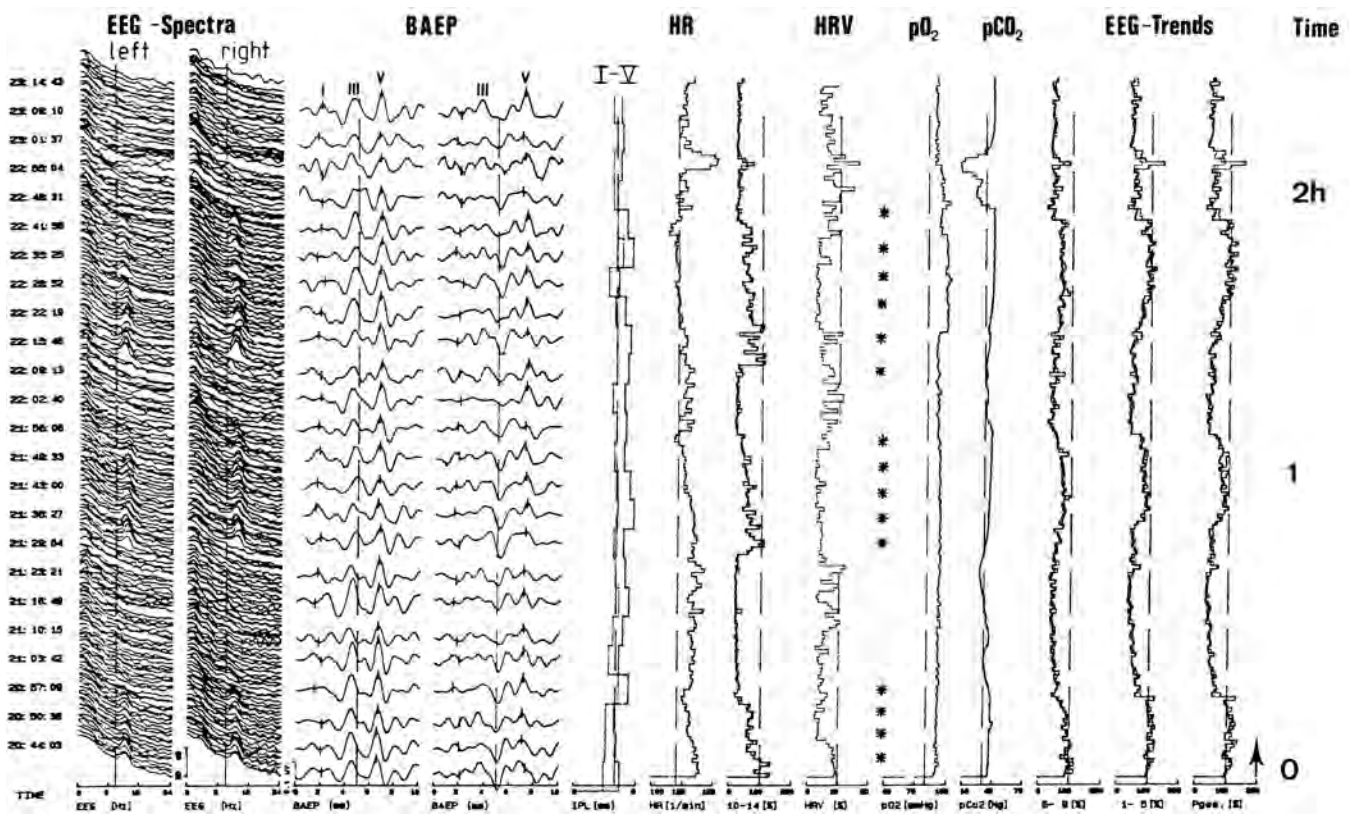


Figure 58.4 Monitoring protocol from a 4 month-old baby during active and quiet sleep. From left to right: Compressed power spectra from left and right hemispheres; BAEPs ipsi- and contralateral to auditory stimulation; BAEP interpeak latency (I-V); 10- to 14-Hz power trend; HRV; pO₂; pCO₂; and EEG power trend curves. For further explanation see text.

Copyright © 2010. Wolters Kluwer Health. All rights reserved.

REFERENCES

1. Nuwer MR. *Evoked Potential Monitoring in the Operating Room*. New York, NY: Raven Press; 1986.
2. Maresch H, Pfuertscheller G, Schuy S. Brain function monitoring: a new method for simultaneous recording and processing of EEG power spectrum and brainstem potentials. *Biomed Tech*. 1983;5:117–122.
3. Pfuertscheller G, Schwarz G, Schroettner O, et al. Continuous and simultaneous monitoring of EEG-spectra and brainstem auditory and somatosensory evoked potentials in the intensive care unit and the operating room. *J Clin Neurophysiol*. 1987;4(4):389–396.
4. Steller E, Litscher G, Maresch H, et al. Multivariables Langzeitmonitoring von zerebralen und kardiovaskulären Größen mit Hilfe eines Personal-Computers. *Biomed Tech*. 1990;35:90–97.
5. Hilz MJ, Litscher G, Weis M, et al. Continuous multivariable monitoring in neurological intensive care patients—preliminary reports on four cases. *Intensive Care Med*. 1991;17:857–893.
6. Branston NM, Ladds A, Lindsay S, et al. Somatosensory evoked potentials in experimental brain ischemia. In: Pfuertscheller G, Jonkman EJ, Lopes da Silva FH, et al., eds. *Brain Ischemia: Quantitative EEG and Imaging Techniques, Progress in Brain Research*. Vol. 62. Amsterdam: Elsevier; 1984:185–199.
7. Anderson DC, Bundlie S, Rockswold GL. Multimodality evoked potentials in closed head trauma. *Arch Neurol*. 1984;41:369–374.
8. Greenberg RP, Newlon PG, Hyatt MS, et al. Prognostic implications of early multimodality evoked potentials in severely head-injured patients. *J Neurosurg*. 1981;55:227–236.
9. Guerit JM. Medical technology assessment EEG and evoked potentials in the intensive care unit. *Clin Neurophysiol*. 1999;29(4):301–317.
10. Sayers B. Analysis of heart rate variability. *Ergonomics*. 1973;16:17–32.
11. Schwarz G, Pfuertscheller G, Litscher G, et al. Quantification of autonomic activity in the brainstem in normal, comatose and brain dead subjects using heart rate variability. *Funct Neurol*. 1987;2:149–154.
12. Mehta SK, Super DM, Connuck D, et al. Heart rate variability in healthy newborn infants. *Am J Cardiol*. 2002;89:50–53.
13. Ako M, Kawara T, Uchida S, et al. Correlation between electroencephalography and heart rate variability during sleep. *Psychiatr Clin Neurosci*. 2003;57(1):59.
14. Grundy BL. Intraoperative monitoring of sensory-evoked potentials. *Anesthesiology*. 1983;58:72–87.
15. Schick U, Dohnert J, Meyer JJ, et al. Prognostic significance of SSEP, BAEP and serum S-100B monitoring after aneurysm surgery. *Acta Neurol Scand*. 2003;108(3):161–169.
16. Prior PF, Maynard DE. *Monitoring Cerebral Function*. Amsterdam: Elsevier; 1986.
17. Pichlmayr I, Lips K, Künkel H. *The Electroencephalogram in Anesthesia. Fundamentals, Practical Applications, Examples*. Berlin: Springer-Verlag; 1984.
18. Brass M, Kravath R, Glass L. Death-scene investigation in sudden infant death. *N Engl J Med* 1986;315:100–105.
19. Steinschneider, A. Prolonged apnea and the sudden infant death syndrome: clinical and laboratory observations. *Pediatrics*. 1972;50:646–654.
20. Bastuji H, Larrea LG, Bertrand O, et al. BAEP latency changes during nocturnal sleep are not correlated with sleep stages but with body temperature variations. *Electroencephalogr Clin Neurophysiol*. 1988;70:9–15.

